Synthesis and Test of Peptides and Peptoids for the Inhibition of Cytokines

TECHNISCHE
UNIVERSITÄT
DARMSTADT

Synthesis and Test of Peptides and Peptoids for the Inhibition of Cytokines

Zur Erlangung des Grades eines Doktors der Naturwissenschaften (Dr. rer. nat.)
genehmigte Dissertation von Dorothea Helmer aus Rastatt
— Darmstadt — D 17

TECHNISCHE
UNIVERSITÄT
DARMSTADT

Synthesis and Test of Peptides and Peptoids for the Inhibition of Cytokines

Genehmigte Dissertation von Dorothea Helmer aus Rastatt

Tag der Einreichung: 28. Oktober 2014
Tag der Prüfung: 12. Januar 2015

Darmstadt — D 17

Synthesis and Test of Peptides and Peptoids for the Inhibition of Cytokines

Vom Fachbereich Chemie

der Technischen Universität Darmstadt

zur Erlangung des akademischen Grades eines

Doctor rerum naturalium (Dr. rer. nat.)

genehmigte

Dissertation

vorgelegt von

Dipl.-Chem. Dorothea Helmer

aus Rastatt

Referent: Prof. Dr. Katja Schmitz
Korreferent: Prof. Dr. Harald Kolmar
Tag der Einreichung: 28. Oktober 2014
Tag der mündlichen Prüfung: 12. Januar 2015

Darmstadt 2015

D 17

Meinen Eltern

Contents

1 Zusammenfassung

Chemokine sind kleine Signalproteine des menschlichen Immunsystems, die an der Steuerung und Regulierung von Entzündungsprozessen beteiligt sind. Unregulierte Entzündungsreaktionen können zu Autoimmunerkrankungen und chronischen Entzündungen führen, daher ist die gezielte Beeinflussung der Chemokinwirkung durch regulatorische oder inhibitorische Substanzen von großer Bedeutung für die Entwicklung anti-inflammatorischer Wirkstoffe. Das Ziel dieser Arbeit war es, neue Liganden für das Chemokin CXCL8 zu finden, die die Wirkung von CXCL8 unterdrücken.

Die Wechselwirkung von CXCL8 mit seinem G-Protein gekoppelten Rezeptor CXCR1 wurde seit ihrer Entdeckung eingehend untersucht. In dieser Arbeit wurde durch flexibles Protein-Protein Docking ein Modell des CXCL8:CXCR1 Komplexes entwickelt, welches die experimentellen Befunde zur Interaktion von CXCL8 mit CXCR1 widerspiegelt. Insbesondere die in der Literatur beschriebene Möglichkeit einer Wechselwirkung zwischen dem N-terminalen ELR Motiv von CXCL8 mit Aminosäuren im Bereich der extrazellulären Domänen EZD3 und EZD4 von CXCR1 wurde durch das Modell bestätigt. Basierend auf dieser Wechselwirkung wurde ein Peptid ('IL8RPLoops') entworfen, welches die beiden ELR-bindenden Bereiche nahe EZD3 und EZD4 von CXCR1, bestehend aus α-Helices mit je einer Windung, durch einen 6-Aminohexansäure-Linker verbindet. Mit CD-Spektroskopie konnte nachgewiesen werden, dass IL8RPLoops teilweise helikale Struktur aufweist, was darauf hindeutete, dass die helikale Struktur der zwei zugrundeliegenden Rezeptorsequenzausschnitte im Peptid erhalten wurde. Es wurde nachgewiesen, dass IL8RPLoops CXCL8 mit einer Affinität von $K_d = 0.5 \pm 0.3$ μM bindet und die durch CXCL8 induzierte Migration von humanen neutrophilen Granulozyten inhibiert. FACS-Messungen und zellbasierte Versuche mit fluoreszenzmarkiertem CXCL8 zeigten, dass IL8RPLoops die Wechselwirkung von CXCL8 mit CXCR1 auf humanen neutrophilen Granulozyten und CXCR1-transfizierten HEK293 Zellen unterdrückte. CXCL8-Proteinmuster auf Glas, erzeugt durch maskenlose Projektionslithographie, konnten mit fluoreszent markiertem IL8RPLoops selektiv angefärbt werden.

Strukturelle Ähnlichkeit zu Peptiden, kombiniert mit höherer Stabilität und Bioverfügbarkeit machen Peptoide zu geeigneten Verbindungen für die Entwicklung neuer Wirkstoffe. Im zweiten Teil dieser Arbeit wurden *one-bead-one-compound* (OBOC) Peptoid-Bibliotheken auf TentaGel-Syntheseharz systematisch auf ihre Fähigkeit zur Bindung an fluoreszenzmarkiertes CXCL8 untersucht. Der Untersuchungsprozess (Screening) basierte auf der Analyse von Mikroskopiebildern der Harzpartikel aus einer entsprechenden Bibliothek und wurde computerbasiert durch eine speziell entwickelte Software oder durch individuelle Bildbetrachtung durchgeführt. Die Eigenfluoreszenz des TentaGel-Syntheseharzes sowie die Zunahme der Fluoreszenz desselben durch die Anbindung von Aminen – insbesondere Tryptamin – wurde untersucht. Die Screening-Parameter wurden hinsichtlich Belichtungdauer und Analyse anhand der Bindung von fluoreszent markiertem CXCL8 an IL8RPLoops auf TentaGel Harz optimiert. Geringe Belichtungsdauern von 40 ms unterdrückten den Verlust von Fluoreszenzintensität durch Photobleichen und hielten Autofluoreszeneffekte minimal. Die Betrachtung von FITC/RHO Mischkanalbildern der Harzpartikel stellte sich als effektivste Untersuchungsmethode heraus, mit der fluoreszierende Partikel leicht identifiziert werden

konnten. Auf diese Weise wurde eine einfache und kostengünstige Methode zum Screening von OBOC Bibliotheken auf TentaGel-Harz entwickelt. Erste Tests mit Magnetpartikel gebundenem CXCL8 für die Selektion von CXCL8-bindenden Peptiden verliefen ebenfalls erfolgreich und könnten zu einer weiteren Screening-Methode ausgebaut werden.

Die entwickelte Methode für fluoreszenzbasiertes Screening wurde angewandt, um eine Peptoid-Bibliothek mit einem theoretischen Maximum von 117649 Sequenzen auf die Bindung an fluoreszenzmarkiertes CXCL8 zu untersuchen. Es wurden 44 Peptoid Sequenzen als potentielle CXCL8-Liganden identifiziert, von denen 15 auf Grund ihrer ausgeprägten Hydrophobizität von weiteren Tests ausgeschlossen wurden. Aus den verbleibenden 29 Sequenzen wurden durch Nachuntersuchungen (Re-Screening) 18 CXCL8-bindende Peptoide mit Affinitäten zwischen 11 μM und 112 μM identifiziert. Vier dieser Peptoide unterdrückten die durch CXCL8 induzierte Aktin-Polymerisation in humanen neutrophilen Granulozyten. Zwei der vier Peptoide wurden außerdem in Zellmigrationsassays mit humanen neutrophilen Granulozyten getestet, zeigten dort allerdings keinen Einfluss auf die Zellmigration. Die gefundenen Peptoide sind vielversprechende Leitstrukturen für die Entwicklung von CXCL8 Inhibitoren, deren inhibitorische Wirkung in weiterführenden Experimenten durch Dimerisierung oder Erhöhung der Rigidität mittels Zyklisierung verbessert werden könnte.

2 Summary

Chemokines are small signalling proteins that are involved in a number of autoimmune diseases. The selective inhibition of chemokines is thus a promising strategy for the discovery of anti-inflammatory drugs. The aim of this work was to find novel CXCL8 ligands capable of inhibiting CXCL8 function.

Profound study on the interaction of CXCL8 with its receptor CXCR1 first led to the discovery of a novel, potent CXCL8 inhibiting peptide. Computational docking of CXCL8 to CXCR1 based on previously reported interactions and important amino acids confirmed the regions of the extracellular domains ECD3 and ECD4 of CXCR1 as possible interaction sites with the N-terminal ELR motif of CXCL8. The Peptide 'IL8RPLoops' was designed from two short sequence motifs of extracellular domains ECD3 and ECD4 connected by a linker in an attempt to mimic the receptor binding site. CD spectroscopy confirmed a partial helical structure of IL8RPLoops in accordance with the structure of the receptor scaffold. IL8RPLoops was determined to bind CXCL8 with a K_d of 0.5 ± 0.3 μM and to effectively inhibit CXCL8-induced migration of human neutrophils. FACS and cell fluorescence microscopy experiments suggested that IL8RPLoops prevented CXCL8:CXCR1 interaction on human neutrophils and HEK293 cells stably transfected with CXCR1. IL8RPLoops was also successfully employed in the staining of fluorescently labelled CXCL8 immobilized on glass by maskless projection photolithography.

In a second approach, peptoids were chosen as suitable compounds for inhibitor synthesis due to their structural similarity to peptides but superior stability *in vivo* and easy production. CXCL8 binding peptoids were discovered by screening peptoid one-bead-one-compound (OBOC) libraries on TentaGel resin with fluorescently labelled CXCL8. The screening process was based on image analysis of pictures taken with a fluorescence microscope. TentaGel autofluorescence was studied and it was found that unfunctionalized TentaGel resin fluorescence intensity increases during synthesis. Especially peptoid and peptide sequences with tryptamine side chains displayed increased fluorescence in the FITC channel. Screening parameters were tested and optimized by imaging the interaction of fluorescently labelled CXCL8 with IL8RPLoops on TentaGel macrobeads. Optimized exposure time of 40 ms reduced photobleaching and kept autofluorescence effects to a minimum. Imaging of FITC and RHO channel with consecutive analysis of overlay images proved to be an effective, quick and cost efficient method for library screening. Initial tests of bead isolation by selection with CXCL8-functionalized magnetic spheres also proved successful.

A peptoid one-bead-one-compound (OBOC) library with a statistical maximum of 117649 members was screened for binding fluorescently labelled CXCL8 by the developed microscopy-based two-channel method. MALDI TOF MS/MS sequence identification yielded 44 peptoid sequences, of which 15 were excluded from further testing due to high side chain hydrophobicity. The 29 remaining sequences were synthesized in parallel and re-screened. 18 peptoid sequences that bind CXCL8 with affinities between 11 μM and 112 μM could thus be identified. Four peptoids showed promising inhibitory activity in actin polymerization assay. Testing of two of the four peptoids in cell migration assays however did not provide further proof of the inhibition of CXCL8 function. The discovered peptoids are promising leads for the development of

CXCL8 inhibitors and in further experiments peptoids may be dimerized or their structural rigidity may be increased by cyclization to improve their inhibitory effects.

3 Introduction

The objective of this work was to find peptides and peptoids capable of inhibiting cytokines. The focus lies on a special class of cytokines, the so-called chemokines. Section 3.1 gives a basic overview of chemokine structure and function with special focus on the chemokine CXCL8 (see Section 3.1.1). A main function of CXCL8 is the recruitment of leukocytes into inflamed tissue. To enter into the tissue, leukocytes have to leave the blood vessel across the endothelial border. This process is called 'extravasation' and is explained in Section 3.1.2. The directed movement to the site of inflammation is called 'migration' and the underlying cellular processes are summarized in Section 3.1.3. Chemokines are an interesting target for drug development due to their involvement in a number of diseases, some of which are described in Section 3.1.4. An overview of previously reported chemokine inhibitors is given in Section 3.1.5. Possible strategies for the discovery of novel protein ligands by library screening are shown in Section 3.2 with focus on chemical (see Section 3.2.1) and biological (see Section 3.2.2) libraries. Screening success can be verified by testing affinities of novel discovered compounds in ligand binding assays whose basic principles are explained in Section 3.2.3. Fluorescence anisotropy is a simple yet effective method for studying protein:ligand interactions in solution and is described in detail in Section 3.2.3. Peptidomimetics possess a structure similar to peptides but have several advantages like increased stability and better bioavailability when compared to peptides. Peptoids, the class of peptidomimetics used for the discovery of novel CXCL8 ligands in this work, are characterized in Section 3.3.

3.1 Chemokines

The human immune system is divided into two major sectors: the innate immune system and the adaptive immune system. Innate immunity refers to a non-specific defense system which is capable of attacking pathogens such as bacteria or viruses at the site of inflammation. Neutrophil granulocytes (neutrophils), a type of polymorphonuclear leukocytes (PMN) are the predominant cell type acting in the innate immune system and the most abundant type of white blood cells (leukocytes) in the human body.[1] Their defense mechanisms include phagocytosis, respiratory burst (release of reactive oxygen species, ROS) and the degranulation leading to the release of antimicrobial substances and enzymes from their characteristic granula.[2] The peripheral leukocytes routinely circulate the human blood ready to defend the host against pathogens. Given that the intrusion of a pathogen most likely takes place at mucous membranes and skin (in particular damaged parts thereof) the crucial step of the innate immune defense is the contact of leukocytes with pathogens outside the blood vessel. This can only be achieved by an intricate process involving the directed migration of white blood cells out of the artery into adjacent inflamed tissue (extravasation or diapedesis).[3–6] This directed cell movement is orchestrated by chemotactic cytokines, the so-called chemokines. Apart from leukocytes also various other blood cells, epithelial cells, glial cells and muscle cells secrete chemokines upon stimulation by pathogens or proinflammatory cytokines.[7–10]

Chemokines are small proteins of 8-12 kDa. They posess a highly conserved tertiary structure though their sequence can vary significantly.[11] They display high pI values that lead to a positive overall molecule charge under physiological conditions. Chemokines are therefore preset for binding to negatively charged molecules such as glycosaminoglycans (GAG) on cell-surfaces.[12] They interact with G-protein coupled receptors (GPCRs) on leukocytes or endothelial cells to initiate signalling that ultimately leads to integrin activation, actin polymerization and oxidative burst.

To this day around 50 chemokines and 20 chemokine receptors have been discovered in the human body.[11] They are divided into four subclasses dependent on the number and distribution of the cysteine residues at the N-terminus. With zero, one or three amino-acids in between cysteine residues there are CC-chemokines, e.g. CCL5 (RANTES), CCL2 (MCP-1), CCL11 (eotaxin-1), CXC-chemokines, e.g. CXCL8 (interleukin-8), CXCL12 (SDF1-α) and CX$_3$C-chemokines, e.g. CX$_3$CL1 (fractalkine). Two C-chemokines with only one cysteine residue have also been discovered: XCL1 (lymphotactin) and XCL2 (SCM1-β). This 'cysteine-code' is followed by an 'L' for *ligand* when referring to a chemokine, or by an 'R' when referring to a *receptor*. CXC chemokines are further divided into ELR$^+$CXC and ELR$^-$CXC chemokines, depending on whether they posses the 'ELR-motif', a sequence of glutamic acid, leucin and arginine at the N-terminus (in front of the first N-terminal cysteine residue); ELR$^+$CXC chemokines display angiogenic activity while ELR$^-$CXC chemokines display angiostatic activity.[13] The tertiary structure of all known chemokines is highly conserved and consists of an unstructured N-terminus followed by an antiparallel three-stranded β-sheet and a C-terminal α-helix.[14]

3.1.1 The Chemokine CXCL8

CXCL8 (or interleukin-8, IL-8) is a pro-inflammatory chemokine that was first described in 1987 as a tissue-derived neutrophil-activating protein.[15,16] Earlier names for CXCL8 include neutrophil activating factor (NAF), granulocyte chemotactic peptide (GCP) and monocyte-derived neutrophil chemotactic factor (MDNCF). It has a molecular mass of 8386 g/mol and possesses an overall positive charge at physiological pH values due to its high isoelectric point that has been reported to be 8.3[17] and is calculated to be 9.0 with ExPASy.[18] CXCL8 is the best studied member of the subfamily of angiogenic ELR$^+$CXC chemokines and possesses strong neutrophil activating and recruitment properties. CXCL8 can be produced by leukocytes like neutrophils, monocytes, T-cells, natural killer cells, as well as by endothelial cells, fibroblasts and epithelial cells.[19] CXCL8 is produced as an inactive 99 amino acid precursor with a 20 amino acid signal sequence.[17,20] 79-, 77-, 72-, 71-, 70- and 69-amino-acid isoforms have been isolated from cultured human blood cells.[16,21] The most active form of CXCL8 *in vivo* is the 72 amino acid isoform.[19]

CXCL8 binds two different GPCRs: CXCR1 and CXCR2[32,33] with an affinity of approximately 2 nM for both receptors.[34] CXCR1 is only activated by CXCL8 and CXCL6, CXCR2 is activated by CXCL8 and multiple other chemokines.[35] Monocytes, eosinophils, neutrophils and basophils all express both CXCR1 and CXCR2 receptors but neutrophils show the highest tendency to migrate upon CXCL8 stimulation.[36] While neutrophils express both receptors in roughly the same amounts, CXCR2 seems to be the predominant receptor in basophils, eosinophils and monocytes.[37] The interactions between CXCL8 and its receptor CXCR1 have been studied extensively. From early on, the ELR motif at the CXCL8 N-terminus was discovered to be essential for receptor activation.[29,30] CXCL8(6-72) without the ELR motif still binds to CXCR1 though with reduced affinity.[29] Early mutational studies with CXCR1/2 in-

Table 3.1: Structure and functional intra- and intermolecular interactions of CXCL8.

Part of CXCL8	Length	Part of Sequence	Interactions
α-helix	17 aa	55-72	Interaction with GAG[22–24]
50S loop	4 aa	52-55	
β$_3$ strand	5 aa	48-51	Disulfide bond with second cysteine (C9),[25] interaction with CXCR1(1-38)[26,27]
40S loop	3 aa	44-47	Interaction with CXCR1(1-38)[26,27]
β$_2$ strand	6 aa	38-43	
30S loop	9 aa	29-37	Disulfide bond with first cysteine (C7)[25]
β$_1$ strand	7 aa	22-28	Dimerisation site[28]
3$_{10}$ helix	3 aa	19-21	Interaction with CXCR1(1-38)[26,27]
N-loop	9 aa	10-18	Interaction with CXCR1(1-38),[26,27] Y13-F17 for CXCR1/CXCR2 specificity[14]
N-terminus	9 aa	1-9	Receptor activation,[29,30] possible interaction with Arg199, Arg203, Asp265 of CXCR1[31]

tersubtype chimeric receptors showed, that the N-terminus of the CXCR1/2 receptors was responsible for chemokine specificity and thus was a likely chemokine:receptor interaction site.[38] NMR studies of the N-terminus of CXCR1, CXCR1(1-40) with ^{15}N-labelled CXCL8(1-72) suggested the N-loop, 3$_{10}$ helix, 40S loop, β$_3$ strand and α-helix as CXCL8:receptor interaction sites.[26] However, the α-helix as interaction site is disputable since studies with truncated CXCL8(1-51) suggested that the α-helix was not necessary for receptor binding.[29,39] Mutational studies of CXCR1 implicated the involvement of E275, R280[40] as well as R199 and R203[31] in CXCL8:receptor binding. These residues are situated near extracellular domains ECD3 and ECD4 of CXCR1 and discussed as a possible interaction site for the ELR motif.[31] Since two interaction sites on CXCR1, N-terminus and ECD were considered likely, a two-site model was suggested for the binding of CXCL8 to CXCR1. In this model the CXCL8 N-loop first interacts with the CXCR1 N-terminus (site I) and the CXCL8 N-terminus containing the ELR motif then interacts with ECD3 and ECD4 (site II).[41–43] Recent NMR studies of CXCL8 with parts of the receptor in a lipid bilayer supported the CXCL8:CXCR1(1-38) interaction reported earlier by Clubb *et al.*[26] but failed to provide experimental proof of the interaction between ELR motif and CXCR1 extracellular domain regions.[27] However, it was lately reported that ECD4 enhances binding affinity of the CXCR1 N-terminus for CXCL8 when ECD4 and N-terminus of CXCR1/2 were fused onto a soluble protein scaffold that retains the orientation of ECD and N-terminus of the chemokine receptor structure original (chemokine receptor elements on a soluble scaffold, *CROSS*).[44] The CROSS protein uniting CXCR1 N-terminus and ECD4 bound CXCL8 with an affinity of 0.8 ± 0.3 μM while ECD4 without an additionally fused CXCR1 N-terminal part did not bind

CXCL8. Despite the lack of definite proof, the hypothesis of synergistic binding effects between two regions of CXCL8 is still considered valuable.
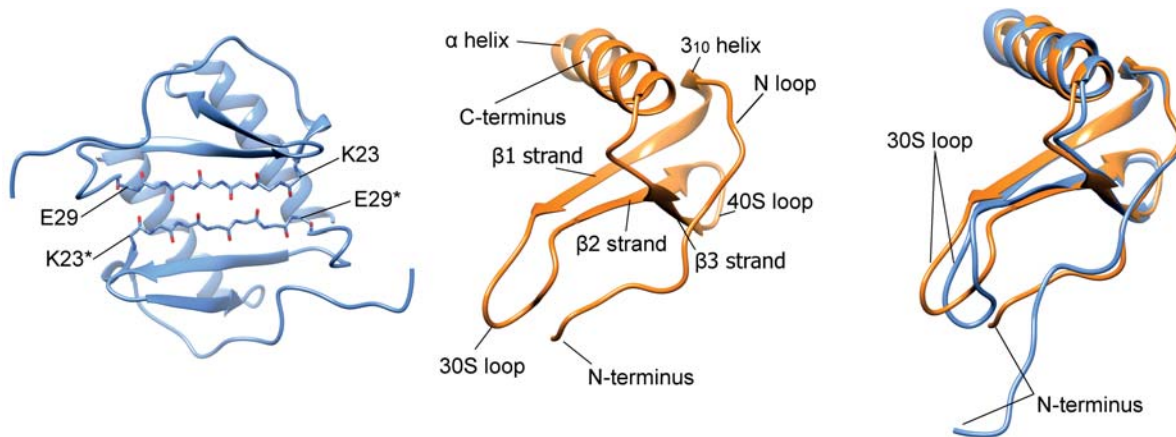

Figure 3.1: Left: CXCL8 dimer structure based on NMR (pdb id: 1IL8)[25] with peptide backbone of the dimerisation interface reaching from residues K23 to E29 (mainly β$_1$ strand).[28] The sequence misses the first serine S1 of the 72 amino acid isoform and starts with alanine A2. Middle: one chain of the CXCL8 dimer structure based on NMR refined by X-ray data (pdb id: 3IL8),[28] the sequence starts with arginine R6. Right: superimposition of X-ray (orange) and NMR (blue) structure shows significant differences in 30S loop and N-terminus, which are the largely unstructured parts of the chemokine and major CXCL8:CXCR1 interaction sites.

From early on NMR and crystal structures suggested that CXCL8 is capable of forming homodimers.[25,28] The β1 strands of two CXCL8 molecules align to form a six-stranded antiparallel β-sheet stabilizing the dimer (see Figure 3.1).[45] The dimerisation interface comprises mainly the β$_1$ strand residues K23 to E29.[28] The dimerisation constant of CXCL8 was reported to be between 0.1 μM and 20 μM.[46–48] There is still some debate about the CXCL8 monomer and dimer form and their respective biological activity. The monomeric form of CXCL8 is likely to be the active form that binds CXCR1.[27,47–49] However, recent *in vivo* studies with trapped monomer and trapped dimer variants of CXCL8 show neutrophil recruitment ability for both variants.[50,51] It was hypothesized that CXCL8 dimerisation could lead to negative regulation.[52] A conclusive hypothesis that takes all the findings into account is not yet available.

A monomer/dimer equilibrium can lead to significant complication of experiments, e.g. the evaluation of binding data.[53] To further study the influence of the monomer/dimer equilibrium on CXCL8 function, several different CXCL8 variants have been produced. First, a 'nonassociating' monomer CXCL8-L25NMe with a backbone methylation at L25 was synthesized by solid phase peptide synthesis.[49] NMR studies revealed a loss of helical structure in residues 67-72 (pdb id: 1IKL).[49] It was concluded that the outer end of the C-terminal α-helix of CXCL8 was merely stable when the dimer was formed.[54] Later studies determined the affinity of CXCL8L25NMe for CXCR1 to be $K_d = 0.8 \pm 0.3$ nM, which is equivalent to wild type CXCL8 within the error of the binding assay.[55] Secondly, the non-dissociating dimer CXCL8-R26C with an affinity of $K_d = 55.0 \pm 6.7$ nM for CXCR1 was reported.[55] Several other CXCL8 mutants with mutations at the dimer interface have been described: L25Y/V27R, being still monomeric at 10 μM, E24L/L25E, V27A,[56,57] as well as L25F/V27F with a dimerisation constant of $K_d = 7$ μM.[58] Furthermore, a shortened variant of CXCL8, CXCL8(1-66), was reported to be monomeric and characterized by ultracentrifugation, nuclear magnetic resonance (NMR) and circular dichroism (CD) spectroscopy.[59,60]

Another important aspect of CXCL8 function is the binding to gylcosaminoglycans (GAG) on the endothelium in order to form stable haptotactic gradients *in vivo*.[22,61–63] Heparin has been used as the representative GAG in studies in the literature, because it is more easily obtained and cheaper than other GAG and it has a similar structure to heparan sulfate, the most abundant GAG that is expressed on 'virtually every cell in the body'.[64,65] Interaction with GAG is a feature of many different proteins and not restricted to the chemokine family. Consensus sequences for GAG-interaction, e. g. XBBXBX or XBB-BXXBX, where B is 'the probability of a basic residue and X is a hydropathic residue', have been identified in several proteins.[66] Protein:GAG interactions largely depend on the type and spacing of basic residues and the affinity depends largely on the arginine to lysine ratio in positions that pair with GAG anions.[67] Hydrophobic interactions between N-acetylated groups have also been suggested to play a role in specific binding to heparan sulfate.[67] The heparin:CXCL8 interaction is mediated by basic residues K67, K64, R68 and R60 on the C-terminal α-helix of CXCL8.[22–24] When the α-helix is missing, CXCL8 can no longer bind to GAGs on endothelial cells and there is no consecutive internalization and transcytosis of CXCL8 across endothelial cells as shown in experiments with rabbit skin.[24]

3.1.2 Leukocyte Extravasation

Pattern-recognition receptors (PRRs) can bind to specific pathogen-associated molecular patterns (PAMPs) to ensure the detection of invading microorganisms.[68] The recognition of pathogens in the human body is ensured by a class of PRR called toll-like-receptors (TLR) that are expressed by endothelial cells.[69] Bacterial proteoglycans or lipopolysaccharides (LPS) bind to a plasma-protein such as lipopolysaccharide-binding protein (LBP). This complex is recognized by the phagocytes via binding to the cell-surface protein CD14 (cluster of differentiation 14). This protein complex is capable of activating TLR4 which induces a signalling pathway that eventually causes inflammation by activating DNA-promotors for the transcription of genes that code for pro-inflammatory proteins like chemokines that guide white blood cells to the site of inflammation (see Figure 3.2).[70,71] To reach the inflamed tissue, leukocytes have to leave the blood vessel across the endothelial border ('extravasation' or 'diapedesis'). An important factor in the process of leukocyte extravasation is the interaction between leukocytes and endothelial cells in the blood vessel. Apart from chemokines also selectins and integrins play a key role in the 'leukocyte adhesion cascade' that is characterised by the following steps: leukocyte tethering, rolling, activation, arrest, intravascular crawling and transmigration.[72]

Leukocyte tethering and rolling is mainly dependent on selectins. Selectins are a class of sugar-binding transmembrane glycoproteins with a highly conserved extracellular structure.[73] The extracellular N-terminus consists of a sugar-binding lectin-domain, an EGF-like (epidermal growth factor-like) domain and a number of consensus repeats of complement regulatory protein (CR) homologous domains depending on the type of selectin: two repeats for L-selectins (*l*eukocyte), six repeats for E-selectins (*e*ndothelium) and nine repeats for P-selectins (*p*latelet).[74] Inflamed vascular endothelial cells express increased amounts of P- and E-selectins which are able to bind P- and E-selectin glycoprotein ligand-1 (PSGL-1, ESGL-1) on the membrane surface of leukocytes with a calculated P-selectin:PSGL-1 dissociation constant between $K_d = 3 \pm 2$ nM and $K_d = 320 \pm 20$ nM.[75,76] The binding strength is dependent on shear stress which means that the blood flow strengthens the bond ('catch-bond') thereby facilitating the capture, i. e. teth-

ering, of the leukocyte. The binding between the lectin-domain and the glycosylated protein is reversible which enables the leukocyte to perform a rolling-motion on the vascular endothelium.[72,77–79]
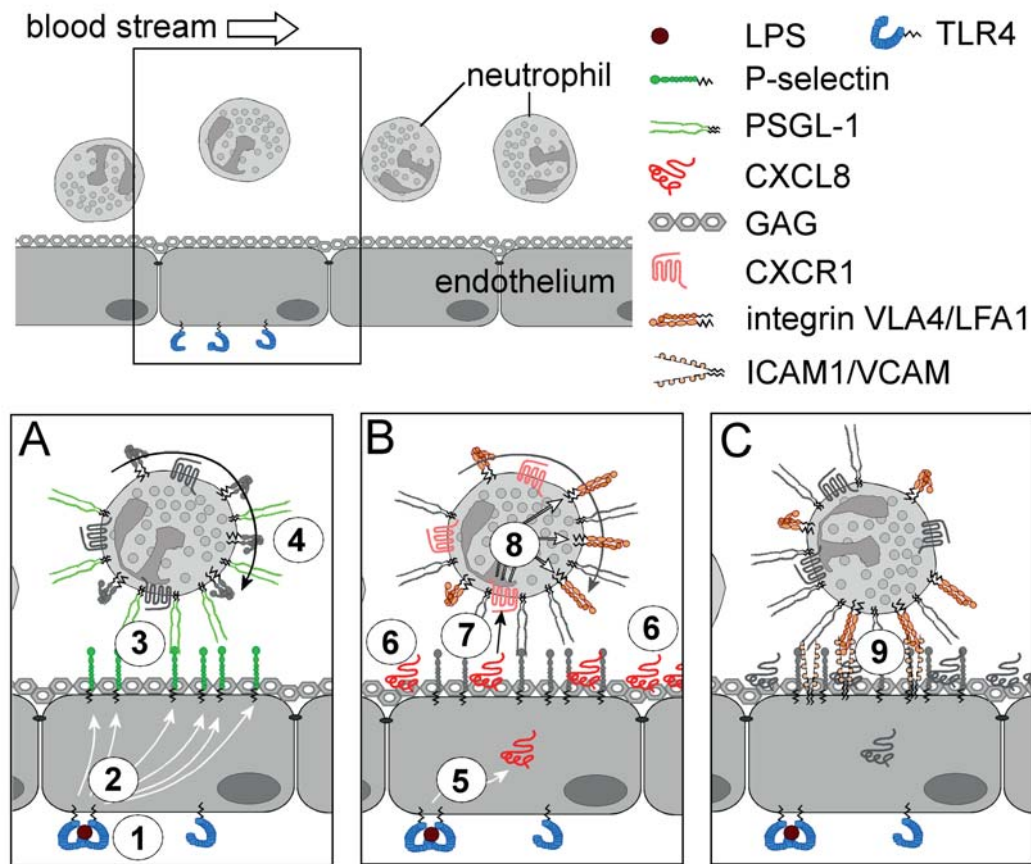

Figure 3.2: The involvement of chemokines in the extravasation of leukocytes. Neutrophils regularly circulate the blood. (A) When a foreign substance enters the body (e.g. a bacterial lipopolysaccharide LPS), it is detected by binding to a receptor ① (e.g. a toll-like receptor TLR4). This initiates a signalling cascade ② that leads to an increased expression of P-selectins. ③ P-selectins bind to P-selectin binding glycoprotein ligand PSGL-1 on neutrophils. This interaction is dependent on shear stress ('catch bond') and leads to a rolling motion ④ of the neutrophil on the endothelium. Leukocyte rolling is also observed in the absence of pathogens, since P-selectins are expressed regularly on the endothelium. The effect is however increased by enhanced P-selectin expression. (B) The TLR-4 activation also leads to the expression of chemokines ⑤ (e.g. CXCL8) that are presented on the endothelial glycosaminoglycans (GAG) ⑥ in the blood vessel. ⑦ Chemokine CXCL8 activates the G-protein coupled receptor (GPCR) CXCR1. This interactions leads to the activation of integrins (e.g. very late antigen 4 VLA4 and lymphocyte function-associated antigen 1 LFA1) ⑧ on the neutrophil (switchblade-like movement, affinity regulation) most likely via the expression of talin-1 and/or kindlin-3. (C) The firm adhesion of the neutrophil to the endothelium due to the interaction of the integrins with cell-surface glycoproteins like intercellular adhesion molecule 1 (ICAM1) or vascular cell adhesion molecule (VCAM1) ⑨ leads to the arrest of the neutrophil on the endothelium. The neutrophil then extravasates into the tissue where it is guided to the site of inflammation by a chemokine gradient that may be stabilized by CXCL8:GAG interactions.

The arrest and firm attachment of leukocytes to the endothelium is mediated by integrins. Integrins are transmembrane receptor proteins that enable cells to attach to extracellular matrices (e.g. fibrinogen,

fibronectin) or cells (via integrin-binding cell adhesion molecules, CAMs).[73] They are non-covalently associated heterodimers consisting of α- and β-subunits which both possess one transmembrane region.[80] They combine to form the integrin structure via association of their amino-terminal extracellular loop domains. When chemokines are secreted during inflammation, they activate integrins on leukocytes through G-Protein coupled receptor-dependent signalling: Chemokines bind to their GPCR thereby activating several different pathways such as the PI3K, the RhoA and RAP1 pathway ultimately leading to the enhanced production of talin, a 250 kDa cytosceletal protein with a C-terminal actin-binding domain and an N-terminal region for integrin-binding. Talin binds the intracellular parts of the integrin β-chain, leading to a conformational change.[81] This switchblade-like movement of the integrin head, which initially is bent towards the membrane, increases the affinity for integrin ligands (affinity regulation) such as intercellular adhesion molecule (ICAM1) or vascular cell adhesion molecule (VCAM1). The binding strength may be further enhanced by the interaction of several integrins on a localized spot of the plasma membrane, the so called integrin-clustering (valency regulation).[81–83] The activation of integrins through GPCR signalling is referred to as 'inside-out signalling'.[84,85] The neutrophil, being firmly attached to the endothelium, may then start to crawl on the endothelium. This crawling on the endothelial surface enabled by the integrin:CAM interaction is referred to as two-dimensional 'haptokinesis'.[3] Neutrophil:VCAM interactions cause an increase in intracellular calcium ions that leads to the phosphorylation of cadherins (calcium dependent glycoproteins) which causes loosening of cell-cell interactions.[6] Neutrophils may then extravasate between endothelial cells and, guided by a chemokine gradient, migrate into underlying tissue disrupting the extracellular matrix by release of enzymes like elastase.[86]

3.1.3 Cell Migration

The two dimensional migration of white blood cells on the endothelium is directed towards an increasing amount of chemoattractant and may therefore be classified as 'chemotaxis' (if the chemoattractant is dissolved in the surrounding fluid) or 'haptotaxis' (if the chemoattractant is immobilized on a surface, e. g. chemokines bound to GAG on the cell surface). Cell migration is dependent on the rearrangement of the cytoskeleton, namely the rapid polymerisation and depolymerization of actin. Actin is one of the most abundant proteins in eukaryotic cells.[87] Filamentous F-actin is formed by the association of globular G-actin enabled by rotation of the two G-actin subunits relative to each other.[88,89] All directed cellular movements rely on motor proteins like myosin that bind to and move along cytoskeletal filaments like actin.[89,90] Myosin (non-muscle myosin II) movement along actin filaments is based on a conformational change of the actin-binding head referred to as 'power stroke' that requires the hydrolysis of adenosine triphosphate (ATP) to adenosine diphosphate (ADP). Myosin therefore has ATPase activity. In association with myosin, electron microscopy images of actin filaments look like the close follow-up of arrowheads, so one end is called the pointed or (-) end and the other is called barbed or (+) end.[87] Actin polymerization is diffusion-dependent, i. e. dependent on the rate of G-actin/F-actin collision at the (+) end of the filament. Rate constants for ADP- and ATP-actin association and dissociation vary at the (+) and (-) ends of the filament. The – compared to ADP-G-actin – higher association rates of ATP-G-actin at the (+) end together with the high dissociation rates of ADP-G-actin at the (-) end lead to a 'treadmilling' of G-actin monomers from the (+) to the (-) end.[87] The rate of polymerisation is thus dependent on the amount of monomeric ATP-G-actin available in the cell as well as the availability of barbed (+) ends for polymeriza-

tion. Regulatory proteins like profilin and thymosin-β4 help to keep the amount of G-actin high: profilin binds one side of G-actin and thus suppresses the association of G-actin at the (+) end. Thymosin-β4 stops actin polymerization altogether and competes with profilin for the binding of G-actin.[87] Capping proteins prevent further polymerization at the barbed (+) ends. F-actin polymerization in cells can be studied by phalloidin-staining. Phalloidin is a toxic bicyclic heptapeptide isolated from the death cap fungus (*Amanita phalloides*) that binds F-actin and prevents filament depolymerization.[91,92] When treated with phalloidin labelled with a fluorophore, the amount of filamentous actin can be directly measured by means of fluorescence intensity.[92] Cells are fixed with formaldehyde at different timepoints seconds after stimulation with a chemoattractant and consecutively stained to visualize the effect of increased actin-polymerization by binding of fluorescently labelled phalloidin.[93,94]

Amoeboid movement of neutrophils starts with the polarization of the cell, i.e. the change of cell morphology that leads to an asymmetric, flattened cell shape that makes it possible to distinguish cell front and rear (see Figure 3.3).[95–97] The frontal structure is characterized by the lamellum, a flat protruding cell structure of finger-like, outward pointing actin filaments.[98] Nucleus and other organelles are concentrated at the rear, the so-called uropod. The outer rim of the lamellum, the lamellipodium, is characterized by an increased amount of actin-polymerization with Arp2/3 crosslinked, myosin-free actin filaments ('dendritic actin'). Behind the outer lamellipodium, the lamellum is characterized by thick bundles of actin, myosin and actin-binding proteins.[99] Polarization is followed by protrusion: actin filaments push the membrane forward by polymerizing towards it (elastic Brownian ratchet model) thus forming pseudopods.[100,101] The force of the F-actin pushing towards the membrane also leads to a backwards push of the filaments towards the uropod, also termed 'retrograde actin flow', characteristic for the lamellum.[102] Focal adhesions (e.g. by the interaction of actin filaments with integrins, mediated by proteins like talin) between cell and substrate can provide points of force transfer enabling a faster migration (integrin clutch hypothesis).[102,103] Myosin contracts the filamentous network in the lamellum and with the retraction of the uropod the cell moves forward.[102]

The role of CXCL8 signalling in actin polymerization, pseudopod formation and ultimately amoeboid movement is complex and not understood in detail. Early studies showed the CXCL8-induced calcium release in neutrophils is sensitive to pertussis toxin.[110] CXCL8 receptor CXCR1 was thus believed to associate with $G_{i\alpha}$ (*inhibitory*) G-proteins.[111,112] The increase in calcium can be explained by the G-protein βγ subunit activating phospholipase Cβ of the IP_3 (inositol-1,4,5-triphosphate) signalling pathway.[113–115] Calcium ions are however not responsible for actin polymerization but rather facilitate actin depolymerization.[116] More recent studies found that CXCR1 may also associate with G-protein $G_{\alpha16}$.[117] CXCL8 increases phosphatidyl-inositol-3,4,5-triphosphate (PIP_3) content in human neutrophils through PI3K activation; inhibition of PIP_3 formation results in reduced rate of pseudopod formation upon CXCL8 stimulation.[107] PIP_3 activates protein kinase B (Akt/PKB) and leads to the activation of several proteins involved in actin polymerization and cytoskeleton rearragement (e.g. myosin light chain kinase MYLK for cell spreading). Small GTPases like Rho, Rac and Cdc42 are major factors in rearrangement of the cytoskeleton.[118] Cdc42 for instance leads the activation of Arp2/3, a protein that is responsible for actin crosslinking to enhance filament stability.[107–109]
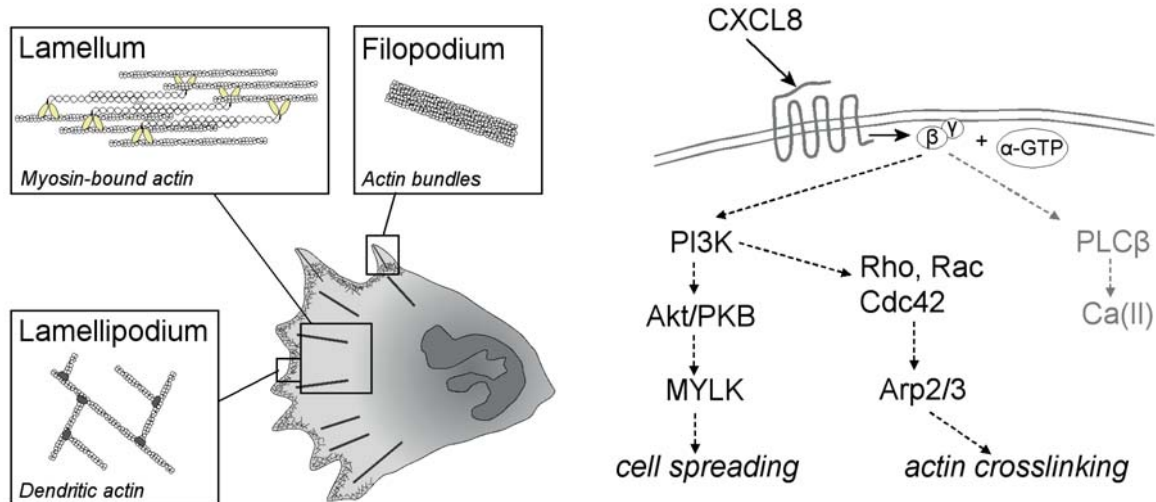
Figure 3.3: Actin polymerization in human neutrophils in the process of cell migration. The amoeboid movement during migration depends on restructuring of the cytoskeleton, especially the actin filaments in the cell. Stimulated cells polarize by developing a flat outstretching structure in the front. This so-called lamellum is characterized by myosin-bound actin bundles that enable cell contraction. At the outermost rim of the cell the lamellipodium, a tight network of short, Arp2/3 crosslinked myosin-free actin filaments ('dendritic actin') allows for rapid actin reorganization and changes in movement direction. Filopodia of stable actin bundles are pushed outwards to scan the environment and enable protrusion of the cell.[99, 102, 104] CXCL8 plays an important role in actin polymerization but only parts of the signalling cascade are known.[105] After GPCR-activation, the G-protein βγ subunit activates phosphatidyl-inositol-3-kinases (PI3K) that phosphorylate PIP2 to PIP3, an important factor in neutrophil chemotaxis.[106, 107] Further down the cascade, protein kinase B (Akt/PKB) is activated and may activate myosin light chain kinase (MYLK), a process likely to be important for cell spreading.[108] Small GTPases like Cdc42 are also activated by PI3K leading to the activation of Arp2/3, the protein that enables the crosslinking of actin filaments in the lamellipodium.[107–109] The pathway of phospholipase Cβ leading to the formation of inositol-3,4,5-triphosphate (IP3) and ultimately to the release of calcium ions into the cytosol is also activated, the role of calcium for cell migration is not entirely clear though.

3.1.4 Chemokines and Diseases

Inflammation-stimulating (proinflammatory) chemokines like CXCL8 provoke an immune responses of the host system. This initial response is primarily focussed on the destruction of invading pathogens. When recruited, neutrophils can release aggressive substances like reactive oxygen species (ROS) or proteases and other enzymes to ensure pathogen destruction. Wrongly induced or persistent inflammation however may lead to autoimmunity and chronic inflammation and thus to unwanted damage of the host organism. Examples for chemokine-related diseases are autoimmune disorders like multiple sclerosis and rheumatoid arthritis and inflammatory diseases like asthma.

Multiple sclerosis (MS) is a degenerative disease of the nervous system where the nerve-protecting myelin sheath is attacked by the immune system. Elevated levels of CCL3 (MIP1α), CCL4 (MIP-1β) and CCL5 (RANTES) were found in the affected tissue of MS patients. Also high levels of CXCL10 (IP-10) and abnormally low levels of CCL2 (MCP-1) were detected in the cerebrospinal fluid,[119–121] though an even

greater number of chemokines may be involved in the disease.[122] The etiology of MS or even details about how chemokines influence the development of the disease are unknown. One hypothesis suggests that chemokines induce immune cells to cross the blood-brain barrier, a prerequisite for attacking cells in the central nervous system.[123]

In rheumathroid arthritis an unknown cause leads to the prolonged inflammation of the joints with progressive cartilage and bone damage. Chemokines are thought to be involved in the extravasation of leukocytes through the vascular endothelium into the synovium and the persistent recruitment of macrophages into the joint.[124] It is hypothesized that an imbalance in the complexly regulated system of cytokines with a multitude of different receptors and ligands/effectors has an influence on cell differentiation.[124] Especially chemokines CCL5 (RANTES), CCL3 (MIP-1α) and CCL2 (MCP-1) are believed to be a critical factor in the proliferation of T-cells.[125, 126]

Apart from the production pool in the bone marrow, there are three marginated pools of neutrophils in the body: lung, liver and spleen each contain an elevated amount of neutrophils due to the prolonged passing time (margination time) through these organs.[2] Neutrophils pass most slowly through the lung making it prone to diseases related to damage caused by neutrophil attacks. Asthma is broadly defined as a reduced function of the lung due to allergens causing prolonged inflammation that leads to severe airway damage. Eosinophils have been identified as the cell type mainly involved in the disease. Chemokines like eotaxin induce the migration of eosinophils and are therefore implicated in the process of lung inflammation. In a mouse-model it has been proven that eotaxin-1 (CCL11) and eotaxin-2 (CCL24) both play a crucial role in recruiting eosinophils into the lung.[127] The high levels of eosinophilia were lost in mice lacking the eotaxin receptor CCR3. The eotaxin/CCR3 pathway is therefore likely to play a major role in the development of the disease.

An increased amount of chemokine receptors in cancer cells suggests an involvement of chemokines in cancer development.[128] The angiogenic nature of chemokines that possess the ELR motif (glutamic acid - leucine - arginine sequence close to the N-terminus) has been identified from early on.[13] Chemokines can thus play a crucial role in cancer development not only regarding the migration of cancer cells that leads to metastasis but also the development of new blood vessels that supply a tumor with oxygen and nutrients. A correlation between the expression of CCR7 and the aggressiveness of lung-cancer has been described.[129] Another well-discussed tumor survival strategy is autocrine signalling, the production of growth factors, chemokines and other proteins by the tumor cells themselves.[130] Many chemokines were found to play a role in tumor autocrine signalling *in vitro*: CXCL8 for example has been implicated in the growth of human skin cancer melanoma and colon, liver as well as pancreatic cancer cells.[131–133]

Another prominent example for the involvement of chemokines in diseases is the infection of human immune cells by the human immunodeficiency virus (HIV) that leads to the acquired immunodeficiency syndrome (AIDS). A viral glycoprotein-complex binds the CD4 receptor on human T-helper cells or macrophages followed by a conformational change in the glycoprotein-complex and the subsequent binding of a co-receptor, usually of the chemokine class, like CXCR4 or CCR5.[134] Eventually the viral membrane fuses with the membrane of the cell thereby releasing the viral DNA into the cell.[135] Monocyte chemoattractant protein-1 CCL2 (MCP-1) levels in the plasma were found to correlate with the virus titer in HIV.[136] Furthermore, in a tissue culture of the human blood-brain-barrier, the stimulation with CCL2 lead to the transmigration of

HIV-infected leukocytes across the barrier.[137] This way, the virus could enter the central nervous system and cause NeuroAIDS or HIV-associated dementia by attacking and destroying brain tissue.

3.1.5 Chemokine Inhibitors

Since chemokines are affiliated with a number of different severe diseases (see previous Section) there has been a keen interest in finding inhibitors of chemokine functions during the past two decades. There are two obvious approaches for inhibiting the effect of chemokines: the inhibition of the receptor of the respective chemokine or the inhibition of the chemokine itself. The chemokine network is very complex with several chemokines binding to the same receptors. The inhibition of a receptor therefore has an effect not only on the targeted chemokine, but also on all other chemokines interacting with the receptor. In order to suppress the function of a single chemokine, it is therefore favourable to target the chemokine itself. This section therefore focuses on inhibitors for chemokine ligands. Several different classes of chemokine inhibitors are known: peptides, small molecules, proteins. Also several antibodies against various chemokines are commercially available.

As early as 1993 the first peptides capable of inhibiting CXCL8 were studied. It was found, that the N-terminus of CXCL8, CXCL8(3-25) was capable of inhibiting the binding of CXCL8 to human neutrophils and inhibited the chemotactic activity of recombinant human CXCL8.[138] The short peptide Ac-RRWWCR-NH$_2$, later named 'antileukinate', was discovered through the screening of a synthetic peptide combinatorial library of mixtures of hexapeptides.[139] The sequence was initially tested for antimicrobial activity against *Staphylococcus aureus* but was later found to inhibit the binding of CXCL8 to human neutrophils and thus also inhibit CXCL8-induced neutrophil chemotaxis.[140] Further studies revealed that the peptide also suppresses the staphylococcal enterotoxin A (SEA)-induced recruitment of neutrophils into the lung of rabbits and that it is capable of preventing CXCL1 from binding to human melanoma cells.[141–143]

Peptides like Ac-MWDFDD-*spacer*-MPPADEDYSP-NH2 which are derived from the extracellular N-terminus of CXCR1, one of the binding sites for CXCL8, bind to CXCL8 and possess K_i values in the lower micromolar range.[144, 145] The complex of one of these peptides, CXCR1-p1, i.e. CXCR1(9-14) linked to CXCR1(20-29) by 6-aminohexanoic acid (sequence: MWDFDD-Ahx-MPPADEDYSP, $K_i = 7$ μM), with CXCL8 was further studied by NMR (pdb id: 1ILQ).[42] Experiments revealed that CXCR1-p1 is unstructured (see Figure 3.4) and retains the previously confirmed[26, 27] interaction sites of CXCL8 with the N-terminus of CXCR1: N-loop, 3$_{10}$ helix, 40S loop, β$_3$ strand. In a similar approach, peptides derived from the N-terminal domain of CCR3 have been found to be potent CCL11 (eotaxin) inhibitors while peptides based on the sequence of the first and third extracellular loops showed no binding capacity.[146] Peptides derived from the N-terminus of rabbit CXCR1 have also been reported.[147] In 2009 consensus sequences from several different chemokine receptors were presented on recombinant phage and screened on microarrays for their binding affinities to 31 different chemokines.[148] The rationale was to find low-affinity chemokine-binding peptides that are capable of simultaneously modulating the function of several chemokines in the chemokine network. Peptides LFGNDCE and WVFGNAMCK were found to be active in delayed type contact hypersensitivity (DTH) in mice. Phage display has also been employed for the discovery of high affinity chemokine inhibitors: the peptide CPWYFWPC has been shown to inhibit the interaction of CCL11 with its receptor CCR3, and SAMWDF as well as FWDDFW were found to interfere with CXCL8:receptor interaction thus inhibiting CXCL8-induced neutrophil migration.[149, 150] It is however

not specified, if these peptides bind to the chemokine or the receptor. CROSS proteins (chemokine receptor elements on a soluble scaffold) were designed to study the interactions of chemokines with their receptors, by fusing chemokine receptor sequence parts onto a protein scaffold (B1 domain of streptococcal protein G) that retains the spatial orientation of parts in the native receptor.[44, 151] They have not been tested for inhibitory effects but they have been found to bind to chemokines with affinities in the low micromolar range.

The first small molecules known to bind CXCL8 were (R)- and (S)-ketoprofene (see Figure 3.4). They suppress the chemotactic activity of human monocytes and human polymorphonuclear neutrophils *in vitro*.[152, 153] Chalcones (see Figure 3.4), similar structures derived from 1,3-diphenylurea reduce the binding of CXCL12 to CXCR4, inhibit calcium response, prevent receptor internalization in human kidney cells and block the recruitment of eosinophils into the airways of ovalbumin-challenged mice *in vivo*.[154, 155]
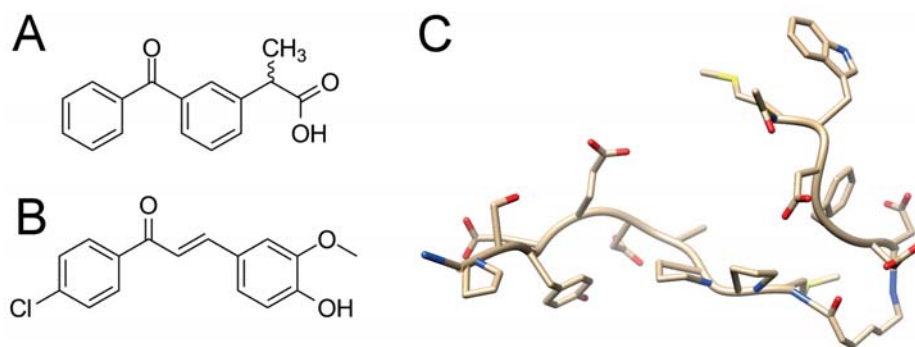

Figure 3.4: Examples of known chemokine inhibitors. (A) Ketoprofene isomers bind to CXCL8 and inhibit neutrophil migration.[152, 153] (B) Chalcone 4 binds CXCL12 and inhibits the interaction with its receptor CXCR4.[154] (C) NMR-based structure of CXCR1-p1 (pdb id: 1ILQ), a peptide derived from the N-terminal sequence of CXCR1 that binds CXCL8.[42, 145]

NOXXON pharma introduced D-RNA aptamers with promising binding capabilities that were resynthesized as L-RNA oligonucleotides and named 'spiegelmers' ('mirrored', German: *'spiegeln'*). They are stable against nucleases and therefore could serve as potential drugs. An inhibitor of CCL2 (MCP-1) is commercially available and proved to be effective in the treatment of lupus nephritis in mice.[156] A commercially available anti-CXCL12 (SDF1-α) spiegelmer proved to effectively reduce the migration of chronic lymphocytic leukemia cells in Transwell assays.[157] A broad-range aminolactam chemokine inhibitor (FX125L) is being tested in clinical trials mainly for the treatment of asthma.[158]

To evade immune responses, some organisms in nature prevent the release of or inhibit the function of chemokines in order to be able to live on the host. Tick saliva is known to contain small proteins called 'evasins', which show chemokine neutralizing activity: Evasin-1 for instance is specific for CCL3, CCL4 and CCL12 and binds to these chemokines with an affinity in the low to sub-nanomolar range.[159] Large DNA viruses like the herpes- and poxviruses produce chemokine-mimicking proteins as well as chemokine-receptor mimics and chemokine-binding proteins that prevent the interaction of chemokines with their receptors.[160, 161] Myxoma virus T7-glycoprotein binds the GAG-binding domain of CXCL8 and is believed to thus interfere with neutrophil recruitment.[162]

Proteins are involved in all types of cellular processes, e.g. signalling and detection, catalysis and reproduction. All these reactions depend on the interaction of different classes of proteins like receptors and signalling proteins, enzymes and cofactors. Influencing the interactions of proteins can have desirable effects for the host organism and lead to the development of new drugs. Protein-binding substances, or 'ligands', can be found in many substance classes: small molecules, peptides/proteins, peptidomimetics or nucleic acids.
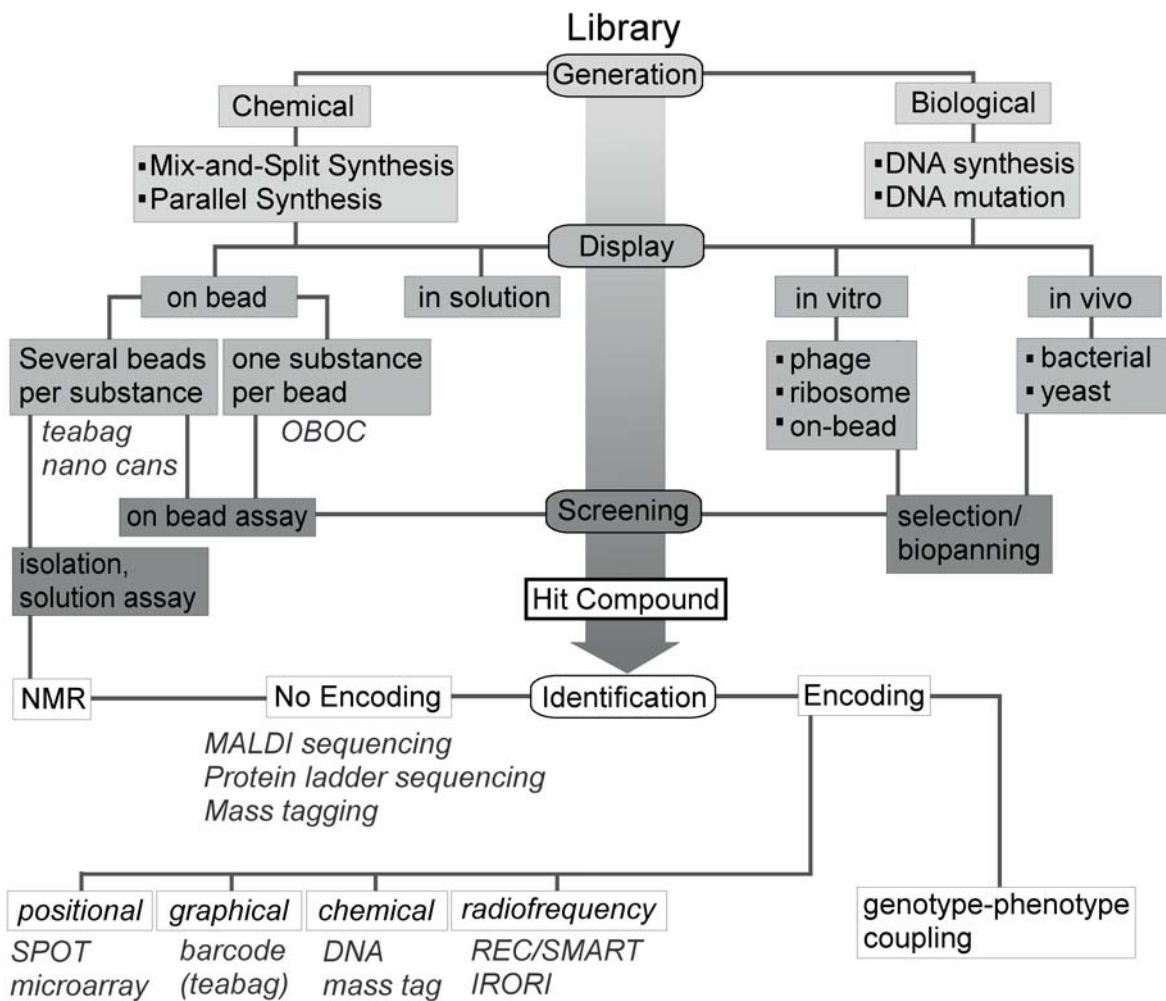

Figure 3.5: Finding novel protein ligands by library screening: Overview of different methods for library generation, display, screening and hit identification. Libraries are generated by chemical synthesis (peptides, DNA) or mutation (DNA, RNA) to give 'chemical' and 'biological' libraries. They are displayed on bead, on phage or on microorganisms. Different types of libraries are screened by testing compounds in *in vitro* or *in vivo* assays that produce a readout (like fluorescence intensity) for each compound, permitting to find active compounds (hits). Hits are then identified by sequence deconvolution or their assay-specific encoding. Chemical, positional, graphical and radiofrequency encoding have been described for chemical libraries.[163] Biological libraries are characterized by their genotype-phenotype encoding. Identified hits may be re-tested and further characterized for their biochemical properties.

The discovery of novel protein ligands either relies on rational ligand design or on the synthesis of large compound collections (libraries) that are tested (screened) in biochemical assays to find compounds with certain desired properties. Methods for the synthesis as well as for the screening of compound libraries are diverse. An experimental approach to studying protein-protein interactions is the parallel or combinatorial synthesis of a large number of potential binding molecules and a subsequent assay for the visualization of a positively interacting substance. The use of a large number of substrates increases the possibility of finding a specific protein ligand and minimizes the problem of synthetic bias that occurs when synthesizing and testing only a small number of previously chosen substances. To this day several different types of libraries with different kinds of protein-targeting molecules are known. They are generally divided into synthetic (or chemical) and biological libraries. Chemical library synthesis relies on the concept of combinatorial chemistry: the generation of compounds by repetitive or combined use of well-characterized, high-yield chemical reactions (like amide-coupling or click-chemistry, respectively). Biological libraries on the other hand are created by the use of microorganisms for peptide synthesis, e.g. the synthesis and presentation of peptides on phages in a phage display library.

The screening of compounds in chemical and biological libraries usually comprises an *in vitro* or *in vivo* assay that allows a simple readout (e.g. by fluorescence intensity or luminescence) to distinguish between binding or active compounds and non-binding or inactive compounds. Promising candidates identified by the readout are termed 'hits' or 'screening positives'. The chemical identity or sequence of the hits is then identified depending on the mode of library encoding. Hits may then be re-synthezised and further characterized for affinity and activity. The different types of libraries and encoding methods are described more closely in the following paragraphs and are summarized in Figure 3.5.

3.2.1 Chemical Libraries

Most chemical library synthesis reactions are carried out on solid support. Solid phase synthesis was introduced by Merrifield in 1963 for the synthesis of peptides on chloromethylated crosslinked polystyrene.[164] In general the attachment to solid support ensures an easy removal of unattached reaction side products after each synthesis step, enables the use of chemicals in excess and facilitates the automation of the synthesis which can provide a large number of substances in small or large quantities. Limitations of solid-phase synthesis are the inability to perform purification steps to remove side-products like truncated or erratic sequences during the synthesis and the consecutive analysis of small quantities of compounds. For the synthesis and screening of large libraries the question of compound analysis is essential. There are different approaches to overcome the problem of direct substance identification: Several kinds of library encoding methods have been reported, like positional, chemical, graphical and radiofrequency encoding.[163]

Non-Encoded Libraries

The basic variant of combinatorial libraries is non-encoded: various compounds are synthesized in a combinatorial process, and important sequences are only identified after positive screening results. This determination of compound identity is also termed 'deconvolution'. At first, the synthesis of compounds and the presentation as an array for screening were two seperate steps: compounds were synthesized and then presented on a solid support for screening ('spotted' onto a surface). Sometimes the term 'probe' is used for

a spotted compound with a known identity, while 'target' describes an unknown compound in an array.[165] The dot blot is an early example for pre-synthesized DNA probes spotted onto nitrocellulose filters in an array format.[166] When the printed spots became smaller and the compound collections were printed on a minimal space, the term 'microarray' was introduced: a densely printed collection of biomolecules on surfaces (biochips) for screening purposes,[167] e.g. microarrays of DNA,[168] peptides[169] and natural products.[170] These techniques link a compound to a certain space on an array, but do not directly identify the sequence, which has to be determined by further analysis.

The synthesis and presentation of the library can also be combined in one process. A combinatorial process known as the 'mix-and-split' (also 'mix-and-pool') method was reported by Furka in 1991.[171] It is especially useful for the synthesis of polymeric, repetitive structures like peptides: the first amino acid is coupled to the resin and the resin is split into several portions, each portion is reacted with a different amino acid and the resin is pooled and mixed. After splitting, the next set of amino acids is attached and so on (see Figure 3.6). The number of possible peptides N is dependent on the amount of amino acids A_i per cycle i and the number of residues of the peptide n (equals the total number of synthesis cycles):
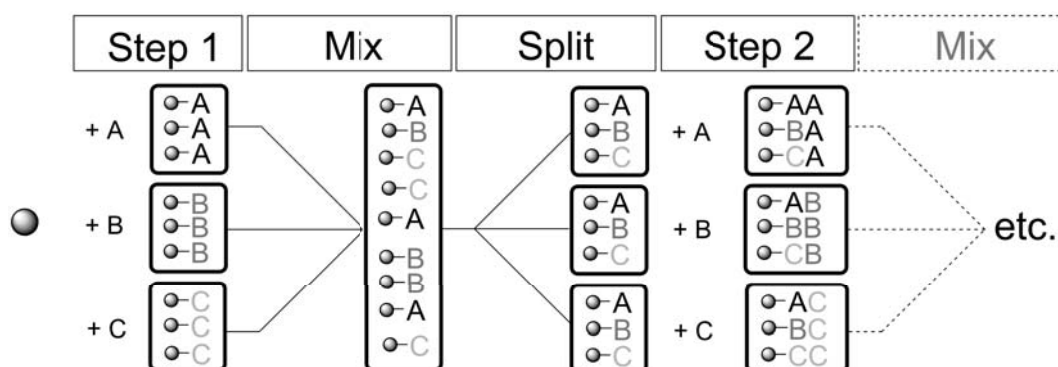
$$N_n = \prod_{i=1}^{n} A_i \tag{3.1}$$

Figure 3.6: Schematic explanation of mix-and-split synthesis. One synthesis cycle consists of reaction step, mixing and splitting of the reactants. The number of compounds synthesized increases exponentially with the number of synthesis cycles.

The mix-and-split method was further developed by Lam to produce libraries in which each individual resin bead carries one sequence, the so-called 'one-bead-one-compound' (OBOC) libraries.[172] Compounds from this type of library can be easily screened 'on-bead': proteins are incubated with the library and give a certain signal readout, e.g. by fluorescence intensity of an attached fluorophore. OBOC libraries with various non-peptide oligomers and small molecules have been reported and have been reviewed, e.g. by Lam *et al.*[173] The sequence deconvolution relies on classical fragmentation or sequencing methods like matrix-assisted laser desorption/ionization time-of-flight mass spectrometry with ion fragmentation (MALDI TOF MS/MS) or Edman degradation. The analysis is therefore largely restricted to peptides, peptidomimetics and nucleic acids. The OBOC method needs no additional synthesis steps and no further specialized decoding instrumentation and thus keeps synthesis and analysis prizes low. Mass spectrometric analysis of unlabeled peptide or peptoid OBOC libraries may be facilitated by protein ladder sequencing.[174,175]

Ladder sequencing produces terminated peptide fragments from every coupling step, i. e. a bead with the sequence ABCD shows A, AB, ABC and ABCD fragments after ladder sequencing. This 'fragmentation' is accomplished by Edman degradation of the bead-bound peptide sequence with a mixture of 95 % phenylisothiocyanate and 5 % phenylisocyanate. The phenylcarbamyl peptides formed by phenylisocyanate are resistant to further degradation cycles while the phenylthiocarbamyl peptides are cleaved. This way, the only instrumentation needed for sequence deconvolution is a MALDI TOF MS without fragmentation ability. The addition of mass spectrometry tags to the compound structure can facilitate sequence analysis by mass spectrometry. Tags may either be attached after cleavage or parallel to compound syntheses with multi-functional beads. Such co-functionalization of compound beads can be accomplished with bifunctional resin.[176] Bifunctional beads have been used for the generation of a small-molecule OBOC library co-functionalized with chlorine and bromine labelled mass spectrometry tags.[177] The halogenated tags may be cleaved independently from the resin and identify the compound sequence. In other approaches, the post-screening cleavage of peptides or peptoids from the resin followed by the functionalization with a halogen mass tag simplifies the recognition of the fragmentation pattern in mass spectrometry.[178]

Non-encoded libraries may also be synthesized in solution: a rigid core molecule is equipped with different functionalities and reacted simultaneously with various building blocks with reactivities complementary to the functional groups of the core.[179] This way a statistical mixture of all possible (small) molecules is generated in solution. Screening of the mixtures of chemical compounds created by this method is complex and requires the preparation and screening of a number of sublibraries for sequence deconvolution in an iterative process.[180]

Encoded Libraries

Graphical encoding links the synthesis product to a graphical identification tag like a barcode. One of the first examples is the teabag-synthesis where the solid support is kept and reacted inside labelled polypropylene 74 μm mesh bags.[181] The bags are unambiguously identified by a code that may be read out with a scanner. The syntheses in small containers leads to high compound yields so that even analysis methods like NMR can be employed.

Radiofrequency Encoded Combinatorial chemistry (REC™) combines the tea-bag approach of a multitude of beads in one reaction compartment (called 'nano can') with the storage of synthesis information by a Single or Multiple Addressable Radiofrequency Tag (SMART™).[182] Commercial methods like the IRORI MiniKans are available.[183, 184]

In a library encoded by position, a particular compound identity is linked to a specific location on an array. As opposed to early dot blot-like strategies or microarray-printing these arrays are synthesized directly on the solid support (e. g. *in situ* microarray synthesis) and thus couple the solid phase synthesis of a compound to its spatial position on the solid support. One of the earliest example for this approach is the multipin-synthesis of peptides on acrylic-acid-grafted polystyrene rods.[185] An array of 96 polymer rods was dipped into individual reaction mixtures in a 96-well plates in a defined order, so that after synthesis the peptide sequence on each rod was known. A more sophisticated version of this positional encoding is the spatially adressable parallel synthesis of compounds on a glass slide, developed in the late 1980s by Fodor at Affymetrix.[186, 187] 1024 penta-peptides were synthesized on a 1.6 mm^2 array by a circular process of

selective photodeprotection of light-sensitive peptide protecting groups and amide-coupling. The process yielded only picomoles of substance and screening relied on strong interactions of printed peptides with antibodies. Another method for *in situ* microarray synthesis relies on the delivery of reagents to confined areas,[165] e.g. through drop-on-demand ink-jet technology[188] or flow channels.[189] A similar approach for the synthesis of targets on surfaces is the SPOT-synthesis, where peptides are synthesized on spots on a cellulose membrane.[190]

Chemically encoded libraries facilitate compound identification by co-synthesizing or adding a chemical tag that may be more easily identified than the actual compound. The earliest form of chemical encoding was the addition of co-synthesized DNA-sequences on peptide OBOC library beads.[191] DNA is an especially suited molecule since very small amounts may be amplified by PCR and consecutively identified by sequencing. The encoding of small-molecule libraries with peptoids on bifunctional beads was reported recently.[192]

3.2.2 Biological Libraries

Biological libraries exploit biological replication systems such as peptide or DNA production by microorganisms. A characteristic feature of molecular displays is the coupling between genotype (DNA or RNA) and phenotype (peptide and its affinity/specificity or RNA). Such displays exist *in vivo* on bacteria and yeast and *in vitro* on bacteriophage, ribosomes and particles. Genotype/phenotype coupling enables the rapid amplification and sequencing of library hits.

The most employed method is the *in vitro* phage display method.[193] Phages are viruses that can insert their DNA into bacteria. The M13 phage of the Ff phage family is one of the most widely used phages for phage display. It can infect *E. coli* cells with a *fertility* (F)-plamide that enables the horizontal gen transfer between bacteria through cell-to-cell connections of small 'membrane-tunnels', the so-called 'F-pili'. The phage DNA encodes for major and minor coat proteins. The major coat proteins flank the rod-like shape of the filamentous virion, while the minor proteins cap the ends of it. Only one side of the phage is able to bind the F-pilus of *E. coli*.[194] In M13 phages, gene III of the single-strand DNA encodes for minor coat protein pIII on the pilus-binding end of the virion. Foreign DNA sequences can be inserted into the amino-terminal half of pIII on the outside of the virion. This leads to the presentation of the DNA-encoded protein on the outside of the phage.[193] Required DNA libraries can be produced by randomization (chemical DNA synthesis), mutation or recombination (biological DNA synthesis).[195] Phage libraries are screened by incubation with molecules of interest and the bound phage population is enriched by further screening steps ('biopanning'). Phage 'hits' can be used to infect *E. coli* which leads to amplification of the phage DNA that may be sequenced to decode the peptide sequence. Up to 40 amino acids can be incorporated into the pIII gene of the M13 phage.[196] Libraries of up to 10^9 different peptides on phages are routinely produced and tested for their interaction with proteins, DNA or other biomolecules. Due to the amount of peptide sequences that may be screened at once and the easy deconvolution, phage display has been a convenient method for the discovery of antibody Fab fragments from early on.[197] Similar display techniques are carried out with bacteria and yeast.[198, 199]

Another method of displaying peptides is the so-called ribosome display.[200] Synthetic ribosomes are assembled *in vitro* and a library of mRNA sequences (transcribed from a pool of DNA) are added. The active

ribosomes translate the mRNA-sequences into peptides. Addition of antibiotics or the lack of a stop codon results in the protein as well as the mRNA remaining attached to the ribosome. Like in phage display, biopanning yields a number of binding peptides attached to the corresponding ribosomes. The mRNA is translated into cDNA, amplified by PCR and analyzed to identify the peptide sequence.[201]

Recently a method for genotype-phenotype coupling on beads was reported. In the ORBIT bead display,[202] streptavidin beads are coated with homogeneous DNA (i. e. DNA of the same sequence, one sequence per bead) from a library where each sequence contains a 27 basepair epitope, the gene for β-2-microglobulin and the gene for streptavidin binding peptide. An emulsion PCR (where one bead is incorporated into one emulsion droplet) ensures the amplification of the DNA template on the beads. Emulsion *in vitro* transcription/translation (IVTT) translates the DNA into peptides that are presented on β-2-microglobulin and immobilization on the bead is ensured by the streptavidin binding peptide. The beads then carry both peptide template and corresponding DNA. Ligand selection via on-bead assay with subsequent DNA sequencing of selected beads can be executed in high-throughput.[202]

3.2.3 Analysis of Ligand Binding

Protein-ligand interactions may be characterized by the affinity of the ligand for the protein. The main objective of binding assays is to determine the affinity of the ligand for its receptor, i. e. the binding strength of the ligand-protein iteraction. In the simplest case, one ligand molecule L binds reversibly to one receptor R to form a receptor-ligand complex RL:

$$R + L \underset{k_{-1}}{\overset{k_1}{\rightleftharpoons}} RL \tag{3.2}$$

At equilibrium the concentrations (denoted by letters in brackets) of the reactants are connected to the dissociation constant K_d by the following equation:

$$K_d = \frac{k_{-1}}{k_1} = \frac{[R][L]}{[RL]} \tag{3.3}$$

The concentration of free receptor $[R]$ at equilibrium is related to the total receptor concentration $[R]_0$ and the amount of receptor bound in the complex $[RL]$ as follows:

$$[R] = [R]_0 - [RL] \tag{3.4}$$

Combination of Equation 3.3 and Equation 3.4 gives:

$$\frac{[RL]}{[R]_0} = \frac{[L]}{K_d + [L]} \tag{3.5}$$

The term $[RL]/[R]_0$ corresponds to the fraction f of receptor bound in the complex, sometimes also referred to as B:

$$B = f = \frac{[RL]}{[R]_0} \tag{3.6}$$

When B is plotted against the concentration of the free ligand $[L]$, Equation 3.5 corresponds to a hyperbolic curve shaped as shown in Figure 3.7. When displaying the curve with logarithmic x-axis, a dose-response curve with a sigmoid shape results (see Figure 3.7). The dissociation constant K_d can be found on the x-axis at the point of inflection, and corresponds to the amount of ligand required to bind 50 % of the receptor in the complex.
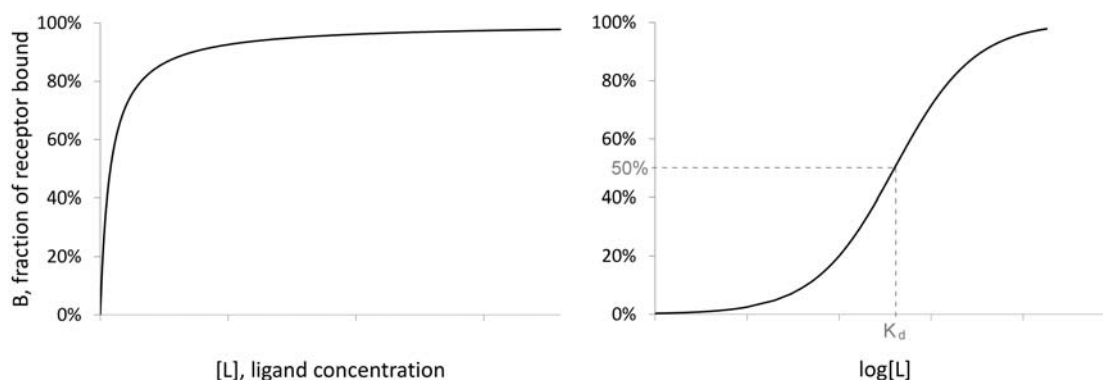

Figure 3.7: Left: Hyperbolic curve corresponding to Equation 3.5: fraction of receptor bound as a function of ligand concentration. Right: Sigmoid dose-response curve that results by displaying logarithmic ligand concentrations on the x-axis. K_d corresponds to the x-value at the point of inflection or the amount of ligand required to bind 50 % of the receptor in the complex.

The analysis of binding properties like the K_d value of newly discovered ligands relies on receptor-ligand binding assays (here, 'receptor' is equal to 'protein', and usually refers to the binding partner with the higher molecular weight). Receptor-ligand binding assays can be classified by two major characteristics: labelling and homogeneity.[203] In order to acquire a readout signal, most assays require the attachment of a label like radioisotopes (e. g. radioligand binding filtration assay, scintillation proximity assay) or fluorophores (e. g. fluorescence filtration assay, FRET, fluorescence anisotropy). Since those labels may interfere with ligand binding, a label-free assay is generally favourable. Label-free assays like surface plasmon resonance (SPR) however require the immobilization of one of the binding partners. Completely label-free assays like isothermal titration calorimetry, ITC on the other hand require expensive instrumentation. The second assay criterion is homogeneity. Following the classification of immunoassays, a homogenous assay in pharamacology refers to an assay without separation steps ('mix and measure').[203,204] One of the most inexpensive yet sensitive and homogenous labelled methods is fluorescence anisotropy (equal to fluorescence polarization).

Fluorescence Anisotropy

The following explanations unite the necessary information about fluorescence anisotropy and were largely taken from textbooks: 'Molecular Fluorescence: Principles and Applications',[205] 'Principles of Fluorescence Spectroscopy',[206] 'Methods in Molecular Biology: Fluorescence Polarization Assay to Quantify Protein-Protein Interactions',[207] additional sources are marked in the text.

In 1926 Perrin observed that fluorophores which are excited by polarized light also emit polarized light upon returning to the ground state.[208] Thus the emitted fluorescence is polarized or 'anisotropic'. Fluorescence anisotropy measurements are based on the polarization of light, i. e. electromagnetic waves. Electromagnetic waves are characterized by an electric field vector $\vec{e}$ that is perpendicular to the magnetic field vector $\vec{m}$. Light waves are transverse meaning their vector of propagation is perpendicular to $\vec{e}$ and $\vec{m}$. For considerations regarding fluorescence anisotropy measurements, the magnetic field can be omitted. When the orientation of the electric field vector during propagation is not random, the wave is called polarized. Most natural light sources emit non-polarized light: the emitted waves share no uniformly directed electric field vectors. For fluorescence anisotropy measurements, linearly polarized light is of interest: the electromagnetic waves oscillate in just one plane perpendicular to propagation (see Figure 3.8). Polarization can be achieved by a polarizer most commonly through absorption or reflexion processes.
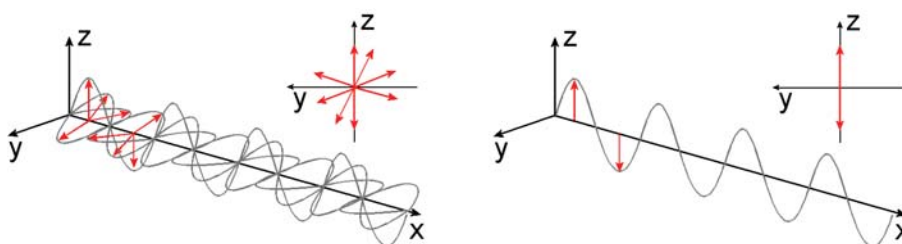
Figure 3.8: Visualization of unpolarized and polarized light. Light waves are shown in grey, their respective electric field vectors $\vec{e}$ are shown in red. Left: unpolarized light is a mixture of randomly polarized light waves with electric field vectors pointing into random directions. Right: linearly polarized light with the electric field vector oscillating in one direction (z); with the wave propagating into a perpendicular direction (x) the polarization plane is the x/z plane.[205, 206]

In order for the electromagnetic wave to interact with a molecule, the molecule has to possess a dipole moment $\vec{\mu}$. Simplified, this corresponds to an axis along which electrons in the molecular orbitals can move more easily. Such an axis is often observed for aromatic systems, since they are planar and the electrons can move in the delocalized π orbitals. The movement of the electrons corresponds to a transition to another (excited) state and the dipole moment is therefore also named transition moment (or transition dipole moment). In different excited states the transition moment vector can possess different orientations. The larger the transition moment, i.e. the length of the vector $\vec{\mu}$, the higher the probability for absorption of light. Fluorophores in solution are randomly oriented and only those molecules whose transition moment vector $\vec{\mu}$ possesses a component in the direction of the field vector $\vec{e}$ can absorb light and thus can be excited. This is called the 'photoselection rule'. The probability of light being absorbed by a fluorophore is proportional to the square of the vector ϕ between the electrical field and the transition moment $\vec{\mu}$ (see Figure 3.9):

$$P(abs) \propto cos^2\phi \qquad (3.7)$$

Upon transition of a molecule to an excited state, the electrons rearrange inside the molecular orbitals and the orientation of the dipol moment changes. The vector is then referred to as the transition dipole moment of the excited state $\vec{\mu}_E$. When the excited fluorophore returns to the ground state, polarized light

is emitted. This emission of light by a dipole ('dipole radiation') is not random: there is no emission along the dipole axis and the emission is maximal perpendicular to the dipole axis (see Figure 3.9).
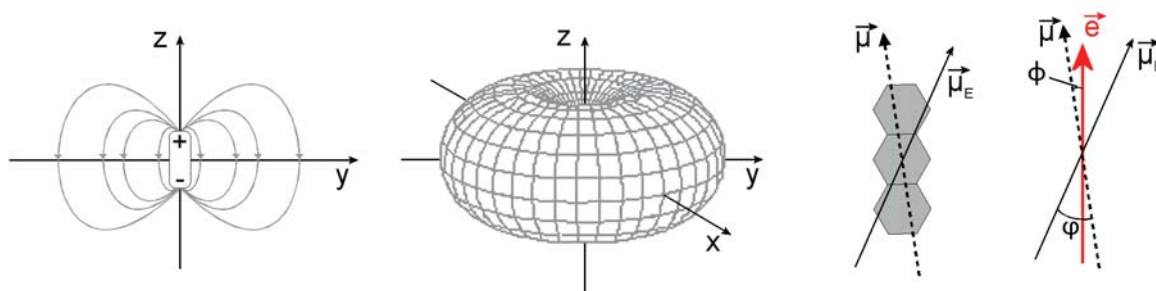

Figure 3.9: Electric fields and dipole moments of a fluorophore. Left: electric field lines of a dipole (analogous to fluorophore). Middle: the three dimensional shape of the electric field around a dipole (or fluorophore) which is symmetrical around the z axis (dipole axis or axis of the transition dipole moment). Right: the dipole moment $\vec{\mu}$ and the transition dipole moment $\vec{\mu}_E$ of an exemplary aromatic fluorophore in an electric field $\vec{e}$ (corresponds to the e-field of the polarized light that is absorbed). The probability of light being absorbed by the molecule is proportional to $cos^2\phi$.[206]

Even though the light emitted by individual fluorophores is always polarized, in a collection of numerous fluorophores in solution (ensemble) the random orientation and movement of the fluorophores leads to an overall isotropic fluorescence. Transition dipole moments of the fluorophores that are excited by photoselection are randomly oriented with respect to the plane of the exciting light. Thus, even without rotation, an intrinsic polarization P_0 (or anisotropy r_0) is measured that is dependent on the angle φ between the absorption dipole moment $\vec{\mu}$ and the emission dipole moment $\vec{\mu}_E$:[209]

$$\frac{1}{P_0} - \frac{1}{3} = \frac{5}{3}\left(\frac{2}{3cos^2\varphi - 1}\right) \tag{3.8}$$

Perrin described the polarization as a function of molecule mobility in solution.[208] The model was based on the diffusion of spherical molecules in solution and resulted in the Perrin equation:[210]

$$\frac{1}{P} - \frac{1}{3} = \left(\frac{1}{P_0} - \frac{1}{3}\right)\left(1 + \frac{3\,\tau}{\rho}\right) \tag{3.9}$$

where P is the measured polarization, P_0 is the intrinsic polarization (polarization in absence of rotation/movement), τ is the lifetime of the excited state and ρ is the rotational relaxation time (the time it takes for a spherical molecule to rotate through 68.5 $°$[211]) which is calculated by:

$$\rho = \frac{3\eta V}{RT} \tag{3.10}$$

where R is the universal gas constant, T is the absolute temperature, V is the effective molar volume of the rotating molecule/complex and η is the viscosity of the surrounding solution. The Perrin equation for the anisotropy is written as follows:

$$\frac{r_0}{r} = 1 + \frac{\tau}{\theta} \tag{3.11}$$

where r_0 is the intrinsic anisotropy (anisotropy in absence of rotation/movement), r is the measured anisotropy, τ is the lifetime of the excited state and θ is the rotational correlation time which is defined as:

$$\theta = \frac{\eta V}{RT} = \frac{1}{3}\rho \tag{3.12}$$

Equations 3.9 and 3.11 show that anisotropy/polarization is dependent on the rotational relaxation and rotational correlation time, respectively, and thus on the effective molar volume V of the rotating molecule. When measurements are conducted with one type of fluorophore in the same environment, i.e. solvent type and temperature kept constant, anisotropy/polarization is solely dependent on the effective molar volume V of the rotating fluorophore. Thus, a significant change in molecular volume leads to slower movement and a higher anisotropy/polarization value. This way, the difference in anisotropy/polarization can be measured when a small molecule (ligand) binds to a larger molecule (protein).

The experimental setup for measuring anisotropy or polarization is shown in Figure 3.10. The light passes through a polarizer before exciting the fluorophores in the sample according to the photoselection rule (see Equation 3.7). The emitted light of the sample (ensemble) is detected through an analyzer which is set either parallel $I_\parallel$ or perpendicular $I_\perp$ to the polarization plane of the exciting light. In case the fluorophores move slowly due to binding a larger molecule, individual fluorophores emit light in a plane only slightly different from the plane of the absorbed light. This results in a high emission intensity in the direction of $I_\parallel$. When fluorophores move quickly the individual fluorophores emit light in almost random orientations and $I_\parallel$ will be low.
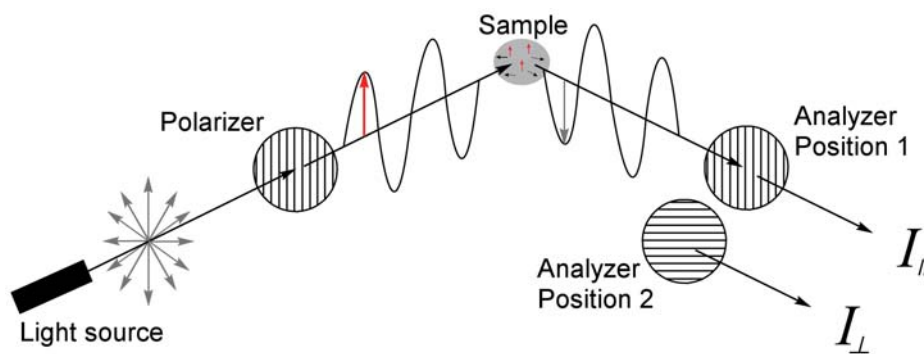

Figure 3.10: Setup of the fluorescence anisotropy measurement. The light passes through a polarizer before interacting with the sample. The residual polarization of the light leaving the sample is calculated by analyzing the light emitted parallel to the polarization plane $I_\parallel$ and the light orthogonal to the polarization plane $I_\perp$. The more light intensity $I_\perp$ is detected in the orthogonal plane (analyzer position 2), the less polarization was retained and the sample shows small anisotropy values. In the opposite case, the more polarization is retained, e.g. the higher the light intensity in the polarization plane $I_\parallel$ (analyzer position 1), the higher the anisotropy value.

The anisotropy r is dependent on the emission intensities $I_\parallel$ and $I_\perp$ and is calculated by:[209]

$$r = \frac{I_\parallel - I_\perp}{I_\parallel + 2\,I_\perp} = \frac{I_\parallel - I_\perp}{I_{tot}} \tag{3.13}$$

$I_\parallel + 2\,I_\perp = I_{tot}$ can be assumed since the electric field of the fluorophore is symmetrical around the z-axis, the axis of the electric field vector $\vec{e}$ (see Figure 3.9). The values of polarization P do not take this symmetry into account:

$$P = \frac{I_\parallel - I_\perp}{I_\parallel + I_\perp} \tag{3.14}$$

Anisotropy is measured in mAU (milli anisotropy units), polarization in mPU (milli polarization units). Fluorescence polarization P and fluorescence anisotropy r describe the same phenomenon and can easily be calculated from one another:

$$r = \frac{2P}{3 - P} \tag{3.15}$$

For measuring a dose-response curve, different dilutions of receptor are mixed with small, constant amounts of labelled ligand. In case of a binding event, the anisotropy increases with increasing amounts of receptor (due to increasing amounts of bound labelled ligand). Binding curves have to be corrected for quenching effects, if the fluorescence intensity of the free fluorophore is not equivalent to the intensity of the bound fluorophore. This can be done by the method of Dandliker *et al.*.[212] The bound to free ratio of the fluorophore is defined as:[212, 213]

$$\frac{F_b}{F_f} = \left(\frac{r - r_f}{r_b - r}\right)\frac{I_f}{I_b} = \frac{r_{corr} - r_f}{r_b - r_{corr}} \tag{3.16}$$

where F_b is the molar concentration of the fluorescent tracer bound in the complex, F_f is the molar concentration of the free tracer, r is the measured anisotropy, r_b is the anisotropy of the bound tracer, r_f is the anisotropy of the free tracer, I_f is the fluorescence intensity of the free tracer, I_b is the fluorescence intensity of the bound tracer and r_{corr} is the corrected anisotropy. The corrected anisotropy is thus calculated from:[212, 213]

$$r_{corr} = \frac{\left(\frac{r - r_f}{r_b - r}\frac{I_f}{I_b}\,r_b\right) + r_f}{1 + \left(\frac{r - r_f}{r_b - r}\frac{I_f}{I_b}\right)} \tag{3.17}$$

Anisotropy and fluorescence intensity of the free fluorophore can be measured, anisotropy and fluorescence intensity of the fluorophore bound in the complex can either be taken from the asymptotes of the binding curve or extrapolated using the following equations, where I and r are the observed fluorescence intensity and anisotropy, respectively:

$$I = I_b + \frac{I_f - I}{[R]_0} \tag{3.18}$$

$$r = r_b - \frac{I_f(r - r_f)}{I_b[R]_0} \tag{3.19}$$

where $[R]_0$ is the concentration of the 'receptor' (the molecule the fluorophore binds to) in the solution. When I is plotted against $\frac{I_f - I}{[R]_0}$, I_b is the y-intersect. Similarly, when r is plotted against $\frac{I_f(r - r_f)}{I_b[R]_0}$, r_b is represented by the y-intersect.

3.3 Peptoids

Peptidomimetics are compounds that mimic peptide or protein structure and retain the ability to interact with a target and produce the same biological effect as the peptide/protein.[214–216] The objective behind synthesis of peptidomimetics is to find structures that are biologically as active as peptides but at the same time possess superior features like increased stability, bioavailability or rigidity. There are three major approaches for the synthesis of peptidomimetics with increased stability that mimick the structure of peptides or corresponding peptide binding pockets: amino acid modifications (in the backbone or sidechain), global restriction by cyclisation to increase stability and achieve a defined three dimensional structure or global restriction by using synthetic scaffolds with functionalities in defined spatial orientations.[216] Peptoids are a class of peptidomimetics with a backbone modification: the side chains are not connected to the α-carbon atom but rather to the nitrogen atom of the backbone, which effectively corresponds to the replacement of the α-CH group by nitrogen and the simultaneous replacement of the NH group by CH_2 in the backbone. This 'switch' in the backbone is the reason for peptoid sequences being synthesized in reverse order compared to the corresponding peptides.
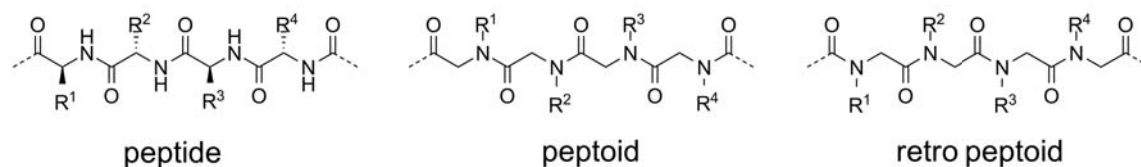

Figure 3.11: The structure of peptides compared to peptoids. When a peptide is translated into a peptoid, the sequence is synthesized backwards (retro peptoid) to ensure that the carbonyl groups and the side chains are in register with the corresponding peptide.[217]

Peptoids were first synthesized in 1992 by Zuckermann and coworkers as 'oligo(N-substituted)glycines'.[217,218] Peptoid synthesis can be carried out with protected monomers as a one-step-coupling reaction, or via a two step acylation/substitution process, the so-called 'submonomer-method' (see Scheme 3.3.1).[218,219] Peptoid coupling reactions can be monitored by the amine-sensitive colorimetric 'chloranil test'.[220–222] Tetrachloro-1,4-benzoquinone (p-chloranil) reacts with secondary amines to give blue 2,3,5-trichloroaminovinyl-1,4-benzoquinone derivatives (see Scheme 3.3.2).

Peptoids, as opposed to peptides, are stable against proteases and possess high oral availability.[141,223,224] Peptoid structures have been described with Ramachandran plots which suggested a greater degree of flexibility in the peptoid structures compared to peptides.[217,225–227] There are significant differences in peptoid compared to peptide structures, however: the amide bond in peptides measured by the dihedral angle ω
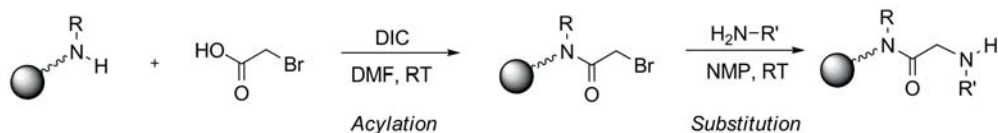
Scheme 3.3.1: Submonomer synthesis of peptoids.[218] (Secondary) amines are acylated with bromoacetic acid and bromine is consecutively substituted with a primary amine to give a secondary amine; the cycle is then repeated.
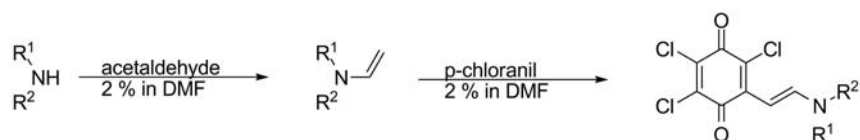
Scheme 3.3.2: Chloranil test for secondary amines. Secondary amines react with acetaldehyde to give the respective enamine. The enamines react with tetrachloro-1,4-benzoquinone (p-chloranil) to give blue 2,3,5-trichloroaminovinyl-1,4-benzoquinone derivatives.

is usually planar and the trans-conformation is favoured over the cis-conformation (with the notable exception of structures that involve the amino acid proline which tends to form a higher degree of cis-amide bonds).[228] In peptoids, the cis and trans ω states are equally populated, giving rise to 2^{n-1} configurational isomers for an n-meric peptoid and 2^n configurational isomers for an N-acetylated peptoid. Interestingly the exchange rate between isomers depends on the localization of the bond in the peptoid structure rather than on the side chains of the nitrogen atoms.[226] Additionally, the amide bond angle ω can differ significantly from planarity ($\omega = 180$ °) to almost 20 °.[227] Due to the N-substitution peptoids lack the ability to form hydrogen bonds within the backbone and thus do not regularly form secondary structures like sheets and helices. Additionally, the lack of C-substitution at the backbone leads to an increased rotational flexibility, as seen in glycine residues of peptides.[217]

Peptoids of up to about 50 residues have been synthesized,[229] and microwave-assisted synthesis of peptoids is a frequently employed technique.[230] Peptoids can be specifically designed to build stable secondary structures making them part of a class of synthetic molecules called 'foldamers'. The first described protein-like secondary structure was a 10-mer peptoid analogue to a collagen triple-helix.[231] It was found that peptoids can be forced into forming α-helical structures by introducing a chiral centre adjacent to the nitrogen atom.[232–234] β-turn structures have also been described.[235] At the beginning, most of these structures proved only stable in organic solvents, until a 36-mer peptoid that forms stable α-helices in aqueous solution was described by Zuckermann *et al.* in 2002.[236] Recently reported peptoid ribbon structures were stable in acetonitrile/water mixtures.[237] Peptoids have been shown to also form multihelical tertiary structures that were able to bind zinc-ions in a zinc-finger protein-like fashion.[238, 239] Peptoids are further regarded as promising biopolymers, the latest development in peptoid-structure research giving rise to stable, self-assembling peptoid nanosheets.[240] Another interesting class of molecules are peptide-peptoid hybrids (sometimes called 'peptomers'). They display an improved stability against proteases combined with desirable features of proteins like secondary and tertiary structures.[241] Peptomer somatostatin-analogues have been shown to possess higher affinity and specificity for certain somatostatin receptors than corresponding peptides as tested by radioligand binding assays on cells and by hormone release *in vivo*.[242] Peptoids have

also been used as antimicrobial substances called 'ampetoids', as antifouling agents on surfaces and as cellular transporters, sometimes functionalized with lipid structures ('lipitoids').[224,243–248]

An optimal system for the nomenclature of peptoids is still under debate and definite rules have not been released. In this work, peptoid monomers start with a capital 'N' (for the N-subsitution in the backbone) that is followed by the three letter code of the amino acid equivalent of the peptoid sidechain. Numbers in superscript provide information about the length of the carbon chain of the side chain: "+0" means the side chain has the same length as in the corresponding amino acid, "+1" points to the fact that the C-chain is one carbon atom longer than in the corresponding amino acid (and so on).

3.3.1 Peptoids for the Inhibition of Protein-Protein Interactions

Many biologically active peptoids have been synthesized so far. It has been found that peptoid sequences that are derived from peptides have similar affinities for their molecular targets. Peptide-analogues are usually synthesized in reverse with respect to the peptide sequence to retain the right order of atoms in the backbone (see Figure 3.11). The translated peptoid sequences range from short ones like the inhibitor of glycolytic enzyme α-amylase Ac-WRY-OMe which has a K_i value of 100 μM as a peptide and 200 μM as a peptoid or thermolysin inhibitor peptoids with an affinity about eight times lower than the corresponding peptide ($K_i = 15$ μM and 1.8 μM).[217,249] For the discovery of novel inhibitor structures, peptoid libraries have also been screened and synthesized. The employed methods included mix-and-split one-bead-one-compound (OBOC) libraries, spatially adressable SPOT synthesis on cellulose membranes and tea bag synthesis.[241,250–253] Protein ligands have also been identified from peptoid microarrays.[254] Among these methods the mix-and-split synthesis with a consecutive on-bead assay is the most suitable for smaller laboratories since it does not require high-priced equipment like printers or robotics.[255] The screening of a peptomer combinatorial library yielded hepta-peptomer HN-Nphe^{+0}Pro-Nphe^{+0}Ntrp^{+0}-SerSerSer-CONH$_2$ that replaces biotin from streptavidin with a half maximal inhibitor concentration of $IC_{50} = 25$ μM, while a similar hepta-peptide FSHPQNT[256,257] showed an IC_{50} over 400 μM under the same conditions.[241]

3.3.2 Peptoid Analysis

Due to the population of *cis* and *trans* states of the peptoid amide bond and the derived number of rotamers one dimensional nuclear magnetic resonance (NMR) measurements of peptoids often yield highly complex spectra due to the slow exchange between the configurational states in linear unrestrained peptoid structures.[226,258] However, short peptoid sequences can be analyzed by NMR and a combination of ^{13}C and ^{1}H NMR has been used to identify trimeric peptoids from combinatorial libraries.[258,259] NMR spectroscopy combined with CD spectroscopy can further be used for analyzing stable peptoid secondary structures.[260] The most widely employed analysis method to determine peptoid sequences is the combination of high performance liquid chromatography (HPLC) and mass spectrometry (MS/MS). Like peptides, peptoids can be fragmented in the mass spectrometer to yield characteristic fragments for sequence analysis (see Figure 3.12).[261,262] C^{α}-CO bond breaks give N-terminal A and corresponding C-terminal X-fragments, CO-NR bond breaks give N-terminal B and corresponding C-terminal Y-fragments and NR-C^{α} bond breaks lead to N-terminal C and corresponding C-terminal Z-fragments. Numbering of the fragments starts at the N-terminus with the first A$_1$/B$_1$/C$_1$-fragments and continues in natural numbers to the last A$_n$/B$_n$/C$_n$-

fragments at the C-terminal end of the peptoid. X, Y and Z-fragments are numbered by subtracting the number of their corresponding N-terminal fragment from the maximum fragment number n. Peptoids fragment preferably at the amide bond and thus show intense Y and B fragments. Due to the increased basicity of the substituted backbone nitrogen in peptoids, a Y+2H fragment is the most abundant in the majority of peptoid mass spectra. The identification of fragments can be improved by applying specific mass-tags like bromine containing molecules characteristic for their isotope-peaks.[178] It is also possible to sequence peptoids by Edman-degradation.[175, 241]
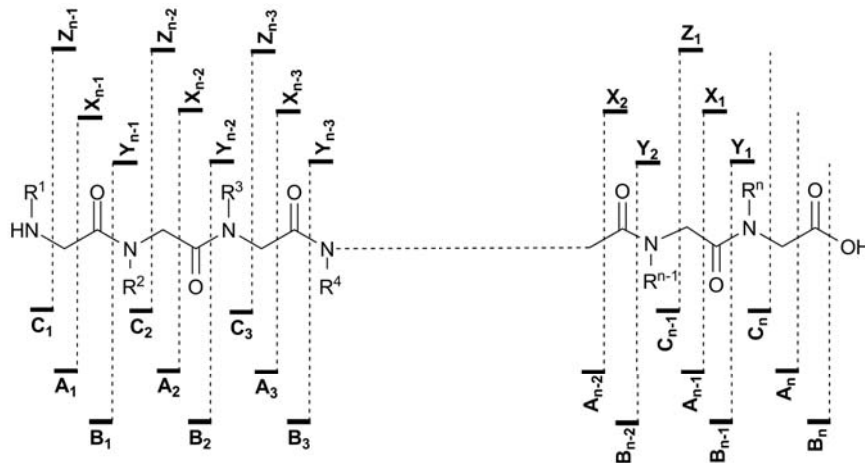
Figure 3.12: Characteristic peptoid fragments detected in MALDI TOF MS/MS.[261]

4 Aim

In case of pathogen invasion, CXCL8 induces the directed migration of neutrophils out of the blood vessel into infected tissue. The neutrophils follow a gradient of CXCL8 that leads them to the source of inflammation, where they release their reactive chemicals to destroy foreign organisms. Wrongly induced inflammation with persistent neutrophil recruitment however leads to the destruction of host tissue and explains the involvement of chemokines like CXCL8 in inflammatory and autoimmune diseases. Therefore the aim of this work is to find novel inhibitors of CXCL8 function. Peptoids were chosen as potential inhibitors due to their structural similarity to peptides, their stability to proteases and ease of synthesis.
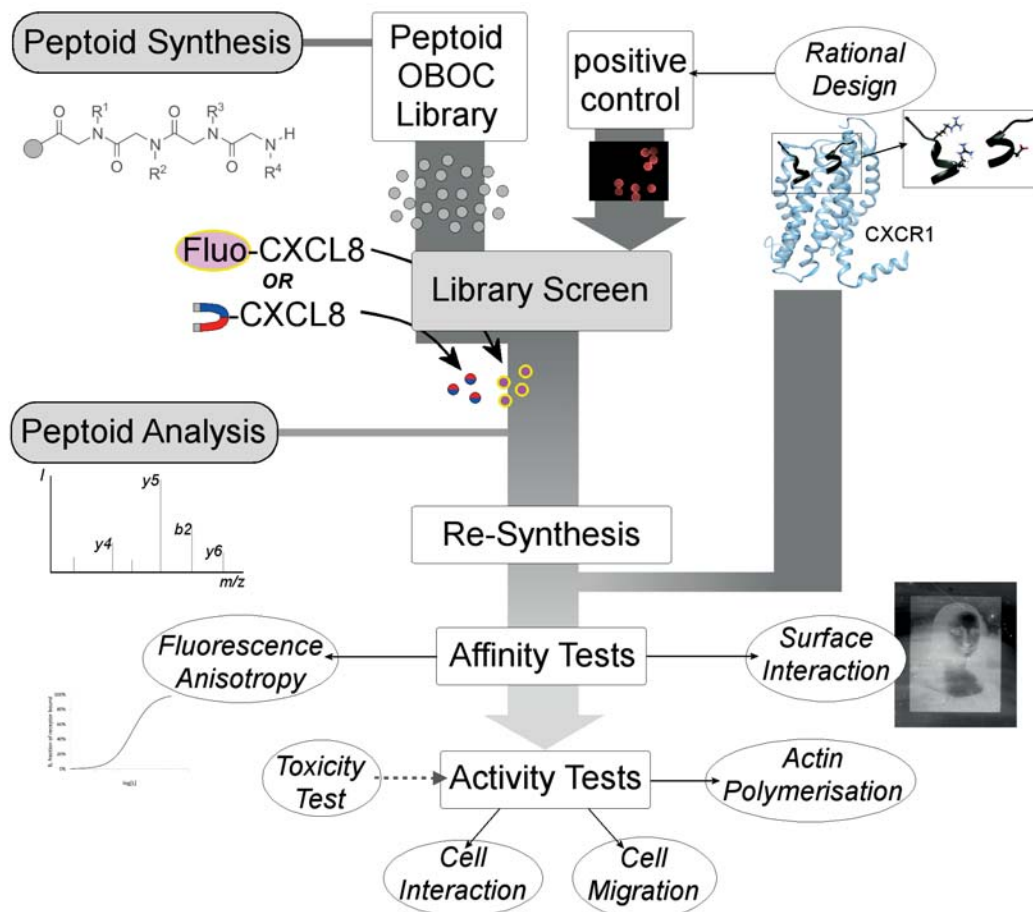
Figure 4.1: Overview of the methods and processes to be employed for the discovery of CXCL8 inhibitor peptoids. A new CXCL8-binding peptide is rationally designed based on a computational model of the CXCL8:CXCR1 complex. The peptide may serve as a positive control for the screening of one-bead-one-compound (OBOC) libraries. After establishing peptoid synthesis and analysis as well as a reliable screening method with either fluorescently labelled CXCL8 or magnetically labelled CXCL8, peptoid OBOC libaries may be screened. Hits from the screening process are identified, synthesized in bulk ('re-synthesis') and tested for affinity and activity.

Different CXCL8-Variants, e.g. the wild type protein, a non-dimerising variant and a fluorescently labelled variant have to be analyzed by CD-spectroscopy to determine their structure and their applicability in ligand binding assays. For ligand-binding analysis a fluorescence anisotropy assay should be established and tested with a known CXCL8-ligand. A computational model of the interaction of CXCL8 with its receptor CXCR1 based on previously reported experimental data should be developed in order to rationally design a new CXCL8-binding peptide. The affinity of the designed peptide for CXCL8 should be determined by fluorescence anisotropy measurements. Further binding assays, e.g. fluorescence on-bead assays and interaction on glass surface, should be executed to ensure that the peptide may serve as a positive control for the screening of one-bead-one-compound (OBOC) libraries.

To find novel CXCL8-inhibiting peptoids, peptoid OBOC libraries should be synthesized and consecutively screened. Before screening, two major prerequisites need to be met: the effective synthesis of peptoids on resin and their unambiguous identification by MALDI TOF MS/MS spectrometry. Screening processes based on magnetic separation or fluorescence which are simple in execution and low in cost with a good signal-to-noise ratio should be tested. For this purpose, fluorescently as well as magnetically labelled CXCL8 has to be synthesized and characterized. A reliable fluorescence-screening method that overcomes problems like resin bead autofluorescence has to be established. Parameters for library screening should be optimized by using the rationally designed peptide positive control. Hits derived from the screening process should be identified and re-synthesized in bulk and tested for their affinity for CXCL8 *in vitro* and for inhibitory effects *in vivo*. Ultimately, the most promising lead structures should be tested for their toxicity as well as for their biological activity by cell-based assays such as actin polymerization and cell migration assay.

5 Results

5.1 CXCL8 Variants

For the study of protein:ligand or protein:receptor interactions different variants of a protein or polypeptide of interest can be useful: a fluorescently labelled form may be used for tracking in cellular assays, mutated forms can show increased or decreased affinities for ligands or receptors. In this work mainly three types of CXCL8 were used for experimental work: first the 72-amino acid isoform of CXCL8[263] (referred to as CXCL8wt **19** for 'wild type') was used for ligand:binding studies and Transwell assays. Secondly, CXCL8L25Y/V27R **21**, a CXCL8 variant with reduced affinity for dimerisation[56,57] that was useful for ligand:binding assays to simulate monomeric CXCL8 was used for fluorescence polarization assays. Thirdly CXCL8S72C-DL550 **23** with a C-terminal cysteine residue that was labelled with a thiol-reactive DyLight550 fluorescent dye[264] was used for on-bead assays, surface immobilization and microscopy.

5.1.1 Folding of CXCL8 Variants

For the structural evaluation, circular dichroism (CD) spectra of CXCL8wt **19**, CXCL8L25Y/V27R **21** and CXCL8S72C-DL550 **23** were recorded.
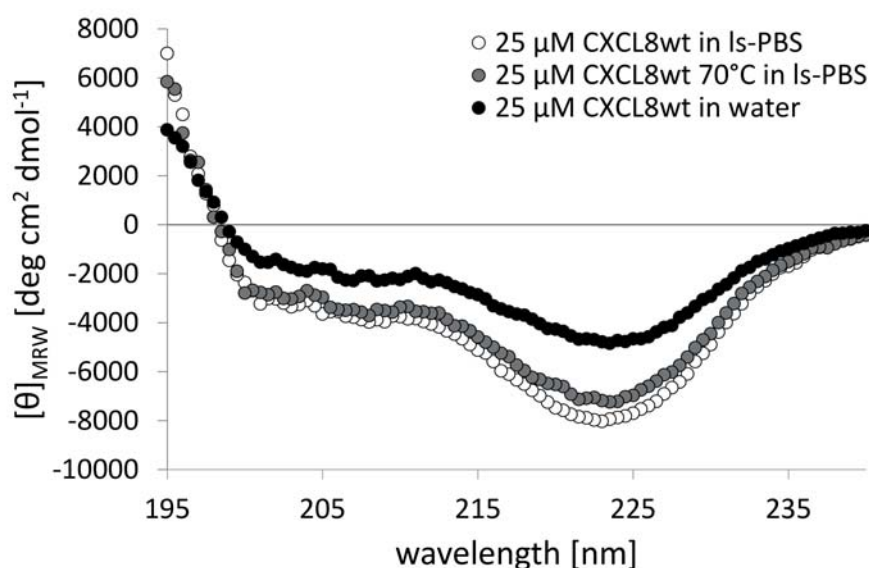
Figure 5.1: Buffer-corrected circular dichroism spectra of CXCL8wt **19** in *ls*-PBS and water. CXCL8 heated to 70 °C for 10 min still retained its three dimensional structure, proving the heat stability of CXCL8 previously reported.[265,266] All show the characteristic shape of CXCL8. Changes in ellipticity were likely due to imprecise determination of concentrations (dry protein samples were weighed).

Two identical samples of CXCL8wt **19** were prepared and one was heated to $70\,°C$ for 10 min to demonstrate CXCL8 heat resistance which was occasionally exploited in our laboratory for CXCL8 purification by heat-denaturation of unwanted proteins. The CD spectra of CXCL8wt **19**, CXCL8wt **19** heated to $70\,°C$ and CXCL8 in water show the characteristic shape of the CXCL8 CD spectra previously reported (see Figure 5.1).[60,263] Changes in mean residue ellipticity are likely artifacts of altered protein concentrations due to protein loss in transfer steps. CD spectroscopy is extremely sensitive to sample concentrations which can make secondary structure element calculation unreliable.[267]
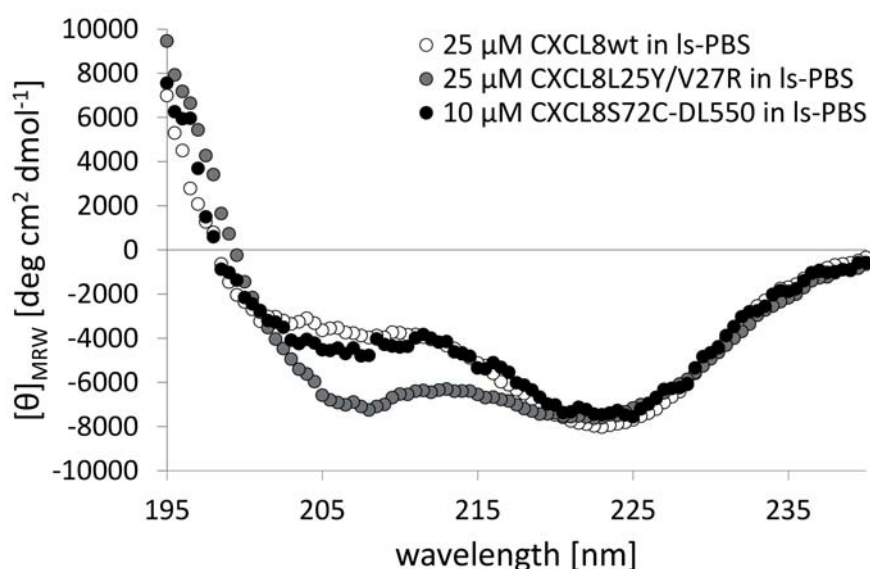
Figure 5.2: Buffer-corrected circular dichroism spectra of CXCL8L25Y/V27R **21** and CXCL8S72C-DL550 **23** compared to CXCL8wt **19**. CXCL8S72C-DL550 **23** retained CXCL8 protein folding after labelling with the fluorophore and was used for fluorescence assays. CXCL8L25Y/V27R **21** retained the fractional helicity of CXCL8wt **19** at 222 nm almost completely, but shows a significantly altered spectrum in the 200 to 220 nm region which points to a significantly altered three dimensional structure. It is not clear, to what extent the exchange of L25 and V27 interfere with CXCL8 protein structure. The CD spectrum also differs greatly from the spectrum of CXCL8(1-66),[59] a previously reported monomeric CXCL8 variant. CXCL8L25Y/V27R **21** is therefore not an ideal choice for a monomeric form of CXCL8.

The mutated forms of CXCL8, CXCL8L25Y/V27R **21** and CXCL8S72C-DL550 **23**, are compared in Figure 5.2. CXCL8S72C-DL550 **23** retains the structure of CXCL8wt **19** and is therefore suitable for replacing CXCL8wt **19** in labelled assays. CD spectra for CXCL8L25Y/V27R **21** have not been previously reported. The measured CD spectrum of CXCL8L25Y/V27R **21** is significantly altered compared to CXCL8wt **19** and CXCL8S72C-DL550 **23** spectra (see Figure 5.2). CXCL8L25Y/V27R **21** shows similar fractional helicity compared to CXCL8wt **19** at 222 nm, but the changes in the region of 205 to 220 nm are significant. Since no CD spectrum of a monomeric 72 amino acid isoform of CXCL8 has been reported so far, the obtained spectrum could not be compared to a spectrum from the literature. However, the CD spectrum of a different monomeric CXCL8 variant, CXCL8(1-66)[59] was reported (no three dimensional structure available).[60] 2D-NMR experiments showed that CXCL8(1-66) adopts a similar structure to CXCL8L25NMe, a monomeric CXCL8 variant with a known NMR structure (PDB id: 1IKL[49]). If the three dimensional structure of all different monomeric CXCL8 variants are similar, also similar CD spectra would be ex-

pected. However, the CD spectrum of the CXCL8(1-66) variant shows a local minimum at 200 nm and a local maximum at 215 nm. Another local minimum at 222 nm shows slightly less mean residue ellipticity compared to CXCL8(1-72), which is expected, since in CXCL8(1-66) parts of the C-terminal α-helix are missing.[60] This is not similar to the spectrum of CXCL8L25Y/V27R **21**. It is however not clear to what extent the exchanges of L25 and V27 disrupt the structure of CXCL8. To gain further insight into the structure of monomeric and dimeric CXCL8 variants, the variants available in the protein database were analyzed regarding their secondary structure elements.

DSSP (define secondary structure of proteins algorithm)[268] calculations* of the CXCL8 variants in the protein database (see Figure 5.3) showed that the monomeric variant CXCL8L25NMe[49] has a lower amount of amino acids assigned to β-sheets (16.7 %) than the NMR (25.0 %) and X-ray structures (23.6 %) of CXCL8 (see Table 5.1). At the same time, the monomeric variant CXCL8L25NMe also possesses a considerably lower amount of amino acids assigned to α-helices (15.3 %) when compared to the NMR (22.2 %) and X-ray (20.8 %) structure. This indicated that in a CD spectrum of a monomeric variant, less α-helical and less β-sheet structures should be detected. The CD spectrum of CXCL8L25Y/V27R **21** (see Figure 5.2) showed a slightly lower amount of helical structure than CXCL8wt **19** but also showed considerably lower mean residue ellipticity between 200 and 220 nm (β-sheet region) and is thus not consistent with structures expected in comparison with monomeric CXCL8 variants reported by Fernando *et al.*.[60] CXCL8L25Y/V27R **21** is therefore most likely not a suitable mutant for CXCL8 dimerisation studies.
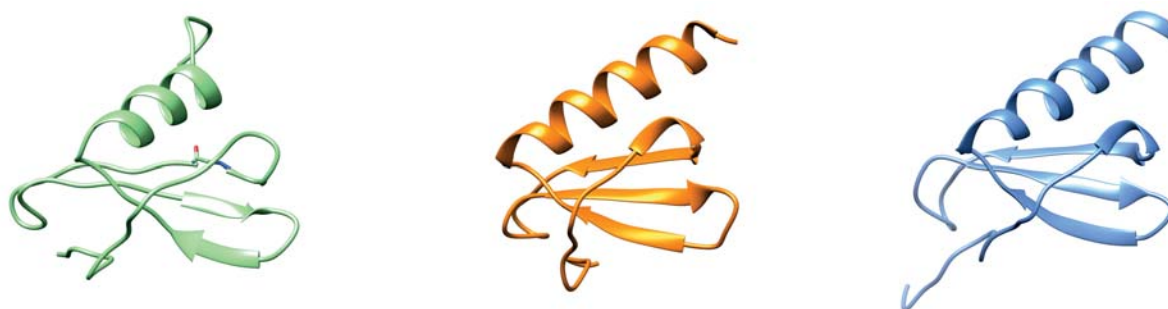
Figure 5.3: Structures of monomeric CXCL8 variant CXCL8L25NMe(4-72) 1IKL[49] (left), dimeric CXCL8(2-72) 1IL8[25] determined by solution state NMR (middle) and dimeric CXCL8(5-72) 3IL8[28] determined by X-ray crystallography (XRC). The monomeric variant possesses a considerably lower amount of amino acids assigned to β-sheets and α-helices.

Table 5.1: Percentage of amino acids (values were calculated for a total amount of 72 amino acids for all three structures since the amino acids missing in the sequences are at the N-terminus, which is unstructured in CXCL8) of CXCL8 monomer and dimer assigned to α-helices and β-sheets calculated by DSSP.[268]

Structure	Source	Description	PDB id	α-helix [%]	β-sheet [%]
Monomer	NMR	CXCL8L25NMe(4-72)	1IKL[49]	15.3	16.7
Dimer	NMR	CXCL8(2-72)	1IL8[25]	22.2	25.0
Dimer	XRC	CXCL8(5-72)	3IL8[28]	20.8	23.6

---

*   Calculated on web server http://www.cmbi.ru.nl/dssp.html, September 2014.

Peptide 'CXCR1-p1' (sequence: Ac-MWDFDD-Ahx-MPPADEDYSP-NH$_2$, Ahx: 6-aminohexanoic acid) was first reported by Attwood *et al.* to replace CXCL8 from its receptors CXCR1/2 on neutrophil membranes with a K_i of 7 µM.[145] Fluo-CXCR1-p1 **89** with an N-terminal fluorescein label was used to test the fluorescence anisotropy assay with CXCL8wt **19** in low-volume, black, transparent bottom microtiter plates (MTP). When fluorescence anisotropy values of Fluo-CXCR1-p1 **89** were measured in dilutions of **19** in *ls*-PBS, the values of the dilutions with the four lowest fluorophore concentrations increased significantly with increasing incubation time (see Figure 5.4). The corresponding fluorescence intensity measurements showed that fluorescence intensities at low fluorophore concentrations decreased (see Figure 5.5). This indicated that quenching occurs, most likely due to adhesion of the peptide to the walls of the MTP. K_d values calculated from the measurement at 0 min incubation time gave 39.5 ± 11.8 µM by omitting the four lowest CXCL8wt **19** concentrations.
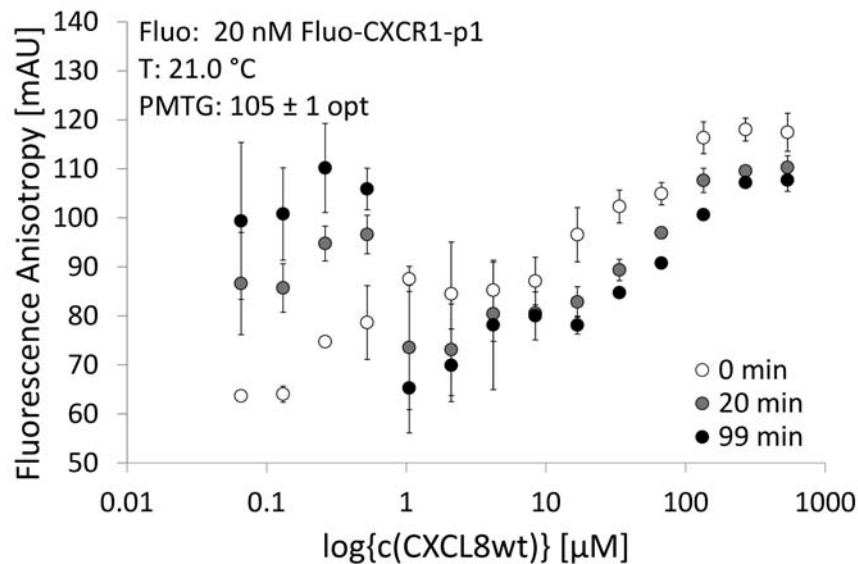
Figure 5.4: Fluorescence anisotropy measurements (λ_{ex}=470 nm, λ_{em}=520 nm) of 20 nM Fluo-CXCR1-p1 **89** in CXCL8wt **19** dilutions in *ls*-PBS at 0 min, 20 min and 99 min incubation time. Measured values at the four lowest CXCL8 concentrations increased with increasing incubation time, indicating the peptide Fluo-CXCR1-p1 **89** adhered to the walls of the microtiter plate (MTP). Calculations with the measurement at 0 min incubation time gave 39.5 ± 11.8 µM by omitting the measurement values at the four lowest CXCL8 concentrations.

When measuring fluorescence intensity values of 20 nM Fluo-CXCR1-p1 **89** in different concentrations of Triton X-100, a steep increase between 1.6 µM and 6.5 µM (0.000097 % and 0.0004 % v/v) Triton X-100 was observed (see Figure 5.6). At ca. 6.5 µM Triton X-100, the maximum fluorescence intensity was reached (ca. 36000 RU), which corresponds to the maximum intensity value in Figure 5.5. This indicated that the detergent prevented the adhesion of the peptide to the walls of the MTP. At high Triton X-100 concentrations, the fluorescence was quenched to an approximately half-maximal, stable intensity value, possibly due to the incorporation of the fluorophore into micelles since the critical micelle concentration of Triton X-100 is 240 µM in water.[269,270]
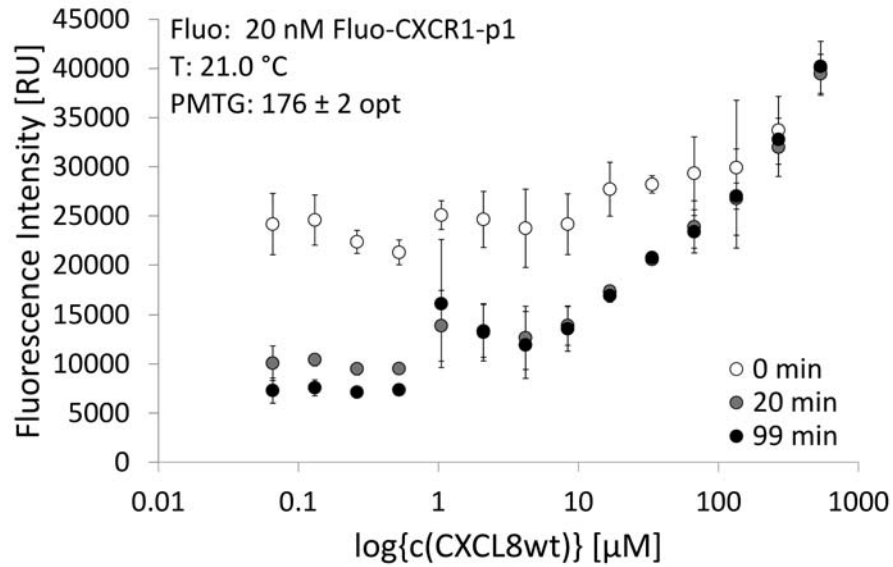
Figure 5.5: Fluorescence intensity measurments (λ_{ex}=488 nm, λ_{em}=520 nm) corresponding to the anisotropy measurement in Figure 5.4 of 20 nM Fluo-CXCR1-p1 **89** in CXCL8wt **19** dilutions in *ls*-PBS at 0 min, 20 min and 99 min incubation time. Measurement points at the four lowest CXCL8 concentrations show quenching of fluorescence intensity, likely due to the fluorophore adhering to the walls of the MTP.
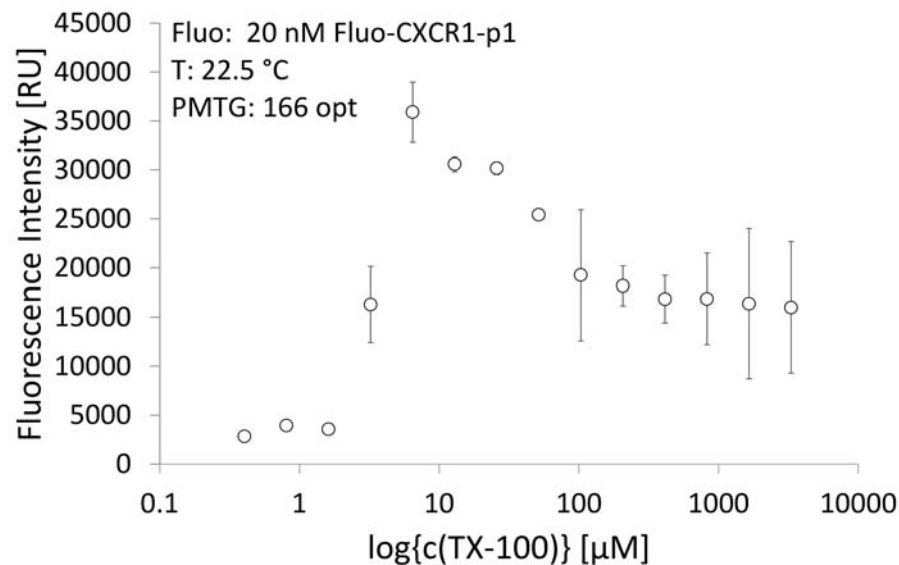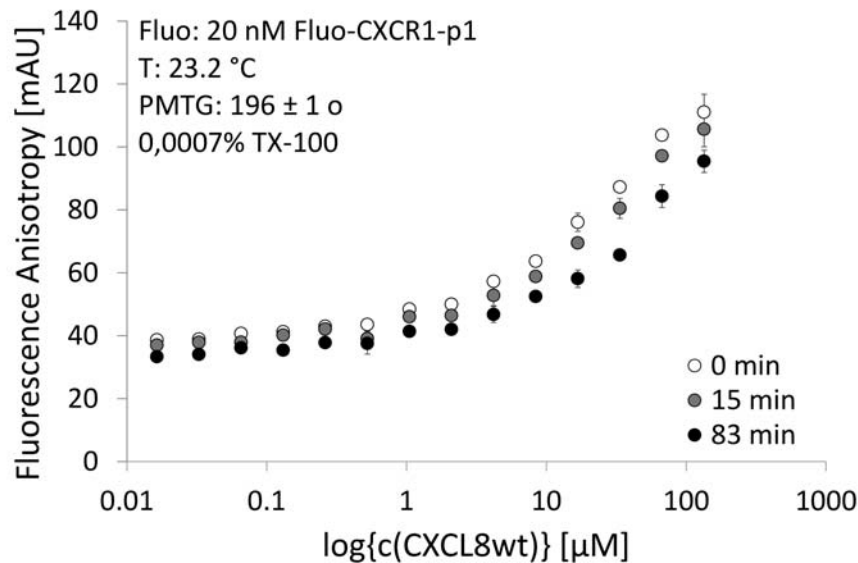

Figure 5.6: Fluorescence intensity (λ_{ex}=488 nm, λ_{em}=520 nm) measurements of 20 nM Fluo-CXCR1-p1 **89** in dilutions of Triton X-100 in *ls*-PBS. The steep increase between 1.6 µM and 6.5 µM (0.000097 % and 0.0004 %) Triton X-100 indicated that the detergent prevented the peptide adhering to the walls of the MTP.

0.0007 % (approximately 10 µM) Triton X-100 appeared like a suitable concentration at which the peptide did no longer adhere to the MTP, while at the same time no quenching of the fluorophore occurred as shown in Figure 5.6. When 0.0007 % Triton X-100 were added to the dilutions, the anisotropy measurements showed well-shaped binding curves (see Figure 5.7). Fluorescence intensity was however quenched upon

binding (see Figure 5.8). K_d values were thus corrected for the fluorescence intensity increase by the method of Dandliker *et al.*.[212] Anisotropy measurement of CXCR1-p1 **89** binding to CXCL8wt **19** were also conducted with 0.1 % (v/v) Triton X-100 (see Figure 5.9).
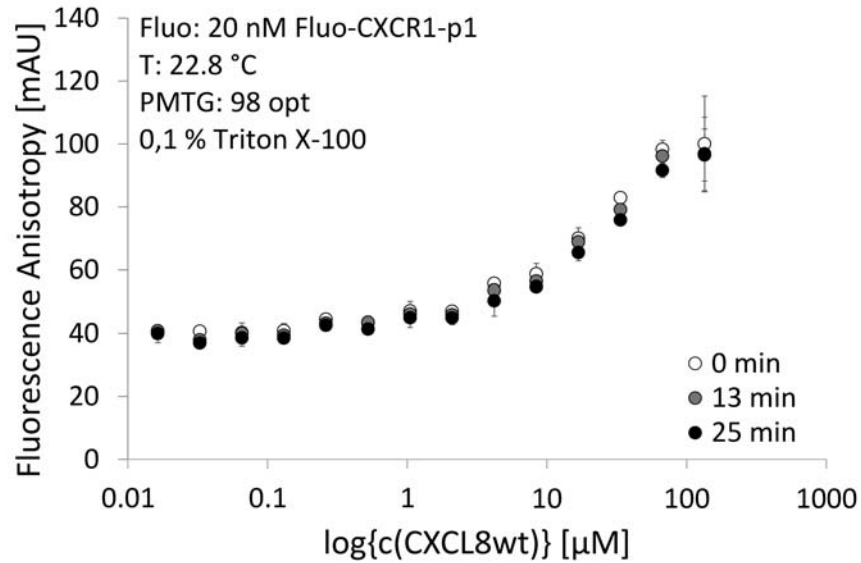

Figure 5.7: Fluorescence anisotropy measurements (λ_{ex}=470 nm, λ_{em}=520 nm) of 20 nM Fluo-CXCR1-p1 **89** in dilutions of CXCL8wt **19** in *ls*-PBS with 0.0007 % Triton X-100.
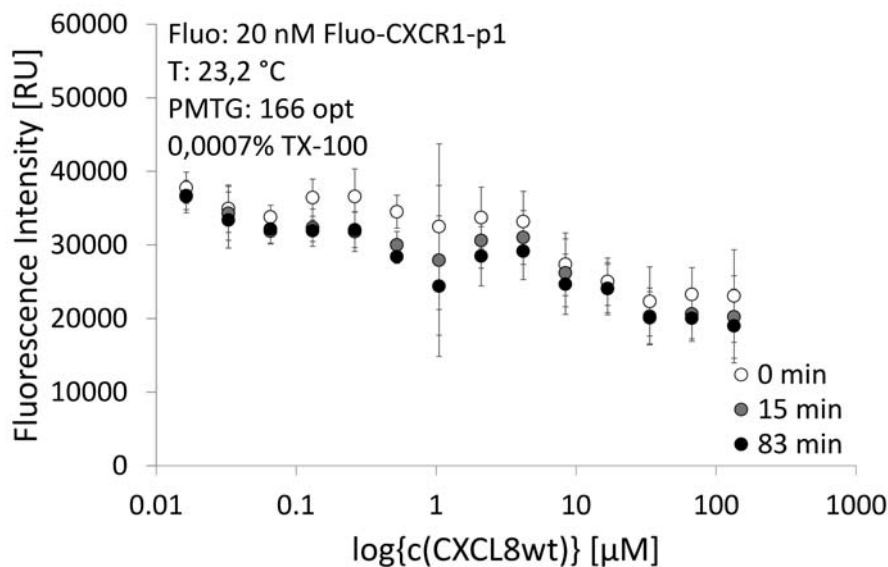
Figure 5.8: Fluorescence intensity measurement (λ_{ex}=488 nm, λ_{em}=520 nm) corresponding to Figure 5.7 of 20 nM Fluo-CXCR1-p1 **89** in dilutions of CXCL8wt **19** in *ls*-PBS with 0.0007 % (v/v) Triton X-100. Upon binding to CXCL8, the fluorescence intensity of Fluo-CXCR1-p1 **89** is quenched.

All calculated K_d values for the binding of Fluo-CXCR1-p1 **89** to CXCL8wt **19** at different concentrations of Triton X-100 and different time points are summarized in Table 5.2. The data shows that without Triton X-100 addition to the buffer, the K_d values were higher than with Triton X-100 and measurements at different time points varied considerably. When Triton X-100 was added to the protein dilutions, K_d

Figure 5.9: Fluorescence anisotropy measurement (λ_{ex}=470 nm, λ_{em}=520 nm) 20 nM Fluo-CXCR1-p1 **89** in dilutions of CXCL8wt **19** in *ls*-PBS with 0.1 % (v/v) Triton X-100.

values became more stable over longer incubation times. Thus the addition of Triton X-100 is beneficial to the determination of the K_d of peptides that adhere persistently to the walls of the MTP. The effects of Triton X-100 on anisotropy measurements are discussed in detail in the next Section.

Table 5.2: K_d values of Fluo-CXCR1-p1 **89** binding to CXCL8wt **19** with different amounts of Triton X-100 (TX-100) added to the protein dilutions in *ls*-PBS and measurements taken at different time points. Values were obtained from fluorescence anisotropy measurements in Figures 5.4, 5.7 and 5.9 . K_d values were corrected for fluorescence intensity increase according to Dandliker *et al.*.[212, 213]

TX-100 (v/v)	incubation time	K_d	corrected K_d
0 %	0 min	39.5 ± 11.8 µM	48.1 ± 14.3 µM
0 %	20 min	47.8 ± 11.7 µM	not determined
0 %	99 min	57.8 ± 22.7 µM	not determined
0.0007 %	0 min	21.1 ± 2.5 µM	13.3 ± 1.7 µM
0.0007 %	15 min	24.2 ± 2.9 µM	11.0 ± 1.6 µM
0.0007 %	83 min	33.5 ± 6.5 µM	13.4 ± 3.0 µM
0.1 %	0 min	22.7 ± 3.2 µM	19.3 ± 2.7 µM
0.1 %	13 min	23.6 ± 3.9 µM	20.0 ± 3.2 µM
0.1 %	25 min	28.3 ± 3.8 µM	23.5 ± 3.3 µM

5.1.3 CXCL8wt Dimerisation and Influence of Triton X-100 on Fluorescence Anisotropy Measurements

The hydrophobic effect leads to the adhesion of proteins and peptides to surfaces and results in reduced molecule mobility. Aggregation of ligands due to the hydrophobic nature of the fluorophore can also be an issue in fluorescence anisotropy. CXCL8S72C-DL550 **23** was used to detect residual CXCL8 in the wells of a microtiter plate (MTP) by fluorescence intensity measurements. It was found that CXCL8S72C-DL550 **23** adhered to the walls of microtiter plates when a solution of the labelled protein came into contact with the MTP well and left a considerable residual fluorescence after its removal (see Figure 5.10). This amount of residual protein correlated with the amount of protein added in solution. A saturation could not be measured due to quenching effects at high concentrations. The adhesion of the protein to the surface could be prevented by adding 0.1 % Triton X-100 (1.65 mM), a non-ionic, polyethylene glycol- (PEG) based detergent, to the protein solutions (see Figure 5.11). Triton X-100 is known to be non-denaturing and has been reported to only bind hydrophobic proteins.[271,272] In binding assays it prevents the aggregation of small, mostly aromatic molecules. Triton X-100 possesses a critical micelle concentration (cmc) of 240 μM in water.[269,270] When the cmc is reached, micelles form spontaneously facilitating the solubilization of membrane proteins and deaggregation of hydrophobic molecules.
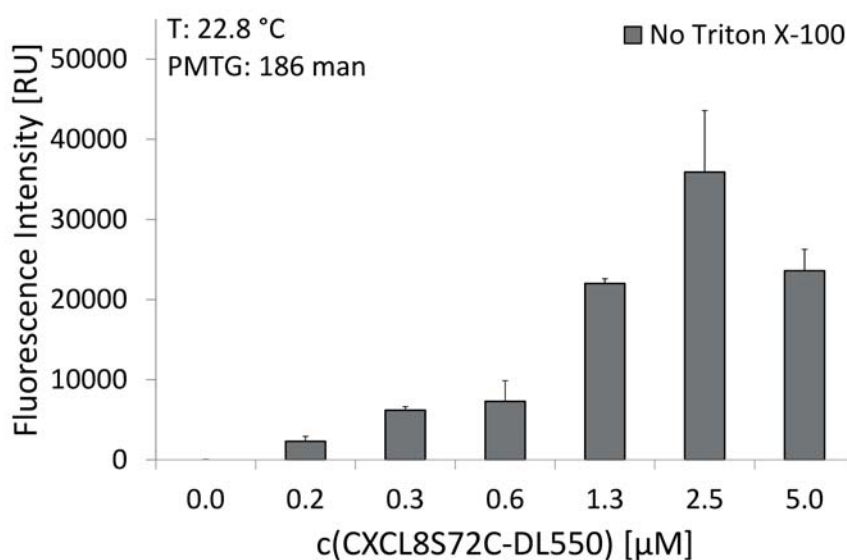
Figure 5.10: Interaction of CXCL8S72C-DL550 **23** with MTP. 30 μL of CXCL8S72C-DL550 **23** in *ls*-PBS were added to the wells of a MTP and removed after 5 min incubation time. The plates were centrifuged inside-out to remove all solvent and 30 μL of *ls*-PBS were added. Fluorescence intensity measurements (λ_{ex}=562 nm, λ_{em}=576 nm) show that a significant amount of the protein remains attached to the well surface. The amount of remaining protein correlates with the initial amount of protein added. At higher concentrations, quenching effects of multiple layers of protein on the wall decrease the fluorescence intensity.

When a constant CXCL8S72C-DL550 **23** concentration of 500 nM was mixed with different concentrations of Triton X-100 a threshold was reached at approximately 10 μM Triton X-100 (ca. 0.0007 % v/v) (see Figure 5.12). From this concentration on, CXCL8S72C-DL550 **23** fluorescence intensity was much higher. This higher fluorescence intensity was retained at increasing Triton X-100 concentrations. This
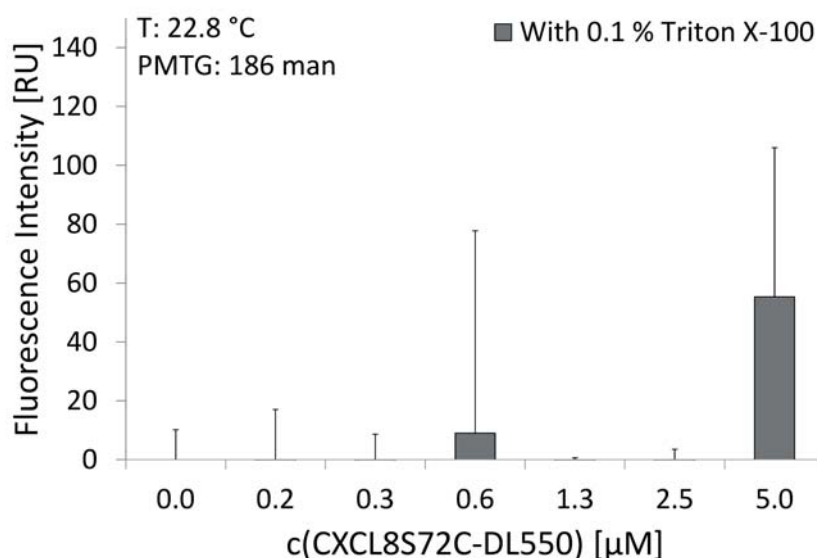
Figure 5.11: Interaction of CXCL8S72C-DL550 **23** with MTP upon addition of Triton X-100 to the protein solution. 30 μL of CXCL8S72C-DL550 **23** in *ls*-PBS with 0.1 % Triton X-100 were added to the wells of a MTP and removed after 5 min incubation time. The plates were centrifuged inside-out to remove all solvent and 30 μL of *ls*-PBS were added. Fluorescence intensity measurements (λ_{ex}=562 nm, λ_{em}=576 nm) show that no detectable amount of protein remains in the wells. This indicates that Triton X-100 prevents the adsorption of protein on the MTP well surface and decreases the quenching effect affiliated with this adsorption.

indicated that increasing amount of Triton X-100 prevented the adsorption of CXCL8S72C-DL550 **23** on the MTP well surface and reduced the quenching effect affiliated with this immobilization. Based on Figure 5.12, 10 μM (0.0007 % v/v) Triton X-100 should suffice to prevent 500 nM CXCL8S72C-DL550 **23** from adhering to the MTP surface.

Fluorescence anisotropy measurements with CXCL8S72C-DL550 **23** in CXCL8wt **19** dilutions were conducted to determine the dimerisation constant of CXCL8. Different amounts of Triton X-100 were added to prevent the protein from adhering to the MTP well. Measurements with 500 nM CXCL8S72C-DL550 **23** in dilutions of CXCL8 in *ls*-PBS with 0 %, 0.0007 % and 0.1 % (v/v) Triton X-100 all reached the same final anisotropy value but varied significantly in the initial anisotropy values (see Figure 5.13). The anisotropy of the free fluorophore increased from ca. 170 to 210 to 235 with increasing amounts of Triton X-100. Thus, by addition of Triton X-100 the dynamic range of the assay was significantly decreased. The higher initial anisotropy values indicate lower mobility of the fluorophore in solutions when higher amounts of Triton X-100 are present. This could indicate an interaction of Triton X-100 with the protein that slows down CXCL8S72C-DL550 **23** movement. The fluorescence intensity measurements corresponding to the anisotropy measurements showed that at 0 % and 0.0007 % (v/v) Triton X-100 the fluorescence intensity of the free fluorophore increased at higher CXCL8wt **19** concentrations (see Figure 5.14).

K_d values were corrected for the quenching effects by the Method of Dandliker *et al.*.[212] The corrected K_d values for CXCL8S72C-DL550 **23** binding to CXCL8wt **19** were 0.9 ± 0.4 μM, 1.1 ± 0.4 μM and 0.4 ± 0.1 μM for the measurement in *ls*-PBS buffer with 0 %, 0.0007 % and 0.1 % (v/v) Triton X-100, respectively (see also Table 5.3). The small dynamic range at 0.1 % (v/v) Triton X-100 complicated K_d
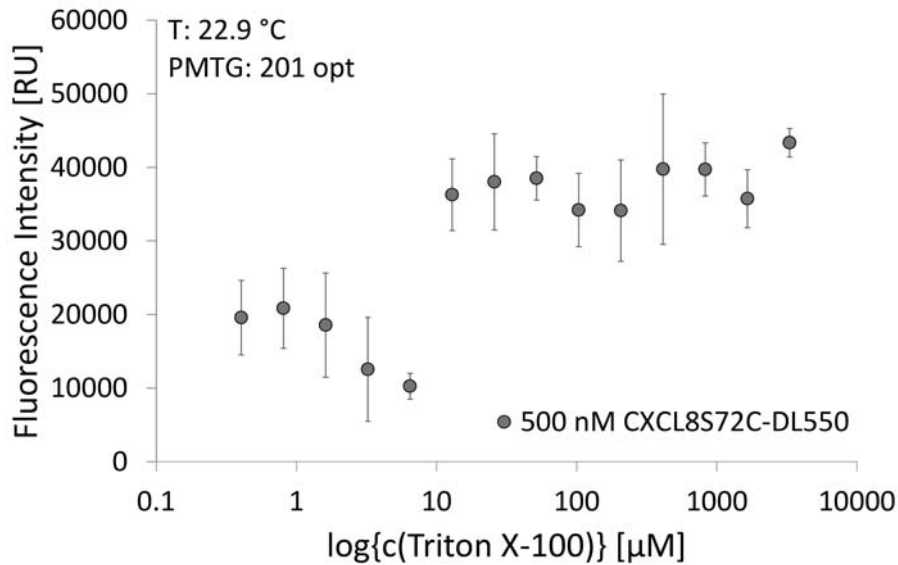
Figure 5.12: Fluorescence intensity (λ_{ex}=562 nm, λ_{em}=576 nm) of 500 nM CXCL8S72C-DL550 **23** in different Triton X-100 concentrations in *ls*-PBS. A steep increase of CXCL8S72C-DL550 **23** fluorescence intensity at approximately 10 μM Triton X-100 (0.0007 % v/v) indicates that Triton X-100 prevents protein aggregation and adsorption to the wells of the MTP.
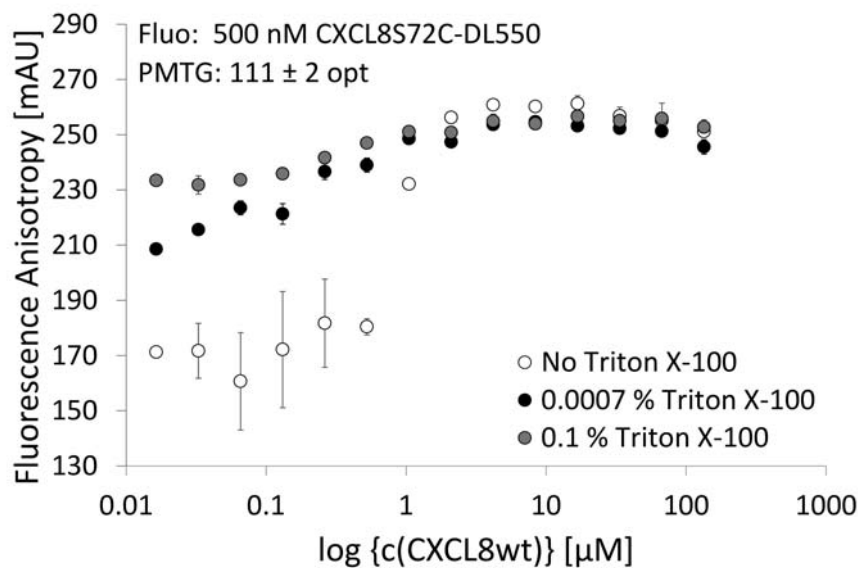

Figure 5.13: Fluorescence anisotropy (λ_{ex}=530 nm, λ_{em}=576 nm) of 500 nM CXCL8S72C-DL550 **23** in CXCL8wt **19** dilutions at different Triton X-100 concentrations. Increasing amounts of Triton X-100 decrease the dynamic range of the assay. A K_d of 0.9 ± 0.4 μM was determined for 0 % Triton X-100.

evaluation and K_d values differed considerably from values determined from measurements with 0 % and 0.0007 % (v/v) Triton X-100. The addition of Triton X-100 should thus be viewed critically due to its unknown interference with protein interactions and the resulting changes in determined K_d values. When planning an experiment it should also be considered that 0.1 % of Triton X-100 are equal to a concentration of ca. 1.65 mM which makes it the most abundant substance in the well (apart from the buffer). This
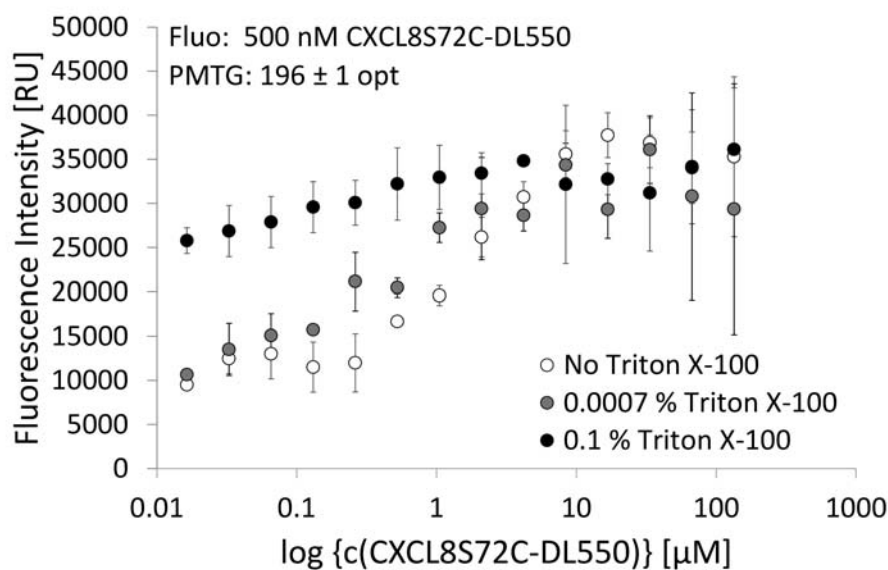
Figure 5.14: Fluorescence intensity (λ_{ex}=562 nm, λ_{em}=576 nm) of 500 nM CXCL8S72C-DL550 **23** in different CXCL8wt **19** concentrations with varying Triton X-100 addition (v/v) in *ls*-PBS.

concentration is also far above the critical micelle concentration of Triton X-100 (240 μM in water[269, 270]). Most anisotropy measurements in this work where therefore carried out in the absence of Triton X-100.

5.1.4 Dimerisation of CXCL8L25Y/V27R

CXCL8 dimerisation plays an important role for binding data since it influences the equilibrium and may complicate data interpretation. The reported dimerisation constant of CXCL8wt **19** varies considerably in the literature and has been reported to be between 0.1 μM and 20 μM, depending on experimental conditions.[46–48] Dimerisation of CXCL8 was investigated by fluorescence anisotropy measurements to obtain a dimerisation constant consistent with the standard conditions employed for anisotropy measurements in this work. CXCL8L25Y/V27R **21** has been reported to have a lower dimerisation constant than CXCL8wt **19**[56, 57] due to the mutations at the dimer interface and was investigated for its suitability for the use as a monomeric variant of CXCL8.

Fluorescence anisotropy measurements with 500 nM CXCL8S72C-DL550 **23** in dilutions of the monomeric CXCL8 variant CXCL8L25Y/V27R[56, 57] **21** were conducted to determine the dimerisation constant of the monomeric CXCL8 variant CXCL8L25Y/V27R **21** (see Figure 5.15). Comparison of fluorescence anisotropy measurements of the interaction of CXCL8S72C-DL550 **23** with CXCL8wt **19** and CXCL8L25Y/V27R **21** indicated that there was no change in the dimerisation constant when comparing CXCL8wt **19** and CXCL8L25Y/V27R **21** (see Figure 5.15). The fluorescence intensity of the fluorophore increased at higher CXCL8L25Y/V27R **21** concentrations (see Figure 5.16). K_d values corrected according to Dandliker *et al.*[212] gave 1.5 ± 0.4 μM without addition of Triton X-100 and 0.4 ± 0.2 μM for measurements with 0.0007 % (v/v) Triton X-100. Dimerisation constants for CXCL8wt **19** and CXCL8L25Y/V27R **21** are summarized in Table 5.3.
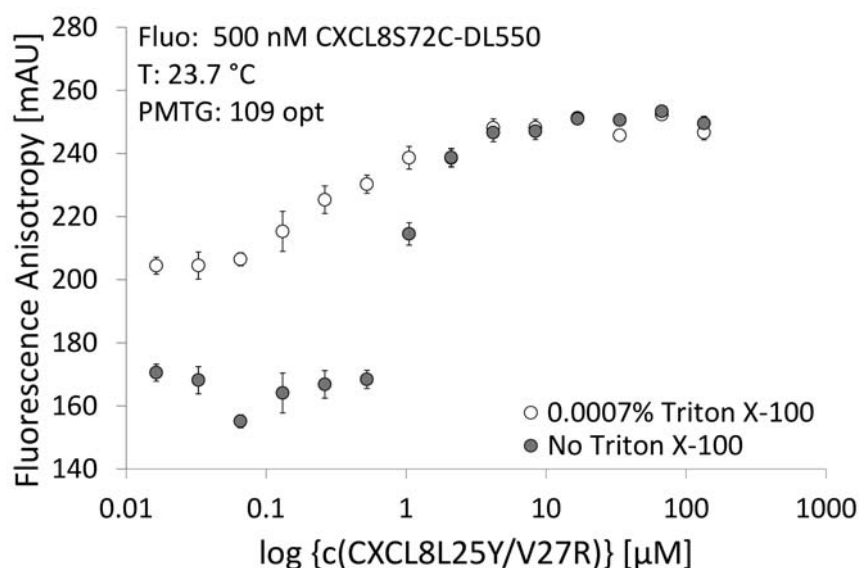
Figure 5.15: Fluorescence anisotropy (λ_{ex}=530 nm, λ_{em}=576 nm) of 500 nM CXCL8S72C-DL550 **23** in CXCL8L25Y/V27R **21** dilutions at different Triton-X concentrations. CXCL8L25Y/V27R[56, 57] **21** is supposed to be a variant of CXCL8 with reduced tendency for dimerisation. K_d values corrected according to Dandliker *et al.*[212] gave 1.5 ± 0.4 µM without addition of Triton X-100 and 0.4 ± 0.2 µM for measurements with 0.0007 % (v/v) Triton X-100. These results suggested, that CXCL8wt **19** and CXCL8L25Y/V27R **21** possess the same affinity for CXCL8wt **19** (see Figure 5.13).
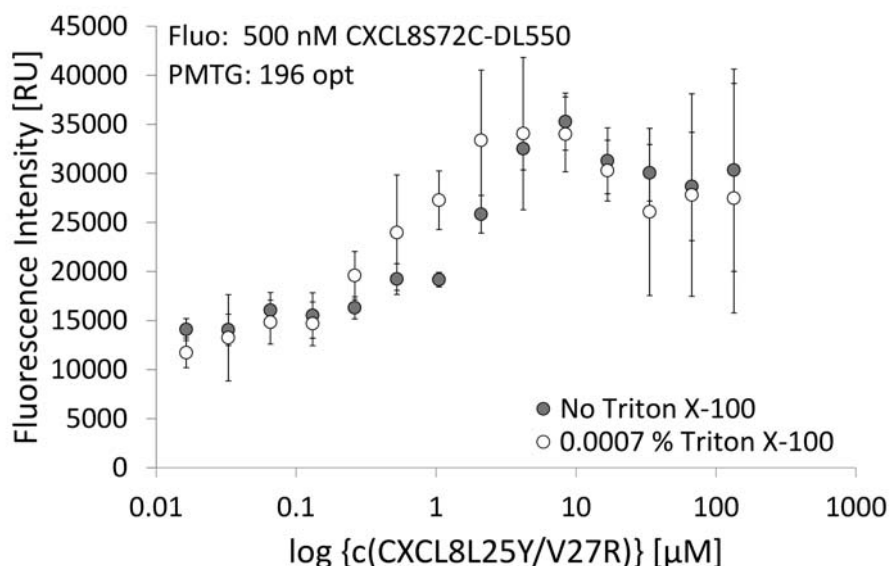
Figure 5.16: Fluorescence intensity (λ_{ex}=562 nm, λ_{em}=576 nm) corresponding to anisotropy measurement in Figure 5.15: 500 nM CXCL8S72C-DL550 **23** in CXCL8L25Y/V27R **21** dilutions at different Triton X-100 concentrations. Fluorescence intensity increased at higher CXCL8L25Y/V27R **21** concentrations and K_d calculations were corrected for that intensity increase.[212]

Table 5.3: K_d values of CXCL8wt **19** and CXCL8L25Y/V27R[56] **21** dimerisation at different Triton X-100 (TX-100) concentrations (v/v). Despite previous reports from Williams *et al.*[57] CXCL8L25Y/V27R **21** does not show significantly lower affinity for dimerisation than wild-type CXCL8. Values were obtained from fluorescence anisotropy measurements in Figure 5.13 and Figure 5.15 and corrected for fluorescence intensity increase according to Dandliker *et al.*.[212,213]

TX-100	CXCL8wt:CXCL8S72C-DL550		CXCL8L25Y/V27R:CXCL8S72C-DL550	
	K_d measured	K_d corrected	K_d measured	K_d corrected
0 %	0.7 ± 0.3 µM	0.9 ± 0.4 µM	1.0 ± 0.4 µM	1.5 ± 0.4 µM
0.0007 %	0.3 ± 0.1 µM	1.1 ± 0.4 µM	0.2 ± 0.1 µM	0.4 ± 0.2 µM
0.1 %	0.3 ± 0.1 µM	0.4 ± 0.1 µM	not determined	not determined

CXCL8L25Y/V27R **21** showed an equally high tendency to form dimers when compared to CXCL8wt **19** and was thus not used as a monomeric CXCL8 variant in fluorescence polarization assays.

5.2 Rational Design of a Novel CXCL8-Binding Peptide

Parts of the section 5.2 have been published.* At the N-terminus of CXCL8 residues 4-6 –glutamic acid, leucine, arginine –form the so-called 'ELR motif'. It is crucial for receptor activation and is conceived to interact with residues near ECD3 and ECD4 of the CXCR1 receptor, i.e. residues R199 (TMH5), R203 (ECD3) and D265 (TMH6).[31,40] A two-site model was proposed for the CXCL8:CXCR1 interaction, were the CXCL8 N-loop region interacts with the N-terminus of CXCR1 (site 1) and the ELR motif interacts with the region of ECD3 and ECD4 (site 2).[41–43] The interaction of ELR-motif and ECD could so far not be directly proven by experiment.[27] A flexible protein-protein docking of CXCL8 to CXCR1 was performed to confirm the plausibility of this interaction by using ROSETTA†.[273] CXCR1 and CXCL8 structures are both available in the protein database. The NMR structure of CXCR1 published by Park (pdb id: 2LNL) lacks the N-terminus, i.e. residues 1-28 and it shows the receptor in an inactive state with no ligand bound,[274] which is not optimal for docking the agonist CXCL8. Therefore conformational changes to CXCR1 were anticipated necessary for an accurate docking with CXCL8, which required a docking protocol that incorporates flexibility into both receptor and ligand. Firstly, the missing N-terminus of CXCR1 was homology modeled based on the structure of CXCR1-p1 (pdb id: 1ILQ), a receptor-derived peptide that replaces CXCL8 from its receptors CXCR1/2 on neutrophil membranes with a K_i of 7 µM first described by Attwood *et al.*.[26,42,145] Secondly, the monomer of the CXCL8 crystal structure (pdb id: 3IL8) was positioned according to the interactions reported by Skelton *et al.*.[42] This process involved a three-way superimposition between the CXCR1-p1 structure, the NMR structure of CXCR1, and the crystal structure of CXCL8, which was performed with CHIMERA.[275] The CXCR1-p1 structure was then removed from the superimposition, leaving an initial 'pre-docked' unoptimized orientation of CXCR1 with respect to CXCL8. Next, the missing residues 1-4 (SAKE) of 3IL8 (CXCL8) were attached using the MODELLER *ab initio* loop prediction method, in such a way as to minimize steric clashes with CXCR1. Finally, flexible protein-protein

---

* Helmer *et al.*, *RSC Advances* **2015**, *5*, 25657-25668. – Reproduced by permission of The Royal Society of Chemistry.
† Computational work by J.A.R. Dalton in the group of J. Giraldo (UAB, Barcelona). Reproduced with permission.

docking with ROSETTA was employed to optimize the interaction between CXCR1 and CXCL8, which involved full flexibility in side-chains and backbones, as well as free rotational and translational movement of each binding partner. Three iterations of ROSETTA relaxation were introduced until energetic convergence was reached. In the final docked structure of CXCR1:CXCL8, the residues E4 and R6 of the ELR motif at the N-terminus of CXCL8 interacted with the crucial receptor residues R203 and D265, while E29 of the CXCL8 30S loop interacted with the receptor residue R199 (see Figure 5.17).
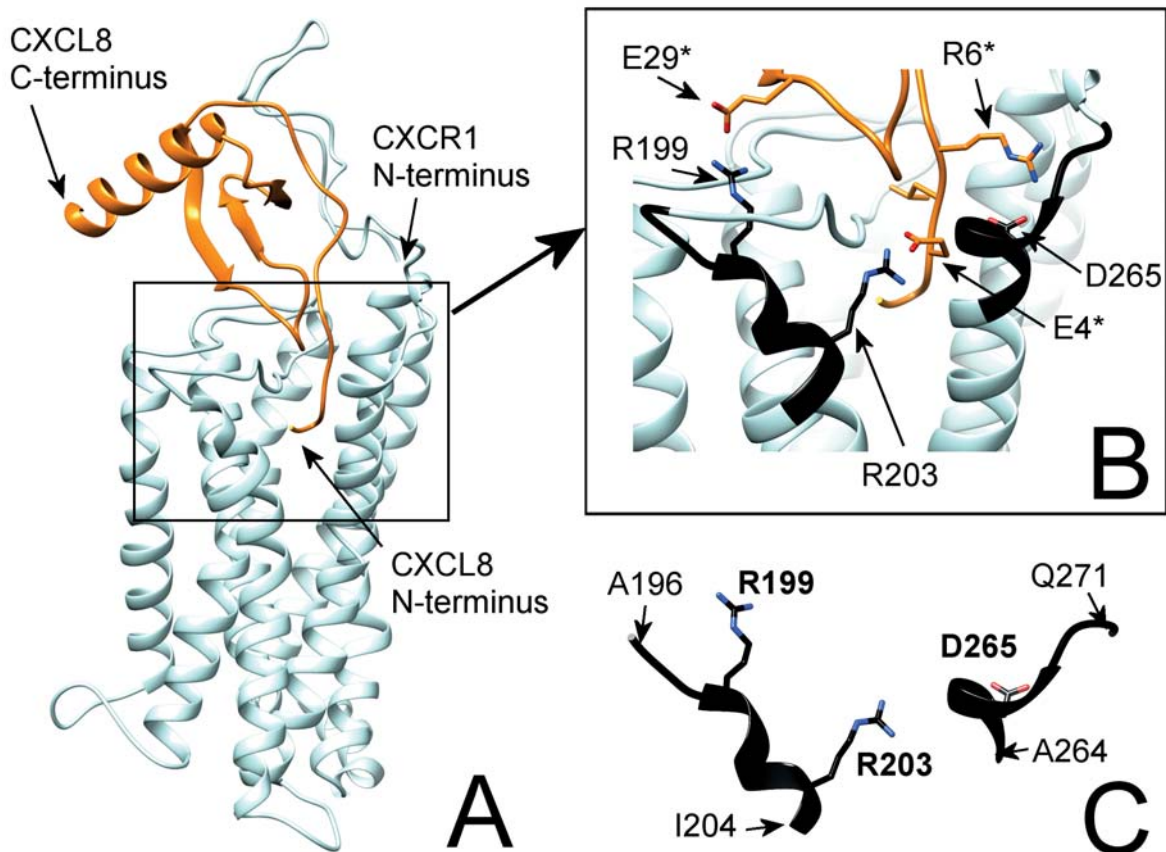
Figure 5.17: Flexible Docking of CXCL8 to CXCR1. A) Docking result based on the interaction of CXCL8 with receptor peptide CXCR1-p1[42, 145] and the proposed interaction of the ELR motif (CXCL8) with R199, R203 and D265.[31] B) Close-up of the interacting of E4* and R6* of the ELR motif with R203 and D265 as well as the interaction of E29* with R199. CXCL8 residues are marked with an asterisk. CXCR1 regions of interest for this interaction are marked in black. C) A196 to I204 (AKWRMVLRI) and A264 to Q271 (ADTLMRTQ) the regions of interest in ECD3 and ECD4 respectively that interact with the CXCL8 N-terminus containing the ELR motif.

Important interactions in the predicted CXCL8:CXCR1 complex were characterized by measuring hydrogen-bond distances. Distances between donor atoms (D) and acceptor atoms (A) should not exceed 3.9 Å and ideally lie between 2.7 Å and 2.9 Å.[276–278] Table 5.4 lists all intermolecular D-A distances in the proposed model (using 2.9 Å as a cut-off distance value for the formation of strong hydrogen bonds) and compares them to previously reported experimentally proven interactions. In accordance with experimental data the model supports the major interaction sites of CXCL8 to be N-loop, 3_{10} helix, 40S loop and β_3 strand (see also Section 3.1).[26, 27]

Table 5.4: Interactions between CXCL8 and CXCR1 as proposed in the model (see Figure 5.17). The fourth column shows previously reported interactions between CXCR1 and CXCL8 as indicated by a colon. If more than one residue was reported to interact, all interacting residues were put in parentheses.

CXCL8 domains (aa)	CXCL8 residues interacting with CXCR1 (distance < 2.9 Å)	CXCR1 residues interacting with CXCL8 (distance < 2.9 Å)	Specific CXCL8:CXCR1 interactions previously reported
N-Terminus (1-9)	S1, A2, K3, E4,[30,279] L5,[30,279] R6,[30,279] C7, Q8[42]	P29,[42] K117, H179, P180, N181, S184, V186, C187, Y188, E189, R203,[31,41] L262, D265,[31,41] T266, R269, T270, Q271, I273, R280,[40] I283, G284, L287	Q8:P29[42]
N-Loop (10-18), 3₁₀-Helix (19-21)	I10,[30,42] K11,[42] T12,[26,42,274] Y13,[42,280,281] K15,[26,42,280] P16, F17,[26,42,274,282] F21[26,42,282,283]	D11,[40] F17, T18, G19, M20, P21,[42] D26,[42] Y27,[42] P29, L32, E33	(I10, K11, Y13):Y27,[42] K11:(D24, E25, D26),[42] (Y13, F17, F21):(P21, P22),[42] CXCR1 N-terminus (1-40),[26] CXCR1 N-terminus (1-39),[274] (H18, F21) of CXCR1 N-terminus[283]
β1-Strand (22-28)	E24, L25, R26, V27, I28	F105, G106, T107, A177, Y178, H179, P180, Y188, L191	
30S-Loop (29-37)	E29, G31, P32, H33, C34	Y188, E189, L191, G192, R199,[31] T266, L267	
β2-Strand (38-43) 40S-Loop (44-47)	I40,[42] L43[42,282] S44,[26,42,274] D45, R47[42]	P21,[42] H179 T5, D6, P7, M9, F12, P22,[42] D24,[42] E25[42]	I40:P29,[42] L43:(P21, P22)[42] F47:(P21, P22),[42] R47:(D24, E25, D26),[42] CXCR1 N-terminus (1-40),[26] CXCR1 N-terminus (1-38)[274]
β3-Strand (48-51)	E48,[26,42,274] L49,[26,42,281] C50[26,274]	P22,[42] E25, Y27,[42] S28, W103, F105	L49:(P21, P22),[42] L49:Y27,[42] CXCR1 N-terminus (1-40),[26] CXCR1 N-terminus (1-38)[274]

Interestingly, during flexible docking, in order to accommodate CXCL8 binding, CXCR1 was observed to change into a more 'active-like' conformation, in a similar fashion seen in the activation of the Adenosine A2A receptor, another class A GPCR.[284] This conformational change involves mainly the tilting of TMH7 (see Figure 5.18). In addition, in the 'active-like' state of CXCR1, E275 at the top of helix 7 forms two strong hydrogen bonds with T34 located on the N-terminus of CXCR1 (see Figure 5.18). E275 was

previously reported to be an important residue for CXCL8:CXCR1 interaction.[40] When E275 was replaced by alanine, binding of radiolabelled CXCL8 to CXCR1 on HEK 293 cells was no longer observed. Since a two-site mechanism involving interactions of several amino-acids of CXCL8 and CXCR1 is proposed for the binding and activation of CXCR1,[41–43, 285, 286] this drastic influence of one residue on receptor function seems surprising. Our model suggests, that E275 is essential for the stabilization of the 'active-like' state of CXCR1 by forming two hydrogen bonds with T34 of TMH1. This could indicate that without E275 the receptor can no longer form a stabilized active state and thus can no longer bind CXCL8, further supporting the proposed model.
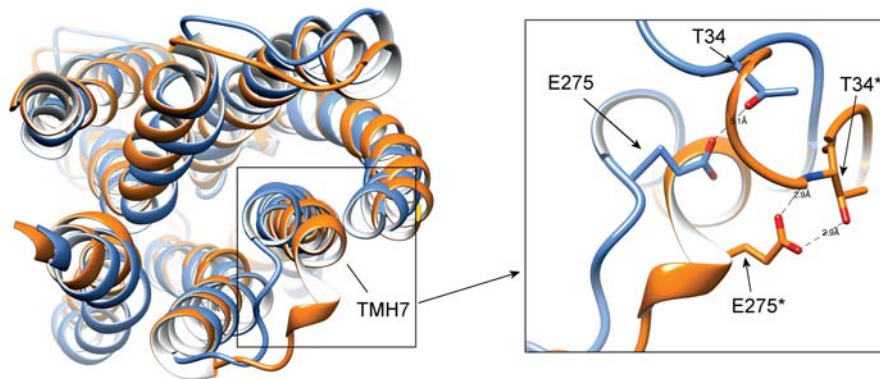
Figure 5.18: During flexible protein-protein docking of CXCL8 to CXCR1, the receptor transformed into an 'active-like' state. This activation was mainly characterized by a tilting of transmembrane helix 7 (TMH 7). A similar tilt is seen upon the activation of adenosine A2A receptor.[284] Left: Extracellular view on CXCR1 in the 'active-like' (orange) and inactive (blue) state. Right: Focus on the region of E275, a residue previously reported to be important for CXCL8:CXCR1-interaction.[40] Only in the 'active-like' state E275 forms two stable hydrogen bonds with T34 (3.1 Å, 5.1 Å in the inactive form, see dashed lines). Active state residues are marked by an asterisk.

The influence of the dimerisation of CXCL8 on receptor activation is not yet fully understood (see Section 3.1.1) and it is not known whether CXCL8 binds the receptor as a monomer or a dimer. In this model, CXCL8 dimerisation is not possible upon binding to the receptor for reasons of steric hindrance (see Figure 5.19).

A second possible influence on CXCL8 function is the interaction with glycosaminoglycans (GAG), see also Section 3.1. In the model presented here the interaction of CXCL8 with GAG is possible: the C-terminal helix of CXCL8 is facing to the top exposing the heparin (a glycosaminoglycan) binding residues K67, K64, R68 and R60 crucial for CXCL8 gradient formation on cell surface.[22, 287] Since the affinity of CXCL8 for GAG is increased in the dimer,[288] it is possible that dimerisation is crucial only for presentation of CXCL8 on endothelial GAG but might not be necessary for receptor activation. The K_d of CXCL8 for heparin-binding has been reported to be 5.5 µM,[22] the dimerisation constant of CXCL8 was reported to have a similar value (see Section 5.1.4). Due to the similar affinity for itself and heparin, CXCL8 is just as likely to show monomeric chemotactic activity as dimeric haptotactic activity. Thus the accessibility of the heparin-binding α-helix is important to explain the influence of dimeric CXCL8 structures *in vivo*. A recently published structure of the CXCL8:CXCR1 complex where the C-terminal α-helix of CXCL8 faces the receptor as recently modelled by Liou *et al.*[289] might therefore not be favourable.
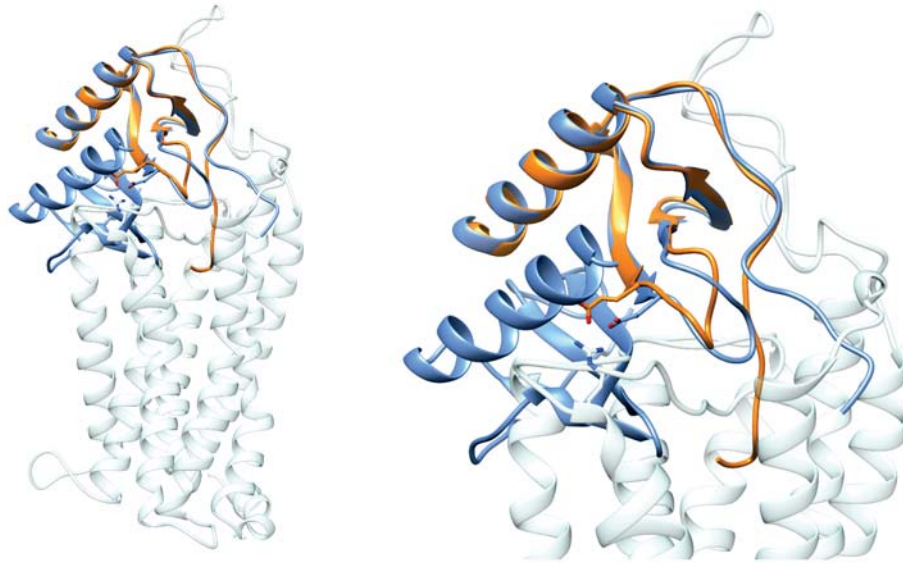
Figure 5.19: In the proposed docking model (see Figure 5.17) dimerisation of CXCL8 is not possible upon receptor binding. The interaction between E29 of the monomer (orange) and R199 of CXCR1 is still possible in the dimer:CXCR1 interaction but the CXCL8 dimer (blue) reaches far into the structure of CXCR1 (light green) making a dimerisation impossible for steric reasons.

According to the docking of CXCR1 with CXCL8 shown in Figure 5.17, R199, R203 and D265 of CXCR1 are involved in the CXCR1:CXCL8 interaction and therefore constitute a promising scaffold for the design of a peptide capable of binding CXCL8. A196 to I204 (ECD3/TMH5) and A264 to Q271 (TMH6/ECD4) were chosen as appropriate parts of the CXCR1 sequence because they incorporate at least one full helix turn each that may be preserved in a peptide (see Figure 5.17). The two domains were linked by 6-aminohexanoic acid (Ahx) because it poses a good compromise between hydrophobicity, length and flexibility and has been employed successfully in the design of CXCR1-p1, a peptide that was derived from the N-terminus of CXCR1 that has been previously reported to bind CXCL8 (see Section 5.1.2).[145] The resulting peptide AKWRMVLRI-Ahx-ADTLMRTQ was named 'IL8RPLoops'. A 100 ns molecular dynamics simulation, performed with MOE2013 software[290] indicated that the peptide possessed a stable, partly helical structure in which the spatial orientation of the critical residues R199, R203 and D265 of the CXCR1 scaffold (corresponding to R4, R8 and D12 in the IL8RPLoops peptide) was largely retained (see Figure 5.20).
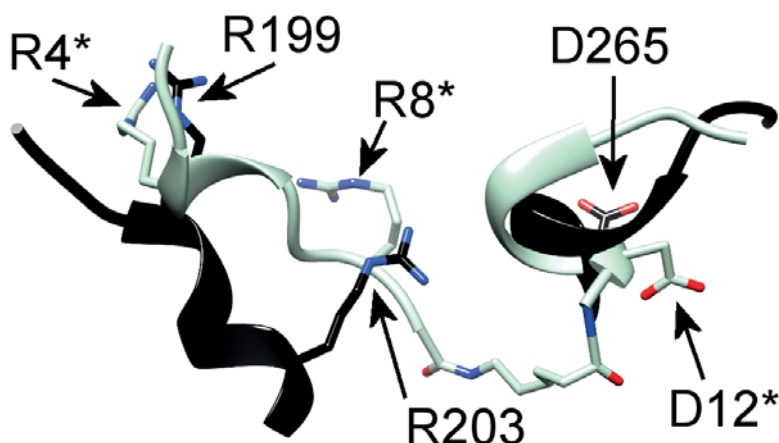
Figure 5.20: Important residues R199, R203 and D265 of CXCR1 as a scaffold for the rational design of a peptide. The CXCR1 sequence motifs important for the CXCL8:CXCR1 interaction as suggested by Leong et al.[31] (in black) (see Figure 5.17) are shown superimposed with the molecular dynamics simulation (100 ns) of the designed peptide IL8RPLoops (in light blue, important residues corresponding to R199, R203 and D265 were renumbered and are marked by an asterisk) in which the two CXCR1 domains were linked by 6-aminohexanoic acid (Ahx). The peptide seems to possess a stable secondary structure with α-helical content so that the structure of the CXCR1 scaffold is retained to a large extent.

5.2.1 Binding Assays in Solution

The peptide (Fluo-)AKWRMVLRI-Ahx-ADTLMRTQ was synthesized via solid phase peptide synthesis using standard Fmoc/tBu strategy.[291] To determine the affinity of IL8RPLoops for CXCL8 the dissociation constant was determined by fluorescence anisotropy measurements (see Section 5.1.2). When the anisotropy was directly measured after mixing of CXCL8wt **19** and Fluo-IL8RPLoops **86** (0 min) the resulting curve was sigmoidal, after 30 min the anisotropy values were significantly higher over the whole concentration range, except for the last two values, making the curve appear bell-shaped (see Figure 5.21). The fluorescence intensity of the measurements shows that the intensity varied significantly in the 0 min measurement, while it had reached an equilibrium at at 30 min (see Figure 5.22). The lower fluorescence intensity of ca. 11000 relative fluorescence units (RU) after 30 min incubation compared to ca. 18000 RU at 0 min incubation pointed to Fluo-IL8RPLoops **86** adhering to the wall of the MTP accompanied by quenching effects. This was supported by the higher anisotropy values detected at 30 min and 60 min incubation time. The elevated fluorescence intensity values at the two highest CXCL8wt **19** concentrations were likely due to the influence of CXCL8wt **19** auto-fluorescence: at high photomultiplier tube gains (PMT Gain, i. e. detector amplification, values 0-255) like 180, CXCL8wt **19** concentrations above 10 µM exhibit detectable fluorescence intensities (see Figure 5.23). At ca. 1 µM CXCL8wt **19** the fluorescence intensity was significantly lower than at any other concentration and shows a significant increase in fluorescence anisotropy.

The loss in intensity at 1 µM indicated that Fluo-IL8RPLoops **86** binding to CXCL8 was accompanied by quenching of the fluorophore. The fact that the anisotropy values decreased at the end of the 30 min and 60 min curve and thus eventually reached the initial anisotropy of the free fluorophore could be a result of the monomer-dimer equilibrium of CXCL8wt **19**. If the affinity of IL8RPLoops for the monomer differs from
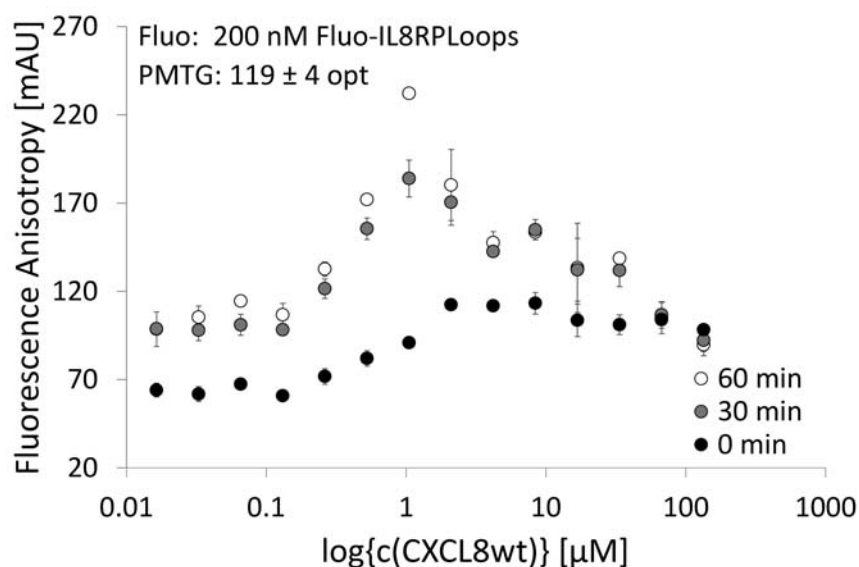
Figure 5.21: Fluorescence anisotropy measurement (λ_{ex}=470 nm, λ_{em}=520 nm) of fluorescein-labelled IL8RPLoops in CXCL8wt **19** in *ls*-PBS. The anisotropy values were determined at 0 min, 30 min and 60 min.
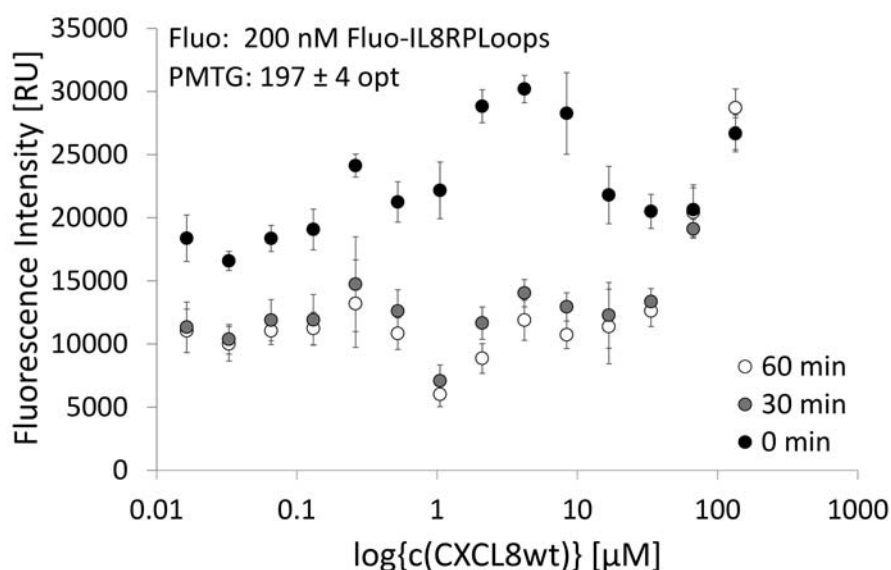

Figure 5.22: Fluorescence intensity measurements (λ_{ex}=488 nm, λ_{em}=520 nm) corresponding to the anisotropy measurements conducted with Fluo-IL8RPLoops **86** (see Figure 5.21) (buffer corrected).

that for the dimer a more complex kinetic model would be appropriate for data analysis. At concentrations above the dimerisation constant of CXCL8wt **19**, i.e. around 1.0 μM (see Table 5.2), the dimer becomes the predominant species. If IL8RPLoops prevented dimer formation and only binds the CXCL8 monomer, anisotropy values would decrease at high CXCL8wt **19** concentrations, because the CXCL8 dimer is formed and Fluo-IL8RPLoops **86** is released from CXCL8wt **19** binding. The decomposition or unfolding of CXCL8wt **19** in the presence of Fluo-IL8RPLoops **86** would also explain the decrease of anisotropy values, either due to a complete loss of binding affinity or due to the faster movement of fluorophores bound to
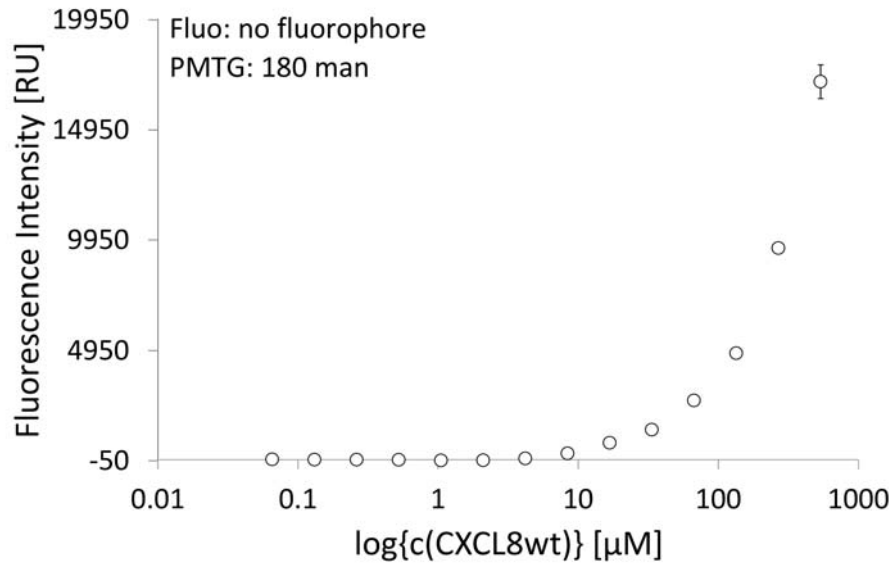
Figure 5.23: Fluorescence intensity measurements (λ_{ex}=470 nm, λ_{em}=520 nm) of CXCL8wt **19** in *ls*-PBS (buffer corrected). CXCL8wt **19** displays measurable fluorescence intensity values above concentrations of 10 μM.

smaller protein segments. This could be ruled out since the circular dichroism spectra of 25 μM CXCL8 mixed with 10 μM (Fluo-)IL8RPLoops or Fluo-IL8RPLoops **86** displayed no change in protein structure (see Figure 5.24). Since the binding of IL8RPLoops to CXCL8 had no influence on CXCL8 structure, the binding event could not be shown by circular dichroism spectroscopy. Analysis of fluorescence anisotropy according to one-site saturation binding gave an apparent K_d of 0.5 ± 0.3 μM at 0 min incubation time (see Figure 5.21).
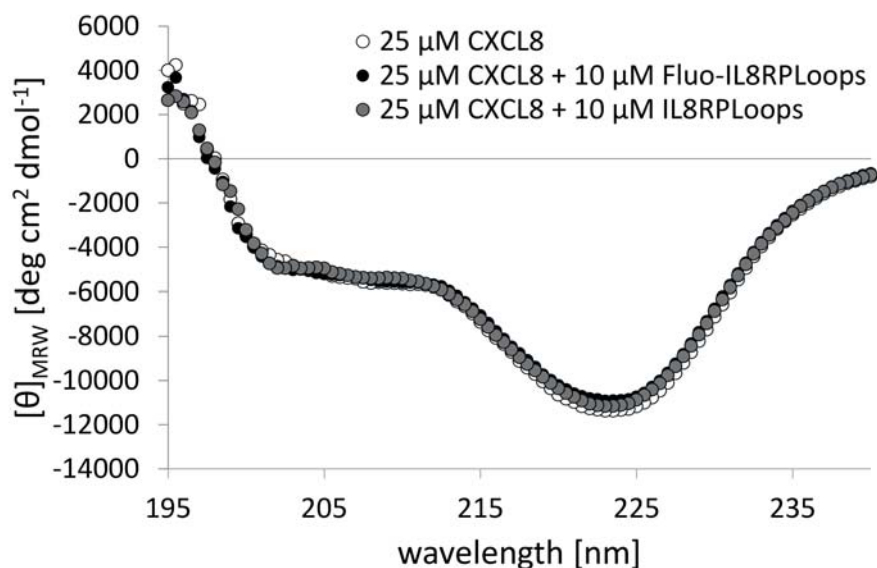
Figure 5.24: Circular dichroism spectra of CXCL8 mixed with IL8RPLoops and Fluo-IL8RPLoops **86** in *ls*-PBS. No significant changes in the curves indicate that at concentrations below 10 μM the peptide has no influence on CXCL8 structure. The binding event could not be detected by CD.

In order to confirm the helical structure of the peptide, CD spectra of the peptide and its fluorescein-labelled derivative Fluo-AKWRMVLRI-Ahx-ADTLMRTQ were measured. The CD spectra showed a strong negative signal at roughly 201 nm, characteristic for a random coil structure as well as a negative signal at 222 nm and a positive signal at 190 nm characteristic for α-helices (see Figure 5.25).
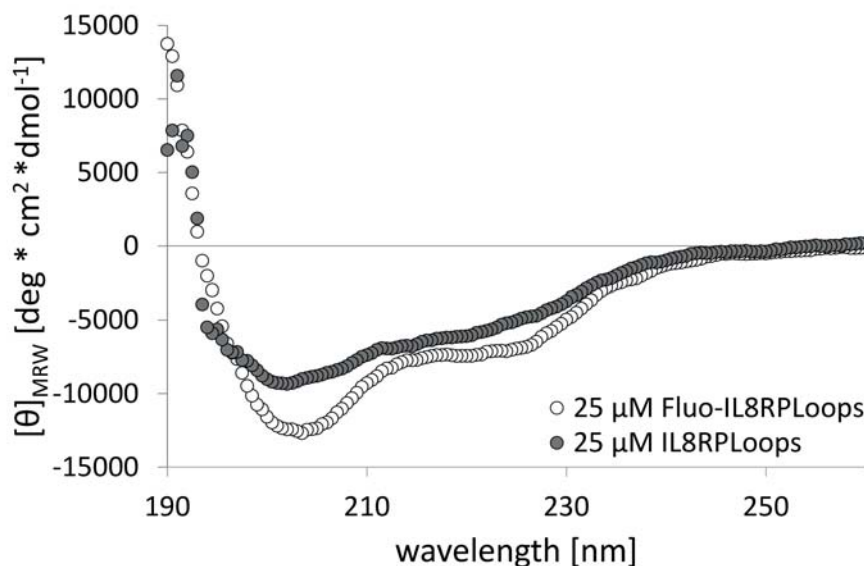

Figure 5.25: CD spectra of IL8RPLoops and Fluo-IL8RPLoops **86** confirmed the results of the MD simulation that predicted α-helical components in the peptide. The negative signal at 201 nm points to a random structure, the shoulder at 222 nm is characteristic for α-helices. The difference detected between Fluo-IL8RPLoops **86** and IL8RPLoops suggested that the fluorescein label had some influence on peptide folding. Further studies with the fluorescein label (described in the text) led to the conclusion that the label most likely stabilized the peptide fold.

To ensure that the fluorescein label had no influence on the binding of IL8RPLoops, a fluorescence anisotropy assay with fluorescein (sodium salt) and CXCL8wt **19** was conducted (see Figure 5.26). Fluorescein possesses a low affinity for CXCL8wt **19** ($K_d > 100$ µM). It was concluded that even at high concentrations fluorescein did not bind to CXCL8wt **19**. Furthermore a competitive binding assay with unlabelled IL8RPLoops was performed (see Figure 5.27). As expected, IL8RPLoops competed for the binding to CXCL8wt **19** and eventually replaced Fluo-IL8RPLoops **86** thus reducing anisotropy values. An IC_{50} value of 43.9 ± 3.7 µM was determined. Using the Cheng-Prusoff equation[292] a K_i of 8.8 ± 3.7 µM was calculated. In an assay in which the competing ligand is equal to the bound ligand except for the label, K_d should be equal to K_i. In this case K_i appears to be higher than K_d, which could be due to unspecific interactions for instance with the MTP well surface.
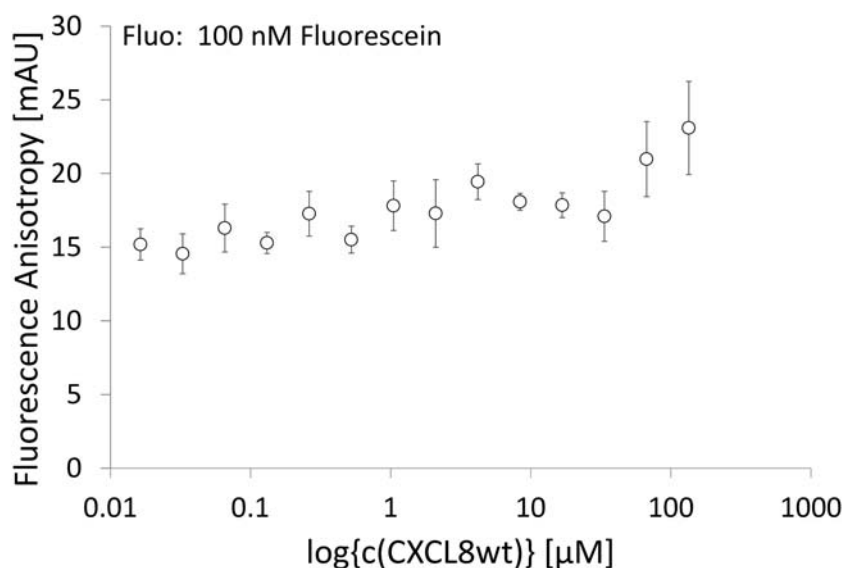
Figure 5.26: Fluorescence anisotropy measurement of fluorescein (sodium salt) binding to CXCL8wt **19**. Fluorescein has a low affinity for CXCL8wt **19** ($K_d > 100$ µM).
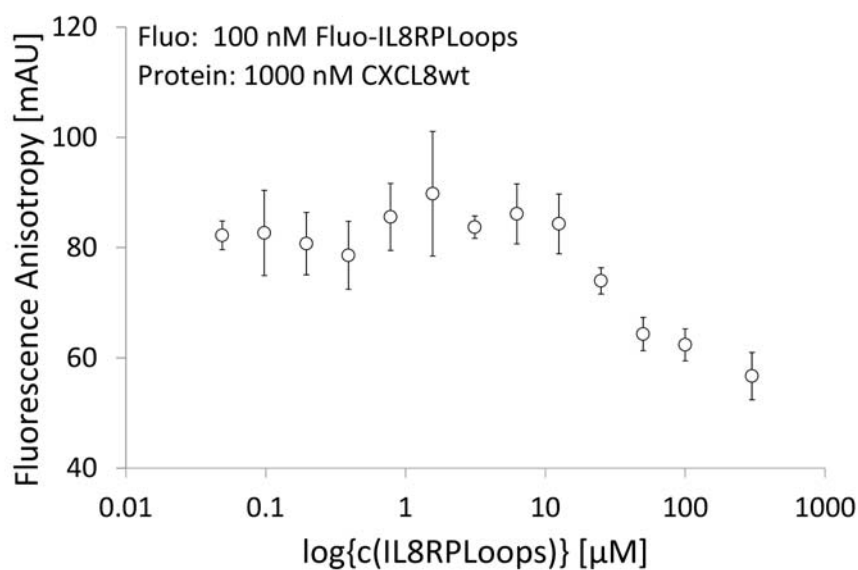

Figure 5.27: Fluorescence anisotropy competition assay (λ_{ex}=470 nm, λ_{em}=520 nm). IL8RPLoops competes with Fluo-IL8RPLoops **86** for the binding to CXCL8wt **19**. At high concentrations, ILRPLoops replaced Fluo-IL8RPLoops **86** which leads to a decrease in anisotropy.

5.2.2 Binding Assay on Surface

The binding of Fluo-IL8RPLoops **86** to CXCL8 was also shown on surface: CXCL8S72C-DL550 **23** was immobilized on BSA-coated glass slides by photobleaching of the fluorescent label by a digital mirror array (DMD)-based, maskless lithography system.[293–296] A glass slide was coated with bovine serum albumin (BSA) by a simple immersion/adhesion process. A solution of CXCL8S72C-DL550 **23** was introduced onto the surface and the fluorophore (DyLight550) was excited by projecting light of 550 nm wavelength onto

the slide with a DMD. Excitation causes the formation of radicals that can cause the covalent attachment of the fluorophore to the surface, resulting in bleaching of the fluorophore. The protein is thus covalently attached to the surface at the site of its fluorescence label, which in this case was attached at the C-terminus. The 1024×768 individual mirrors (in total ca. 5 mm^2 exposure area) projecting the light can oscilate and thereby produce grayscale images corresponding to protein bitmaps. After washing, the remaining protein on the surface can be stained, e. g. by fluorescenctly labelled antibody or small ligands (see Figure 5.28).
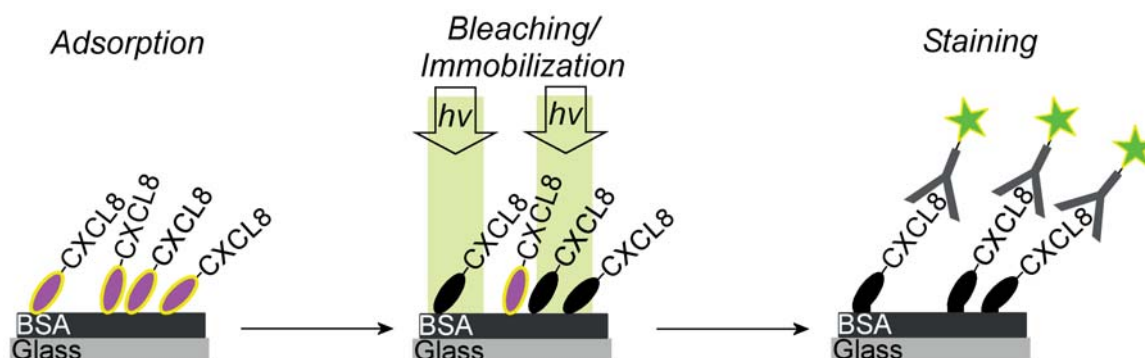
Figure 5.28: Immobilization and staining of CXCL8S72C-DL550 **23** on glass slides by light-induced protein patterning.[293–296]

The results of staining CXCL8S72C-DL550 **23** on surface with Fluo-IL8RPLoops **86** and FITC-anti-CXCL8 were visualized with a microarray scanner. The results showed that both Fluo-IL8RPLoops **86** and FITC-anti-CXCL8 bound the immobilized CXCL8 (see Figure 5.29).

Figure 5.29: Protein bitmap (scale bar: 500 µm) of CXCL8S72C-DL550 **23** on BSA-coated glass showing the Mona Lisa,[297] stained with IL8RPLoops (left image) and FITC-anti-CXCL8 (right image).

In the upper part of the pattern, the signal-to-noise ratio appeared to be better in case of Fluo-IL8RPLoops **86** (see Figure 5.30). Since a fluorescence anisotropy measurement of Fluo-IL8RPLoops **86** in different BSA concentrations showed, that Fluo-IL8RPLoops **86** does not possess a high affinity for
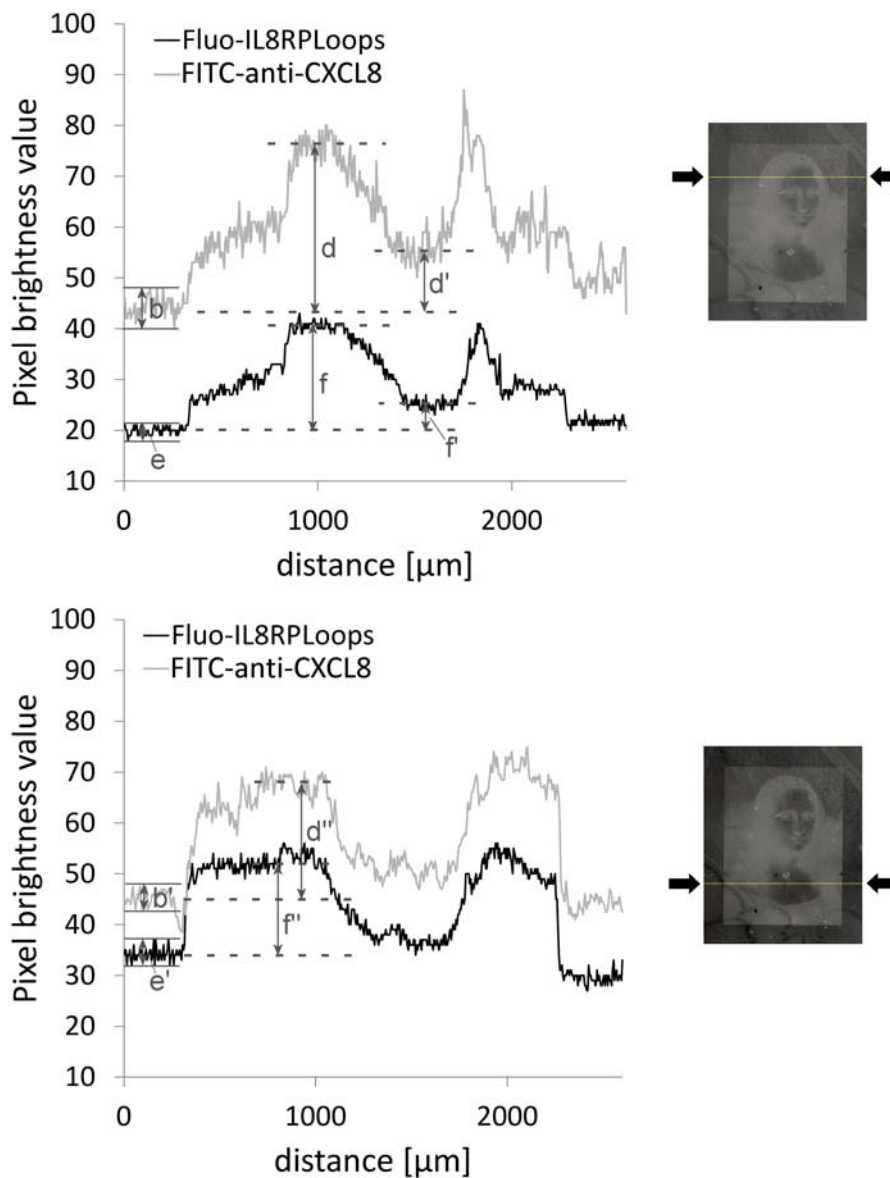
Figure 5.30: Analysis of pixel brightness values across protein patterns of CXCL8S72C-DL550 **23** (see Figure 5.29) stained with IL8RPLoops (black lines) and FITC-anti-CXCL8 (grey lines) with Image J.[298] Two plot profiles were obtained from the upper part of the pattern (top) and the lower part of the pattern (bottom). Locations of the shown plot profiles were marked by arrows on exemplary, contrast-corrected versions of the FITC-anti-CXCL8 pattern on the right side of the graphs. Results showed that the FITC-anti-CXCL8 stained pattern (grey lines) possessed a higher fluorescence intensity compared to the Fluo-IL8RPLoops **86** stained pattern. In the upper part of the image, the signal, i. e. the differences between background colour and image colour, was higher in the FITC-anti-CXCL8 stained pattern (d=33, d'=11) compared with the Fluo-IL8RPLoops **86** stained pattern (f=20, f'=5). The background noise (b=8 and e=2) is considerably lower in the Fluo-IL8RPLoops **86** stained pattern. The signal to noise ratio for the Fluo-Il8RPLoops **86** pattern is thus better compared to the FITC-anti-CXCL8 pattern. These differences are less pronounced in the lower parts of the picture, where contrasts (d''=21 compared to f''=16) and background noise (b'=4.5 and e'=5) and signal-to-noise ratios are largely equal.

BSA ($K_d > 100$ µM) (see Figure 5.31) the low background in the Fluo-IL8RPLoops **86** stained pattern is explicable. The increased background noise value variations in case of the antibody staining indicated either that a varying amount of antibody bound per immobilized CXCL8 molecule or that the amount of immobilized CXCL8 itself varies. If the same amount of CXCL8 is immobilized in both cases, the variations might arise from the size of the antibody, that probably prevented a 1:1 binding between antibody and immobilized CXCL8. In case of Fluo-IL8RPLoops **86**, which is much smaller compared to the antibody, there are less steric hindrances and the binding ratio is stable and thus probably varies less. The immobilization at the C-terminus of CXCL8 presumably leaves the protein in a orientation similar to its spatial arrangement *in vivo* when immobilized on endothelial GAG. This way, the N-terminus of CXCL8 is facing away from the glass and therefore accessible to N-terminal binding peptides. This can be taken as another clue pointing to the Fluo-IL8RPLoops:CXCL8 interaction taking place at the N-terminal side of CXCL8. Interstingly, attempts to stain the protein pattern with Fluo-CXCR1-p1 **89** were unsuccessful.
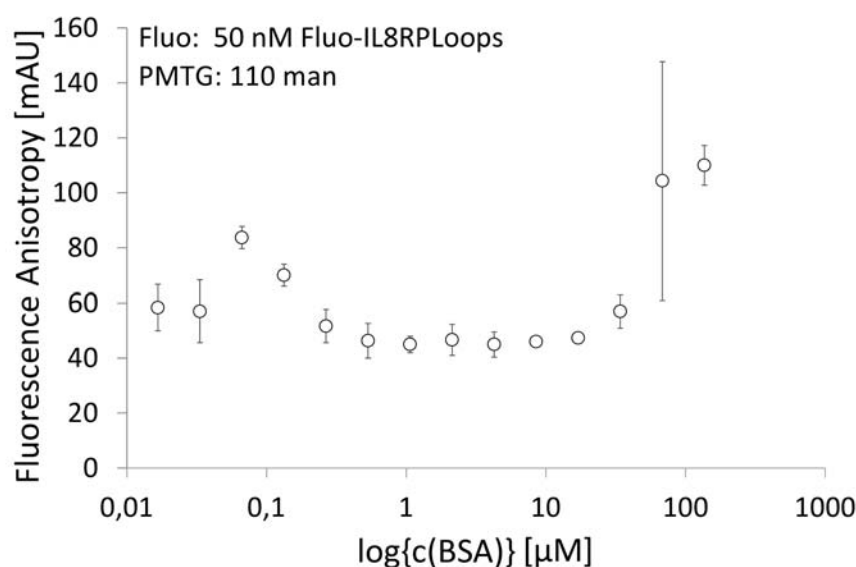

Figure 5.31: Fluorescence anisotropy measurement (λ_{ex}=470 nm, λ_{em}=520 nm) of the binding of Fluo-IL8RPLoops **86** to bovine serum albumin (BSA). Fluo-IL8RPLoops **86** has low affinity for BSA ($K_d > 100$ µM).

5.2.3 Biological Activity

A cell migration Transwell assay, in which activated cells migrate from an upper reservoir through a membrane into a lower cavity, was conducted to investigate if IL8RPLoops binding to CXCL8 had an influence on the CXCL8-induced migration of human neutrophil granulocytes[*]. 10 nM CXCL8wt **19** served as the chemoattractant and the formyl peptide fMLP at 10 nM concentration was chosen as a positive control for it is a strong activator of granulocyte migration. Mixtures of 2.5 µM Fluo-IL8RPLoops **86** with either of the two chemoattractants were added to the cells. After 1.5 h the cells that had reached the lower cavity of the plates were counted using an improved Neubauer chamber. At five times the K_d

---

[*]   Human neutrophil granulocytes were isolated by I. Rink.

concentration (2.5 µM) Fluo-IL8RPLoops **86** proved to selectively inhibit CXCL8-induced migration by about 50 %. Fluo-IL8RPLoops **86** had no influence on fMLP-induced migration proving the selectivity of the inhibition. The migration was succesfully inhibited by anti-CXCL8 antibody.
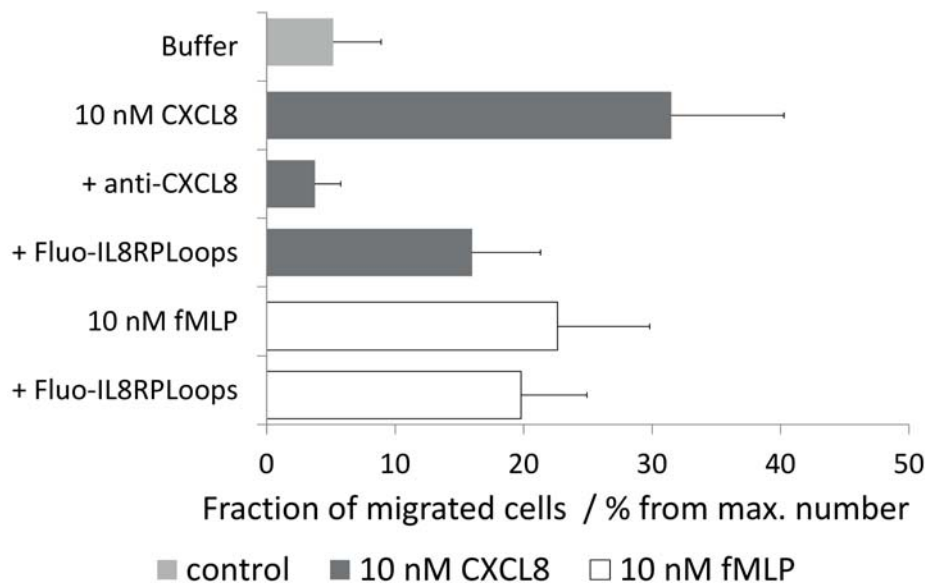

Figure 5.32: Transwell cell migration assay with human neutrophil granulocytes. 2.5 µM Fluo-IL8RPLoops **86** (K_d of 0.5 ± 0.3 µM) significantly inhibited the CXCL8-induced cell migration, fMLP induced migration was not influenced. Results represent three unrelated experiments with standard deviation (STD).

Further cell-based assays were conducted to show the biological activity of IL8RPLoops. The interaction of CXCL8 with its receptors CXCR1/2 was studied with CXCL8S72C-DL550 **23** on human neutrophil granulocytes. CXCL8S72C-DL550 **23** interaction with CXCR1/2 on cells was detected by fluorescence microscopy, where cells with bound CXCL8S72C-DL550 **23** are visible in the RHO channel. Human neutrophil granulocytes were incubated for 1 h at room temperature with either 100 nM IL8S72C-DL550, 500 nM Fluo-IL8RPLoops **86** or a mixture of 100 nM IL8S72C-DL550 and 500 nM Fluo-IL8RPLoops **86**. Cells appear fluorescent in the RHO when treated with IL8S72C-DL550 and show significantly reduced fluorescence when incubated with the mixture of IL8S72C-DL550 and Fluo-IL8RPLoops **86** (see Figure 5.33). Cells treated with Fluo-IL8RPLoops **86** showed no fluorescence in the FITC channel, untreated cells displayed no autofluorescence. This insinuates that Fluo-IL8RPLoops **86** either interferes with the internalization of CXCL8 and its receptor or that IL8RPLoops interferes with CXCL8 receptor binding.

A fluorescence-activated cell sorting (FACS) experiment with HEK293 (human embryonic kidney) cells stably transfected with CXCR1 was conducted[*]. Cells were incubated with CXCL8S72C-CF633 **24**, IL8RPLoops and a mixture of both. Treatment with a control antibody against CXCL8 resulted in a complete loss of cell fluorescence, indicating a complete blocking of CXCL8:CXCR1/2 interactions. Cells incubated with a mixture of CXCL8S72C-CF633 **24** and IL8RPLoops showed a significant decrease of fluorescence at 640 nm emission when compared with cells treated with CXCL8S72C-CF633 **24** alone (see Figure 5.34). At 488 nm emission there was no detectable increase in fluorescence of cells treated with Fluo-IL8RPLoops **86** (see Figure 5.35). The lack in a curve shift at 488 nm shows that Fluo-IL8RPLoops
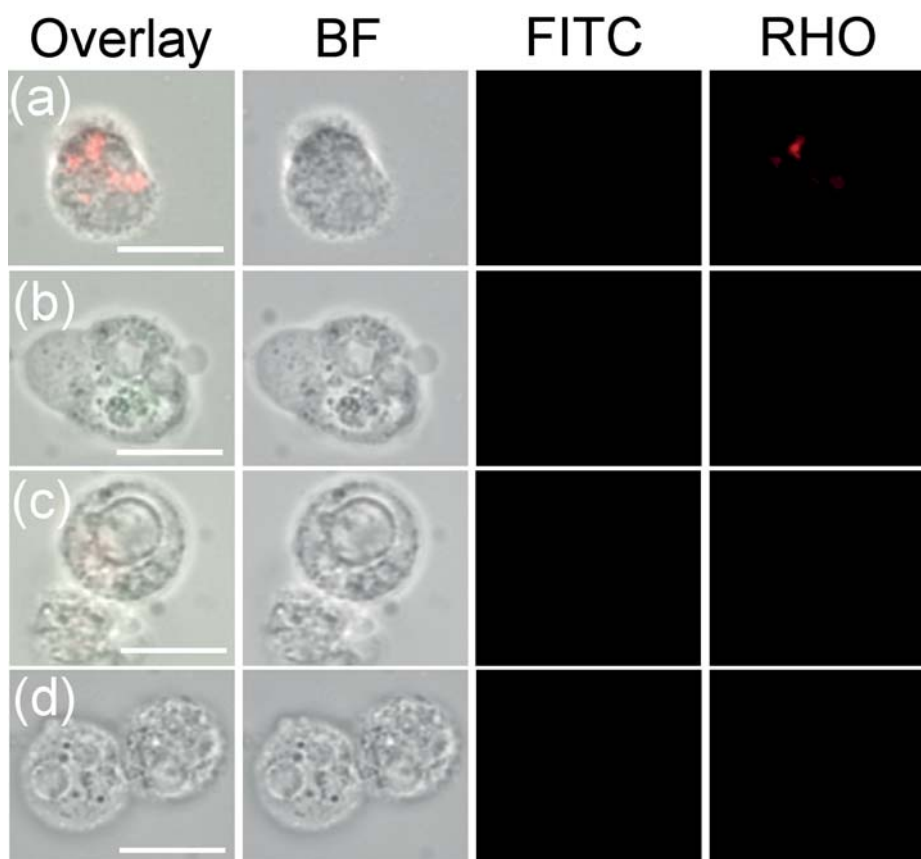
---

[*] FACS analysis by M. Joest.

Figure 5.33: Cell-based fluorescence assay with human neutrophil granulocytes (scale bar: 20 μm). (a) Cells that were incubated with 100 nM IL8S72C-DL550 for 1 h showed strong fluorescence in the RHO channel. (b) Cells treated with 500 nM Fluo-IL8RPLoops **86** showed no detectable fluorescence in the FITC and RHO channel. (c) Cells that were treated with a mixture of 100 nM IL8S72C-DL550 and 500 nM Fluo-IL8RPLoops **86** showed low fluorescence in the RHO channel, indicating the interference of Fluo-IL8RPLoops **86** with CXCL8 receptor binding or internalization. (d) Negative control of untreated cells in buffer showed no autofluorescence.

86 did not interact unspecifically with HEK293 cells. Therefore, biological activity of Fluo-IL8RPLoops **86** was not due to unspecific interaction with cells or interaction with the receptor CXCR1. These results support those from the previous cell-assay conducted with human neutrophil granulocytes and show that IL8RPLoops interferes with either the internalization of CXCL8 or the binding of CXCL8 to its receptor.

To ensure that the observed effects on cells were not due to a toxic effect of IL8RPLoops, a cell viability assay was conducted. Human neutrophil granulocytes (cell titer 5 10^6 cells/mL) were treated with different concentrations of IL8RPLoops and incubated for 5 h at 37 °C. Cells were consecutively stained with resazurin dye over night. Living cells reduce resazurin (dark purple) to resorufin (magenta), which is detected by fluorescence intensity measurements at λ_{ex}=535 nm and λ_{em}=585 nm. Dead cells do not reduce resazurin and show no fluorescence intensity at these wavelengths. Maximum fluorescence intensities (100 % alive) were determined by staining cells in buffer without IL8RPLoops and minimum fluorescence intensities (0 % alive) were determined by staining buffer without cells. All measured fluorescence intensities were calculated as percentages of these maximum/minimum cell numbers. The results showed that IL8RPLoops had an influence on cell viability only at high concentrations, approximately starting from
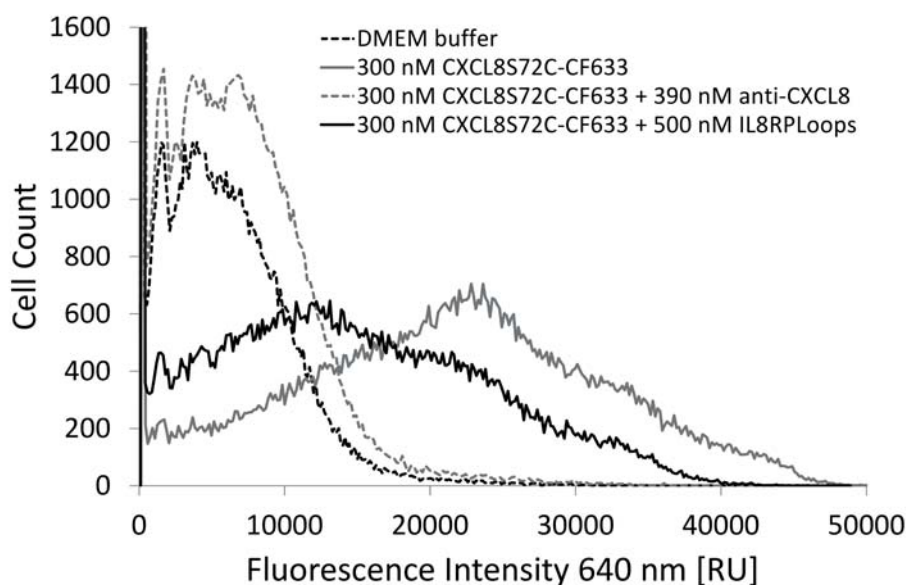
Figure 5.34: FACS analysis histogram of the interaction of CXCL8S72C-CF633 **24** with CXCR1 on stably transfected HEK293 cells. Cells incubated with CXCL8S72C-CF633 **24** showed an increase in fluorescence at 640 nm. Incubation with a mixture of CXCL8S72C-CF633 **24** and Fluo-IL8RPLoops **86** decreased the number of fluorescent cells, i. e. shifted the curve towards lower fluorescence intensities. This indicated that Fluo-IL8RPLoops **86** interfered with cell fluorescence caused by binding or internalization of CXCL8S72C-CF633 **24**.
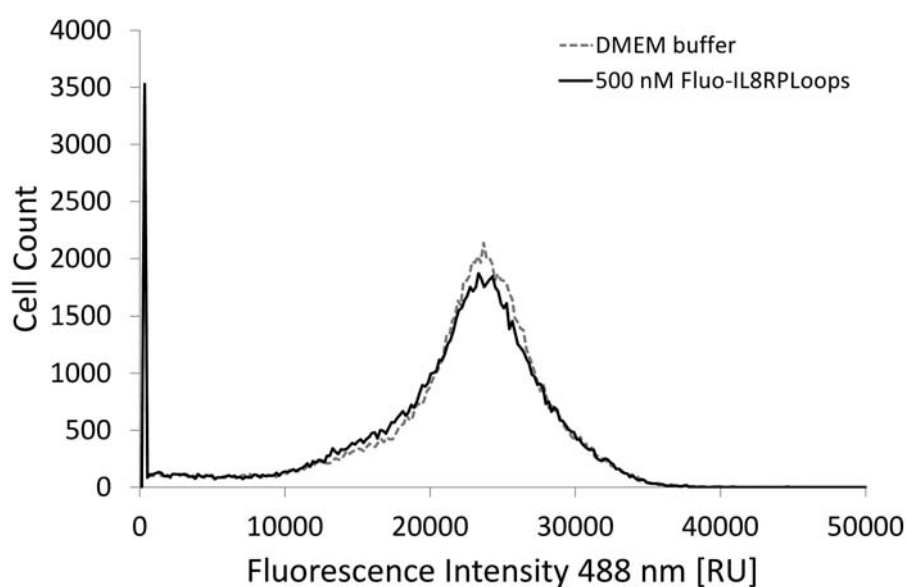
Figure 5.35: FACS analysis of the interaction of Fluo-IL8RPLoops **86** with HEK293 cells. At 488 nm no increase of cell fluorescence was detected after treatment with Fluo-IL8RPLoops **86**. It was concluded that Fluo-IL8RPLoops **86** does not bind to HEK293 cells unspecifically.

280 µM (see Figure 5.36). At the concentrations employed in the cell-assays IL8RPLoops therefore had no toxic effect.
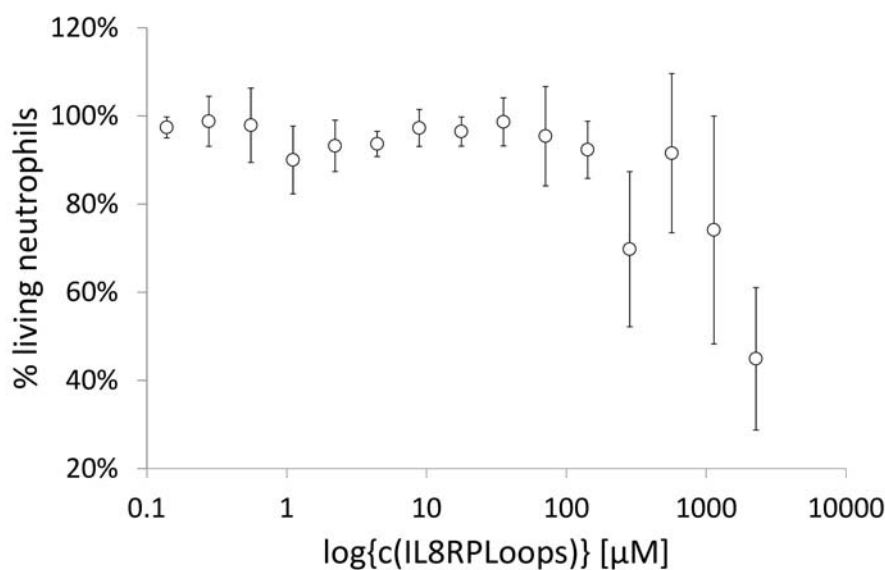
Figure 5.36: Human neutrophil granulocytes were incubated with different concentrations of IL8RPLoops for 5 h at 37 °C and consecutively stained with resazurin overnight. Only at concentrations higher than ca. 280 µM IL8RPLoops showed a toxic effect.

5.2.4 IL8RPLoops:CXCL8 Interactions

The mode of binding of IL8RPLoops to CXCL8 is not yet known. Since the peptide has a similar structure to the receptor scaffold it was designed from (see Figure 5.20) it is possible that it binds to CXCL8 in a fashion similar to the CXCL8:CXCR1 interaction and thus at the N-terminal region of CXCL8 (residues 1-10, incorporating the ELR motif). CXCL8(1-10) **90**, a peptide representing the N-terminal first ten residues of CXCL8 (sequence: SAKELRCQCI) labelled with Rhodamine B (called RhoB-CXCL8(1-10)) was tested for the ability to bind CXCL8wt **19** (see Figure 5.37). In the tested concentration range no binding could be detected between RhoB-CXCL8(1-10) **90** and CXCL8wt **19**. However, RhoB-CXCL8(1-10) **90** competed with CXCL8wt **19** for the binding to Fluo-IL8RPLoops **86** in a mixture of CXCL8wt **19** and Fluo-IL8RPLoops **86** (see Figure 5.38). The K_i was determined to be approximately 25 µM. This indicated an interaction of RhoB-CXCL8(1-10) **90** with Fluo-IL8RPLoops **86**. Since the N-terminus of CXCL8 is unstructured, which is also expected of the short N-terminal peptide CXCL8(1-10) **90**, the results suggested that RhoB-CXCL8(1-10) **90** imitated the N-terminal region of CXCL8 an therefore bound IL8RPLoops. This is an indication that IL8RPLoops does indeed bind the N-terminal region of CXCL8. The binding of CXCL8(1-10) to IL8RPLoops cannot be determined by fluorescence anisotropy since the gain of molecular volume upon binding of Fluo-IL8RPLoops is not high enough and therefore no anisotropy change can be detected.

A binding model of the binding of IL8RPLoops to CXCL8 was proposed by molecular dynamics simulation. The simulation suggests that the N-terminal residues E4 and R6 of CXCL8 as well as E29 are involved in IL8RPLoops:CXCL8 binding (see Figure 5.39). The simulated structure is largely analogous to the CXCR1:CXCL8 complex (see Figure 5.17). E29 is situated on the dimerisation site of CXCL8 and might thus interfere with CXCL8 dimerisation. In accordance with the binding curves that show decreasing
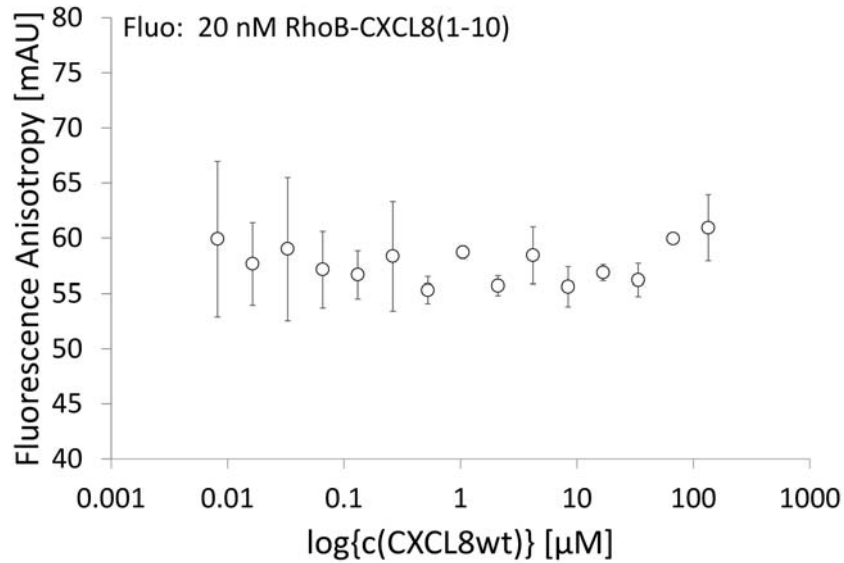
Figure 5.37: Fluorescence anisotropy measurement (λ_{ex}=530 nm, λ_{em}=576 nm) of RhoB-CXCL8(1-10) **90**, the N-terminal peptide of CXCL8 (SAKELRCQCI) labelled with Rhodamine B, binding to CXCL8wt **19**. No binding could be detected over the observed concentration range.
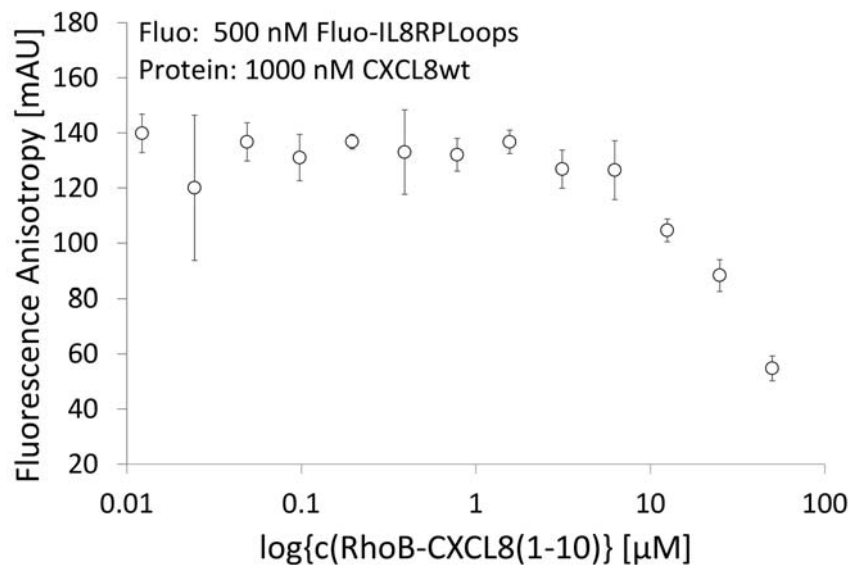

Figure 5.38: Fluorescence anisotropy competition assay (λ_{ex}=470 nm, λ_{em}=520 nm): RhoB-CXCL8(1-10) **90** (peptide of the 10 N-terminal residues of CXCL8) competed for the binding of Fluo-Il8RPLoops **86** to CXCL8wt **19**. Since RhoB-CXCL8(1-10) **90** itself did not bind CXCL8wt **19** (see Figure 5.37) this suggested that RhoB-CXCL8(1-10) **90** bound to Fluo-Il8RPLoops **86**. The K_i was determined to be approximately 25 µM. Since both the N-terminus of CXCL8 and RhoB-CXCL8(1-10) **90** are unstructured they may display similar binding modes to Fluo-IL8RPLoops **86**. The results could thus be an indication of the interaction of Fluo-IL8RPLoops **86** with the unstructured N-terminus of CXCL8wt **19**.

anisotropy values at high IL8RPLoops concentrations (see Figure 5.21), this indicates that IL8RPLoops may prevent CXCL8 dimerisation. This would explain the decrease in Fluo-IL8RPLoops:CXCL8wt (**86:19**)

fluorescence anisotropy binding curves (see Figure 5.21): at concentrations above the dimerisation constant of CXCL8wt **19**, i. e. around 1.0 μM (see Table 5.2), the formation of the dimer at high CXCL8 concentrations causes the displacement of Fluo-IL8RPLoops **86** and decreases fluorescence anisotropy. These results make IL8RPLoops an interesting peptide for the inhibition of the CXCL8:CXCR1 site II interaction that should be further investigated.
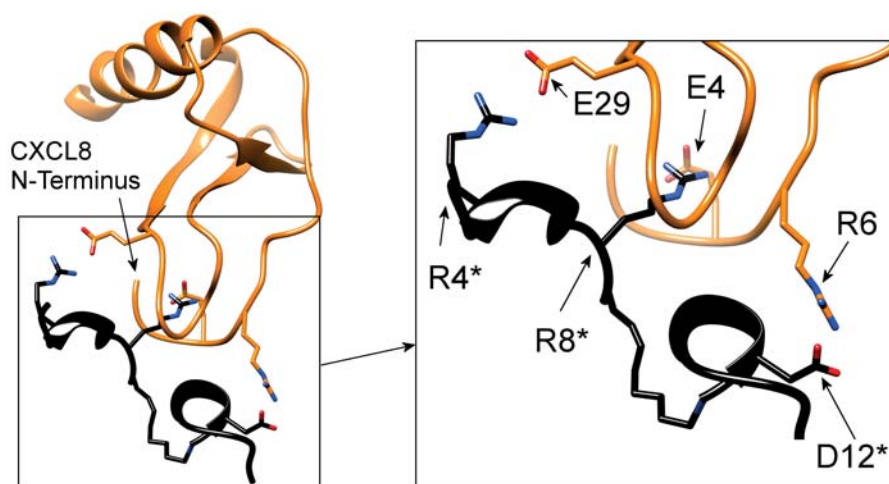

Figure 5.39: Endpoint of the 200 ns molecular dynamics simulation suggested an energetically favoured interaction of R4, R8 and D12 of IL8RPLoops with E29, E4 and R6 of CXCL8. The interaction with E29, a residue at the CXCL8 dimerisation interface, may prevent CXCL8 dimerisation, which would explain the bell-shaped binding curve in Figure 5.21.

IL8RPLoops was shown to be a promising CXCL8 inhibitor that binds CXCL8 with an affinity high enough to detect the CXCL8:IL8RPLoops binding on glass surface (see Figure 5.29). Thus it can be speculated that CXCL8:IL8RPLoops binding could likely be observed also on bead-surface by detecting IL8RPLoops immobilized on-bead with fluorescence labelled CXCL8. IL8RPLoops could thus serve as a positive control for the optimization of on-bead screening assays.

5.3 Peptoid Synthesis and Analysis

In order to obtain peptoid one-bead-one-compound (OBOC) libraries for the screening for ligands of biomolecules, three major aspects have to be taken into account: First the synthesis conditions have to be optimized to obtain sufficient amounts of peptoids of good yield and quality. When synthesis is established, the requirements for screening with biomolecules, e.g. a hydrophilic screening environment, have to be met. Successful screening goes along with the unambiguous analysis of small amounts of peptoids with unknown sequences (see Figure 5.40). Aspect I focuses on the optimization of peptoid synthesis, accompanied by the testing and verification of possible bulk analysis by MALDI TOF MS/MS (matrix assisted laser desorption/ionisation time-of-flight mass spectrometry with ion selection and fragmentation). Aspect II concerns the screening environment, mainly the resin properties which must be chosen so that peptoids stay on-bead and may be screened in aqueous solution. Aspect III stands for the unambiguous identification of unknown peptoid sequences by MALDI TOF MS/MS and limits the amines usable for synthesis. Only if all three aspects are taken into account OBOC libraries fit for screening can be obtained.
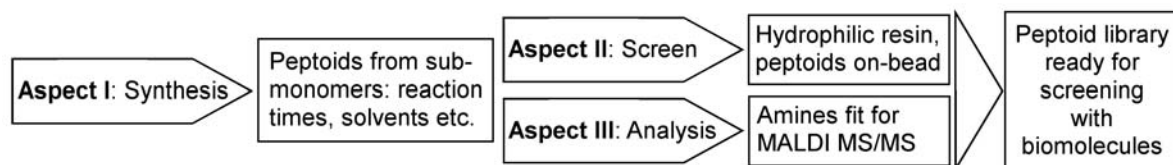
Figure 5.40: The route to peptoid one-bead-one-compound (OBOC) libraries ready for screening with biomolecules is characterized by three aspects: aspect I, the synthesis and analysis of bulk peptoids has to be established to ensure peptoid identification by mass spectrometry. Aspect II focuses on the prerequisites for screening, mainly the choice of resin for hydrophilic on-bead screening. Aspect III covers the analysis by MALDI TOF MS/MS, where unambiguous sequence identification is only possible if the side chains have different molecular weights. Successful analysis of libraries is therefore directly dependent on amine choice.

5.3.1 Aspect I: Peptoid Submonomer Synthesis and Analysis

All peptoids were synthesized by the submonomer method on solid phase originally reported by Zuckermann *et. al* (see Scheme 3.3.1).[218] To this day, a vast number of primary amines and different solid supports have been tested for their applicability in peptoid synthesis.[299] Only primary amines that had already been employed in submonomer synthesis by others and had proven to give high substitution yields were chosen for this work. Peptoid submonomer bulk synthesis was first optimized on HMBA-AM resin, an aminomethyl polystyrene resin with 4-(hydroxymethyl)benzoic acid linker that keeps peptoids immobilized on the resin after acidic deprotection. Only primary amines that lead to peptoid side chains that resemble or equal amino acid side chains were chosen for synthesis. Primary amines used in this work are listed below and are named after the peptide three letter code for the peptide equivalent with a capital "N" because of the backbone N-substitution (see Figure 5.41). See also Section 3.3 for information on the rules for nomenclature in this work.
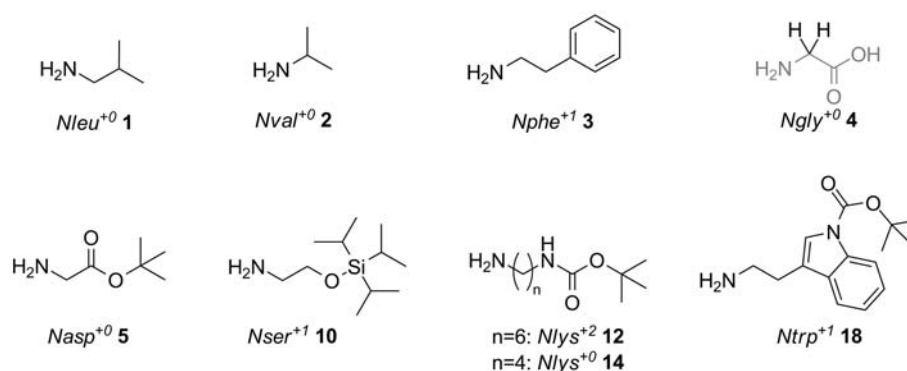

Figure 5.41: Primary amines used for peptoid submonomer synthesis in this work. Peptoids were named after the equivalent amino acid three letter code with a capital "N" to point out the N-substitution of the peptoid backbone. The number in superscript points to the length of the main carbon chain making clear if the peptoid side chain is the exact equivalent of an amino acid "+0" or possesses a longer side chain when compared to the amino acid "+x". Gylcine can be used as a primary amine to give the equivalent of aspartic acid. When introduced into the backbone as a monomer Ngly is equivalent to Gly in a peptide chain.

Primary amines are readily available and low in cost which makes peptoid synthesis generally simpler and more cost efficient than peptide synthesis. Ethanolamine, 1,4-diaminobutane, 1,6-diaminobutane and tryptamine were protected upon receipt. Protection of ethanolamine with triisopropylsilane gave 2-triisopropyl ethanolamine **10** as previously described by Zuckermann and coworkers (see Scheme 5.3.1).[219] Mono-Boc-1,6-diaminobutane **11** and Mono-Boc-1,4-diaminobutane **12** were protected according to the dissertation of T. Schröder (see Scheme 5.3.2).[247, 300] The reported synthesis of Boc-protected tryptamine **13**[301] (see Scheme 5.3.3) was slightly altered as the reaction was not carried out under argon and column chromatography in synthesis steps 1 and step 3 proved unnecessary.
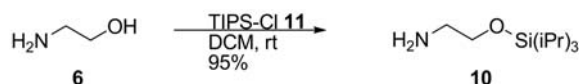
Scheme 5.3.1: Protection of ethanolamine with triisopropylsilyl chloride.
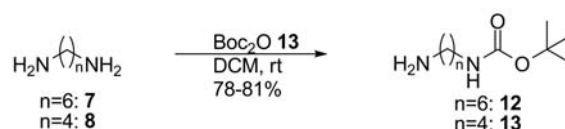
Scheme 5.3.2: Protection of primary amines with di-*tert*-butyl dicarbonate.
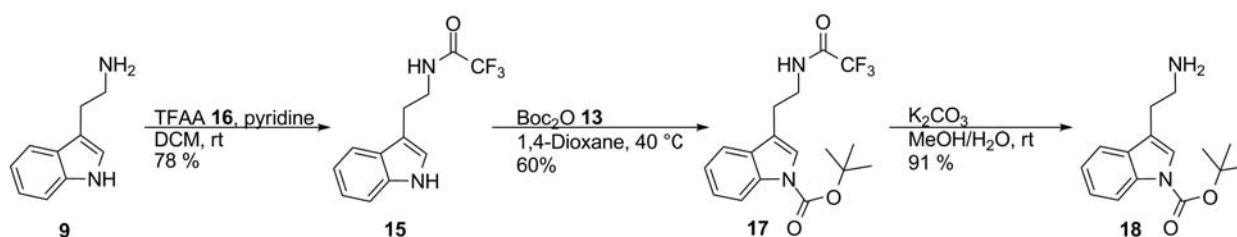
Scheme 5.3.3: Protection of tryptamine with di-*tert*-butyl dicarbonate.

Peptoid submonomer synthesis reaction times vary in different laboratories. In this work, 1 h reaction time for the acylation (room temperature) and 1.5 h for the substitution with amine gave good results* in the synthesis of peptoids **38**-**84** with the amines displayed in Figure 5.41. Elevated temperatures were not necessary and are not advisable when using DMF due to the formation of methylamine which interferes with the substitution reaction. For minimum amine content in the substitution step N-methyl-2-pyrrolidon (NMP) was used as a solvent. As opposed to standard peptide synthesis, the submonomer peptoid synthesis does not require Fmoc-protection of the building blocks rendering the quantification of resin loading by absorption of dibenzofulvene or Fmoc-derivatives impossible. It is however possible to employ a spacer like Fmoc-6-aminohexanoic acid before starting the submonomer synthesis so that resin loading can be determined by Fmoc-deprotection (through measurements of the absorption of dibenzofulvene at 304 nm). Peptoid coupling reactions were monitored by the amine-sensitive colorimetric 'chloranil test' (see Scheme 3.3.2).[220–222] The chloranil test proved to be very sensitive with a prominent blue colouring of amino-functionalized beads that readily appeared after a few seconds after addition of the reagents and required no heating.

---

*   Personal communication, the Zuckermann lab at the Molecular Foundry in Berkeley, California.

Primary amines for peptoid synthesis were equipped with acid-labile protecting groups (see Figure 5.41): *tert*-butyloxycarbonyl (Boc) and triisopropyl (TIPS) protecting groups were cleaved under standard conditions with 95 % trifluoroacetic acid (TFA), 2.5 % triisopropyl silane (TIS) and 2.5 % water for a maximum of 4 h at room temperature. The base-labile HMBA linker was consecutively cleaved by treatment with ammonia gas for 4 h.

To analyse peptoid purity, crude products were purified by high-performance liquid chromatography (HPLC) equipped with reversed phase RP8 or PR18 columns. As opposed to peptides, peptoid crude products could not be obtained by precipitation with cold diethyl ether. TFA cleavage solution therefore had to be removed by evaporation. Peptoids were usually detected at 220-230 nm and 254 nm or when containing aromatic side chains at 280 nm. HPLC chromatograms showed acceptable purity of the crude products in this work (see Figure 5.42).
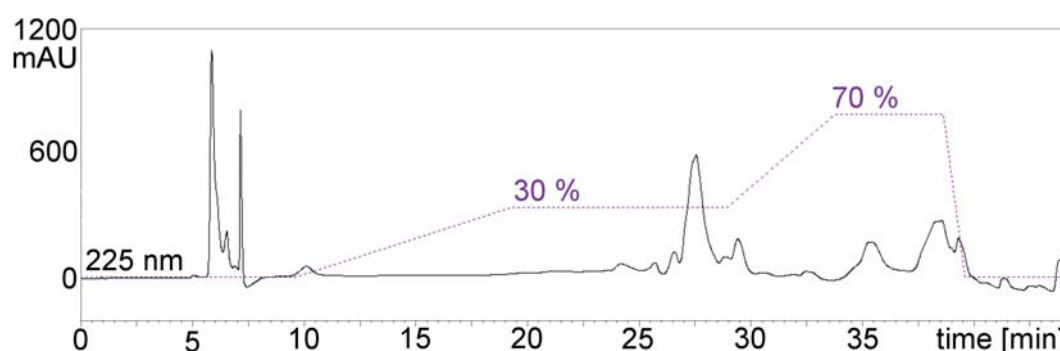
Figure 5.42: Exemplary HPLC chromatogram (RP8 column) of peptoid **61** crude product. Amount of eluent B (see Section 7.2) was increased in a multistep gradient from 10 % to 30 % to 70 % (dotted line). The chromatogram at 225 nm absorption shows the product signal at 27-28.5 min. Signals between 5 and 7.5 min appeared regularly as injection signals.

For the testing of binding and activity it was necessary to attach a fluorescent label to peptoids. Labelling with 5(6)-carboxyfluorescein (Fluo) (λ_{ex}=488 nm, λ_{em}=520 nm) was chosen since the fluorophore is inexpensive and fluorescein-labelled molecules are vastly used in fluorescence anisotropy measurements. The fluorophore was attached by standard 1-hydroxybenzotriazole/diisopropylcarbodiimide (HOBt/DIC) coupling. A massive 5(6)-carboxyfluorescein HPLC signal was observed when purifying crude products (see Figure 5.43). To remove side products washing of peptoids on resin with 20 % piperidine in DMF as suggested by Fischer *et al.* proved effective.[302]

Unpurified peptoid crude products **38**-**84** were analyzed by MALDI TOF MS/MS to confirm successful syntheses. Peptoids produced characteristic MALDI TOF MS/MS Y- and B-fragments (see Figure 3.12). Peptoids **38**-**84** were positively identified by fragmentation. Target peaks were however not always the highest peaks in the mass spectrum. By addition of phosphates to the MALDI matrix mixture MS results could be significantly improved (see Excursus 5.3.1). The fragmentation behaviour of peptoids was studied by comparing data from peptoids **38**-**84**. The following observations were made:

- It is difficult to predict the intensities of peptoid fragments. In most cases the highest (100 %) MS/MS signal is a Y-fragment. Y-fragments are more prominent than B-fragments in most cases, though this cannot be made into a general rule. Only for peptoids **42**, **43**, **44**, **45**, **51**, **52**, **53**, **54**, **77**, **83**
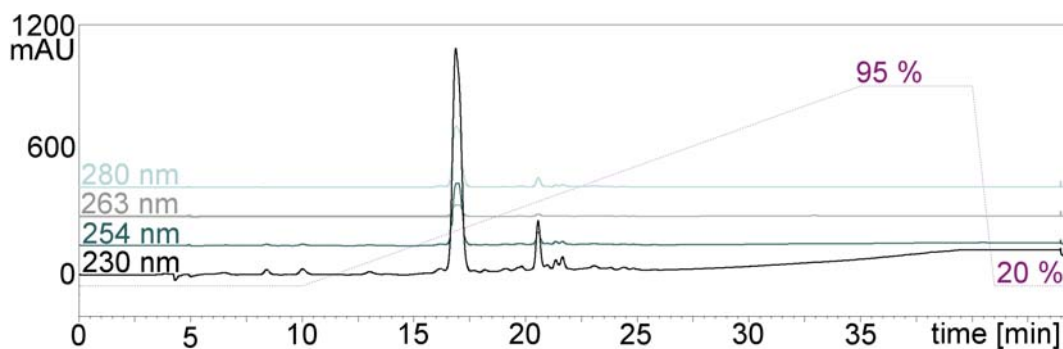
Figure 5.43: Exemplary HPCL chromatogram (RP8 column) of fluorescently labelled peptoid **62** crude product. Amount of eluent B (see Section 7.2) was increased gradually from 10 % to 95 % (dotted line). The chromatogram at 230 nm absorption shows the product signal at 20.5-21.0 min. The signal at 16.5-17.5 min shows the residual 5(6)-carboxyfluorescein after regular washing according to GP002 (see Section 7.6.1).

(22 % of peptoids analyzed) the highest MS/MS signal was a B-fragment. In the case of **42**, **43**, **44**, **45** the incorporation of L-Glycin-*tert*-butylester (Nasp^{+0}) seemed to be the cause for increased B-fragment stability. All peptoids also displayed a number of small non-trivial fragments that could not be identified as Y- or B-fragments.

- Penta-peptoids **51-54** with Ahx linker at the C-terminus and a glycine in position five of the sequence were compared to penta-peptoids **59-62** with the same sequence, except for a hexamethylenediamine at position five instead of the glycine. In peptoids **59-62** the Y_4 fragment is the highest signal, in peptoids **51-54** the B_3 fragment is the highest signal. This shows that fragmentation patterns are influenced by side chains and a peptoid is less likely to fragment at a glycine residue. This is in accordance with the theory that peptoid fragments are stable due to the alkalinity of secondary amines.[262]

- Peptoids of different lengths (penta- and hexa-peptoids) usually break at fragment B_2/Y_{n-2} or B_3/Y_{n-3}. One of this four fragments usually appears as the highest signal of the spectrum. In peptoids where B_2/Y_{n-2} or B_3/Y_{n-3} would cause a break at a glycine residue (e. g. **63**, **64**) the break at B_1/Y_{n-1} is favoured. This rule does not apply for peptoids with a large amount of glycine residues like **75** and **76** where B_1/Y_{n-1}, B_2/Y_{n-2} and B_3/Y_{n-3} all lead to a break at a glycine residue.

- Since peptoids are less likely to fragment at gylcine residues a trimeric glycine linker as used for instance in peptoids **38** to **45** does not produce extra fragments compared to a 6-aminohexanoic (Ahx) acid linker and thus does not complicate analysis. Ahx coupling however only requires one step which is why the Ahx linker was chosen over the trimeric glycine linker for future syntheses.

- When the Boc-protecting group is not removed, it leads to two characteristic signals in the MS/MS spectrum: 56 and 100 units below the target signal (see **38-84**). This makes it easy to distinguish protected and deprotected peptides.

Due to the ionisation of the matrix as well as the target substance in MALDI TOF MS, 'matrix adducts' are formed that complicate spectrum interpretation. The formation of these adducts may be reduced by adding phosphates to the matrix mixture.[303] The effect of matrix concentration and addition of $(NH_4)_2HPO_4$ on the ionisation of peptoids **46**, **48**, **51**, **53**, **58**, **59**, **61**, **62**, **68**, **70**, **72**, **75**, **80** and **83** was investigated. The matrix α-cyano-4-hydroxy cinnamic acid (CHCA) was prepared as 10 $^{mg}/_{mL}$ (matrix M) and 5 $^{mg}/_{mL}$ (matrix M') solution in acetonitrile:water (1:1, v/v). The two matrix solutions were blended with $(NH_4)_2HPO_4$ to give 6 mM and 50 mM phosphate in the matrix, mixed with peptoid solutions in acetonitrile:water (1:1, v/v) and spotted on a MALDI plate. The total detector ion count (TIC), i. e. the amount of ions reaching the detector, and the intensity of the target peaks were analyzed for their relative intensity (peaks in the spectrum were displayed as percentage of the largest peak). As expected, due to interference with the ionization, there is a considerable loss in ion quantity at high phosphate concentrations (see Figures 5.44 and 5.45). The lower amount of CHCA in matrix M' also leads to less ionization, probably due to destruction of target molecules upon absorption of laser light. The addition of phosphate to M or M' leads to a higher target signal in 9 out of the 14 tested cases (see Figures 5.46 and 5.47). The results suggest that a non-ideal MALDI TOF MS spectrum of a peptoid may be significantly improved by adding $(NH_4)_2HPO_4$ to the matrix. The amount of phosphate for ideal results varies and is dependent on the matrix concentration.
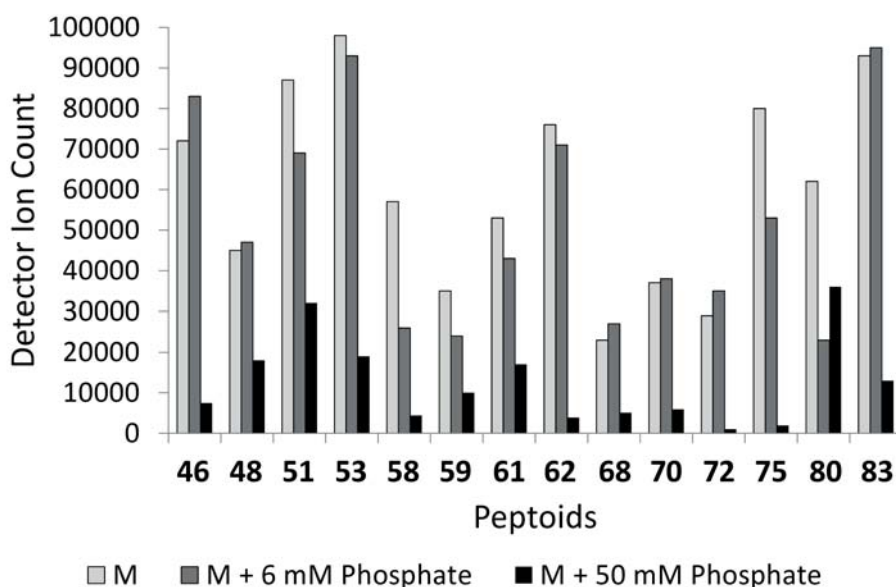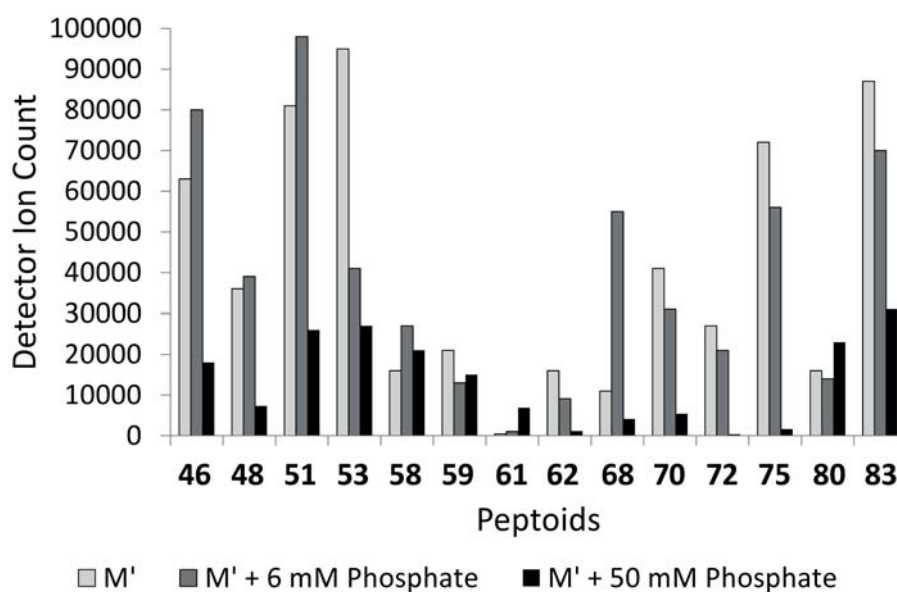

Figure 5.44: MALDI TOF MS detector total ion count (TIC) of peptoids **46**, **48**, **51**, **53**, **58**, **59**, **61**, **62**, **68**, **70**, **72**, **75**, **80** and **83** measured in matrix M (10 $^{mg}/_{mL}$ CHCA) compared to matrix M with phosphate addition. A higher amount $(NH_4)_2HPO_4$ leads to a decrease in ion formation and thus detection.

Figure 5.45: MALDI TOF MS detector total ion count (TIC) of peptoids **46**, **48**, **51**, **53**, **58**, **59**, **61**, **62**, **68**, **70**, **72**, **75**, **80** and **83** measured in matrix M' (5 mg/mL CHCA) compared to matrix M with phosphate addition. A higher amount $(NH_4)_2HPO_4$ leads to a decrease in ion formation and thus detection. Compared to matrix M (10 mg/mL CHCA) matrix M' leads to lower amounts of ions reaching the detector.
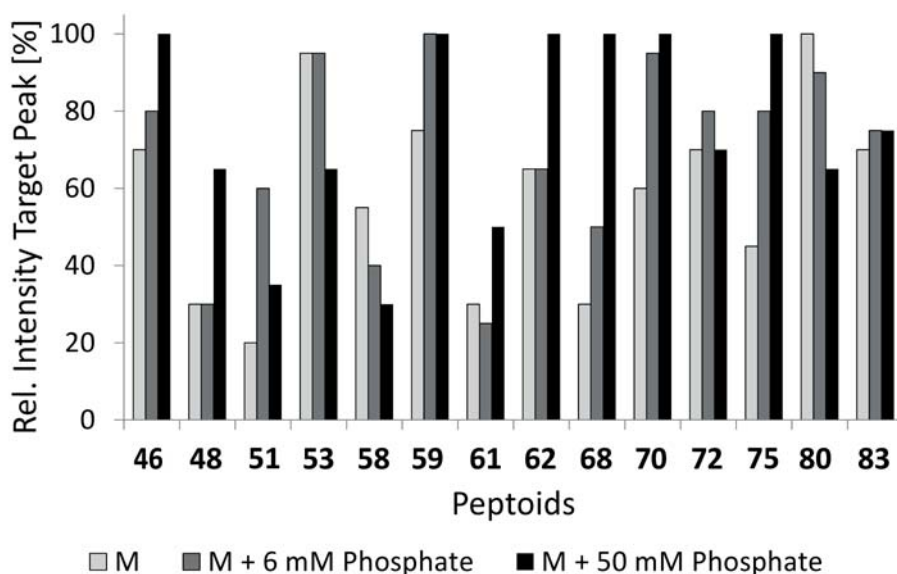

Figure 5.46: MALDI TOF MS relative intensity of the target peak (as percentage of the highest peak of the spectrum) of peptoids **46**, **48**, **51**, **53**, **58**, **59**, **61**, **62**, **68**, **70**, **72**, **75**, **80** and **83** measured in matrix M (10 mg/mL CHCA) compared to matrix M with phosphate addition. A higher amount of $(NH_4)_2HPO_4$ leads to a higher relative intensity of the target peak in 9 out of 14 cases.
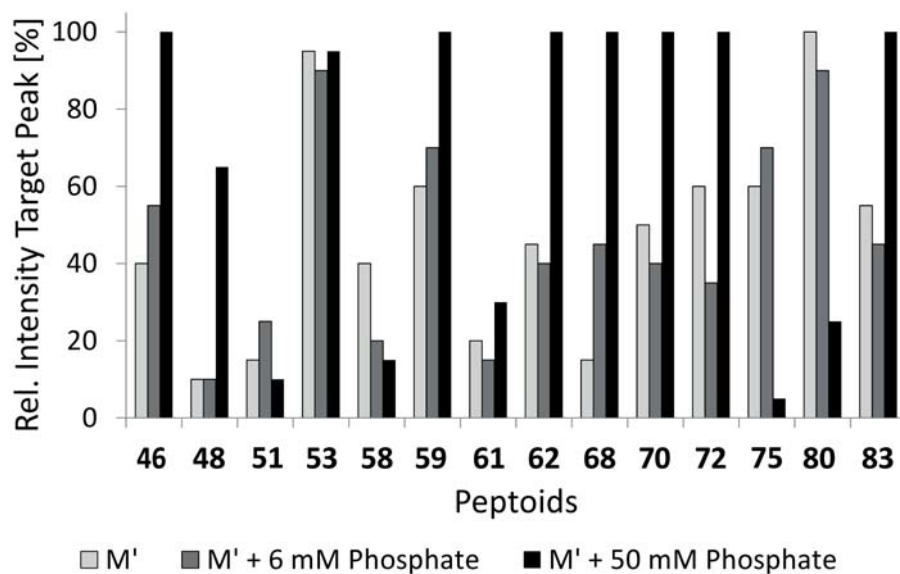
Figure 5.47: MALDI TOF MS relative intensity of the target peak (as percentage of the highest peak of the spectrum) of peptoids **46**, **48**, **51**, **53**, **58**, **59**, **61**, **62**, **68**, **70**, **72**, **75**, **80** and **83** measured in matrix M (10 $^{mg}/_{mL}$ CHCA) compared to matrix M with phosphate addition. A higher amount of $(NH_4)_2HPO_4$ leads to a higher relative intensity of the target peak in 9 out of 14 cases. Compared to the results with matrix M (see Figure 5.46), the differences between M' and M' with 50 mM phosphate addition is higher.

5.3.2 Aspect II: Screening Environment

The choice of the solid support is crucial for the success of library screening. The support chosen should display a minimum of unspecific interactions as well as homogeneous particle size distribution and loading for uniform amounts of synthesis products per bead. It must further possess good swelling abilities in water, thus be hydrophilic, since biological screening is performed in aqueous buffers and the contact of resin with biomolecules in the aqueous phase must be ensured. When handled manually, the size of resin particles should be chosen in such a way that individual particles are easy to observe and to manipulate. If employed for fluorescence screening the particles also must not display inherent fluorescence at the wavelengths of the used fluorophore. In OBOC libraries the peptoids remain on resin for screening and thus the linker cleavage must be orthogonal to any other protection group chemistry. Polyethylene glycol (PEG) based resins are known to show many of the desired properties: low levels of unspecific interactions, homogeneous size distribution, hydrophilicity and thus good swelling ability in water. An appropriate linker for chemical orthogonality to protecting groups is (4-hydroxymethyl)benzoic acid (HMBA), as it is not affected by the acidic condition in peptoid synthesis such as reaction with bromoacetic acid or removal of side-chain protecting groups.

Inspired by Paulick *et al.*[178] the unspecific interactions of several solid supports for peptide synthesis were tested for their tendency for unspecific interactions with a mixture of proteins, i. e. an *E. coli* lysate. Available polystyrene based resins, e. g. aminomethyl resin, Rink amide resin, Sieber resin, synbeads

and 2-chlorotritylchloride resin were compared to PEG-based TentaGel resin[*]. TentaGel consists of a polystyrene core with alkyl-linked tentacle-like polyethylene glycol chains.[304] The protein mixture in PBS buffer was obtained from an *E. coli* BL21 DE3 RIL lysate prepared by sonification, freezing/thawing, DNAse addition and centrifugation. 5.1±0.1 mg of resin support were incubated with lysate and washed with PBS supplemented with 0.1 % Triton X-100. Beads were mixed with 2× Laemmli buffer and heated to 95 °C, ensuring denaturation and removal of any protein adhering to the resin surface. The supernatants were analyzed by SDS-PAGE on a 12 % SDS-PA gel. After staining the SDS-gel by silver staining, no detectable amounts of protein could be seen for the 300 μm TentaGel-HMBA beads, whereas all other solid supports showed several bands of protein that had adhered to the bead surface (see Figure 5.48). Especially the positively charged aminomethyl synbeads (line 7) showed increased protein interaction since the majority of *E. coli* proteins are anionic at the tested pH.

Autofluorescence intensities of peptoid-functionalized polystyrene-based HMBA-AM resin were compared with peptoid-functionalized TentaGel MB HMBA resin (see Figure 5.49). TentaGel displayed a much more homogeneous brightness distribution in aqueous solution. This emphasized the necessity for the resin core to be hydrophilic when employed for screening to ensure a high signal-to noise ratio. Another interesting effect is the massive increase in fluorescence intensity when two TentaGel resin beads lie on top of each other (see Figure 5.49). Taking the above findings into account, TentaGel HMBA macrobeads with 300 μm diameter (capacity: 0.24 mmol/g) were chosen for all library synthesis.

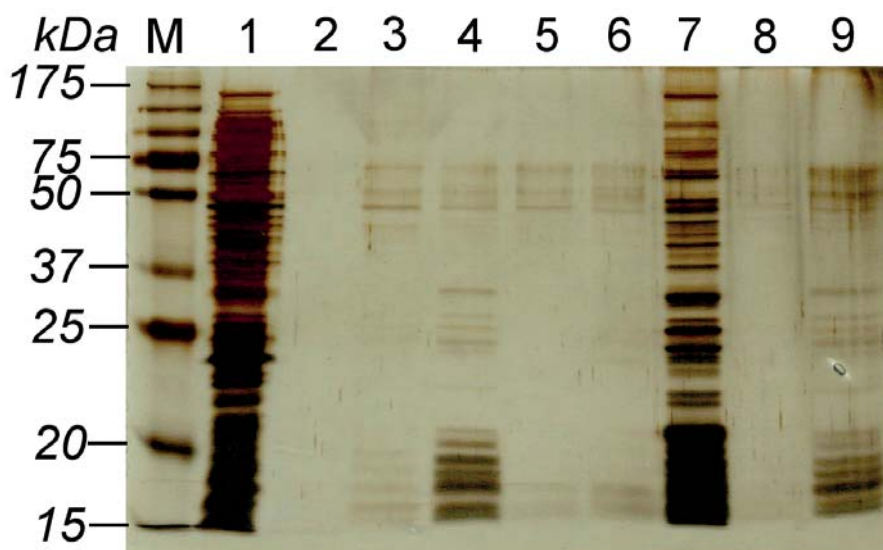Figure 5.48: 12 % SDS polyacrylamide gel (silver stained) showing the unspecific interactions of 5.1±0.1 mg of different solid supports with *E. coli* BL21 DE3 RIL lysate. TentaGel HMBA macrobeads (line 2) are the only resin beads to show no detectable unspecific interactions with the lysate proteins. M=Marker: Prestained Protein Marker, Broad Range 7-175 kDa, (1) Lysate of *E. coli* BL21 DE3 RIL, (2) 300 μm TentaGel-HMBA macrobeads, (3) HMBA-aminomethyl resin (Novabiochem), (4) HMBA-aminomethyl resin (iris biotech), (5) Rink amide resin, (6) Sieber resin, (7) aminomethyl (AM)- synbeads, (8) 2-chlorotrityl chlorid resin, (9) HMBA-aminomethyl resin (iris biotech) with 6-aminohexanoic acid linker attached.

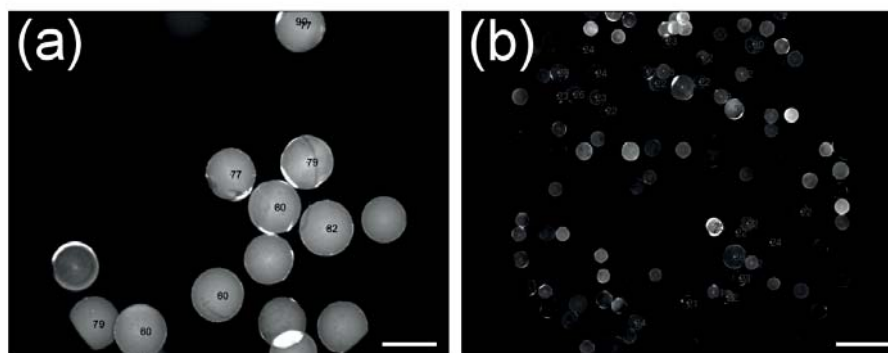[*] TentaGel® is a trademark of Rapp Polymere GmbH, Tübingen, Germany.

Figure 5.49: Comparison of fluorescence intensity in the FITC channel of the microscope of two different resins (scale bar: 300 μm). (a) Hydrophilic TentaGel-HMBA macrobeads functionalized with peptoid **94** in *ls*-PBS. (b) HMBA-aminomethyl (AM) resin functionalized with peptoid **94** in *ls*-PBS. The HMBA-AM resin displays a much greater distribution of fluorescence intensities. Another notable effect is the very strong fluorescence of TentaGel-HMBA macrobeads that lie on top of each other.

It was reported that TentaGel beads possess inherent fluorescence so that any fluorescence screening with the beads was prone to errors due to a low signal-to-noise ratio.[255,305] In this work the TentaGel-HMBA macrobeads did not display intrinsic fluorescence under the microscope at relevant exposure times in the FITC or RHO channel (see Figure 5.50). When functionalized with certain peptides, e.g. FWLDFW **88** however, the beads showed a considerable increase in autofluorescence in the FITC and RHO channel (see Figure 5.51). Based on the data analyzed in this work, it can be assumed that the autofluorescence increases dramatically when the peptide possesses a tryptophan or a peptoid possesses a tryptamine residue.
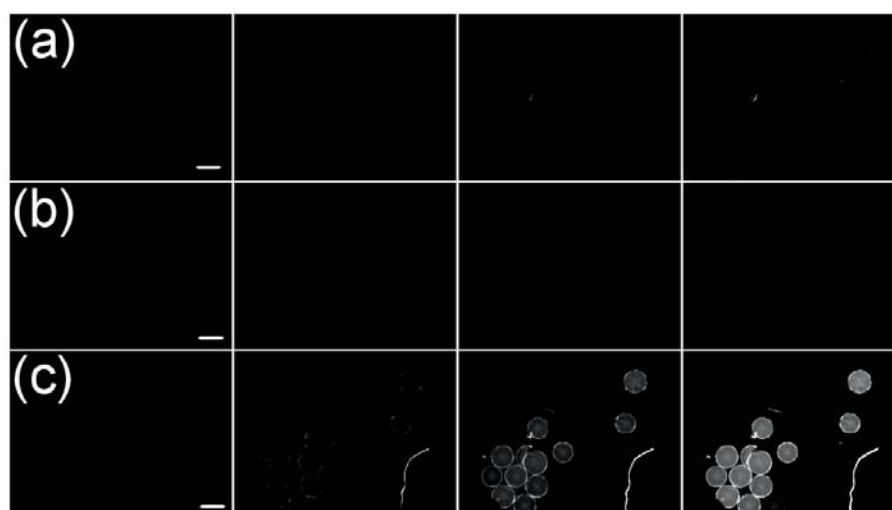

Figure 5.50: Intrinsic fluorescence of TentaGel-HMBA macrobeads under the fluorescence microscope (scale bar: 300 μm) in the (a) FITC, (b) RHO and (c) DAPI channel. Exposure time increases from left to right: 5 ms, 30 ms, 60 ms, 90 ms. TentaGel-HMBA macrobeads display no intrinsic fluorescence in the FITC and RHO channel at these exposure times.
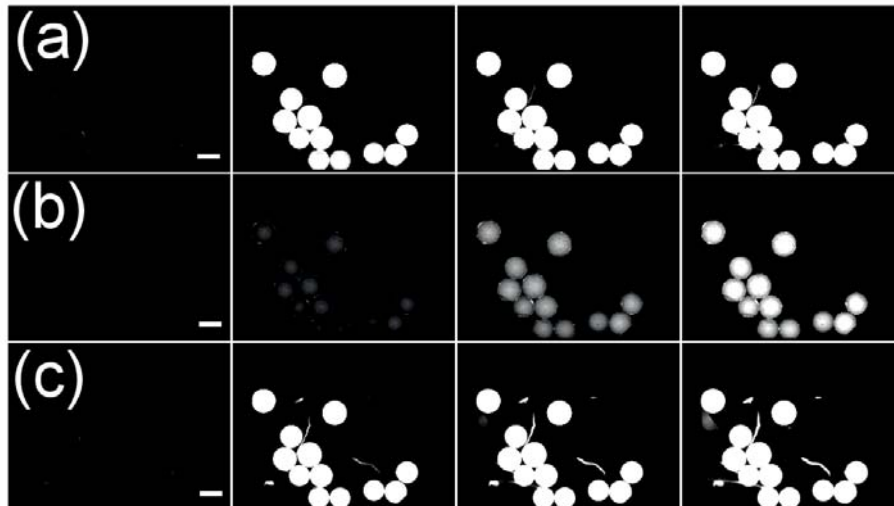
Figure 5.51: Fluorescence of TentaGel-HMBA macrobeads functionalized with the peptide FWLDFW under the fluorescence microscope (scale bar: 300 μm) in the (a) FITC, (b) RHO and (c) DAPI channel. Exposure time increases from left to right: 5 ms, 30 ms, 60 ms, 90 ms. When compared to unfunctionalized TentaGel-HMBA macrobeads (see Figure 5.50), it is evident that the functionalization with peptide caused an increase in bead fluorescence.

PEG itself, represented by a solution of PEG3400* in water, showed autofluorescence in the FITC channel, but the effect was subtle and appears only at high PMT Gain (PMTG) values (see Figure 5.52).
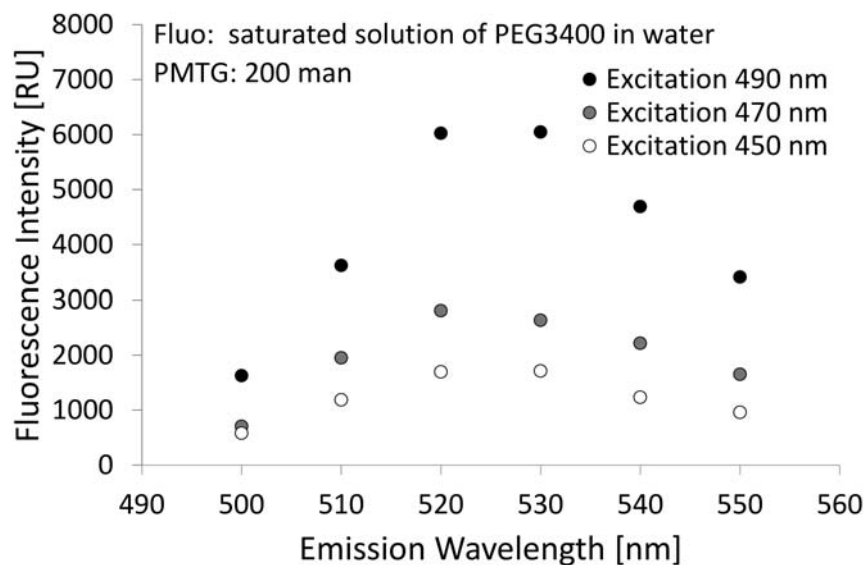
Figure 5.52: Fluorescence intensity of a saturated PEG3400 solution in water at different excitation wavelengths. Slight autofluorescence in the FITC channel can be observed but only at high photomultiplier tube gain (PMTG) values.

---

*   PEG3400 was a kind gift from B. E. Rapp, KIT.

After immersion in liquid (*ls*-PBS or water) TentaGel MB HMBA resin displayed very low autofluorescence in the FITC channel (see Figure 5.53). To explain the high autofluorescence of TentaGel beads loaded with tryptamine residues, tryptamine was dissolved in ethanol and different amounts of a saturated PEG3400 solution in water were added (see Figure 5.54). The experiments showed that the fluorescence of tryptamine (λ_{ex}=450 nm, λ_{em}=530 nm) was increased by addition of PEG3400. This effect is not readily explicable but it may be the reason for the increased bead-fluorescence.
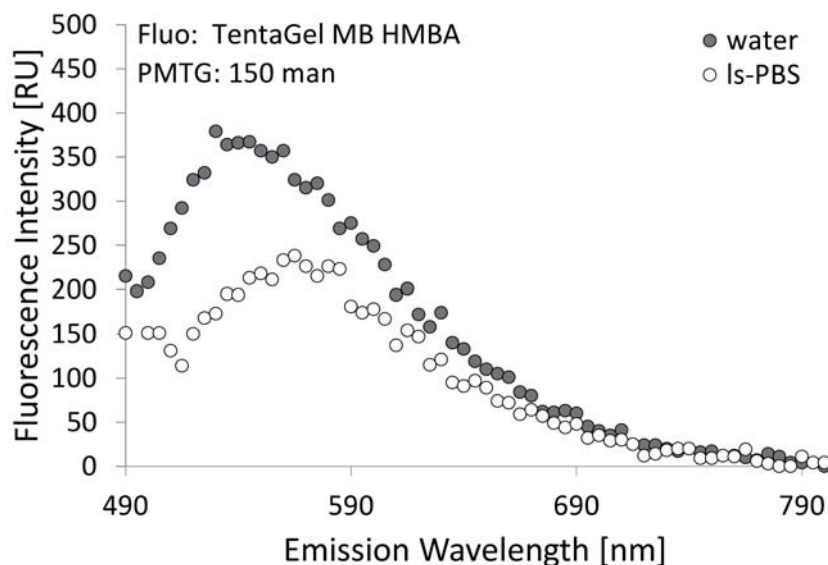
Figure 5.53: Fluorescence intensity (λ_{ex}=488 nm) of TentaGel MB HMBA resin after immersion in water or *ls*-PBS measured by the plate reader. The well of a microtiter plate was filled with approximately half way with resin beads. The beads display very low autofluorescence.

Figure 5.53 suggested that the autofluorescence of TentaGel MB HMBA can vary in different solvents. When just bathed in *ls*-PBS but imaged without buffer the beads displayed higher fluorescence (see Figure 5.55). Differences may have arisen from light scattering on the particle surface. It was then explored whether the well-filling height (i. e. the amount of solvent) had an influence on TentaGel fluorescence. Differing amounts of solvent per well did not lead to differences in bead brightness (see Figure 5.55). Therefore it was possible to quickly distribute bead suspensions into 384-well plates for bead screening without generating artifacts by differing filling heights.
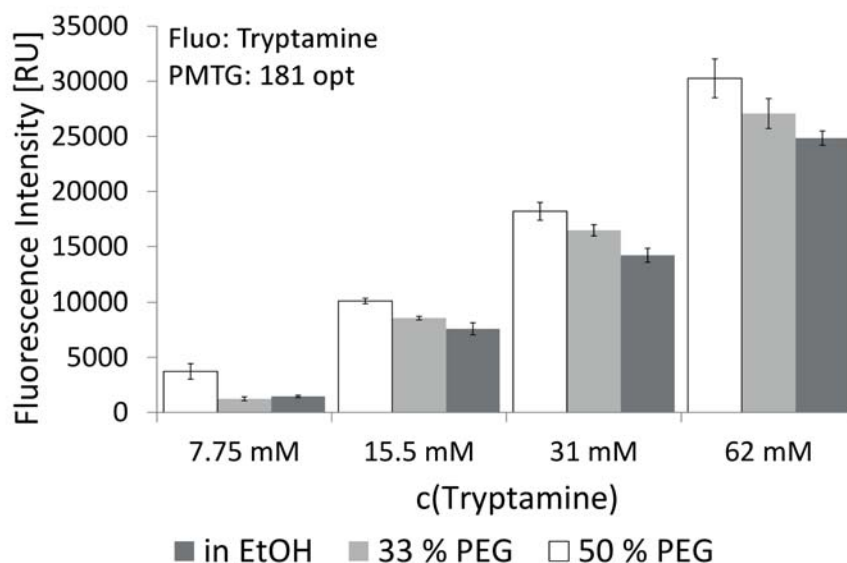
Figure 5.54: Fluorescence intensity of tryptamine (λ_{ex}=450 nm, λ_{em}=530 nm) in ethanol and mixtures of ethanol with a saturated PEG3400 solution in water (v/v). All data are corrected by the respective solvent fluorescence intensity. It shows that the fluorescence intensity of tryptamine at 450 nm excitation and 530 nm emission is increased by addition of PEG3400 to the solution.
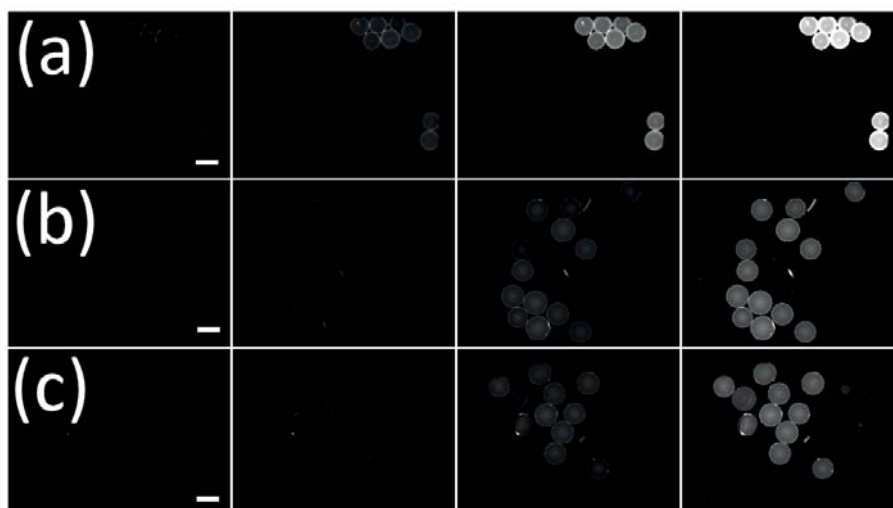

Figure 5.55: Fluorescence intensity of unfunctionalized TentaGel MB HMBA beads under the fluorescence microscope (scale bar: 300 µm) in the FITC channel. Exposure times from left to right in every row: 50 ms, 100 ms, 250 ms and 500 ms. (a) Bathed in *ls*-PBS, imaged without buffer. (b) Imaged in 20 µL *ls*-PBS. (c) Imaged in 100 µL *ls*-PBS. Beads without buffer appear very bright, most likely due to light scattering and reflexion on the bead surface.
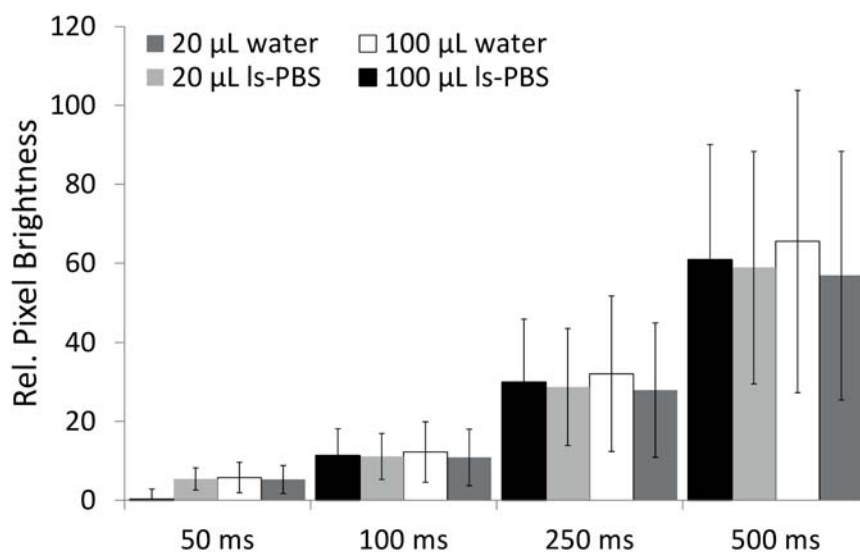
Figure 5.56: Image Analysis (ImageJ[298]) of images from untreated TentaGel MB HMBA beads taken at different exposure times with different amounts of buffer in the wells. The filling height of the well did not influence the fluorescence intensity of the beads, i.e. the pixel brightness of fluorescence images. Error bars represent the STD of pixel brightness in the analyzed image.

5.3.3 Aspect III: Unambiguous Peptoid Identification by MALDI TOF MS/MS

The single-bead MALDI TOF MS/MS analysis and sequencing is crucial when working with OBOC libraries synthesized by the mix-and-split method.[171] This method is characterized by the repetition of synthesis cycles: reaction of beads with different monomers in seperate vessels, mixing of the beads, splitting of the beads followed by the next reaction with another set of components (see Figure 3.6). The number of synthesized sequences increases exponentially with the number of cycles making this an ideal method for quick and efficient library synthesis. One TentaGel MB HMBA bead (Ø 300 µm) weighs roughly 15.7 µg. With a loading capacity of 0.24 $^{mmol}/_g$ one bead thus carries approximately 3.8 nmol of product. MALDI TOF MS/MS is an ideal method for the detection of such small amounts of substance and the method is furthermore capable of peptoid sequencing. For MALDI MS measurements, the peptoid had to be cleaved from the acid-stable HMBA linker after deprotection of *tert*-butyloxycarbonyl (Boc) and triisopropyl (TIPS) protecting groups with 95 % trifluoroacetic acid (TFA), 2.5 % triisopropyl silane (TIS) and 2.5 % water. Cleavage was achieved by exposition of the resin to an ammonia atmosphere for 4 h. Peptoids were washed off the bead with acetonitrile:water (1:1, v/v) with 0.1 % TFA and diluted with MALDI MS matrix solution before spotting on a MALDI MS plate.

The choice of primary amines is important: for sequencing by MALDI TOF MS/MS analysis peptoid side chains must possess different molecular weights so that peptoid sequence permutations may be identified (see Figure 5.57). This was taken into account when choosing amines for submonomer synthesis. Analysis of petoid fragment MS/MS spectra was straightforward. The highest signal was usually (though not always) a Y-fragment. Since the Y- and corresponding B-fragment give the total mass of the peptoid they were

found by subtracting the fragment from the peptoid weight (see Figure 5.58). Subtraction of consecutive Y- or B-signals gave the mass of the monomer between the signals.
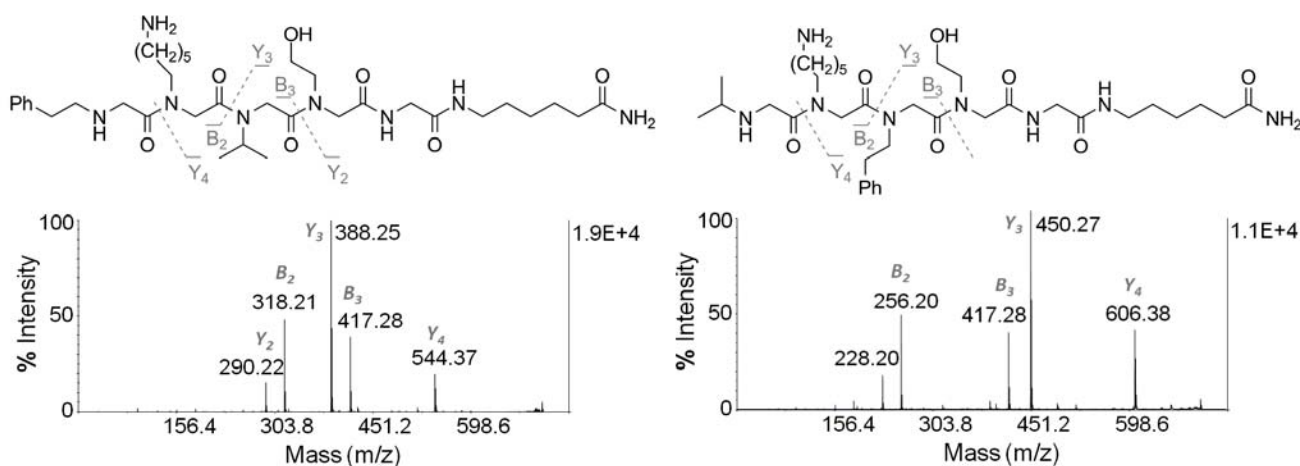

Figure 5.57: Peptoid permutation identification by MALDI TOF MS/MS fragmentation. Two peptoids (**61** and **62**) that possess different sequences consisting of the same amines possess the same molecular weight (705 g/mol). They can be unambiguously identified by MALDI TOF MS/MS if all side chains have different molecular weights.
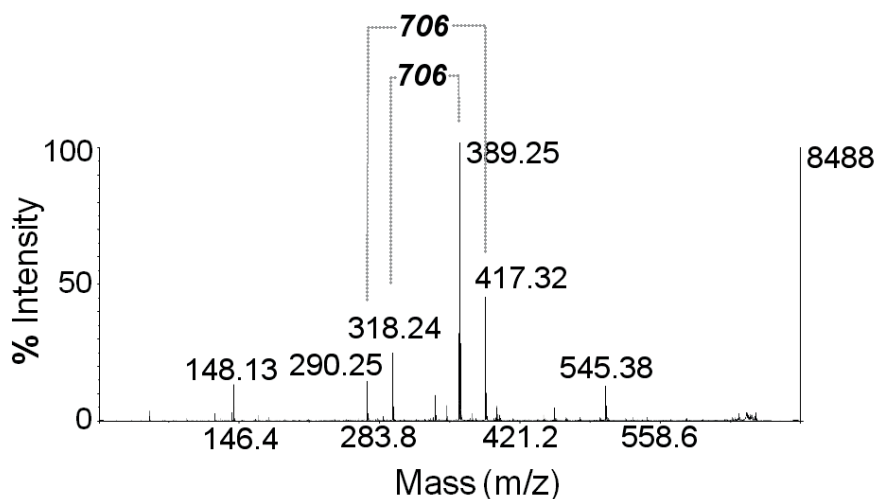

Figure 5.58: MALDI TOF MS/MS spectrum of peptoid **40**. Interpretation of the spectrum was done by finding the corresponding Y- and B-fragments that give the total peptoid mass when summed up (in this case 706 g/mol). Subtracting consecutive signals of one kind like Y_n and Y_{n-1} or B_n and B_{n-1} gives the mass of the monomer between these signals. The highest signal to the right of the spectrum (here: m/z=545) is usually the B_1 fragment due to the loss of the last monomer.

5.4 Peptoid OBOC Libraries

The synthesis and analysis of a small 16-membered combinatorial peptoid library **91** was successful with the non-ambiguous identification of 12 (**92**-**103**) of the 16 possible sequences*. A library of $7^6 = 117649$ peptoid hexamers **104** with seven primary amines chosen from Figure 5.41 was synthesized by mix-and-split synthesis on TentaGel MB HMBA resin (see Figure 7.6.2). Acylation was carried out in a glass filter frit. After acylation the resin was split and substituted with amines in seven individual polypropylene frits. The last mix-and-split cycle led to seven individual polypropylene frits (one for each of the seven amines coupled in the last step, maximum of 16807 sequences each). 18 beads of the library were randomly chosen and analyzed (peptoids **105**-**122**) to determine their sequence. Two of the beads (**111** and **112**) revealed unsuccessful coupling in the last coupling step of L-glycine-*tert*-butyl ester acetate.

5.4.1 Proof of Concept: Screening of Peptoid OBOC Libraries

The synthesis of peptoid OBOC libaries is straightforward (see Section 5.3). The consecutive screening process of a multitude of beads involves the isolation of beads carrying CXCL8-binding peptoids and ultimately the identification of these peptoids. It is therefore crucial to be able to distinguish a CXCL8-binding peptoid (a screening 'hit') from a non-binding peptoid. A simple way to distinguish is the introduction of a label to the protein that visualizes the binding event and allows the separation of the hits. Two kinds of labelling strategies for CXCL8 were tested for this purpose: fluorescence and magnetic properties.

5.4.2 Library Screening Based on Visualization by Fluorescence

Fluorescence intensity can be measured with high sensitivity at low fluorophore concentrations and is thus applicable for screening with small substance amounts in medium and high-throughput assays. CXCL8S72C-DL550 **23**, a fluorescently labelled variant of CXCL8, was produced and proven to be correctly folded after introduction of the fluorescent label (see Section 5.1.1). The fluorophore DyLight550 has an excitation maximum at 562 nm and an emission maximum at 576 nm making it visible in the red 'rhodamine' (RHO) channel of the fluorescence microscope. After incubation of a peptoid OBOC library with CXCL8S72C-DL550 **23**, beads that bound the labelled protein displayed fluorescence under the microscope. In order to reduce quenching of the fluorophore upon observation, i. e. destruction of the fluorophore by light-induced chemical reactions, the exposure time was kept as short as possible. The pictures were evaluated by eye or by image analysis on a computer and beads displaying fluorescence were separated and consecutively sequenced by MALDI TOF MS/MS (see Figure 5.59).

The described method of incubation, imaging, image analysis, separation and sequencing is a modified version of a method previously reported by T. Kodadek.[255] The Kodadek publication describes the analysis of bead populations by the researcher in real-time by eye. However fluorescence intensities of hits compared to non-hits were often poor. Also, the permanent exposure to excitation light during library-screening in real-time can lead to significant fluorescence bleaching. Taking fluorescence images at low exposure times minimized bleaching effects and provided better signal-to-noise ratios.

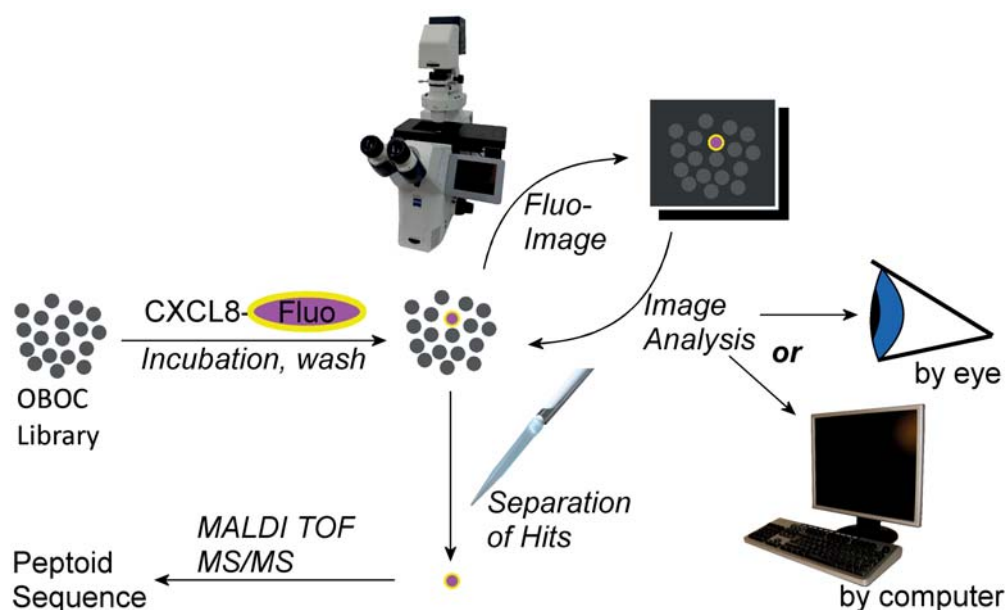* Part of the Bachelor thesis of M. Hau, Hochschule Reutlingen 2012.

Figure 5.59: Overview of the screening of OBOC libraries based on fluorescence. OBOC libraries are incubated with CXCL8S72C-DL550 **23**, washed and imaged in 384-well microtiter plates by fluorescence microscopy. Fluorescent beads (i. e. those that bind CXCL8S72C-DL550 **23**) are separated manually and sequenced by MALDI TOF MS/MS.

Obtaining Fluorescence Image Data

For large OBOC libraries with a multitude of beads fluorescence images must be obtained automatically to ensure imaging in a timely and unbiased manner. After the beads had been incubated with fluorescently labelled protein they were consecutively washed with *ls*-PBS. The dissociation of labelled protein from the bead surface over time is inevitable as a new equilibrium forms. To ensure higher throughput and to facilitate recovery of fluorescent beads, bead images were taken in 384-well black, transparent bottom microtiter plates (MTP). The size of individual wells was ideal for obtaining a single-well-image with a 5× objective under the microscope. Equipped with an automated x/y-table the microscope can generate single and overlay images of desired channels in an automated fashion. The imaging of one 384-well MTP in RHO and FITC channel took roughly 7 min. 25 MTP were needed for screening of the whole library. The most time-consuming step was the manual distribution of beads into the MTP. As previously mentioned (see Figure 5.49) it was crucial for image evaluation that beads did not lie on top of each other for this increases light scattering effects. Therefore it had to be ensured that only a small amount of beads was distributed into each well. The best way to achieve this was the distribution of droplets of bead suspensions into wells by means of a modified pipette tip (see Figure 7.3 in Section 7.7). After the distribution of the beads the MTP was centrifuged to prevent layering and floating of the beads.

To obtain fluorescence images with a good signal-to-noise ratio it was also necessary to set the right exposure time. As shown before (see Figure 5.51) TentaGel beads may display slight autofluorescence in the RHO channel. With the discovery of IL8RPLoops (see Section 5.2) as a positive control it was possible to test the on-bead screening assay for the optimum exposure time. At 40 ms exposure time the binding of CXCL8S72C-DL550 **23** to TentaGel MB HMBA-bound IL8RPLoops **85** could be easily detected.
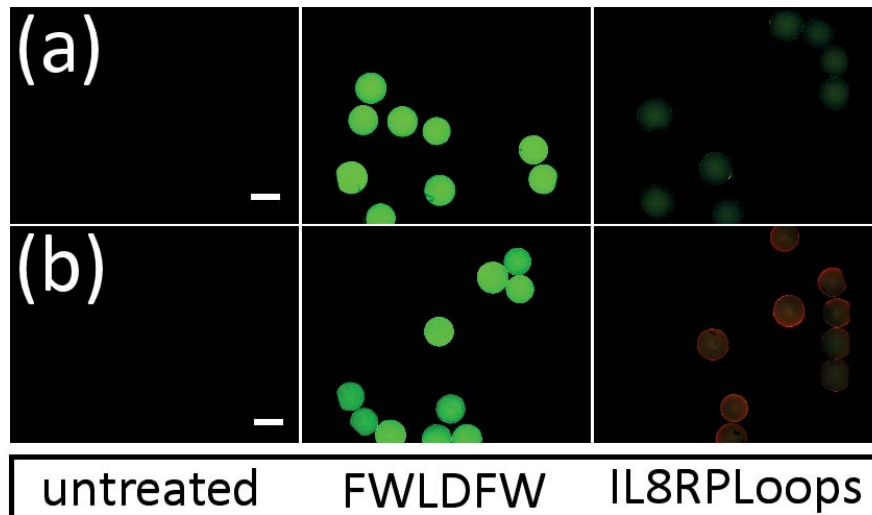
Figure 5.60: Proof of concept of screening by fluorescence intensity. The binding of IL8RPLoops on TentaGel MB HMBA resin TG-IL8RPLoops **85** to CXCL8S72C-DL550 **23** (scale bar: 300 µm) is detectable by fluorescence microscopy in the RHO channel. Images are overlays of FITC (green) and RHO (red) channel. Untreated beads, TG-FWLDFW **88** (a peptide reported to bind CXCL8[150]) and TG-IL8RPLoops **85** were tested. All images were acquired in *ls*-PBS. (a) Images taken at 40 ms exposure time after incubation of the different beads with *ls*-PBS. (b) Images taken at 40 ms exposure time after incubation with CXCL8S72C-DL550 **23** and consecutive washing with *ls*-PBS. CXCL8S72C-DL550 **23** bound TG-IL8RPLoops **85** and is visible in the RHO channel.
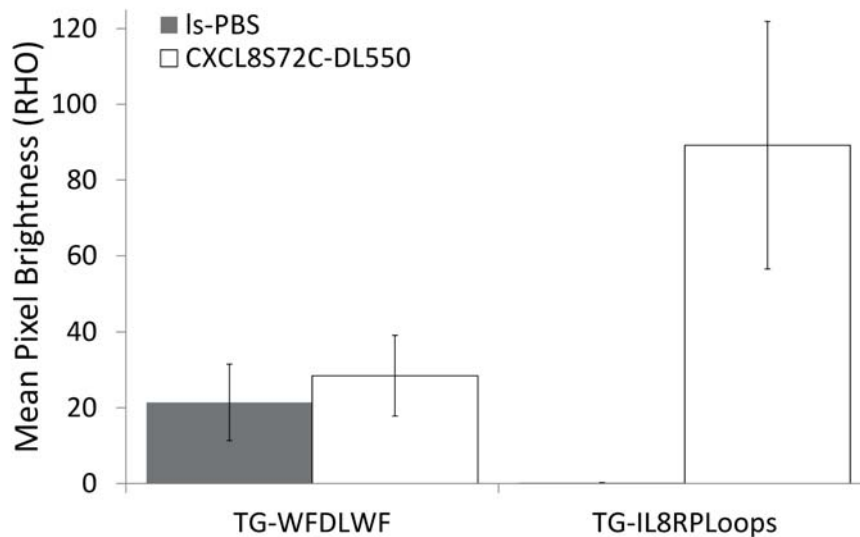
Figure 5.61: Quantification of increase of fluorescence intensity in the RHO channel upon treatment of TentaGel MB HMBA (TG)-WFDLWF **88** and TG-IL8RPLoops **85** with CXCL8S72C-DL550 **23**. The good signal-to-noise ratio enables the facile detection of bound CXCL8S72C-DL550 **23**.

Functionalized TentaGel beads were incubated with CXCL8S72C-DL550 **23** and imaged. Even though the beads functionalized with the FWLDFW peptide and to a certain extent also those functionalized with IL8RPLoops showed fluorescence in the FITC channel, the increase in fluorescence in the RHO channel

was significant (see Figure 5.61). Unfunctionalized TentaGel beads showed no unspecific interactions with CXCL8S72C-DL550 **23**. These results suggested that the detection of CXCL8-binding molecules on TentaGel MB HMBA resin is possible with the method described in Figure 5.59 and autofluorescence is distinguishable from the binding of fluorescently labelled protein.

Evaluation of Fluorescence Image Data

Evaluation of large amounts of fluorescence image data may be accomplished in two ways: images can be compared directly by eye or with the aid of a computer program. Computer based analysis is especially helpful when signal-to-noise ratios are not ideal and unbiased decisions between screening positives and negatives have to be made.

For the evaluation of TentaGel MB HMBA libraries a computer programme was designed in collaboration with and programmed by Markus Reischl and Sophie von Borstel[*]. The programme is MATLAB-based and analyzes TIFF images (1024×1344) of single wells with a maximum of 20 beads per image. An image taken in the fluorescence channel for screening purposes usually consists of three pixel populations of different brightness: the outside of the MTP well which is always black, the inside of the well (the background) that will be slightly less dark than the outside of the well and the beads that appear at higher brightness values (see Figure 5.62).
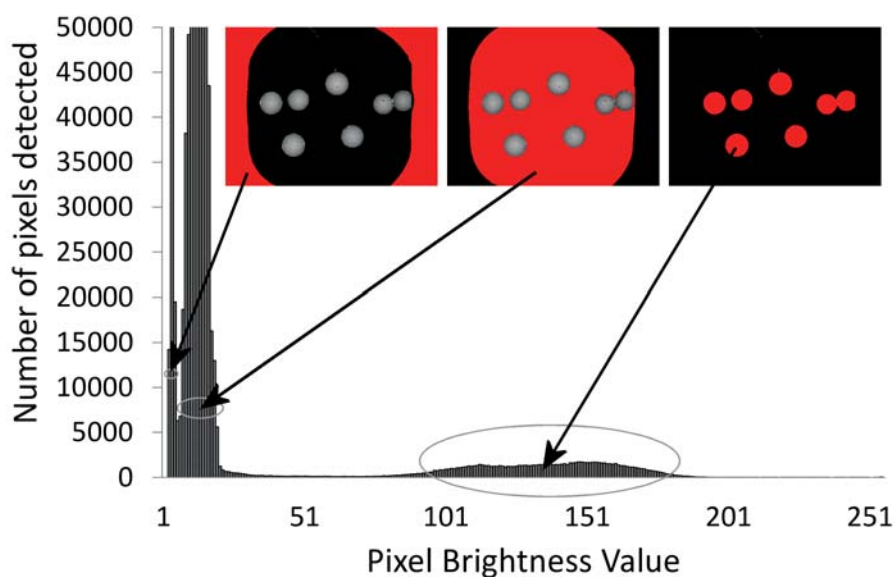

Figure 5.62: Histogram of fluorescence images of library beads with three pixel populations of different brightness. The part of the images corresponding to the histogram populations are shown in red. Left: the very sharp distribution of the completely black, non-transparent outside of the well of the MTP. Middle: the narrow distribution of the background of the transparent MTP well. Right: the broad distribution of the brightness of the beads.

The programme uses the canny edge detector algorithm[306] for detecting the well outline. Bead circular shapes are detected with by the Hough algorithm[307] with an optimized radius detection at 300 μm. To determine fluorescence intensities of individual beads, the mean pixel brightness of the beads is calculated

---

[*]   Part of the Master Thesis of Sophie von Borstel, Institute of Applied Informatics, KIT, 2012.

across the bead circle shape and the background mean brightness value is subtracted. Detected circles are marked with central red dots and green numbers. Reflexion and scattering effects make the edges of beads appear brighter than the rest of the bead area which will influence overall brightness. Therefore an offset of 30 pixels was introduced, that diminishes the area of the beads at the rim as indicated by white circles in the images of individual beads to be analyzed (see Figure 5.63).
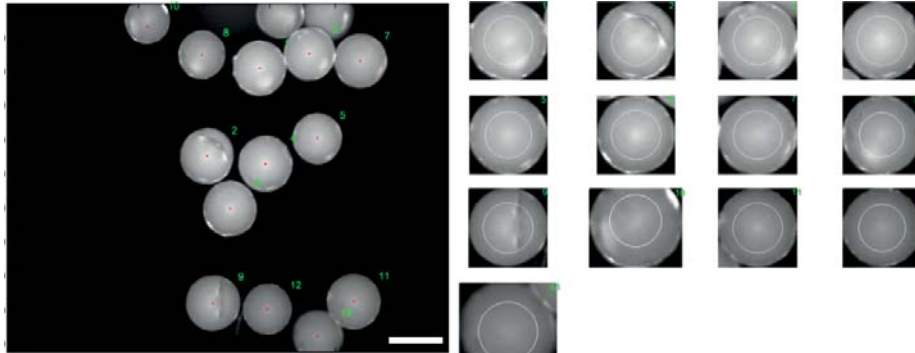

Figure 5.63: Example of automated bead detection with the Hough algorithm.[307] The picture on the left shows the FITC channel image of a single well of a 384-well MTP (scale bar: 300 µm, 100 ms exposure time). Detected circular shapes are marked by a central red spot and a green number. On the right the individual beads as detected by the Hough algorithm are displayed. The bead mean brightness values were automatically calculated in order to detect the ones with high fluorescence intensity. The white circles inside the beads indicate an offset of 30 pixels that was introduced into the calculation of pixel brightness since reflexion and scattering effects make the bead rim appear brighter than the rest of the bead.

The mathematical threshold between homogeneity and inhomogeneity of a bead is given by the variation coefficient c

$$c = \frac{\sigma}{\bar{x}} \tag{5.1}$$

with

$$\sigma = \sqrt{\frac{1}{n-1} \sum_{i=1}^{n} x_i - \bar{x}} \tag{5.2}$$

where n is the number of pixels, x_i is the brightness value of pixel i and $\bar{x}$ is the mean brightness value. The threshold value of the variation coefficient c can be chosen to fit the data at hand. It was found that a value of $c < 1.4$ was a good compromise for rejecting inhomogeneous beads. The restrictive choice of the variation coefficient c solved some issues that caused problems in the screening process: it detected broken and misshaped beads (see Figure 5.64) as well as beads that lay on top of each other since the stacking of beads distorted the pixel brightness due to reflexion and scattering effects (see Figure 5.65). With the calculation of mean brightness of each bead and rejection of inhomogeneous beads by the criterion defined by the variation coefficient c, a list of bead brightness values was generated. This way, the wells with the brightest beads were identified from a set of images.

When signal-to noise ratios are good and screening results are obtained in the RHO channel (where autofluorescence of TentaGel beads is low) the analysis of screening fluorescence images by eye is straightforward. The image of the overlay is generated by addition of the RGB-values of the individual channels,
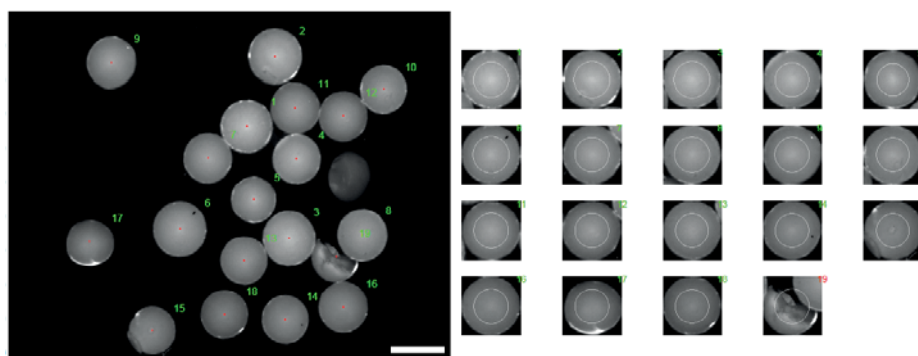
Figure 5.64: Example of screening result with the custom-made MATLAB-based programme: rejection of broken beads. FITC channel image of TentaGel MB HMBA in *ls*-PBS (scale bar: 300 μm, 100 ms exposure time). All detected circular shapes were marked by central red dots green numbers. Number 19 is broken and was detected by the programme due to inhomogeneous brightness values and was rejected for the analysis, indicated by the red number above the individual bead images on the right.
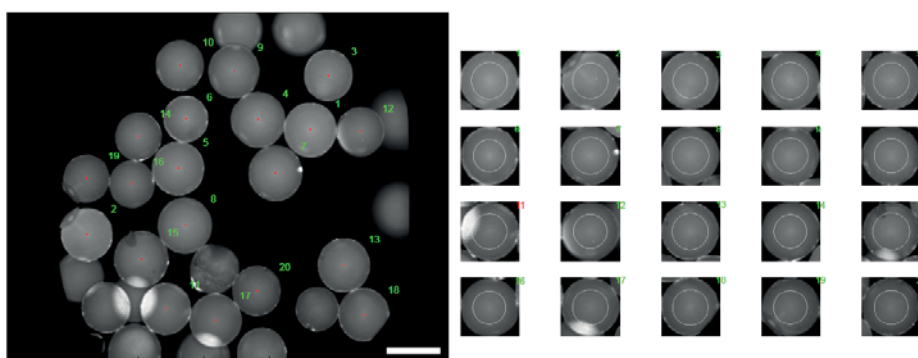

Figure 5.65: Example of screening result with the custom-made programme: rejection of inhomogeneous beads. FITC channel image of TentaGel MB HMBA in *ls*-PBS (scale bar: 300 μm, 100 ms exposure time). As previously discussed (see Figure 5.49), the stacking of beads leads to a distortion in bead brightness. When the distortion occurs on the outer part of the bead it is rejected due to the homogeneity criterion defined by the variation coefficient c.

i. e. when a pixel of the FITC channel image possesses an RGB value of 0/100/0 and the pixel shows an RGB value of 200/0/0 in the RHO channel, the corresponding pixel in the overlay image will have an RGB value of 200/100/0. Colour perception in human trichromats is a result of the interaction of light waves with three types of photoreceptor cells ('cones') on the retina. The cones have sensitivity maxima at 420 nm (S-cones), 534 nm (M-cones) and 564 nm (L-cones).[308] Colour perception is subjective and depends on the number of the respective cone type in the indivual, but in general the human eye is more sensitive to yellow-green light due to the spectral overlap of two (M- and L-cones) of the three colour cones. Red colour is perceived with less sensitivity. Figure 5.66 shows the overlay of the red and green colour RGB-space. The image shows that (a) in an overlay image, beads with very high autofluorescence (FITC, green), i.e. with a G-value above 150 can only appear green, yellow or orange, (b) for a bead to appear red, the R-value should be approximately twice the G-value (and the G-value must be under ca. 150), (c) beads with similar R- and G-values appear orange or yellow. Most beads display fluorescence in the FITC channel due to the immobilized peptoids or peptides on the surface (compare Figures 5.50 and 5.51). Bead autofluorescence in the RHO channel was observed to be of much lower intensity than autofluorescence in

the green channel. Thus the autofluorescence in the RHO channel is completely superseded by the autofluorescence in the FITC channel and only beads with high RGB R-values will appear red in the overlay image. This ensures the selective identification of beads with a high red-to-green ratio. Thus RHO/FITC overlay images were used for effective library analysis by eye (see Figure 5.67).
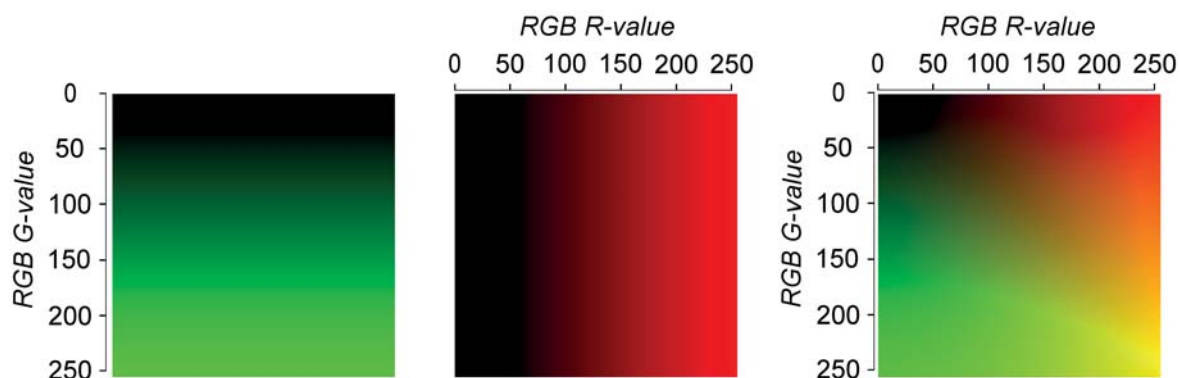

Figure 5.66: RGB colours resulting from the overlay of green (RGB 0/y/0) and red (RGB x/0/0) images (x/y/0) as seen in microscopy overlay images of FITC and RHO channels. Low autofluorescence in the RHO channel is 'masked' by high autofluorescence in the FITC channel that some beads acquire during synthesis. Only beads with a high RGB R-value and a low (ca. <150) RGB G-value are identified as red. This strategy excludes beads with very high green fluorescence and only low red fluorescence.
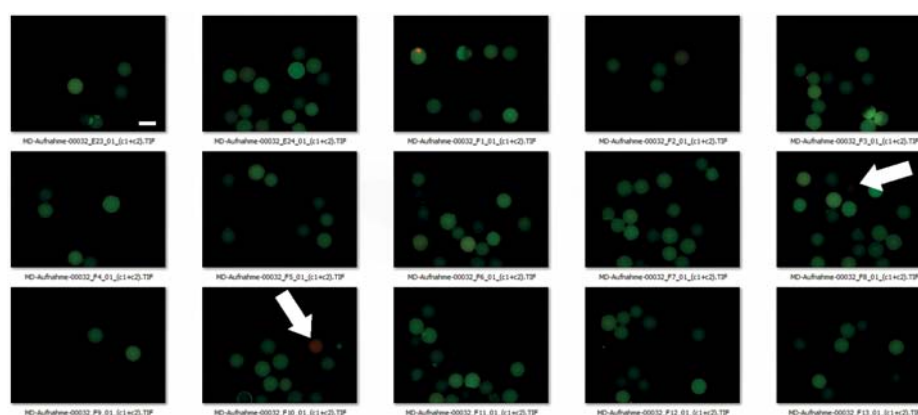

Figure 5.67: Example of the analysis of screening by eye. TentaGel MB HMBA beads from an OBOC peptoid library incubated with 10 μM CXCL8S72C-DL550 **23**, washed and imaged in *ls*-PBS (scale bar: 300 μm, 40 ms exposure time). This is an actual screenshot of images taken from wells of a 384-well MTP as seen in the Windows Explorer®. The red bead in the second picture of the last row is easily identified, another very slightly red bead can be seen in the middle picture on the right (both marked with arrows).

5.4.3 Library Screening Based on Magnetic Selection

The second approach to OBOC library screening relies on the magnetic selection of TentaGel-bound target molecules by CXCL8 immobilized on magnetic particles (see Figure 5.68). Compared to the screening based on fluorescence (see Figure 5.59) less handling and evaluation steps are involved since the identi-

fication and selection of the hits can be achieved in one step. A great challenge in this approach is the control of unspecific interactions between the magnetic spheres and library beads as well as the effective immobilization of CXCL8 onto the magnetic particles.
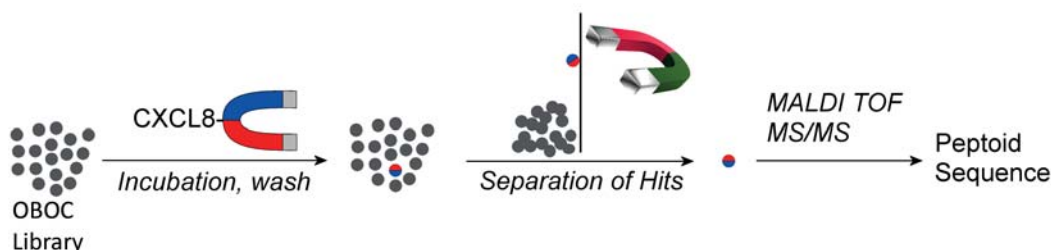

Figure 5.68: Overview of the screening of OBOC libraries based on magnetic properties. OBOC libraries are incubated with CXCL8 immobilized on magnetic particles and washed. The hits are identified and separated in one step. Separated beads are sequenced by MALDI TOF MS/MS. Proportions are not to scale in this figure, the magnetic spheres are 2-3 μm in diameter whilst the OBOC library macrobeads diameter is 300 μm (see Figure 5.69). Therefore several magnetic spheres bind to one macrobead, enhancing the effect of 'magnetization'.

Optimization of Library Screening Parameters

The first step for library screening based on magnetic properties was the effective immobilization of the protein of interest on magnetic spheres. The first approach tested was the immobilization of CXCL8 with an N-terminal hexahistidine tag His$_6$-CXCL8 **22** on magnetic particles with an iminodiacetic acid (IDA) functionality by the formation of an octahedral complex with a copper(II) ion. The 2-3 μm superparamagnetic (M) spheres are based on a polyvinyl alcohol (PVA) matrix with embedded Fe$_3$O$_4$ particles and are therefore called 'M-PVA-IDA'[*]. The particles were loaded with Cu(II) ions (denoted as M-PVA-IDA$^{Cu(II)}$ **34**) and consecutively incubated with N-terminal His-tagged CXCL8 'His$_6$-CXCL8' **22** (denoted as M-PVA-IDA$^{Cu(II)}$:His$_6$-CXCL8 **35**) (see Figure 5.69).

To prove that His$_6$-CXCL8 **22** had been immobilized, the protein was eluted off the magnetic spheres with imidazole which displaced the His$_6$-CXCL8 **22** from the complex. SDS-PAGE (21 % gel) was performed with the supernatant of coordination, washing and elution steps (see Figure 5.70). The SDS-PAGE showed that after incubation of M-PVA-IDA$^{Cu(II)}$ **34** with His$_6$-CXCL8 **22** stock solution (lane 1) the concentration of CXCL8 in the stock solution was decreased (lane 2). After three washing steps no more His$_6$-CXCL8 **22** was detected in the supernatant (lane 5). When treated with elution buffer containing an excess of imidazole, His$_6$-CXCL8 **22** was released from the complex and could be detected in the elution buffer supernatant (lane 6). The immobilization of His$_6$-CXCL8 **22** on magnetic spheres was thus successful.

The immobilization approach with His-tag coordination was further tested for its applicability for Tenta-Gel OBOC library screening. It was investigated by M. Hau in the course of her Bachelor thesis under my supervision[†]. The following paragraph will sum up the results found in the thesis of M. Hau and the conclusions drawn from those results:

A hexahistidine peptide was synthesized on TentaGel HMBA macrobeads with a diameter of 160 μm. The

---

[*]   M-PVA-IDA particles from chemagen were a kind gift from M. Franzreb, Insitute of Functional Interfaces, KIT.

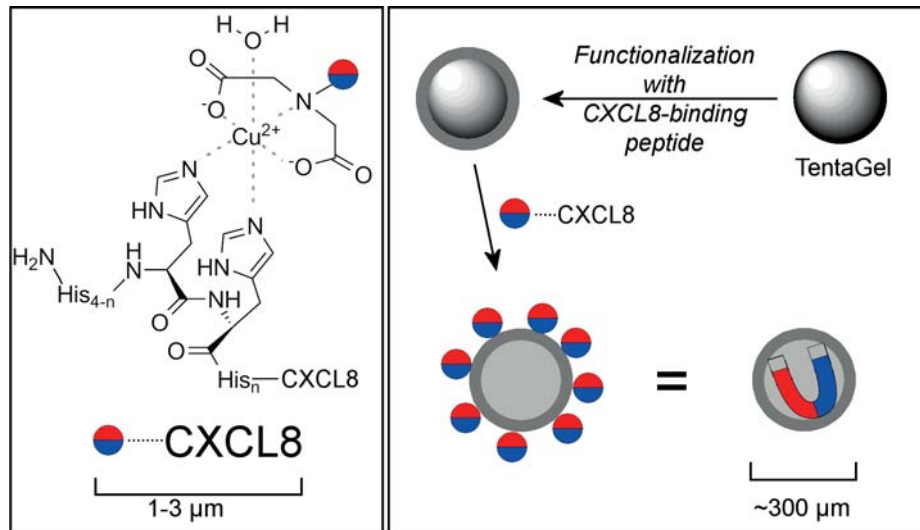[†]   M. Hau, Hochschule Reutlingen 2012, "Screening und Dekonvolution potentieller Interleukin-8 Liganden".

Figure 5.69: Schematic illustration of the immobilization of CXCL8 on magnetic particles by coordination. Left: M-PVA-IDA$^{\text{CuII}}$:His$_6$-CXCL8 **35**, the complex formed between His$_6$-CXCL8 **22** and M-PVA-IDA$^{\text{Cu(II)}}$ **34**. Right: TentaGel MB HMBA beads functionalized with CXCL8-binding peptides bind to several M-PVA-IDA$^{\text{Cu(II)}}$:His$_6$-CXCL8 **35** particles. The result is a TentaGel bead that can be mobilized in a magnetic field.
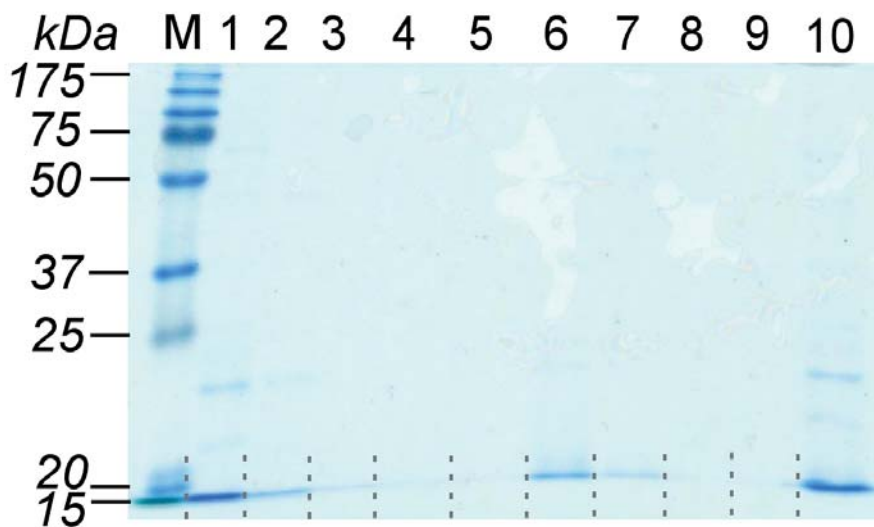

Figure 5.70: 21 % SDS polyacrylamide gel (Coomassie stained) showing the supernatants of coordination, washing and elution of His$_6$-CXCL8 **22** to 1.02 mg M-PVA-IDA magnetic spheres. M=Marker: Prestained Protein Marker, Broad Range 7-175 kDa, (1) and (10) 4 µg His$_6$-CXCL8 **22**, (2) supernatant of M-PVA-IDA$^{\text{Cu(II)}}$:His$_6$-CXCL8 **35**, (3) supernatant of washing step 1 of M-PVA-IDA$^{\text{Cu(II)}}$:His$_6$-CXCL8 **35** with washing buffer, (4) washing step 2, (5) washing step 3, (6) elution step 1 of His$_6$-CXCL8 **22** with imidazole buffer, (7) elution step 2, (8) washing step 1 of M-PVA-IDA$^{\text{Cu(II)}}$ **34**, (9) washing step 2.

complex formed between this His-tag and the M-PVA-IDA$^{\text{CuII}}$ particles (see Figure 5.69) showed high velocity movement when placed in the magnetic field of a small magnet. This proved that the mobilization of TentaGel particles by attachment of small magnetic particles was possible. However two general problems concerning the magnetic spheres were encountered: Firstly, functionalized magnetic particles adhered

persistently to the surface of microcentrifuge tubes forming a thin, largely stable layer. This behaviour interfered with the observation of the beads and led to the use of glassware for separation experiments. Similar unspecific interactions were observed with magnetic spheres and TentaGel-bound peptides. To suppress unspecific interactions 0.3 % BSA were added to buffers. This BSA addition was then found to block all interactions between TentaGel beads regardless of the TentaGel functionalization. Thus, unspecific interactions made it impossible to separate functionalized beads by magnetic particles. Secondly it was found that lose magnetic particles in solution produce a significant current when moving in the magnetic field. This current pulled larger particles like the TentaGel macrobeads alongside the magnetic spheres in the field and thus led to false positive results. Due to these difficulties the ultimate goal of mobilizing TentaGel-CXCR1-p1 particles* could not be achieved.

After the work of M. Hau, a second method for the immobilization of CXCL8 on magnetic particles was tested: the functionalization of the magnetic spheres[†] with thiol-reactive maleimide for the attachment of CXCL8S72C. Compared to the previous method this immobilization is more stable since the protein is covalently bound to the particles instead of being part of a chelate complex which is pH sensitive. Furthermore, by using CXCL8S72C **20** instead of His$_6$-CXCL8 **22**, the attachment of CXCL8 is C-terminal, which leaves the N-terminus accessible. Since the N-terminus rather than the C-terminus plays an important role in CXCL8:CXCR1 interaction and CXCL8-binding peptides like CXCR1-p1 target the N-terminus[42, 145] this form of immobilization is likely to be advantageous.

Carboxy-functionalized magnetic spheres M-PVA were functionalized with mono-Boc-diaminohexane **11**, deprotected and reacted with linker 3-maleimidopropanoic acid N-hydroxysuccinimide ester **26** to give M-PVA-Mal **28** (see Scheme 5.4.1). The quantification of maleimide groups gave 30 $^{\mu mol}$/$_g$ (see Section 7.5). CXCL8S72C **20** was reacted with the maleimide function to give CXCL8-functionalized magnetic particles M-PVA-Mal-CXCL8 **29**.
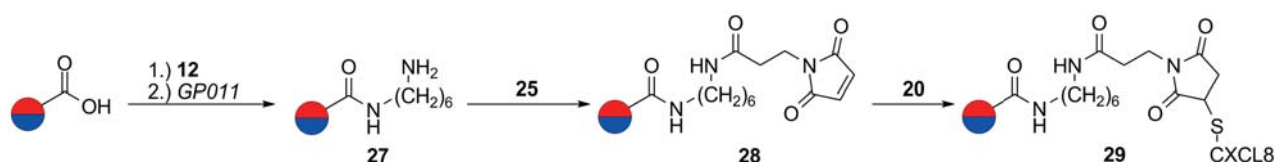
Scheme 5.4.1: Immobilization of CXCL8 on magnetic particles by covalent binding. Magnetic spheres M-PVA were functionalized with N-(6-aminohexyl)-carbamic acid **11**, deprotected according to GP011 and consecutively reacted with 3-maleimidopropanoic acid N-hydroxysuccinimide ester **26** to give maleimide magnetic particles M-PVA-Mal **28**. Thioles like CXCL8S72C **20** can thus be covalently attached.

The screening approach with magnetic particles was tested by preparing a small mixture of 14 TentaGel macrobeads functionalized with peptides FWLDFW **88** and untreated TentaGel beads that was supplemented with two TG-IL8RPLoops particles **85**. After incubation with M-PVA-Mal-CXCL8 **29** TentaGel particles were very carefully transferred into a new vessel to remove the excess of free floating magnetic particles. When the hand magnet was held against the side of the vessel, only two particles could be sep-

---

*   TentaGel-CXCR1-p1: TentaGel macrobeads functionalized by Click chemistry with CXCR1-p1, a peptide based on an N-terminal sequence of CXCR1 that binds CXCL8 with a K_i of 7 µM.[145]

†   M-PVA-COOH particles from chemagen were a kind gift from M. Franzreb, Institute of Functional Interfaces, KIT.
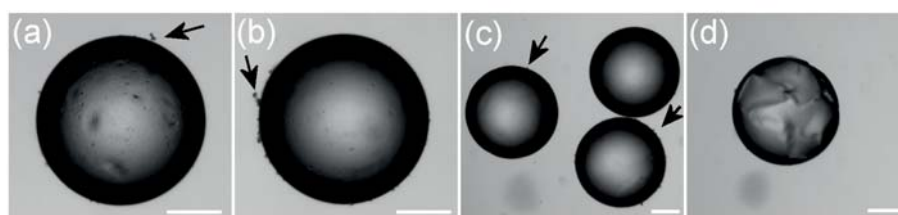
Figure 5.71: Brightfield microscopy images of magnetic particles covalently functionalized with CXCL8 (M-PVA-Mal-CXCL8 **29**) binding to peptides on TentaGel beads, e.g. TG-WFDLWF **88**, AKWRMVLRI-Ahx-ADTLMRTQ TG-IL8RPLoops **85** (scale bar: 100 μm). Magnetic particles **29** can be seen as small dots on the particle surface, some are indicated by black arrows. 14 TentaGel macrobeads functionalized with different peptides were incubated with CXCL8 bound to magnetic particles. (a) and (b) TG-IL8RPLoops **85** particles, that were the only beads that could be separated by a hand magnet out of the mixture. (c) Shows that also beads that were not separated from the mixture can form unspecific interactions with the magnetic particles, indicated by the magnetic particles on the surface. (d) Collapsed beads like the one shown are considerably lighter than normally polymerized beads and in certain cases unspecific interactions with magnetic particles can be sufficient to pull the lighter beads from the mixture leading to false positives.

arated from the mixture. When the particles were observed under the microscope, the seperated particles compared with non-mobilized particles showed the highest amount of bound magnetic spheres (see Figure 5.71). These particles were sequenced by MALDI TOF MS/MS and confirmed to carry IL8RPLoops. This proves that the screening approach is functional. Additionally to the problems observed in the work of M. Hau, another problem with the magnetic screening approach was observed: damaged resin beads with a collapsed structure were considerably lighter than undamaged beads and unspecific interactions with the magnetic sphere were sufficient to lead to the mobilization of those beads (see Figure 5.71d).

Excursus: Functionalization of TentaGel MB and Single-Bead ATR-IR

For on-bead screening with TentaGel MB HMBA it can be convenient to immobilize peptides or peptoids after bulk synthesis rather than performing the synthesis directly on the TentaGel resin. This way, molecules from bulk syntheses may be purified and then immobilized on the bead, e.g. for positive controls. This was achieved by functionalizing TentaGel MB HMBA with 6-aminohexanoic acid and 3-maleimidopropanoic acid N-hydroxysuccinimide ester **26**, so that any molecule with a thiol-group could then be attached to the bead (see Scheme 5.4.2). If the molecule is a substance of high cost or many synthesis steps the analysis of the immobilization should ideally be demonstrated with a minimum amount of beads. When TentaGel was functionalized with 3-maleimidopropanoic acid N-hydroxysuccinimide ester **26** the FT-ATR-IR spectrum showed a clear signal at 1707 cm^{-1} characteristic for maleimidyl groups (see Figure 5.72).[309] The immobilization of CXCL8S72C **20** onto the thiol-active TentaGel particles was shown by staining with primary FITC-antibody and quantified by image analysis (see Figure 5.73). Thus it was found that the analysis of one bead by FT-ATR-IR is possible.
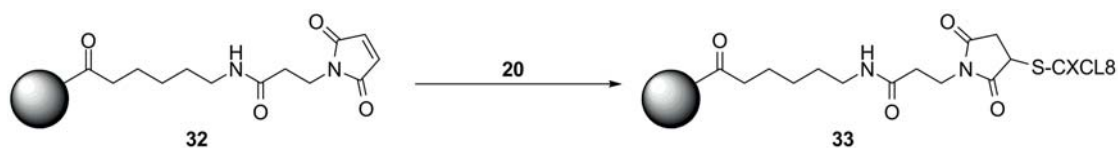
Scheme 5.4.2: Functionalization of TentaGel MB HMBA with 3-maleimidopropanoic acid N-hydroxysuccinimide ester **26** leads to particles that may be used for the immobilization of molecules with thiol groups, e. g. CXCL8S72C **20**.
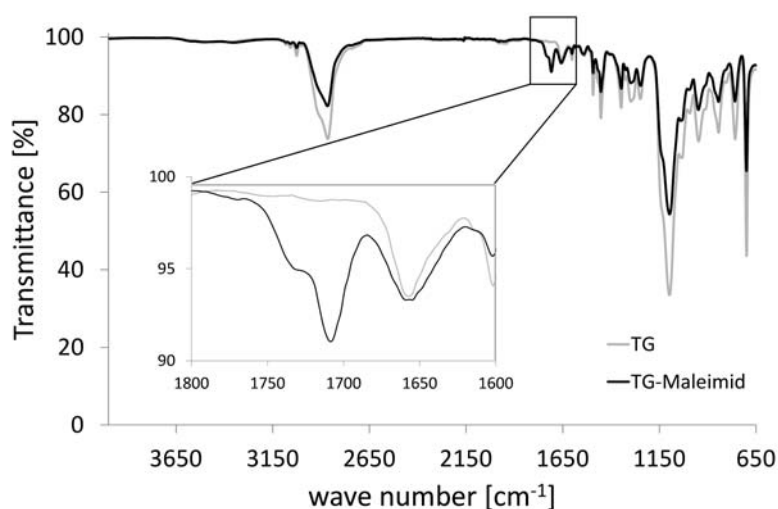

Figure 5.72: The FT-ATR-IR spectrum of a single TentaGel MB HMBA bead functionalized with 3-maleimidopropanoic acid N-hydroxysuccinimide ester **26**. The characteristic antisymmetric stretching of the maleimide group at 1707 cm^{-1} confirms the successful immobilization.
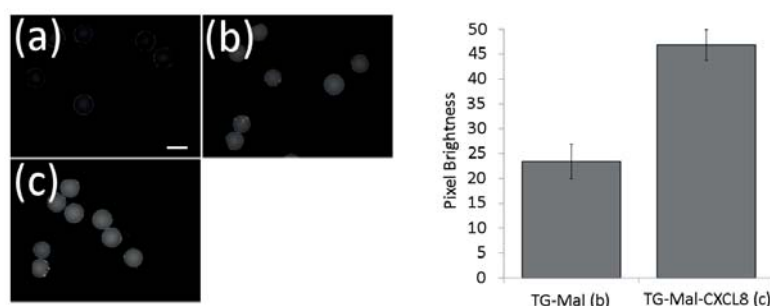
Figure 5.73: Staining of CXCL8 immobilized on TentaGel MB HMBA by primary FITC-antibody . Left: Microscopy images (scale bar: 300 µm, exposure time: 25 ms) (a) Untreated TentaGel MB HMBA show slight autofluorescence in the FITC channel. (b) Maleimide functionalized TentaGel TG-Mal beads **32** show a slightly increased fluorescence intensity after treatment with FITC-anti-CXCL8. (c) TentaGel maleimide particles with attached CXCL8S72C TG-Mal-CXCL8 **33** show increased bead fluorescence intensity after treatment with FITC-anti-CXCL8. Right: ImageJ[298] evaluation of pixel brightness in images (b) and (c).

5.5 CXCL8-Binding Peptoids

With the successful labelling of CXCL8 to give CXCL8S72C-DL550 **23** (see Section 5.1.1) and the synthesis of peptoid OBOC library **104** of 117649 hexamers (see Section 5.4), the optimized screening process based on fluorescence image analysis (see Section 5.4.1) was initiated.

5.5.1 Peptoid OBOC Library Screen

The last step of the mix-and-split routine of library **104** yielded seven 6 mL filter frits (due to the last coupling step of the seven primary amines) with a maximum of 16807 sequences each. The frits were screened individually to keep the number of possible sequences as low as possible and thus simplify sequence identification after screening. Each frit was incubated with 10 μM CXCL8S72C-DL550 **23** in *ls*-PBS. After incubation, the frits were washed three times with *ls*-PBS. The beads were distributed manually into 384-well clear-bottom, black-wall microtiter plates (MTP) and imaged under the fluorescence microscope in the FITC and RHO channel (exposure time: 40 ms). When a red fluorescent bead was detected in the images by eye (see Figure 5.67), the beads of the respective well were individualized by pipetting them into another MTP one by one (see Figure 5.74). This way the red beads could be detected and separated from the rest of the library. The screen yielded 71 TentaGel peptoid particles that showed red fluorescence due to the binding of CXCL8S72C-DL550 **23**.
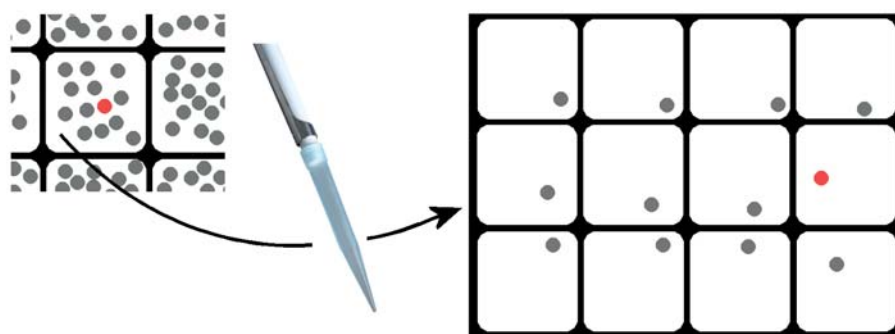

Figure 5.74: After imaging of the library (see Figure 5.59), the beads of the wells of interest containing one or more red beads were individualized by distributing them into a new microtiter plate. The single beads were imaged under the microscope to find the individual red fluorescent bead.

5.5.2 Analysis of Library Hits

The 71 positive TentaGel beads found in the screening process were put in 71 individual microcentrifuge tubes, washed with DCM and dried. The peptoids were cleaved under ammonia atmosphere, dissolved in a 1:1 acetonitrile:water mixture with 0.1 % TFA and diluted with α-cyano-4-hydroxycinnamic acid for MALDI MS measurements. MALDI TOF MS measurements were analyzed between 600-2000 $^m/_z$ to find the peptoid masses. The three highest mass signals detected were then further analyzed by MALDI TOF MS/MS.

To simplify the determination of a sequence out of a multitude of possibilities, an Excel Macro was developed in Visual Basic for Applications (VBA)*. The program 'ChemRetrieve 1.0' is capable of finding possible peptoid sequences of a library by variable primary amine input based on the MALDI TOF MS/MS peaks detected. The program relies on the following equations for the determination of fragment weight. The total weight of the peptoid is determined by:

$$m_{ges} = (m_{monomer,1} + m_{monomer,2} + m_{monomer,3} + \cdots + m_{linker} + 1)\frac{g}{mol} \tag{5.3}$$

with the weight of one monomer n being the weight of the side chain amine n plus 40 g/mol

$$m_{monomer,n} = (m_{amine,n} + 40)\frac{g}{mol} \tag{5.4}$$

and, if present, the 6-aminohexanoic acid linker (with an amide group instead of a carboxyl group due to cleavage conditions)

$$m_{linkerfrag} = (m_{linker} - 2)\frac{g}{mol}. \tag{5.5}$$

The masses of the characteristic B- and Y-fragments of the peptoids are calculated as follows:

$$m_{fragB,n} = \sum_{i}^{n} (m_{fragB,i} + 1)\frac{g}{mol} \tag{5.6}$$

and

$$m_{fragY,1} = (m_{ges} - m_{fragB,n-1} + 2)\frac{g}{mol}. \tag{5.7}$$

The primary amines for synthesis are letter-coded and listed in a permutation matrix. The program has an error function that calculates the deviation of the measured mass spectrometry signal from the calculated peak. The deviations are summed up to give a total error that may be adjusted in order to find a larger set of possible sequences with higher deviations from the measured signals. The signals of the MS/MS spectrum along with the total molecular weight are enlisted, the error coefficient is set and the program is run, giving the list of possible sequences along with their calculated B- and Y-fragments.

Of the 71 red TentaGel beads, 44 peptoid sequences (62 %) were unambiguously identified by MALDI TOF MS/MS, one sequence (**142**) was found twice. Some particles were lost in the separation process before analysis, other spectra could not be interpreted. 14 sequences (**123**-**136**) of the 44 determined sequences consisted only of aromatic side chains and were thus exceedingly hydrophobic. Those peptoids were likely to show a very low bioavailability and they were therefore not investigated any further. The remaining 29 peptoids **137**-**165** were considered peptoids of interest and studied in detail.

To check for hits or false positives **137**-**165** were first re-synthesized on TentaGel MB HMBA. The beads were analyzed by MALDI TOF MS/MS to confirm successful synthesis and the results of the MS/MS spectra

---

* Written by C. Helmer.

were compared to the spectra obtained from the single beads: All spectra were found to be equal, confirming the determination of sequences **137**-**165**. 10 macrobeads of each of the re-synthesized 29 peptoid sequences were then incubated with CXCL8S72C-DL550 **23**, washed and consecutively imaged under the fluorescence microscope. The results showed that not all of the 29 sequences of interest bound to CXCL8S72C-DL550 **23** in this re-screening experiment. Peptoids **154** and **157**-**164** did not bind CXCL8S72C-DL550 **23** at all, peptoids **155** and **156** show reduced binding affinities (see Figure 5.75). When comparing peptoid sequences, it is obvious that the non-binding peptoids **154** and **157**-**164** all contain one or more tryptamine side chain, which is also the reason for the high fluorescence in the FITC channel compared to other sequences (see Section 5.3.2). This shows that the library screening in the RHO channel is not beyond error and tryptamine-containing sequences can cause problems due to unspecific interactions. Peptoids **137**-**153** and **165** were thus confirmed as the 18 hits of library **104**. The discovery of these 18 hits is summarized in Figure 5.76. The 18 sequences discovered show a high amount of basic 1,4-diaminobutane side chains ($Nlys^{+0}$) (see Table 5.5). This is interesting since CXCL8 is a basic polypeptide with a pI of 9.0.[310] This excludes the possibility of the CXCL8:peptoid interaction consisting purely of unspecific electrostatic interactions.
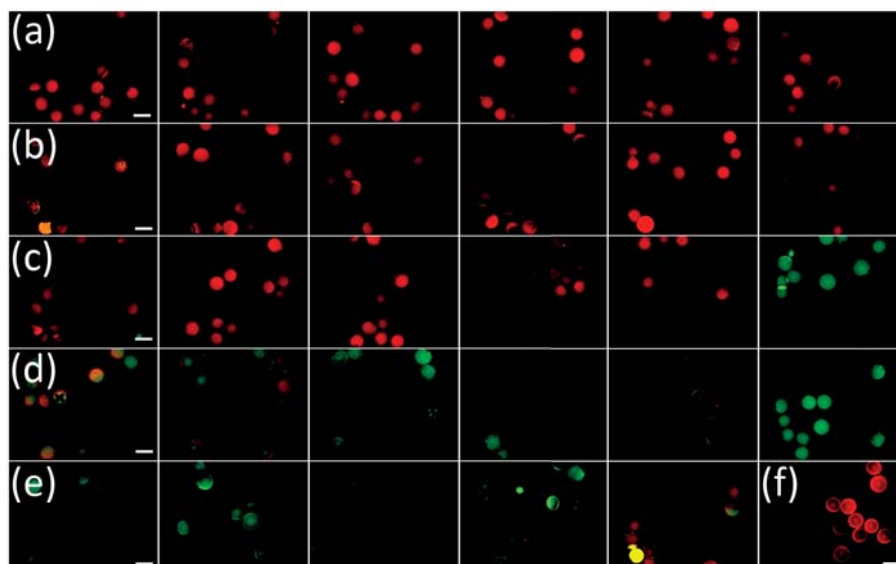

Figure 5.75: Re-screening of peptoids **137**-**165** with CXCL8S72C-DL550 **23** (scale bar 300 μm, exposure time 80 ms). The mix of FITC and RHO channel images are shown. Peptoids are listed from left to right. (a) Peptoids **137**-**142**, (b) Peptoids **143**-**148**, (c) Peptoids **149**-**154**, (d) Peptoids **155**-**160**, (e) Peptoids **161**-**165**, (f) Positive control: TG-IL8RPLoops **85**. Peptoids **154** and **157**-**164** show no binding to CXCL8S72C-DL550 **23**. Peptoids **155** and **156** show reduced binding to CXCL8S72C-DL550 **23**.
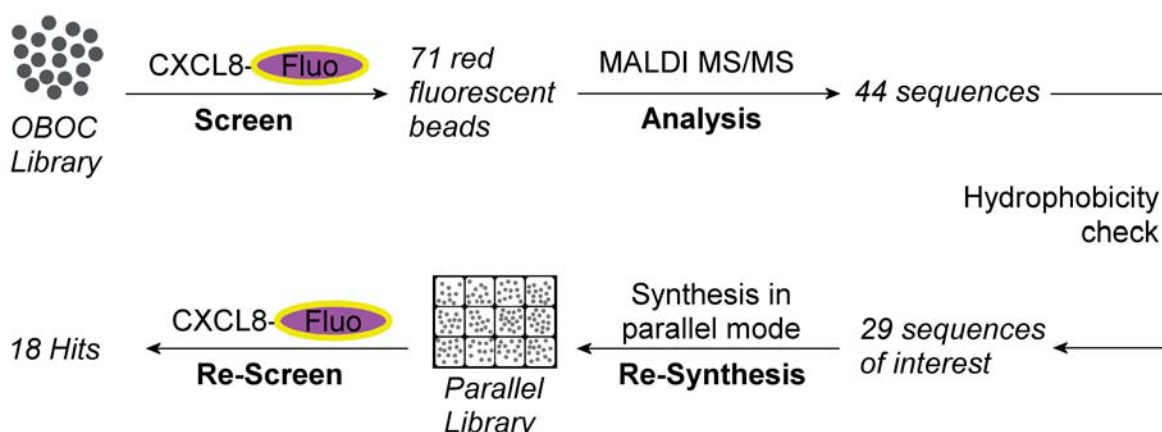
Figure 5.76: Summary of the discovery of 18 peptoid 'hit' sequences of library **104** that bind CXCL8S72C-DL550 **23** as described in this and the previous section.

Table 5.5: Sequences of the 18 peptoid hits **137**-**165** discovered in the screening process (see Figure 5.76).

Hit Number	Peptoid Number	Sequence
1	**137**	H_2N-Ahx-Nlys^{+0}Nlys^{+0}Nlys^{+0}Nval^{+0}Nleu^{+0}Nser^{+1}-H
2	**138**	H_2N-Ahx-Nlys^{+0}Nlys^{+0}Nlys^{+0}Nleu^{+0}Nval^{+0}Nasp^{+0}-H
3	**139**	H_2N-Ahx-Nlys^{+0}Nlys^{+0}Nser^{+1}Nlys^{+0}Nlys^{+0}Nleu^{+0}-H
4	**140**	H_2N-Ahx-Nlys^{+0}Nlys^{+0}Nleu^{+0}Nlys^{+0}Nval^{+0}Nleu^{+0}-H
5	**141**	H_2N-Ahx-Nlys^{+0}Nlys^{+0}Nval^{+0}Nlys^{+0}Nphe^{+1}Nleu^{+0}-H
6	**142**	H_2N-Ahx-Nlys^{+0}Nlys^{+0}Nval^{+0}Nleu^{+0}Nleu^{+0}Nleu^{+0}-H
7	**143**	H_2N-Ahx-Nlys^{+0}Nlys^{+0}Nval^{+0}Nlys^{+0}Nphe^{+1}Nasp^{+0}-H
8	**144**	H_2N-Ahx-Nlys^{+0}Nlys^{+0}Nphe^{+1}Nlys^{+0}Nphe^{+1}Nleu^{+0}-H
9	**145**	H_2N-Ahx-Nlys^{+0}Nleu^{+0}Nlys^{+0}Nlys^{+0}Nphe^{+1}Nasp^{+0}-H
10	**146**	H_2N-Ahx-Nlys^{+0}Nleu^{+0}Nlys^{+0}Nphe^{+1}Nlys^{+0}Nasp^{+0}-H
11	**147**	H_2N-Ahx-Nleu^{+0}Nlys^{+0}Nlys^{+0}Nleu^{+0}Nlys^{+0}Nleu^{+0}-H
12	**148**	H_2N-Ahx-Nleu^{+0}Nlys^{+0}Nlys^{+0}Nval^{+0}Nphe^{+1}Nasp^{+0}-H
13	**149**	H_2N-Ahx-Nleu^{+0}Nleu^{+0}Nlys^{+0}Nlys^{+0}Nphe^{+1}Nasp^{+0}-H
14	**150**	H_2N-Ahx-Nval^{+0}Nlys^{+0}Nlys^{+0}Nphe^{+1}Nlys^{+0}Nleu^{+0}-H
15	**151**	H_2N-Ahx-Nphe^{+1}Nlys^{+0}Nlys^{+0}Nleu^{+0}Nlys^{+0}Nleu^{+0}-H
16	**152**	H_2N-Ahx-Nphe^{+1}Nlys^{+0}Nlys^{+0}Nval^{+0}Nphe^{+1}Nasp^{+0}-H
17	**153**	H_2N-Ahx-Nphe^{+1}Nlys^{+0}Nser^{+1}Nlys^{+0}Nval^{+0}Nleu^{+0}-H
18	**165**	H_2N-Ahx-Nphe^{+1}Ntrp^{+1}Nphe^{+1}Ntrp^{+1}Nphe^{+1}Nlys^{+0}-H

5.5.3 Affinity of CXCL8-binding Peptoids

All 18 hits (peptoids **137**-**165**) of library **104** (see Table 5.5) were re-synthesized without 6-aminohexanoic acid linker on 2-chlorotrityl-chloride resin, labelled with 5(6)-carboxyfluorescein and purified by HPLC to give fluo-peptoids **167**-**184**[*]. Peptoids were analyzed by MALDI TOF mass spectrometry. Peptoids were weighed and dissolved in *ls*-PBS to give 1000 μM or 100 μM stock solutions. Binding affinities of peptoids

---

[*]   Purification by HPLC executed by K. Brahm

167-**184** for CXCL8 were determined by fluorescence anisotropy measurements (see Appendix Section 9 for binding curves).

K_d values were calculated using SigmaPlot one-site saturation ligand binding regression. Experiments were repeated between two and four times. The values varied considerably in some cases but all K_d values were found between ca. 10 and 100 µM. Peptoids **167**, **168** and **174** showed the highest affinities for CXCL8 (see Table 5.6).

Table 5.6: K_d values of the binding of the fluorescently labelled equivalents **167**-**184** of the 18 peptoid hits **137**-**165** (see Table 5.5) to CXCL8 in *ls*-PBS.

Peptoid	$K_d \pm$STD [µM]	Peptoid	$K_d \pm$STD [µM]	Peptoid	$K_d \pm$STD [µM]
167	11.6±1.8	**173**	19.0±2.4	**179**	71.4±35.3
168	20.0±2.9	**174**	16.7±4.8	**180**	51.1±15.4
169	42.9±9.2	**175**	25.0±7.4	**181**	39.8±13.9
170	65.3±1.3	**176**	43.3±5.1	**182**	35.4±10.9
171	41.4±17.6	**177**	47.6±12.8	**183**	21.4±6.1
172	57.2±19.7	**178**	112.3±36.1	**184**	27.6±6.4

5.5.4 Biological Activity of CXCL8-binding Peptoids

Before testing the biological activity of peptoids **167**-**184** peptoid toxicity was investigated. Peptoids were diluted in 384-well black MTP and human neutrophil granulocytes were added to the dilutions. After incubation cells were stained with resazurin and incubated overnight before measuring fluorescence intensity. Results show, that none of the tested peptoids have a toxic effect on human neutrophil granulocytes even at concentrations above 50 µM (see Appendix Section 9). **180**, **181** and **184** were not tested, they were lacking in quantity. Resazurin fluorescence intensity increased at high concentrations of peptoids **170**, **171** relative to the control with untreated cells (see Figure 9.8). This points to increased resazurin reduction rates in the peptoid-treated cells. The mechanism of resazurin reduction is not fully understood: some resazurin fluorescence was found in the nucleus and cytoplasms of stained cells but it is still not clear, whether reduction occurs in the medium or inside the cells.[311] If reduction occured inside the cells, the peptoids might have served as transporters[246, 247] and increased the amount of resazurin available for reduction which could have led to increased fluorescence intensity of the samples. This is further supported by the positive charge of the tested peptoids, which is a characteristic feature for peptoid transporters.

The influence of peptoids **167**-**184** on CXCL8-induced actin polymerization in human neutrophil granulocytes was investigated. A momentary increase in actin polymerisation is a characteristic response to stimulation with chemoattractants. Cells were stimulated with 11.93 nM CXCL8 and mixtures of 11.93 CXCL8 and potential peptoid inhibitors (12 µM or 24 µM). Equal portions of the suspension of stimulated cells were fixed with formaldehyde at different timepoints of 0-300 seconds after stimulation. After permeabilization of the cells F-actin content was visualized by phalloidin-iFluor555 fluorescence staining. A positive control of stimulation with CXCL8 and a negative control of stimulation with medium was included in every 96-well black assay plate (see Figure 5.77). All assays shown displayed a CXCL8 signal and no signal from the medium alone. When cells were stimulated with a mixture of peptoid and CXCL8

four peptoids showed an influence on phalloidin-iFluor555 fluorescence compared to the CXCL8 signal: **174**, **180**, **181** and **182** (see Appendix Section 9).
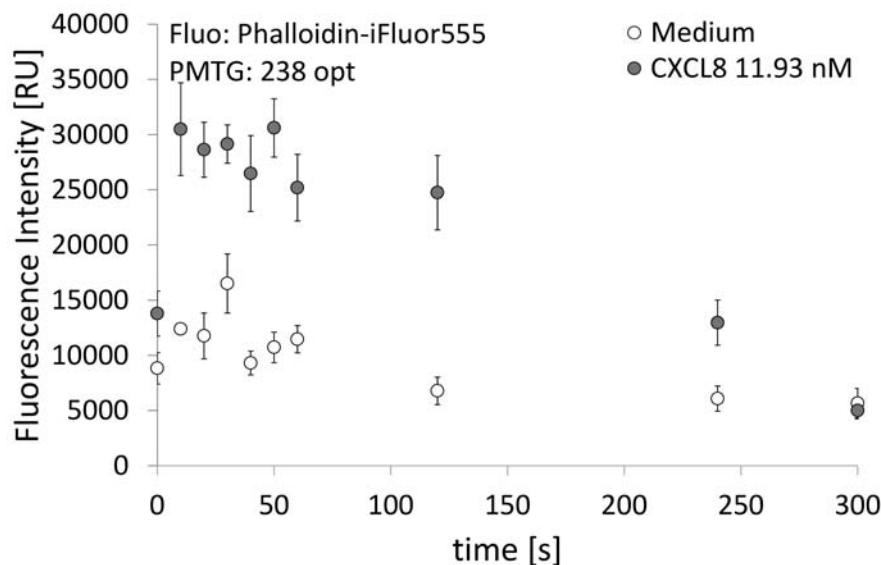

Figure 5.77: Actin polymerisation assay with human neutrophil granulocytes stimulated with CXCL8wt **19** in RPMI$_{(-)}$. The difference between stimulated and unstimulated cells is observed in fixed, permeabilized cells stained by phalloidin-iFluor555 (0.24 $^{ng}/_{mL}$).
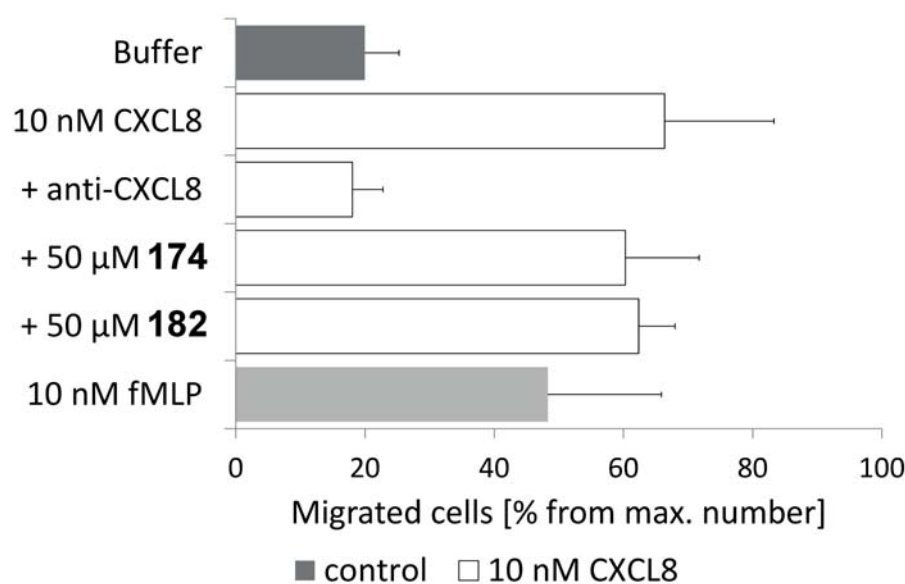

Figure 5.78: Human neutrophil migration assay in 24-well Transwell plates with peptoids **174** and **182**. Both peptoids show no inhibition of CXCL8-induced migration.

Peptoids **174** and **182**, the two peptoids with the lowest K_d values (see Table 5.6) that showed activity in the actin polymerization assay were further tested in a Transwell migration assay. Mixtures of chemoattractant (10 nM CXCL8 or 10 nM fMLP) and peptoids (50 µM) were placed in the lower cavity of a Transwell chamber and human neutrophil granulocytes were placed in the upper cavity. After 1.5 h incubation the cells that had reached the lower cavity were stained with resazurin and incubated for 5 h.

Resazurin fluorescence intensity was measured to determine the number of cells that had migrated into the lower cavity. All three assays with independent donors showed the same result: peptoids **174** and **182** did not inhibit CXCL8-induced migration. Since peptoid concentrations were varied between 50 µM and 100 µM but showed the same results, just one assay is shown (see Figure 5.78).

6 Discussion and Outlook

The aim of this work was to find novel CXCL8-binding peptides and peptoids that suppress CXCL8 function. A fluorescence anisotropy assay was established for ligand-binding studies. Different CXCL8 variants were tested in this assay, and the influence of Triton X-100 on the measurements was studied. The proposition of a model for the interaction of CXCL8 with its receptor CXCR1 developed in cooperation with J. A. R. Dalton in the group of J. Giraldo (UAB Barcelona) laid the foundation for the rational design of the CXCL8-binding peptide 'IL8RPLoops'. The peptide derived from regions near extracellular domains ECD3 and ECD4 of CXCR1 proved to effectively capture fluorescently labelled CXCL8 on the surface of TentaGel resin beads. IL8RPLoops was also shown to bind to CXCL8 immobilized on glass in a protein pattern ('biobitmap') and to successfully inhibit neutrophil migration in Transwell assays. Peptoid parallel synthesis on TentaGel resin and analysis by MALDI TOF MS/MS were tested and established. A small 16-membered peptoid library was synthesized by the mix-and-split method and peptoid sequences were unambiguously identified thus showing the successful combination of combinatorial synthesis and analysis by mass spectrometry. IL8RPLoops served as a positive control for on-bead screening of peptoid OBOC libraries on TentaGel resin with fluorescently labelled CXCL8 in an image-analysis based screening process. Sequences of peptoid hits were determined by MALDI TOF MS/MS spectrometry and re-synthesized in bulk. Peptoids were then tested for their binding affinity in fluorescence anisotropy measurements with CXCL8. The most promising peptoids with the highest affinities were tested for their activity *in vivo* by actin polymerization and Transwell assay. In addition, a screening method based on magnetic separation was tested, whose applicability was proven by initial experiments.

This work led to the discovery/design of a novel CXCL8-binding peptide that poses an interesting lead structure for drug discovery and may be further tested for its effect on the function of different chemokines. A method for the screening of peptoid on-bead libraries based on image-analysis was established, and the screening of a 117649-member peptoid library yielded 18 peptoids that bind to CXCL8. The discovered peptoid-sequences are an interesting starting point for the development of chemokine-inhibitors and additional studies and development of their structure and rigidity may be done to improve their activity.

6.1 Setup of Fluorescence Anisotropy Assay

Fluorescence anisotropy measurements are a widely used method for the determination of protein-protein and protein-ligand interactions.[211, 312–314] Conditions for fluorescence anisotropy measurements in this work were tested with CXCR1-p1, a peptide previously reported to displace CXCL8 from its receptors CXCR1/2 on neutrophil membranes with $K_i = 7$ µM.[145] The addition of Triton X-100 prevented the peptide from adhering to the MTP surface, which led to quenching of fluorescence intensity and increased anisotropy values. If the fluorescence intensity changed during anisotropy measurements, K_d values were corrected with the Method of Dandliker *et al.*.[212, 213] Without addition of Triton X-100 the determination of K_d for

0 min incubation time gave 39.5 ± 11.8 μM and 48.1 ± 14.3 μM when corrected according to Dandliker. At longer incubation times the fluorescence intensities of dilutions with low fluorophore concentrations were severely quenched and the determination of K_d led to high values with high standard deviations: 47.8 ± 11.7 μM and 57.8 ± 22.7 μM. Upon addition of Triton X-100 the binding curves became more stable over the same range of incubation times. However, higher concentrations of Triton X-100 led to quenching effects, probably due to the incorporation of the fluorophores into micelles. The critical micelle concentration (cmc) of Triton X-100 is 240 μM (0.0145 % v/v) in water,[270] and likely varies slightly in salt buffers. With 10.0 μM Triton X-100 (0.0007 % v/v) an average corrected K_d for three incubation times of 12.6 ± 3.8 μM was determined. For 1.65 mM Triton X-100 (0.1 % v/v) the average corrected K_d was 21.0 ± 5.3 μM. This test showed, that the addition of Triton X-100 can be essential for the measurement of well-shaped binding curves. It is likely that hydrophobic peptides preferably adhere unspecifically to the polystyrene surface of microtiter plate (MTP). The GRAVY (Grand Average of Hydropathicity, ExPASy[18]), where the hydropathic values according to Kyte and Doolittle[315] are summed and devided by the number of amino acids in a sequence, determines the hydrophathicity of a peptide. A negative value points to a hydrophilic, a positive value points to a hydrophobic sequence. CXCR1-p1 without 6-aminohexanoic acid linker and fluorescein label possesses a GRAVY of -1.275 and is rather hydrophilic. It is thus not clear why that peptide shows a tendency to adhere to MTP. The role of Triton X-100 in fluorescence intensity and anisotropy measurements was further investigated (see next Section).

6.2 Influence of Triton-X 100 on Fluorescence Anisotropy Measurements

Unspecific interactions pose a problem in fluorescence anisotropy binding assays (see also previous Section) and the addition of Triton X-100 has been recommended to improve assay results.[316] Triton X-100 as a non-ionic, non-denaturing, PEG-based detergent is supposed to suppress interactions of proteins with hydrophobic surfaces like the walls of MTP. Triton X-100 has been reported to exclusively bind hydrophobic proteins and prevent aggregation of small molecules and is therefore added to various binding assays.[269, 271] The influence of Triton X-100 on the fluorescence anisotropy measurements was investigated. In this work it was confirmed that Triton X-100 prevents CXCL8S72C-DL550 **23** adhering to the wall of the MTP. When mixed with different concentrations of Triton X-100, CXCL8S72C-DL550 **23** fluorescence intensity showed a dramatic increase at approximately 10 μM (0.0007 % v/v) Triton X-100 in *ls*-PBS. This increase was also observed for other fluorescently labelled structures like peptides and peptoids and always occured at the same Triton X-100 concentrations. This points to Triton X-100 covering the surface of the MTP with its aromatic ring, exposing the PEG chains into the well thus preventing unspecific interactions. At high Triton X-100 concentrations however, the fluorescence intensity of the fluorophores decreased. This could point the the incorporation of proteins or fluorophores into micelles. A possible interaction between Triton X-100 and proteins may also interfere with the binding to the protein or protein ligand. In measurements with fluorescently labelled CXCL8, Triton X-100 also significantly decreased the dynamic range of the anisotropy assay by causing considerably higher anisotropy values of the free fluorophore. High concentrations of Triton X-100, i.e. concentrations above the cmc (240 μM, 0.0145 % v/v) are therefore not advised.

6.3 CXCL8 Variants and CXCL8 Dimerisation

The monomer/dimer equilibrium of CXCL8 can influence binding assays and complicate kinetics: a ligand can influence the equilibrium by interacting with parts of CXCL8 that are close to the dimerisation site, thereby preventing dimerisation, or ligand interaction may only be possible with the dimer. The dimerisation constant of CXCL8wt **19** was reported to be between 0.1 μM and 20 μM, depending on assay conditions.[46–48] The capability of CXCL8 and related chemokines to form homodimers[25,28] raised the question whether monomeric or dimeric CXCL8 is the active form of the protein capable of activating its receptor CXCR1. The first dimerisation experiments yielded a K_d of 18 ± 6 μM for CXCL8 which is too high to be relevant *in vivo*.[47] Studies with CXCL8L25NMe[49] a trapped monomer form of CXCL8 showed that CXCL8 binds the N-terminal region of CXCR1 as a monomer.[48] The trapped monomer CXCL8L25NMe was more active than the trapped dimer CXCL8R26C in calcium-mobilization and in chemotaxis of human neutrophils.[52] In an NMR binding study of the trapped monomer CXCL8(1-66), the trapped dimer CXCL8R26C and CXCL8wt **19**, only the monomer was capable of binding the N-terminus of rabbit CXCR1(11-34).[53] Further NMR studies suggested that human CXCR1(1-38) binds the CXCL8 monomer with a 1:1 stochiometry.[27] Another aspect of dimerisation is the fact, that only dimeric CXCL8 binds to glycosaminoglycans (GAG) on the endothelium.[288] The binding to GAG enables the formation of a stable gradient with localized high concentrations of CXCL8.[24,61,62] In this work, CXCL8L25Y/V27R **21**, a mutant that was reported to be 'still monomeric at 10 μM'[56,57] was studied for its applicability in fluorescence anisotropy measurements. The K_d under conditions employed in this work was determined by fluorescence anisotropy measurements with CXCL8S72C-DL550 **23** in *ls*-PBS to be approximately 2 μM. The CD spectrum of CXCL8L25Y/V27R **21** in ls-PBS revealed that this variant does not display the characteristic CXCL8wt **19** CD-spectrum and appears to possess a significantly altered three-dimensional structure. If the dimerisation site is conserved in the mutated CXCL8 variant, the mutations at the dimer interface K23 to E29 of CXCL8[28] should prevent dimerisation with a *wild type* sequence of CXCL8. The heterodimerisation of CXCL8L25Y/V27R **21** and CXCL8S72C-DL550 **23** however showed the same dissociation constant as the binding of CXCL8wt **19** to CXCL8S72C-DL550 **23**: approximately 2 μM in *ls*-PBS. CXCL8L25Y/V27R **21** is therefore not an ideal variant for CXCL8 monomer/dimer studies. For future experiments, another CXCL8-variant, e. g. CXCL8(1-66), should be expressed and tested for its folding by CD and its dimerisation constant should be determined. Any potential CXCL8 ligand can then be tested for its inhibitory effects on monomeric CXCL8 as well as CXCL8wt **19**. Differences in affinities or inhibitory effects between monomeric and *wild-type* CXCL8 can point to the inhibitor interfering with the CXCL8 monomer/dimer equilibrium. A ligand that would keep CXCL8 from dimerising without interfering with receptor binding could bring new insights into the question of monomer/dimer potency *in vivo* and the influence of CXCL8 dimerisation on CXCL8:GAG interactions could be studied further.

6.4 Proposed Model of CXCL8:CXCR1 Interaction

The N-terminus and especially the ELR-motif (amino acids 4-6) of CXCL8 were found to be important for receptor activation.[29,30,282] A two-site binding model that involves the interaction of CXCL8 N-loop and CXCR1 N-terminus (site I) and the interaction of the ELR motif the regions of ECD3 and ECD4 (site

II) was proposed.[41–43, 285, 286] The model is in accordance with early studies that suggested an interaction between the ELR-motif and residues R199, R203 and D265 of CXCR1.[31, 40] Recently a model of the CXCL8:CXCR1 complex in a lipid bilayer was proposed by Liou *et al.*.[289] The model was based on rigid docking of CXCL8 to CXCR1 followed by MD simulation to optimize the docking. It resulted in monomeric CXCL8 binding the receptor mainly with its N-loop and the C-terminal α-helix. There are however several problems with the reported approach. Firstly, the structure of CXCR1 in the database[274] misses the N-terminus (1-29) and was homology modelled after the N-terminus of bovine rhodopsin, a well-described G-protein coupled receptor (GPCR).[317, 318] Rhodopsin is not an ideal choice since it possesses only 21 % sequence homology to CXCR1 for the whole sequence and 23 % to the N-Terminus (1-29) in particular. Furthermore rhodopsin has a covalently attached ligand deep in its binding pocket and as opposed to chemokine receptors does not bind diffusible ligands *in vivo*. Secondly, due to the rigid docking approach the receptor does not change its conformation and there is no indication it does so after MD simulation, either. This is unlikely since it is widely accepted that GPCRs change their conformation to an active state during binding of the ligand.[319] Thirdly, one aspect of chemokine function *in vivo* is the tethering of the C-terminal α-helix to glycosaminoglycans (GAG) on the cell surface, e. g. on endothelial cells.[22–24] This interaction may help in forming stable chemokine gradients on the endothelium to guide neutrophils to the source of inflammation. The C-terminal α-helix binding CXCR1 as proposed by Liou *et al.* is not in accordance with this concept. NMR studies previously suggested that the α-helix of CXCL8 was involved in binding,[26] experimental studies with truncated CXCL8 sequences showed however, that the α-helix was not necessary for receptor binding.[29, 39]

In this work, a flexible protein-protein docking of CXCL8 to CXCR1 was simulated in cooperation with J. A. R. Dalton in the group of J. Giraldo of the Institute of Neuroscience at the UA Barcelona. CXCR1 and CXCL8 structures were taken from the Research Collaboratory for Structural Bioinformatics Protein Data Bank (RCSB PDB[320]). The NMR-structure of CXCR1[274] was extended to include the missing N-terminal part (residues 1-28) and the monomer of the crystal structure of CXCL8[28] was positioned relative to CXCR1 according to the interaction of CXCR1-p1 (peptide based on the CXCR1 N-terminus reported by Attwood[145] and modelled in complex with CXCL8 by Skelton[42]) with CXCL8. Missing residues 1-4 (SAKE) of CXCL8 were attached in such a way that they were close to extracellular parts of CXCR1 to enable possible interactions. During flexible docking, transmembrane helix 7 (TMH 7) of CXCR1 was tilted slightly to accomodate CXCL8 binding. In this 'active-like' conformation of CXCR1, E275 in TMH 7 forms two novel, strong hydrogen bonds with T34 at the N-terminus of CXCR1. It was previously reported, that when E275 was changed to alanine, all binding of radiolabelled CXCL8 was lost.[40] Since a two-site mechanism for CXCL8:CXCR1 binding that involves the interaction of several different amino acids on both sides was proposed, this drastic effect of one amino acid change seems surprising. This could point to the fact that either the receptor is completely misfolded or without E275 the active-state of the receptor cannot be stabilized and the ligand CXCL8 cannot bind. This would further validate the proposed model and the 'active-like' conformation of CXCR1. In the final structure of the CXCR1:CXCL8 interaction, residues E4 and R6 of the ELR motif at the N-terminus of CXCL8 interact with the essential receptor residues R203 (ECD3) and D265 (TMH6), while E29 of the CXCL8 30S loop interacts with R199 (TMH5) of CXCR1. The model is in excellent accordance with numerous experimentally studies on CXCL8:CXCR1 interactions reported by various groups. In this model, CXCL8 can only bind as a monomer, which supports

the notion of the monomer being the active species *in vivo*.[27,47–49] An important feature of chemokine gradient formation *in vivo* is the interaction with GAG on the endothelium. Interactions according to the proposed model should enable binding to GAG at the C-terminus of CXCL8 while interacting with the receptor at the N-terminus.

6.5 Rational Design of CXCL8-Binding Peptide

The herein proposed model of CXCL8:CXCR1 interaction led to the design of a peptide derived from the CXCR1 sequence, that comprises of a part of TMH5/ECD3 and of ECD4/TMH6 linked by 6-aminohexanoic acid. The peptide was shown by circular dichroism (CD) spectroscopy to retain the helical structure of its scaffold as well as the spatial orientation of amino acid residues to a large extent (MD simulation). The peptide, called IL8RPLoops, was found to bind CXCL8 with a K_d of $0.5 \pm 0.3\,\mu$M. CXCR1-p1, a peptide derived from the N-terminus of CXCR1 previously reported by Attwood *et al.*[145] showed a lower K_d of approximately 10 μM. IL8RPLoops shows low toxicity on human neutrophils, causing the death of 50 % of the cells at a concentration of around 1000 μM. IL8RPLoops was shown to significantly inhibit neutrophil migration in a Transwell assay. Fluorescence microscopy of cells treated with CXCL8S72C-DL550 **23** displayed a significantly lower amount of fluorescence in the RHO channel when treated with a mixture of CXCL8S72C-DL550 **23** and IL8RPLoops. This suggested that IL8RPLoops either prevents the binding of CXCL8 to its receptor or interferes with receptor internalisation. The same effect was observed when analyzing HEK293 cells stably transfected with CXCR1 treated with CXCL8S72C-DL550 **23** and a mixture of Fluo-IL8RPLoops and CXCL8S72C-DL550 **23** by FACS. FACS experiments also showed no unspecific interaction of IL8RPLoops with the cells, ruling out the possibility of Fluo-IL8RPLoops interacting with CXCR1. Fluo-IL8RPLoops was also shown to bind to CXCL8S72C-DL550 **23** immobilized on glass. CXCL8S72C-DL550 **23** was immobilized by maskless photolithography[296] and consecutively stained with IL8RPLoops. The immobilization relies on the bleaching of the fluorophore at the C-terminus of CXCL8. The immobilization at the C-terminus is similar to the orientation *in vivo*, when CXCL8 binds to GAG on the surface of endothelial cells. With its C-terminus tethered, the N-terminus of the chemokine is still accessible for interactions with receptors like CXCR1. It is therefore likely, with the C-terminus of the chemokine facing the glass surface, that Fluo-IL8RPLoops binds at the region of the CXCL8 N-terminus facing away from the glass. A computer-simulated model for the CXCL8:IL8RPLoops interaction was suggested that placed the peptide similar to the position of the protein scaffold in the CXCL8:CXCR1 complex. The original interactions of the ELR motif of CXCL8 with R199, R203 and D265 (equal to R4, R8, D12 of the peptide) were retained. The N-terminus of CXCL8, peptide CXCL8(1-10), competed with CXCL8 for the binding to IL8RPLoops (IC_{50} between 25 μM and 50 μM). The N-terminus of CXCL8 as well as CXCL8(1-10) are both unstructured, and an interaction of IL8RPLoops with both structures could therefore be likely. This was the first experimental hint for the interaction at the N-terminus.

In fluorescence anisotropy measurements of IL8RPLoops binding to CXCL8, anisotropy values at high CXCL8 concentrations decreased to give the binding curve a bell-shape. The decomposition or unfolding of CXCL8 upon IL8RPLoops addition was ruled out by CD measurements. The decrease of anisotropy may be explained by IL8RPLoops interfering with the CXCL8 monomer/dimer equilibrium: CXCL8 dimerisation and CXCL8:Fluo-IL8RPLoops possess K_d values in the same order of magnitude, 2 μM and 0.5 μM. At CXCL8 concentrations above 2 μM, the dimer becomes the predominant species in so-

lution. If Fluo-IL8RPLoops only binds the monomeric form of CXCL8, the binding curve will decrease for high concentrations of CXCL8 dimer. Taken all the data together, a new promising CXCL8 inhibitory peptide was developed that should be further investigated. Future binding experiments should be conducted with a CXCL8 mutant without ELR motif to see if the ELR motif indeed is the major site of interaction. Mutations in the peptide sequence could also identify peptide residues essential for interaction with CXCL8. Also, increased rigidity through peptide cyclisation could increase the affinity of IL8RPLoops for CXCL8. Binding experiments with non-dimerising variants of CXCL8, e. g. CXCL8(1-66), and Fluo-IL8RPLoops should be performed to show that binding curves do not display a bell-shaped curve, when CXCL8 does not dimerize. This would be further proof to IL8RPLoops only binding the monomeric form of CXCL8 with high affinity. The kinetics of IL8RPLoops interaction with CXCL8 monomer/dimer should be described in a mathematical model to accurately describe the influence of protein dimerisation on binding curves. Since a considerable number of all proteins in different species form homodimers[321] an accurate binding model for ligands interfering with homodimerisation is of high interest. To make IL8RPLoops stable against proteases, its sequence could be translated into a peptoid sequence and tested for its binding affinity.

6.6 Synthesis of Peptoid One-Bead-One-Compound Libraries

Peptoids are peptidomimetics that were first reported in 1992.[217,218] They may be synthesized on resin by solid phase peptide synthesis- (SPPS) like monomer-based synthesis or by submonomer synthesis, in which secondary amines are acetylated with bromoacetic acid and bromine is subsituted by the next primary amine. They may be analyzed by Edman degradation[322] or partial Edman-degradation (protein ladder sequencing[174]) coupled with MALDI TOF MS[175] or by MALDI TOF MS/MS with fragmentation.[261,262] In this work, peptoids were synthesized by the submonomer method due to its simplicity and cost-efficiency. They were analyzed solely by MALDI TOF MS/MS of single resin beads. In most cases, Y-fragments were the predominant fragments in the MS/MS spectrum, as observed by Heerma *et al.*[261,262] Addition of phosphates to the MALDI MS-samples as previously suggested by Zhu and Papayannopoulos were shown to improve peptide spectra considerably by suppressing matrix adduct signals and thus improving signal-to-noise ratios.[303]

The synthesis and screening of compound libraries is an effective method for the discovery of novel protein ligands. A simple method for the generation of such libraries is the mix-and-split method that was first described in 1991.[172] For OBOC libraries, on-bead screening methods are the most efficient way of finding ligands: a tagged protein is incubated with the library directly after synthesis and binds to a small number of beads which can be identified by the protein tag. This method is dependent on a solid support that is compatible with organic library synthesis as well as screening of biomolecules in aqueous environment. Hydrophilic tentacle polymers based on PEG were first reported in the eighties[323] and possess excellent swelling properties in organic solvents and in water.[324] This made them the first-choice-resin for library synthesis in organic solvent followed by on-bead assay in aqueous environment. In 1997, untagged and tagged TentaGel-NH$_2$ single-beads were studied by confocal microscopy for their single-bead fluorescence properties and showed a rather limited autofluorescence.[325] In 2003, the Kodadek lab mentioned the autofluorescence of TentaGel macrobeads, that proved an inconvenience in fluorescence screening in the FITC channel. They therefore turned to screening in the RHO channel.[326] Since autofluorescence was also

claimed for the RHO channel, quantum dots were then introduced as fluorescent protein tags for screening.[305] In this work TentaGel autofluorescence was studied in detail. Fluorescence intensity depends on exposure time and autofluorescence was not observed for untreated TentaGel HMBA macrobeads in the FITC and RHO channel below 100 ms exposure time. It was observed however, that TentaGel beads can acquire significant fluorescence in the FITC (less so in the RHO) channel by the attachment of peptoids or peptides, as recently also suggested by Hintersteiner.[327] The fluorescence intensity increase was only significant when aromatic sidechains, especially tryptamine, were introduced into the peptoid sequence. These findings are supported by fluorescence intensity measurements with tryptamine in PEG3400 solutions in water:ethanol (1:1, v/v) that showed that tryptamine fluorescence in the FITC channel is increased when mixed with PEG in solution. This suggested that high bead-fluorescence in the FITC channel points to tryptamine content of the sequences attached. It was further observed, that CXCL8S72C-DL550 **23** persistently stuck to highly fluorescent beads: when left to incubate overnight, beads with high FITC channel fluorescence intensity still showed RHO channel fluorescence as opposed to less fluorescent peptoids that lost CXCL8S72C-DL550 **23** fluorescence to a large extend when left to incubate overnight. This may either point to an increased amount of unspecific interactions with TentaGel beads presenting tryptamine-rich peptoid sequences or to a high autofluorescence in both channels. This was further supported by analyzing library hits after re-synthesis in bulk, where all sequences containing tryptamine turned out to be false positives. In future experiments, the correlation between tryptamine-content and TentaGel FITC and RHO channel fluorescence should be further investigated and the effect should be quantified. Proteins bound to highly fluorescent, tryptamine-rich beads could be removed from the bead-surface by non-denaturing electrophoresis and compared to wild-type protein to discover probable differences in protein folding.

6.7 Screening of Peptoid OBOC Libraries Based on Fluorescence

Since the first report of the OBOC method, many types of molecules have been synthesized using the technique and were reviewed by Lam *et al.*.[173,328] The first peptoid library was reported by Zuckermann and coworkers.[219] This library was not synthesized in one pool, which is why it is referred to 'resin splitting method' instead of OBOC method. Yet the technique is based on the same stochastical bead-distribution[171] and is regarded as the first peptoid OBOC library. The 18 individual peptoid pools were cleaved from the resin and screened in solution following an iterative process with synthesis of sub-libraries and screening.[180] This kind of screening procedure is only recommended for short sequences that can be synthesized quickly and at low costs since it involves repeated re-synthesis of parts of the library. Several OBOC peptoid libraries have been reported since, especially by the Kodadek Lab.[175,305,326] In this work, the synthesis and one-bead MALDI TOF MS/MS analysis of peptoid OBOC library was straightforward. Only amines that had been previously shown to give very good coupling yields were used for submonomer synthesis.[299] All single-beads picked randomly from peptoid libraries were unambiguously identified by MALDI TOF MS/MS. Previously reported screening routines for OBOC libraries rely on the COPAS bead sorting machine or on microscopic bead inspection. Non-automated microscopy based methods with constant light exposure lead to photobleaching of the tagged proteins. A bead sorting machine enables a much faster separation process and reduces photobleaching but does not overcome the problem of bead autofluorescence. The suggested method of sorting beads prior to screening to exclude highly fluorescent beads[255,329] is not

advisable, since, as has been shown in this work, bead autofluorescence depends on the target sequences on the resin and thus increases during library synthesis. Therefore a library with aromatic compounds may not be screened and important sequences might be lost in the exclusion process. Hintersteiner *et al.* found two ways of dealing with the autofluorescence problem. First, the introduction of confocal nanoscanning (CONA), where individual beads are scanned at a focus plane approximately in the middle of the bead.[330] Since this focal plane cuts through the bead, a positive bead only shows fluorescence as a ring around the outer rim (increased fluorescence ring intensity). An autofluorecent bead on the other hand displays fluorescence inside the bead circle as well. An algorithm was used to successfully distinguish between ring intensity and autofluorescence. Beads were consecutively picked with an automated picker capillary, which is much slower than the bead sorting process in a COPAS. The second approach therefore focused on optimizing the COPAS screening routine by detecting autofluorescence in two channels and excluding beads that displayed fluorescence in the RHO and FITC channel.[330] However, all receeported methods except for microscopy require highly specialized, expensive equipment that is not easily accessible for most laboratories. In this work, autofluorescence and photobleaching issues were overcome by employing a screening method based on image-analysis: the library was incubated with CXCL8S72C-DL550 **23**, distributed into 384-well MTP and images of the wells were taken in the FITC and RHO channel with a fluorescence microscope equipped with a x/y table. The exposure time was kept constant at 40 ms and thus autofluorescence and photobleaching was kept at a minimum. For image analysis by eye the overlay images of FITC and RHO channels proved effective. Due to the generation of the overlay images by RGB value addition (a RHO channel image with RGB values x/0/0 is mixed with a FITC channel image with RGB values 0/y/0 to give an overlay of x/y/0 for each pixel) and the sensitivity of the human eye to green-yellow light, only beads with very high red fluorescence intensities appear red in the overlay image. Only pixels with an RGB R-value approximately twice as high as the RGB G-value will appear red. This way, the extensive autofluorescence in the FITC channel 'conceals' minor autofluorescence in the RHO channel. Hits could thus be easily identified as red beads amongst a number of green beads. For the separation of hits from a well, the beads were distributed individually into MTP wells and imaged at low exposure times. With the described method, 18 novel peptoids that bind CXCL8 with affinities between 11 μM and 112 μM were discovered. All sequences displayed a high amount of 1,4-diaminobutane residues. Since CXCL8 itself posseses a high pI value, both structures have an overall positive charge at physiological conditions. This points to the fact that the peptoid:CXCL8 interaction is not merely a non-specific long-range electrostatic interaction, but might involve more specific interactions like short-range electrostatic interactions, e. g. van der Waals forces, hydrogen bonds or hydrophobic interactions. Thus a practical cost-efficient screening method with conventional equipment like a fluorescence microscope with an x/y-table and a MALDI TOF/TOF mass spectrometer, that exploits simple labelling techniques was established.

Four of the discovered peptoid structures showed promising inhibitory activity in actin polymerization assay. Three of these peptoids were tested further in migration assays and showed no inhibitory activity. The toxicity tests with resazurin staining showed no toxix effect of the peptoids on neutrophils, but showed an increase in cell activity at high peptoid concentrations. This might point to a transporter-like activity of the peptoids that led to intracellular resazurin reduction. The peptoids not yet tested in a Transwell assays should be tried for their inhibitory potential. Peptoid structures could be made more rigid by cyclisation, which could be beneficial for their affinities for CXCL8.[331] The peptoids might also be tested for their affinity for other chemokines.

For libraries with a poorer signal-to-noise ratio an image analysis program was created in cooperation with M. Reischl and S. Borstel of the Institute of Applied Informatics (IAI) at the Karlsruhe Institute of Technology (KIT). The program automatically detects round bead shapes and calculates the mean pixel brightness of individual beads that may then be compared to find beads of high fluorescence. Beads that do not possess a round shape, possibly due to fragmentation, are not analyzed. It was found that the outer rim of the beads always appears more fluorescent than other areas, so that a 30 pixel offset was introduced for the pixel brightness calculations. A variation coefficient threshold was introduced to set a limit for bead homogeneity, that ensures the rejection of inhomogeneous, misshapen beads.

6.8 Screening of Peptoid OBOC Libraries Based on Magnetic Separation

Library screening based on magnetic separation is an elegant method that considerably facilitates screening routines. The separation of proteins or cells by antibody-coated magnetic particles is routinely employed. In the one-bead-one-compound library approach, the screening of libraries on-bead by employing magnetic spheres could be an alternative to other tagging methods, though literature is scarce on the topic. One major issue with this method are unspecific interactions of the magnetic spheres with the library on solid support. Hu *et al.* reported a two-stage screening process of peptides on PEGA 500 μm resin (polyacrylamide crosslinked with PEG).[332] Peptides of the library that could serve as substrates for transglutaminase (TGase) were incubated with the enzyme and a biotin-like functionalized enzyme substrate. TGase attached the biotin-like molecule ('desbiotin') to conserved lysine residues on the library beads. The library was then incubated with streptavidin magnetic particles to seperate biotinylated peptides. The desbiotinylated species were then visualized on-bead by fluorescently labelled streptavidin. The second screening step differentiated the amount of desbiotin on the beads and thus the effectiveness of the peptide as an enzyme substrate. This method proved that the on-bead screening with magentic particles was possible. Astle *et al.* reported a method, where OBOC peptide/peptoid libraries on 75 μm TentaGel beads were screened on-bead by incubation with anti-FLAG antibody and screening with a secondary antibody immobilized on magnetic spheres. A second screening refinement step was introduced by spotting peptides of interest after identification onto microarray slides for affinity titration. In this work, the protein of interest was directly immobilized on magnetic support. Immobilization of CXCL8 on magnetic particles was achieved covalently and by complexation. The covalent attachment by maleimide-functionalization of magnetic spheres and consecutive reaction with CXCL8S72C **20** was found to be more stable and less prone to unspecific interactions. In a proof-of-principle experiment, the separation of TG-IL8RPLoops **87** by CXCL8 attached to magnetic particles out of a small mixture of peptides on TentaGel beads was successful. In future experiments, the number of maleimide groups on the magnetic particles could be increased to achieve a more effective immobilization of CXCL8 and thus a more efficient mobilization of the magnetic-bead/library-bead complex. Furthermore, an experiment with different amounts of target on beads could show, how many interactions between magnetic beads and library bead are necessary to mobilize a large resin particle. A larger library should be screened by magnetic separation and results should be compared to fluorescence-based screening methods.

7 Materials and Methods

7.1 Chemicals and Materials

All materials and equipment were purchased at the following companies: VWR (Darmstadt, Germany), Roth (Karlsruhe, Germany), TH Geyer (Renningen, Germany), Sigma Aldrich (Taufkirchen, Germany), Iris Biotech (Marktredwitz, Germany), Orpegen (Heidelberg, Germany), Carbolution (Saarbruecken, Germany), Rapp Polymers (Tuebingen, Germany), PL-Laboratories (Port Moody, Canada), AB SCIEX (Framingham, MA, USA), Shimadzu (Duisburg, Germany), Bruker (Ettlingen, Germany), Merck (Darmstadt, Germany), Merck Novabiochem (Darmstadt, Germany), Macherey & Nagel (Dueren, Germany), Tecan (Maennedorf, Swiss), Zeiss (Jena, Germany), Ditabis (Pforzheim, Germany), Christ (Osterode am Harz, Germany), Corning (Kaiserslautern, Germany), Rettberg Laborgeraete GL (Goettingen, Germany), Sartorius/Denver Instrument (Goettingen, Germany), Kern (Balingen, Germany). Organic solvents for High Performance Liquid Chromatography were purchased at VWR. Other organic solvents were purchased at VWR, Roth, TH Geyer, Acros and Sigma-Aldrich. Solvents were used as received without further purification. For peptoid and peptide synthesis solvents were purchased as "peptide grade", low in water and amine contents from VWR, TH Geyer and Roth. Coupling reagents for peptide synthesis were purchased at Iris Biotech, Orpegen, TH Geyer.

Primary amines were purchased at Sigma-Aldrich and if necessary protected with appropriate protective groups. Reactive derivatives of protective groups were purchased at Carbolution and Sigma-Aldrich.

TentaGel MB HMBA macrobeads were purchased at Rapp Polymers. Chlorotritylchloride resin was purchased at PL-Laboratories.

7.1.1 Buffer and Media

Distilled water (Merck MilliQ System) was used for the preparation of all buffers.

Table 7.1: Important Buffers and Media used in this work.

Abbreviation	Name	Composition	pH
PBS	Phosphate buffered saline	137 mM NaCl, 2.70 mM KCl, 10 mM $Na_2HPO/_4$, 2 mM $KH_2HPO/_4$	7.41
ls-PBS	Low-salt PBS	35 mM NaCl, 40 mM $Na_2HPO/_4$	7.41
PBS_{BSA}	PBS with bovine serum albumine	0.2 % BSA in PBS	7.41
$RPMI_{(-)}$	RPMI-1640 medium	With L-glutamine and $NaHCO_3$ without phenol red	8.2 ± 0.3
$RPMI_{(BSA-)}$	RPMI-1640 medium with BSA	0.2 % BSA (w/v) in $RPMI_{(-)}$	8.2 ± 0.3

7.1.2 Synthesis Resins and Particles

Table 7.2: Synthesis Resins and Particles used in this work.

Name	Supplier	Specifications
TentaGel MB HMBA	Rapp Polymers	TentaGel macrobeads $\varnothing$ 300 µM with 4-(hydroxymethyl)benzoic acid (HMBA) linker, capacity 0.24 mmol/g
2-Chlorotritylchloride resin	PL Polymer Laboratories	Polystyrene resin with 2-chlorotritylchloride linker, 1.5 mmol/g, $\varnothing$ 90 µM
HMBA-AM resin	Merck Novabiochem	Aminomethyl polystyrene resin with HMBA linker, 1.1 mmol/g, $\varnothing$ 300 µM
HMBA-AM resin	Iris Biotech	Aminomethyl polystyrene resin with HMBA linker, 1.1 mmol/g, $\varnothing$ 300 µM
Rink amide resin	Iris Biotech	Fmoc-Rink Amide linker on aminomethyl polystyrene resin
Sieber amide resin	PL Polymer Laboratories	Polystyrene resin with Sieber's xanhydrylamine linker
AM-Synbeads	Iris Biotech	Aminomethyl methacrylate resin
TCEP resin	Thermo Scientific	Disulfide reducing gel, tris(2-carboxyethyl)phosphine on beaded agarose resin
M-PVA-IDA	Chemagen	Superparamagnetic particles, Fe_3O_4 embedded in polyvinyl alcohol polymer matrix with iminodiacetic acid linker

7.1.3 Proteins, Antibodies, Labelling Reagents

Table 7.3: Proteins and Antibodies used in this work.

Name	Supplier/Origin	Specifications
CXCL8wt **19**	Expressed in our laboratory, see Wiese and Schmitz[263]	CXCL8(1-72)
CXCL8L25Y/V27R	Expressed in our laboratory	Monomeric CXCL8 variant[56,57]
CXCL8S72C	Expressed in our laboratory	CXCL8(1-72) variant with C-terminal cystein instead of serine
His$_6$-CXCL8	Expressed in our laboratory	CXCL8(1-72) with N-terminal hexa-histidine tag
BSA	Carl Roth	Bovine serum albumin Fraction V

| anti-human-IL8 | Sigma Aldrich I2519 | monoclonal anti-CXCL8 antibody, mouse |
| FITC-anti-human-IL8 | BioLegend 514604 | anti-CXCL8 antibody labelled with FITC |

Table 7.4: Reagents used for fluorescence labelling in this work.

Name	Supplier	Specifications
DyLight550 maleimide	Thermo Scientific	DyLight fluorescence dye with maleimide functionalization λ_{ex}=562 nm, λ_{em}=576 nm
CF633 maleimide	Sigma Aldrich	Originally named cyanine-based fluorescent dyes λ_{ex}=633 nm, λ_{em}=650 nm
5(6)-carboxyfluorescein	Sigma Aldrich	Fluorescein derivative for peptide and peptoid labelling λ_{ex}=488 nm, λ_{em}=520 nm

7.2 Equipment and Instrumental Methods

Matrix Assisted Laser Desorption/Ionization Time of Flight Mass Spectrometry (MALDI-TOF/TOF MS)

Matrix assisted laser-desorption/ionization time of flight spectrometry (MALDI-TOF MS) was performed on a 4800 Plus MALDI TOF/TOF Analyzer from AB SCIEX at the Institute of Functional Interfaces, KIT. The α-cyano-4-hydroxy cinnamic acid (CHCA) matrix was prepared as a 10 mg/mL solution in acetonitrile/water (1:1, v/v) containing 0.1 % TFA. Liquid samples were mixed 1:1 with matrix and 1 µL was spotted on a 384-spot MALDI plate. Solid samples were diluted in acetonitrile/water (1:1, v/v) containing 0.1 % TFA and also mixed 1:1 (v/v) with matrix. For single-bead analysis, beads were placed in individual microfuge tubes and the loaded molecules were cleaved from the resin. The beads were immersed in 5 µL acetonitrile/water (1:1; v/v) with 0.1 % TFA. 1 µL of the bead supernatant was mixed with 1 µL of CHCA solution and 1 µL of the mixture was spotted on the target plate. Peptoids and peptides were detected in reflector mode. Proteins were detected in linear mode. Spectra were converted to txt-files, displayed and analyzed using TOPPView.[333]

Electrospray-Ionization Time of Flight Mass Spectrometry (ESI-TOF MS)

ESI-TOF MS Spectra were recorded with a Mariner-Spec of PerSeptive Biosystems Incorporated at the Institute of Functional Interfaces, KIT. H_2O/MeOH (1:1) alone ('L1') or with 0.1 % acetic acid ('L2') was used as solvent. Alternatively, ESI-TOF MS was conducted on a Shimadzu LCMS2020 analyser equipped with a C4 analytical column at the AK Kolmar, TU Darmstadt. Samples were prepared as 10 mg/mL solutions in acetonitrile/water (1:1; v:v).

Nuclear Magnetic Resonance Spectroscopy (NMR)

NMR spectra were recorded on a Bruker AvanCe300 300 MHz spectrometer. All chemical shifts δwere measured in parts per million (ppm), the respective solvent served as spectrum reference peak: [D_6]-Dimethyl sulfoxide (δ= 2.50 ppm), D_2O (δ= 4.80 ppm), $CDCl_3$ (δ = 7.25 ppm). Signal multiplicity: s = singlet, d = doublet, t = triplet, q = quartet, m = multiplet. All spectra were treated as first order spectra. Coupling constants are given in Hertz [Hz]. Ar-H denotes aromatic protons.

Thin Layer Chromatography (TLC)

Thin layer chromatography was performed on Merck TLC Silicagel 60 F_{254} aluminum plates. Plates were stained with the following staining mixtures: *iodine staining* - elementary iodine for unsaturated or aromatic compounds, *ninhydrin staining* - 1.5 g of ninhydrin in 100 mL in n-butanol and 3 mL of glacial acetic acid for amines, *permanganate staining* - 0.75 g $KMnO_4$, 5 g of K_2CO_3 and 0.75 mL 10 % NaOH for oxidizable components, *Seebach staining* - 2.5 g phosphomolybdic acid, 1 g $Ce(SO_4)_2$, 6 mL concentrated sulfuric acid in 94 mL water as a universal stain. Plates were dipped into the respective solutions and heated to 160 °C using a heat gun.

High Performance Liquid Chromatography (HPLC)

High performance liquid chromatography was conducted on a Shimadzu LC20-AD two pump-system equipped with an SPD20A photo diode array detector. Peptoids and peptides were purified usind a Supelco C18 RP column (250 × 10 mm Discovery HS C18, Supelco, Sigma-Aldrich), proteins were purified using a Nucleosil C8 RP column (250 × 10 mm, Macherey & Nagel).
Purification programmes were executed in gradient mode with eluent A (95 % water/5 % acetonitrile/0,1 % TFA) and B (95 % acetonitrile/5 % water/0.1 % TFA). Standard procedure for peptide purification: after injection eluent B was increased to 5 % over 1 column volume (CV). Then the acetonitrile concentration was elevated linearly to reach 80 % eluent B after 5 CV at a flow rate of 1 mL/min. Absorption was monitored at 254 nm and 495 nm. Fractions were collected manually and freeze-dried.

UV-VIS Spectroscopy

UV-VIS spectra or absorbance values were recorded using a Genesys 10S UV-Vis from Thermo Fisher Scientific (or the Tecan M1000 plate reader, see below). Measurements were conducted in 2 mL fused silica cuvettes. The respective solvent was always used as a reference (*Blank*).

Attenuated total reflection infrared spectroscopy (ATR-IR)

Single-bead ATR-IR spectra were recorded with a Perkin Elmer Spectrum 100 fitted with an UATR-IR (Ge) unit at the Ernst-Bertl Institute, TU Darmstadt. Single beads were dried *in vacuo* and placed onto the germanium crystal of the ATR-IR unit and pressed onto the plate to record spectra.

Plate reader

Fluorescence anisotropy measurements, fluorescence intensity measurements and absorption measurements were conducted on a Tecan Infinite M1000 plate reader. The reader was operated by the Tecan i-control software. The photomultiplier tube gain (PMTG) was chosen 'optimal' for regular measurements, or chosen manually between values of 40-255 when comparing two measurements. Bandwidth for excitation and emission filters was set to 5 nm. Standard settings for the resting time (0 s) and the number of light flashes (10) were used. The Z-factor was manually set (24209 µm) for 384-well MTP. Corning 384-well low volume, black, transparent bottom (type 3540) MTP, Corning 384-well UV transparent microplates (type 3675) MTP were used. The G-factor was determined to be 1.158.

Microscopy

Microscopy images were taken on a Zeiss Axio Observer.Z1 microscope equipped with a Hal 100 halogen lamp for brightfield images and a HXP 120 C lamp for fluorescence imaging. The microscope was equipped with an automated x/y-table and was operated by the AxioVision (Rel. 4.8) software. Images were taken with the AxioCam MR 12bit black and white camera. The following filter sets were used: filter set 49 ('DAPI-channel' ex 300-400 nm, em 420-470 nm), filter set 38HE ('FITC-channel' ex 450-490 nm, em 500-550 nm), filter set 43HE ('RHO-channel' ex 538-562 nm, em 570-640 nm).

Shaker, Stirrer and Heater

Synthesis frits and microcentrifuge tubes were shaken using a Ditabis HLC MHR 20/23 shaker. Larger vessels were shaken using a Heidolph Vibramax 100. Reaction vessels were stirred and heated with a VWR magnetic stirrer. TLC plates were heated using a heatgun Type 8384 purchased at Rettberg Laborgeräte.

Freeze-dryer

Peptoids, peptides and proteins were freeze-dried using the Christ Alpha 2-4 LD Plus connected to an Ilmvac P6Z-101 vacuum pump. Samples were frozen in liquid nitrogen prior to drying.

Vacuum pumps

For filtration or desiccator evacuation purposes, a KNF laboport N840.1.2.FT.18 pump was used. For high-vacuum drying a Vacuubrand RZ6 pump connected to a high-vacuum-line was used.
Rotary evaporator: Organic solvents were removed from synthesis mixtures using a Heidolph Laborota 4000 efficient rotary evaporator operated with an adjustable water bath routinely operated at 40 °C and an Ilmvac LVS 210T pump stand.

7.3 Synthesis of Submonomers

$Nleu^{+0}$: isobutylamine **1**, $Nval^{+0}$: isopropylamine **2** and $Nphe^{+1}$: 2-phenylethyl amine **3** were purchased at Sigma Aldrich, $Ngly^{+0}$: glycine **4** was purchased at Iris Biotech, $Nasp^{+0}$: Glycine *tert*-butyl ester acetate **5** was purchased at Merck. These amines were used without further purification. Ethanolamine **6**, hexamethylenediamine **7**, 1,4-diaminobutane **8** and tryptamine **9** were purchased at Sigma Aldrich and protected as described below to give $Nser^{+1}$ **10**, $Nlys^{+2}$ **11**, $Nlys^{+0}$ **12** and $Ntrp^{+1}$ **13**.
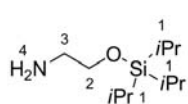
$Nser^{+1}$, *2-[(Triisopropylsilyl)oxy]ethylamine*[219] **10**: 6.30 mL (92.7 mmol, 4.00 eq) ethanolamine **6** were mixed with 25 mL of DCM in a round-bottom flask. 5.00 mL (23.5 mmol, 1.00 eq) triisopropylsilyl chloride TIPS-Cl **14** were added to the mixture under vigorous stirring. The solution was stirred overnight. 50.0 mL DCM are added and the solution was washed three times with saturated sodium bicarbonate, three times with water and three times with saturated sodium chloride solution. The organic phase was dried over $MgSO_4$. Removal of the solvent *in vacuo* yielded 4.85 g of a colourless oil (95 %).
– ^1H-*NMR* (300 MHz, $CDCl_3$), δ/ppm: 1.07-1.03 (m, 18 H, $CH_3(1)$); 2.79 (t, $^3J = 5.26$ Hz, 2 H, $CH_2(3)$); 3.63 (bs, 2 H, $NH_2(4)$); 3.70 (t, $^3J = 5.31$ Hz, 2 H, $CH_2(2)$).
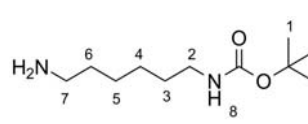
Nlys^{+2}, N-(6-Aminohexyl)-carbamic acid tert-butyl ester[247] **11**: 16.4 g (141 mmol, 1.00 eq) hexamethylenediamine **7** were dissolved in 100 mL 1,4-dioxane to give a yellow solution. 4.00 g (18.3 mmol, 0.13 eq) di-*tert*-butyl dicarbonate (Boc$_2$O) **15** were dissolved in 60.0 mL of 1,4-dioxane and added dropwise to the amine solution. The mixture was stirred overnight. Parts of the solvent were removed *in vacuo* and 100 mL water were added to the white slurry. The white precipitate was filtered off and the yellow solution was extracted three times with ethyl acetate. Removal of the solvent *in vacuo* yielded 3.09 g (78 %) of a slightly yellow oil.

– ^{1}*H-NMR* (300 MHz, CDCl$_3$), δ/ppm: 1.27-1.32 (m, 4 H, CH$_2$(4, 5)); 1.42-1.47 (m, 13 H, CH$_2$, Boc(1, 3, 6)); 2.64 (t, ^{3}J = 7.00 Hz, 2 H, CH$_2$(7)); 3.09-3.05 (m, 2 H, CH$_2$(2)); 4.60 (bs, 1 H, NH(8)).
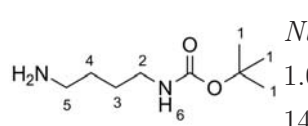
Nlys^{+0}, N-(4-Aminobutyl)-carbamic acid tert-butyl ester[247] **12**: 57.0 g (647 mmol, 1.00 eq) 1,4-diaminobutane **8** were dissolved in DCM and cooled on an ice bath. 14.1 g (64.7 mmol, 0.13 eq) di-*tert*-butyl dicarbonate (Boc$_2$O) **15** were dissolved in 200 mL DCM and added dropwise to the 1,4-diaminobutane under vigorous stirring. The white precipitate was filtered off and the solvent and residual 1,4-diaminobutane were removed *in vacuo*. The reaction yielded 9.9 g (81 %) of a slightly yellow oil.

– ^{1}*H-NMR* (300 MHz, CDCl$_3$), δ/ppm: 1.41 (s, 9 H, Boc(1)); 1.43-1.51 (m, 4 H, CH$_2$(3, 4)); 2.69 (t, ^{3}J = 6.70 Hz, 2 H, CH$_2$(5)); 3.09-3.10 (m, 2 H, CH$_2$(2)); 4.73 (bs, 1 H, NH(6)).
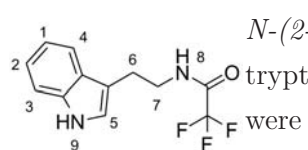
N-(2-(1H-Indol-3-yl)ethyl)-2,2,2-trifluoroacetamide[301] **16**: 5.40 g (34.0 mmol, 1.00 eq) tryptamine **9** were dissolved in 50.0 mL DCM. 25.0 mL (310 mmol, 9.11 eq) pyridine were added to give a brown solution. 5.00 mL (34.0 mmol, 1.05 eq) trifluoroacetic acid TFAA **17** were added dropwise under vigorous stirring. The solution was stirred for 48 h at rt. 100 mL DCM were added and the organic phase was washed three times with saturated sodium bicarbonate solution, three times with a saturated ammonium chloride solution and three times with water. The organic phase was dried over magnesium sulfate. The solvent was removed *in vacuo*. Residual pyridine was removed by adding small amounts of toluene to the residue and removing the liquid *in vacuo*. The reaction yielded 6.80 g (78 %) of a brown solid.

– ^{1}*H-NMR* (300 MHz, CDCl$_3$), δ/ppm: 2.94 (t, ^{3}J = 6.70 Hz, 2 H, CH$_2$(7)); 3.60 (dd, ^{3}J = 6.50 Hz, 2 H, CH$_2$(6)); 6.00 (bs, 1 H, NH(8)); 6.93 (d, ^{3}J = 2.30 Hz, 1 H, Ar-H(5)); 7.04 (t, ^{3}J = 7.60 Hz, 1 H, Ar-H(1)); 7.13 (t, ^{3}J = 7.60 Hz, 1 H, Ar-H(2)); 7.28 (d, ^{3}J = 8.10 Hz, 1 H, Ar-H(3)); 7.48 (d, ^{3}J = 7.90 Hz, 1 H, Ar-H(4)); 8.03 (bs, 1 H, NH(9)).
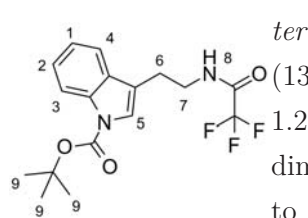
tert-Butyl 3-(2-(2,2,2-trifluoroacetamido)ethyl)-1H-indole-1-carboxylate[301] **18**: 3.40 g (13.3 mmol, 1.00 eq) **16** were dissolved in 25.0 mL 1,4-dioxane. 3.48 g (16 mmol, 1.2 eq) di-*tert*-butyl dicarbonate (Boc$_2$O) **15** and 0.08 g (0.67 mmol, 0.05 eq) 4-dimethylaminopyridine were added to the solution. The reaction mixture was heated to 40 °C for 3 h. The solution was diluted with DCM and the organic phase was washed four times with water and once with saturated sodium chloride solution. The organic phase was dried over magnesium sulfate. The solvent was removed *in vacuo* and the residue was purified by chro-

matography on silica gel (5 % (v/v) ethyl acetate in cyclohexane). Purification yielded 2.86 g (60 %) of a yellow oil that freezes to a white solid upon storage at -8 °C.

– ^{1}H-NMR (300 MHz, CDCl$_3$), δ/ppm: 1.68 (s, 9 H, Boc(9)); 3.00 (t, ^{3}J = 6.90 Hz, 2 H, CH$_2$(6)); 3.70 (dd, ^{3}J = 6.60 Hz, 2 H, CH$_2$(7)); 7.27 (t, ^{3}J = 7.60 Hz, 1 H, Ar-H(5)); 7.36 (t, ^{3}J = 7.70 Hz, 1 H, Ar-H(1)); 7.45 (bs, 1 H, Ar-H(2)); 7.53 (d, ^{3}J = 7.70 Hz, 1 H, Ar-H(3)); 8.16 (d, ^{3}J = 7.70 Hz, 1 H, Ar-H(4)).
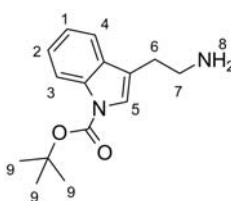
Ntrp^{+1}, 1-Boc-tryptamine[301] **13**: 1.70 g (4.78 mmol, 1.00 eq) **18** were dissolved in 20.0 mL water (20 %) in methanol. 1.73 g (12.5 mmol, 2.62 eq) potassium carbonate was added and the reaction mixture was stirred for 4 d at rt. The reaction mixture was poured into 140 mL water and the product was extracted with DCM. The organic phase was washed with saturated sodium chloride solution and dried over magnesium sulfate. The solvent was removed *in vacuo*. The reaction yielded 1.13 g (91 %) of a colourless oil.

– ^{1}H-NMR (300 MHz, CDCl$_3$), δ/ppm: 1.67 (s, 9 H, Boc(9)); 2.84 (dt, ^{3}J = 6.60 Hz, ^{4}J = 0.90 Hz, 2 H, CH$_2$(7)); 3.05 (t, ^{3}J = 6.50 Hz, 2 H, CH$_2$(6)); 7.14-7.27 (m, 1 H, Ar-H(5)); 7.29-7.35 (m, 1 H, Ar-H(1)); 7.42 (bs, 1 H, Ar-H(2)); 7.54 (dq, ^{3}J = 7.70 Hz, ^{4}J = 0.70 Hz, 1 H, Ar-H(3)); 8.14 (d, ^{3}J = 8.11 Hz, 1 H, Ar-H(4)).

7.4 Protein Expression and Labelling

Expression of CXCL8wt, 72 amino acid variant **19**: Protein expression was executed by I. Rink, A. Imrich, K. Brahm and M. Joest. *E. coli* BL21 DE3 RIL were transformed with a pET-22b vector containing the codon optimized sequence of human CXCL8.[263] Proteins were expressed and purified by a procedure modified from Wiese and Schmitz.[263]

The transformed cells were grown in LB-medium containing ampicillin (60 μg/mL). At an optical density OD600 of 0.6-0.8 expression was induced by addition of IPTG (0.1 mM final concentration). Expression was continued for 3 h at 30 °C. Cells were harvested by centrifugation (45 min at 5000 × g) and resuspended in buffer A (40 mM Na$_2$HPO$_4$, 90 mM NaCl, pH 7.4) supplemented with 1 mM EDTA, 0.2 mg/ml lysozyme, 0.1 mg/ml DNase I and incubated on ice for 1.5 h. After addition of 0.5 % Triton X-100, the suspension was sonified three times for 30 s at 50 % intensity (Sonopuls, Bandelin Electronics). After additional incubation with DNase I the sample was heated to 70 °C for 10 min to precipitate host cell proteins. The lysate was centrifuged at 4 °C and 4500 × g for 45 min. The protein was purified from the supernatant via HPLC on an ÄKTA purifier 10 system (GE Healthcare) using a 5 mL HiTrap SP FF column (GE Healthcare). Gradient of 0-30 % of buffer B (1.5 M NaCl and 40 mM Na$_2$HPO$_4$, pH 7.5) in buffer A (90 mM NaCl, 40 mM Na$_2$HPO$_4$, pH 7.5). Protein fractions were lyophilized and desalted on a centricon (Vivaspin20; Sartorius) using water.

Expression of CXCL8S72C **20**: Protein expression was executed by I. Rink, A. Imrich, K. Brahm and M. Joest, based on the 72 amino acid variant of CXCL8. *E. coli* BL21 DE3 RIL were transformed with a pET-22b vector containing the sequence of human CXCL8 with a C-terminal cysteine residue.[264] The proteins were expressed and purified by a procedure modified from Wiese and Schmitz (see **19**).[263]

Expression of CXCL8L25Y/V27R **21**: Protein expression was executed by I. Rink according to K. Jaeger*. Based on the 72 amino acid variant of CXCL8. – *MALDI-TOF* (matrix: CHCA, linear mode), m/z (%): 8516.20 (100) $[M+Na]^+$, 4230.55 (100), 7875.84 (25).

Expression of His$_6$-CXCL8 **22**: Protein expression was executed by A. Imrich according to D. Wiese†, based on the 72 amino acid variant of CXCL8. *E. coli* BL21 DE3 RIL were transformed with a pET-28a vector containing the sequence of human CXCL8 with an N-terminal TEV-protease cleavage site EN-LYFQ/S followed by an N-terminal hexa-histidine tag.
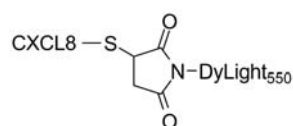
Labelling of CXCL8 with DyLight550 maleimide, CXCL8S72C-DL550 **23**: 150 μL (1.20 μmol, 4.80 eq) Tris(2-carboxyethyl)phosphine reducing gel (TCEP gel) was washed three times with 400 μL PBS with 20.0 mM EDTA (pH 7.00) and once with 400 μL low-salt PBS. 2.10 mg (0.250 μmol, 1.00 eq) CXCL8S72C **20** dissolved in 500 μL low-salt PBS was added to the TCEP gel and incubated for 30 min at room temperature. The supernatant was transferred into another microcentrifuge tube and the TCEP gel was washed twice with 200 μL low-salt PBS. The washing solutions were combined with the supernatant. 0.50 mg (0.469 μmol, 1.88 eq) DyLight550 maleimide (10 mg/mL in DMF, 1065 g/mol) were added to the supernatant and incubated for 2.5 h at room temperature. The product was isolated by HPLC: RP C8 matrix, multistep gradient (0-5 min 5 % eluent B, 5-25 min linear gradient to 40 % eluent B), CXCL8S72C eluted at 27 min, product CXCL8S72C-DL550 eluted after 28 min. The procedure yielded 1.00 mg (0.106 μmol) CXCL8S72C-DL550 (42 %). – *MALDI-TOF* (matrix: CHCA, linear mode), m/z (%): 9396.98 (100) $[M+H]^+$, 4688.07 (25) $[M+H]^{(2+)}$, 18786.84 (6).
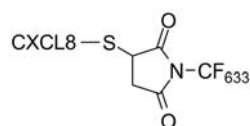
Labelling of CXCL8 with CF^{TM} maleimide, CXCL8S72C-CF633 **24**: Synthesis by M. Joest. 150 μL (1.20 μmol, 4.80 eq) Tris(2-carboxyethyl)phosphine reducing gel (TCEP gel) was washed three times with 400 μL PBS with 20.0 mM EDTA pH 7.00 and once with 400 μL low-salt PBS. 1.20 mg (0.143 μmol, 1.00 eq) CXCL8S72C **20** dissolved in 1.00 mL low-salt PBS was added to the TCEP gel and incubated for 30 min at rt. The supernatant was transferred into another microcentrifuge tube and the TCEP gel was washed twice with 50.0 μL low-salt PBS. The washing solutions were combined with the supernatant. 0.41 mg (0.429 μmol, 3.00 eq) CF^{TM} maleimide (19 mg/mL in DMSO) were added to the supernatant and incubated overnight at 8 °C. The product was isolated by HPLC (0-10 min 20 % B, linear gradient 10-45 min to 45 % B) and eluted after 39 min. – *ESI LC/MS* (C4 LC column), m/z (%): 1168.8 (100) $[M+8H]^{8+}$, 1335.6 (80) $[M+7H]^{7+}$, 1038.2 (50) $[M+9H]^{9+}$, 1558.0 (20) $[M+6H]^{6+}$, 935.2 (20) $[M+10H]^{10+}$, 1869.4 (5) $[M+5H]^{5+}$.

---

*   K. Jaeger, practical course 'Herstellung einer nicht dimisierenden Variante von Interleukin-8 durch Mutagenese', TU Darmstadt, 2012.

†   D. Wiese, PhD Thesis 'Herstellung rekombinanter humaner Chemokine in *E. coli*, KIT 2011.
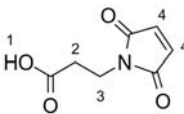
3-(Maleimido)propanoic acid **25**: 4.00 g (44.9 mmol, 1.00 eq) β-alanine and 4.40 g (44.9 mmol, 1.00 eq) maleic anhydride were dissolved in 25.0 ml glacial acetic acid each. The two solutions were combined and stirred at rt for 10 h. The solvent was removed *in vacuo* to yield 8.30 g of a white powder (99 %). – ^{1}*H-NMR* (300 MHz, DMSO-D$_6$), δ/ppm: 2.49 (t, ^{3}J = 7.40 Hz, 2 H, CH$_2$(2)); 3.61 (t, ^{3}J = 7.40 Hz, 2 H, CH$_2$(3)); 7.00 (s, 2 H, CH(4)); 12.33 (bs, 1 H, COOH(1)).
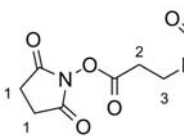
3-Maleimidopropanoic acid N-hydroxysuccinimide ester linker **26**: 6.44 g (44.8 mmol, 1.00 eq) 3-(Maleimido)propanoic acid were dissolved in 25 mL DMF and stirred on an ice bath at 0 °C. 6.44 g (56.0 mmol, 1.25 eq) N-hydroxysuccinimide (NHS) and 18.5 g (89.6 mmol, 2.00 eq) N,N'-dicyclohexylcarbodiimide (DCC) were added. The reaction mixture was stirred for 10 h at room temperature. The urea precipitate was removed by filtration. The product in DMF was concentrated *in vacuo* and the remaining brown solution was poured into 100 mL water. The beige precipitate was removed by filtration and dried *in vacuo*. The reaction yields 9.50 g (80 %) of a beige powder. – ^{1}*H-NMR* (300 MHz, DMSO D$_6$), δ/ppm: 2.79 (s, 4 H, CH2(1)); 3.04 (t, ^{3}J = 6.80 Hz, 2 H, CH$_2$(2)); 3.74 (t, ^{3}J = 6.80 Hz, 2 H, CH$_2$(3)); 7.00 (s, 2 H, CH(4)).
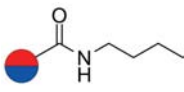
M-PVA magnetic particles functionalized with protected amino-groups **27**: 25.0 mg (23.8 µmol, 1.00 eq) M-PVA-COOH (polyvinyl alcohol, carboxy terminated) high-load magnetic particles (50 ^{mg}/$_{mL}$ suspension in water) were washed twice with 500 µL coupling buffer (10 mM K$_2$HPO$_4$, 400 mM NaCl, pH 5.0). 4.00 mg (34.8 µmol, 1.50 eq) N-hydroxysuccinimide (NHS) were dissolved in 900 µL deionized water and 4.50 mg (29.0 µmol, 1.30 eq) 1-ethyl-3-(3-dimethylaminopropyl)-carbodiimide hydrochloride (EDC) were dissolved in 100 µL deionized water. NHS and EDC solutions were mixed, added to the M-PVA-COOH particle suspension and incubated for 15 min. 33.0 mg (131 µmol, 5.50 eq) N-Boc-1,6-hexanediamine **11** were dissolved in 300 µL NMP, added to the reaction mixture and incubated overnight. The particles were washed with washing buffer (TRIS 10 µM, NaCl 150 µM, pH 7.5).
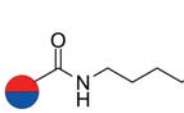
M-PVA magnetic particles functionalized with maleimide groups, M-PVA-Mal **28**: The Boc-group of **27** was removed by treatment with 95 % TFA, 2.5 % and 2.5 % water for 1 h at room temperature. The particles were washed three times with 500 µL washing buffer and three times with NMP. 14.5 mg (54.5 µmol, 2.30 eq) **25** in NMP were added and shaken for 4 h. The particles were washed three times with NMP and three times with washing buffer. Maleimide-functionalized magnetic beads can be stored for up to three days in the refrigerator. *Quantification of maleimide groups on magnetic particles*: Roughly 4 mg of **28** were transferred into a microcentrifuge tube with determined weight. As a control, ca. 4 mg **27** were transferred into a second microcentrifuge tube with known weight. Particles were sedimented using a magnetic rack and the supernatant was removed. The particles were washed three times with 500 µL NMP. 10.0 mg of Fmoc-L-cysteine in 500 µL NMP were added to each tube and shaken for 4 h at room temperature. The

beads were washed twice with NMP, and once with DMF. 20 μL 2 vol% of DBU in DMF were added to the tubes and the mixtures were shaken for 30 min at room temperature. 8 μL of the supernatant was diluted in 992 μL acetonitrile and the amount of dibenzofulvene in these dilutions was determined by measuring absorption at 304 nm. The beads were washed with DCM and dried under vacuum to determine the exact weight. Unspecific binding to M-PVA-HMDA-Boc routinely resulted in a loading of 17 μmol/g, while M-PVA-maleimide particles gave 30 μmol/g.
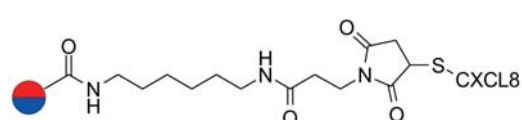
M-PVA-COOH magnetic particles functionalized with CXCL8, M-PVA-Mal-CXCL8 **29**: 1.00 mg (0.190 μmol, 1.00 eq) CXCL8S72C in 250 μL PBS were added to **28** and shaken overnight. The particles were washed three times with washing buffer (TRIS 10 μM, NaCl 150 μM, pH 7.5). M-PVA-CXCL8 particles can be stored for up to three days.
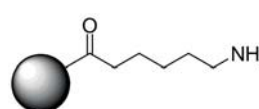
TentaGel MB HMBA functionalized with amino-groups, TG-NH₂ **30**: 100 mg (24 μmol, 1.00 eq) TentaGel MB HMBA resin was swollen in DCM (GP001). DCM was then removed. 84.4 mg (240 μmol, 10.0 eq) Fmoc-6-aminohexanoic **31** were dissolved in 2.00 mL DMF, 18.6 μL DIC (120 μmol, 5.00 eq) and 0.30 mg DMAP (2.40 μmol, 0.10 eq; 15 mg/mL in DMF) were added and the mixture was added to the resin. The resin was shaken overnight and washed five times with DMF (1 mL per 100 mg of resin). Fmoc was removed by treatment with 20 % piperidine in DMF for 20 min. The resin was washed five times with DMF (1 mL per 50 mg of resin).
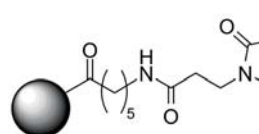
TentaGel MB HMBA functionalized with maleimide groups, TG-Mal **32**: 63.8 mg 3-maleimidopropanoic acid N-hydroxysuccinimide ester **26** (240 μmol, 10.0 eq) were dissolved in DCM added to resin **30** and shaken for 4 h. The resin was washed five times with DMF, three times with DCM and dried. – *UATR-IR* (single particle): $\nu = 1707$ cm⁻¹.
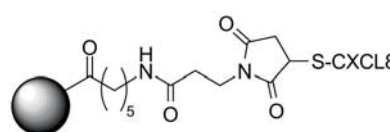
TG-Mal functionalized with CXCL8S72C, TG-Mal-CXCL8 **33**: 100 μL (1.00 μmol, 17.0 eq) tris(2-carboxyethyl)phosphine reducing gel (TCEP gel) was washed three times with 400 μL PBS with 20.0 mM EDTA pH 7.00 and once with 400 μL low-salt PBS. 0.50 mg (0.06 μmol, 1.00 eq) CXCL8S72C **20** dissolved in 500 μL low-salt PBS was added to the TCEP gel and incubated for 4 h at room temperature. The supernatant was transferred into another microcentrifuge tube and the TCEP gel was washed twice with 200 μL low-salt PBS. The washing solutions were combined with the supernatant. 10 individual TG-Mal beads **32** were added to the microcentrifuge tube and shaken for 1 h at rt. A decrease of the maleimide antisymmetric stretching signal in UATR-IR compared to TG-Mal **32** indicated a successful reaction. Particles were also stained with FITC-anti-human-CXCL8 to detect CXCL8 on the surface (see Figure 5.73 in the Results Section).

M-PVA-IDA^{Cu(II)}: Loading of M-PVA-IDA Magnetic Particles with Cu²⁺ [334] **34**: 10.0 mg M-PVA-IDA (polyvinylalcohol-based magnetic particles with iminodiacetic acid functionalization) were immersed in

1.50 mL of loading buffer (50.0 mM $CuSO_4$, 200 mM NaCl). Particles were shaken for 15 min at rt and the buffer was removed. Particles were washed twice with 2 mL binding buffer: 20.0 mM NaH_2PO_4, 200 mM NaCl, pH 6.8.

M-PVA-IDA$^{Cu(II)}$:His$_6$-CXCL8: Coordination of CXCL8 to Magnetic Particles[334] **35**: 1 mL of His$_6$-CXCL8 (1 $^{mg}/_{mL}$ in PBS) was added to particles **34** and the suspension was shaken at rt for 15 min. Particles were washed twice with 2 mL of binding buffer. *Elution of His$_6$-CXCL8 off M-PVA-IDA$^{Cu(II)}$*: Particles **35** were immersed twice in 1 mL of elution buffer (200 mM imidazole, 200 mM NaCl, pH 7.8).

Immobilization of CXCL8S72C-DL550 on Glass: Clean room glass slides (Nexterion Slides, Glass B, Schott, Germany) were immersed in 4 mL 3 % BSA in PBS and shaken for 10 min. Slides were washed by immersion in 4 mL PBS and shaken for 5 min at room temperature. The PBS washing step was repeated twice with fresh PBS. Slides were immersed in water and dried by centrifugation. A HybriWell chamber (Grace Bio-Labs, USA) was attached to the slide, filled with 50 µM CXCL8S72C-DL550 in *ls*-PBS, sealed and exposed to a projected greyscale image at 550 ± 20 nm generated by the maskless lithography system developed by Waldbaur *et. al* for 6 min.[296] HybriWell chambers were removed and slides were washed by immersion in PBS (3×4 mL), washed with water and dried by centrifugation.

Staining of CXCL8S72C-DL550 Immobilized on Glass: CXCL8S72C-DL550 slides were covered with HybriWell chambers and filled with fluorescent staining solution of FITC-anti-CXCL8 (Biolegend) or Fluo-IL8RPLoops in *ls*-PBS and sealed. They were incubated under tinfoil for 10 min at rt. HybriWell chambers were removed and slides were washed with water and dried by centrifugation. Slides were analyzed by a GenePix 4000B microarray scanner (Molecular Devices, USA).

7.6 Peptoid and Peptide Synthesis

Peptides were synthesized following a standard Fmoc/*t*Bu solid phase peptide synthesis (SPPS) protocol.[291] Peptoids were synthesized following submonomer synthesis protocol. General Procedures for both protocols are listed below.

7.6.1 Solid Phase Peptoid and Peptide Synthesis

General Procedures (GP) for Peptoid and Peptide Synthesis

GP001: Swelling of Resin Beads
Resin beads are weighed into polyethylene or glass columns equipped with a filter frit. Columns are closed with a luer cap or in case of larger columns with the attached teflon stopcock. The resin is swollen in DCM (about 1.00 mL per 50.0 mg of resin) for at least 15 min at room temperature with shaking at 600 rpm. Prior to any further reaction DCM is removed by suction filtration.

GP002: Washing of Resin Beads
The resin is washed consecutively five times with DMF (about 1 mL per 50 mg of resin).

GP003: Attachment of first Compound to Resins with HMBA-Linker
3.00 equivalents (with respect to the loading capacity of the resin) of the compound are dissolved in DCM. If the linker does not dissolve completely, DMF is added dropwise. The mixture is stirred at 0 °C in an ice bath and 0.10 eq of 4-dimethylaminopyridine (DMAP) (from a stock solution of 15.0 mg/mL DMAP in DMF) are added. 4.00 eq N,N'-diisopropylcarbodiimide (DIC) are added to the mixture and the solution is stirred for 5 minutes on ice. The solution is then immediately added to the resin. The suspension is shaken for 4 h or over night at rt at 600 rpm.

GP004: Attachment of first Compound to Chlorotritylchloride Resin
3.00 equivalents (with respect to the loading capacity of the resin) of the compound are dissolved in N-methylpyrrolidinon (NMP). If the linker does not dissolve completely, DCM is added dropwise. 3.00 equivalents of DIPEA are added to the solution and the whole mixture is added to the resin. The suspension is shaken for 4 h or over night at rt at 600 rpm.

GP005: Acylation with Bromoacetic Acid
Bromoacetic acid is prepared as a 1.20 M solution in DMF. 10.0 equivalents (with respect to the loading capacity of the resin) of bromoacetic acid are added to the resin. 9.00 equivalents of DIC are added and the suspension is shaken for 1 h at 600 rpm at room temperature. It is not recommended to perform this reaction overnight.

GP006: Subsitution with Primary Amine
20.0 equivalents of primary amine acquired directly from the supplier are added undiluted to the bromoacetylated resin (in case of liquids) or weighed and dissolved in a small amount of NMP and consecutively added to the resin. In each case a small amount of NMP can be added afterwards to facilitate mixing of the suspension. For amines that were modified after receipt (**10**, **11**, **12**, **13**) only 10.0 equivalents were used per reaction.

GP007: Attachment of Amino Acids
Method A: 1.20 equivalents of amino acid in DMF, 1.20 equivalents of DIC and 1.20 equivalents of hydroxybenzotriazole (HOBt, 30.0 mg/mL in DMF) are mixed and added to the resin.The suspension is shaken for at least 2 h or overnight at rt. *Method B:* 3.00 equivalents of amino acid in DMF, 3.00 equivalents of HBTU and 6.00 equivalents DIPEA are mixed and added to the resin. The suspension is shaken for at least 2 h or overnight at room temperature.

GP008: Removal of Fmoc-Protective Group
Fmoc-group was removed by 20.0 vol% piperidine in DMF (about 1.00 mL per 50.0 mg of resin), shaken at 600 rpm for 20 min at room temperature.

GP009: Preparation of Resin Beads for Drying

The resin is washed consecutively three times with DMF (about 1.00 mL per 50.0 mg of resin) and twice with DCM (1.00 mL per 50.0 mg of resin).

GP010: Drying of Resin Beads

The resin is thoroughly washed with DCM and pre-dried by vacuum filtration. The resin pellet or individual bead is dried under vacuum overnight.

GP011: Removal of Protective Groups on Resins with HMBA-Linker

Sequences without cysteine residues: The dried resin is incubated with 95.0 % TFA, 2.50 % water and 2.50 % TIS and shaken at 600 rpm for at least 2 h (but no longer than 4 h) at room temperature. The resin is then washed with DCM until the beads float on the DCM surface. Sequences with cysteine residues: The dried resin is incubated with 94.0 % TFA, 2.50 % water, 2.50 % TIS and 1.00 % 1,2-ethanedithiol and shaken at 600 rpm for at least 2 h (but no longer than 4 h) at room temperature. The resin is then washed with DCM until the beads float on the DCM surface.

GP012: Cleavage of Product from Resins with HMBA-Linker

The dried resin is placed in a vacuum desiccator with 20.0 mL 25 % ammonia solution and evacuated until the ammonia gas forms bubbles in the water. The resin is left for at least 4 h in the ammonia atmosphere.

GP013: Removal of Protective Groups and Cleavage from Chlorotritylchloride Resin

The dried resin is treated with a mixture of 95.00 % TFA, 2.50 % water and 2.50 % triisopropysilane (TIS). If cysteine residues are present, an alternative mixture is used: 94.0 % TFA, 2.50 % water, 2.50 % 1,2-ethanedithiol, 1.00 % TIS. The suspension is shaken at 600 rpm for at least 2 h (but no longer than 4 h) at rt. The solution is collected and the resin is washed twice with the respective cleavage mixture.

GP014: Precipitation of Product

For peptide precipitation, cold diethyl ether is added directly to the TFA cleavage cocktail. The mixture is centrifuged and the supernatant is decanted. The precipitate is washed twice with cold diethyl ether and dried *in vacuo*. In case of peptoids, the product usually does not precipitate upon addition of diethyl ether. The TFA cleavage cocktail is removed *in vacuo* and the solid residue is washed twice with diethyl ether.

GP015: Attachment of Fluorescence Label

The reactive derivative of the fluorophore (3 eq, with respect to loading capacity of the resin) is dissolved in DMF. 1-Hydroxybenzotriazole (HOBt, 3 eq) is added as a solution of 300 mg/mL in DMF. Diisopropylcarbodiimide (DIC, 3 eq) is added and the whole mixture was added to the resin and incubated for at least 4 h at rt. The resin is washed according to GP002 and additionally washed five times with 20.0 % piperidine in DMF.[302]

GP016: Determination of Resin Loading by Fmoc-Removal

In case of TentaGel resin, ten dry TentaGel MB HMBA beads are manually transferred into three microfuge tubes. The beads are centrifuged to the bottom of the tube and incubated for 30 min with 8 µL of 2 vol% 1,8-diazabicyclo[5.4.0]undec-7-ene in DMF. The bead suspension is diluted with 992 µL acetonitrile and absorption is measured at 304 nm. Three different probes are prepared and measured. Extinction coefficient of dibenzofulvene in DBU/DMF/acetonitrile: $\epsilon = 7624$ M^{-1}cm^{-1},[335] resin mass is calculated according to information from Rapp Polymere: 15.7 µg per bead TentaGel MB HMBA. A correction factor of 1.17 has to be introduced by comparing results from this method with the method from Gude.[335] Loading was calculated according to the following equation:

$$loading \left(\frac{mol}{g}\right) = \frac{Abs_{304}\ nm}{1.17 \cdot \epsilon \cdot 1\ cm \cdot 15.7 \cdot 10^{-6}\ g} \tag{7.1}$$

GP017: Equal Splitting of Resin Slurry

DMF is added to the resin to give a known volume of slurry. The slurry is vigorously resuspended with a pipet (preferable 5.00 mL tips with large outlet) and the desired amount of resin is taken out of the slurry.

GP018: Automated Peptide Synthesis

A standard Fmoc/*t*Bu SPPS protocol is used for the peptide synthesizer (Liberty, CEM, USA) equipped with a microwave reactor (Discover, CEM, USA). Amino acids are prepared as 0.20 M solutions in DMF. The Fmoc-protecting group is removed with 20.0 % piperidine in DMF. Activating solution with the following concentration is used: 0.25 M HOBT and 0.25 M HBTU in DMF. Activator base is prepared as 1.00 M DIPEA in NMP.

GP019: Chloranil-test for Detection of Secondary Amines

Solution 1: 2 % (w/v) tetrachloro-*p*-benzoquinone ('chloranil') is dissolved in DMF. Solution 2: 2 % (v/v) acetaldehyde are mixed with DMF. A small amount of resin beads is transferred into a microcentrifuge tube and 40 µL of solution 1 and 2 are added consecutively. The beads are incubated for 5 min at room temperature. Blue coloured beads indicate secondary amines. The staining is usually instantly visible upon adding both solutions. Fmoc-protected amines can give a very pale blue colour. Both solutions should be stored at -8 °C and can be used for one month at maximum.
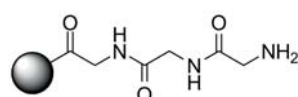
GGG-Linker on HMBA-AM resin **36**: 30.0 mg (0.033 mmol, 1.00 eq) HMBA-AM resin was swollen according to GP001. 29.4 mg (0.099 mmol, 3.00 eq) Fmoc-6-aminohexanoic acid and 4.05 mg (0.033 mmol, 1.00 eq) DMAP were added (dissolved in DMF). 25.5 µL (0.165 mmol, 5.00 eq) DIC were added and the mixture was shaken at 600 rpm overnight. The Fmoc-group was removed (GP008) and the resin was washed (GP002). 11.8 mg (0.040 mmol, 1.20 eq) Fmoc-N-glycine and 5.00 mg (0.040 mmol, 1.20 eq) HOBt were added (dissolved in DMF). 6.13 µL (0.040 mmol, 1.20 eq) DIC were added and the slurry was shaken for 3 h at room temperature. The Fmoc-group was removed (GP008), the resin was washed (GP002) and the last three steps were repeated to attach the third N-Fmoc-glycine residue.
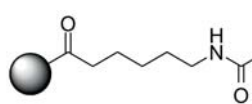
Ahx-G-Linker HMBA-AM resin **37**: 10.0 mg (0.011 mmol, 1.00 eq) HMBA-AM resin was swollen according to GP001. 11.7 mg (0.033 mmol, 3.00 eq) Fmoc-6-aminohexanoic acid and 1.35 mg (0.011 mmol, 1.00 eq) DMAP were added (dissolved in DMF). 8.52 µL (0.055 mmol, 5.00 eq) DIC were added and the mixture was shaken at 600 rpm overnight. The Fmoc-group was removed (GP008) and the resin was washed (GP002). 3.92 mg (0.013 mmol, 1.20 eq) Fmoc-N-glycine and 2.02 mg (0.013 mmol, 1.20 eq) HOBt were added (dissolved in DMF). 2.04 µL (0.013 mmol, 1.20 eq) DIC were added and the slurry was shaken for 3 h at room temperature. The Fmoc-group was removed (GP008) and the resin was washed (GP002).
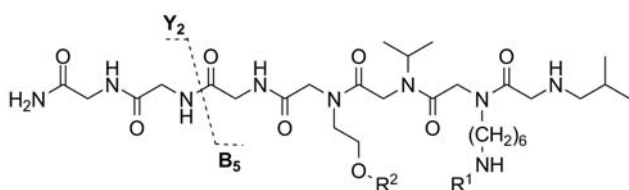
$H_2N\text{-}GGG\text{-}Nser^{+1}Nval^{+0}Nlys^{+2}Nleu^{+0}\text{-}H$ **38**: The resin **36** was acylated with bromoacetic acid (GP005) and washed (GP002). Bromine was substituted with **10** (GP006) and the resin was washed (GP002). The cycle of acylation (GP005), washing (GP002), substitution (GP006), washing (GP002) was repeated with the remaining amines: Isopropylamine, **11** and isobutylamine. Each acylation/substitution step was monitored by the chloranil test (GP019). The resin was split and from one half the Boc and TIPS protecting groups were removed (GP011) and the peptoid was cleaved from the resin (GP012). The peptoid was washed off the resin with DCM and dried. $-R_1$=Boc, $-R_2$=TIPS – *MALDI-TOF* (matrix: CHCA), m/z (%): 914.70 (100) $[M+H]^+$, 927.73 (45), 856.65 (43). – *MALDI-TOF/TOF* (matrix: CHCA), m/z (%) [fragment]: 858.49 (100) $[M-tBu]^+$, 815.50 (23) $[M-Boc]^+$, 801.48 (18) $[Y_6+2\,H]^+$, 642.34 (18), 602.35 (20), 585.32 (30), 545.33 (50) $[Y_5+2\,H]^+$, 469.32 (15) $[B_3]^+$, 413.26 (10), 370.25 (15) $[B_2]^+$, 314.19 (10), 229,11 (55). $-R_1$=H, $-R_2$=H – *MALDI-TOF* (matrix: CHCA), m/z (%): 771.61 (100), 811.61 (95), 700.53 (64), 754.51 (58), 658.51 (45) $[M+H]^+$. – *MALDI-TOF/TOF* (matrix: CHCA), m/z (%) [fragment]: 545.37 (25) $[Y_6+2\,H]^+$, 482.40 (6), 429.25 (2), 401.27 (4), 389.24 (100) $[Y_5+2\,H]^+$, 383.33 (35), 369.31 (40) $[B_3]^+$, 341.31 (10), 327.30 (5), 315.30 (10), 270.23 (40) $[B_2]^+$, 265.15 (8), 242.20 (15).
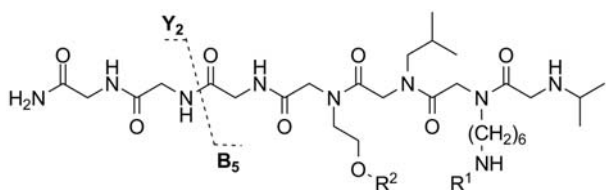
$H_2N\text{-}GGG\text{-}Nser^{+1}Nleu^{+0}Nlys^{+2}Nval^{+0}\text{-}H$ **39**: The resin **36** was acylated with bromoacetic acid (GP005) and washed (GP002). Bromine was substituted with **10** (GP006) and the resin was washed (GP002). The cycle of acylation (GP005), washing (GP002), substitution (GP006), washing (GP002) was repeated with the remaining amines: Isobutylamine, **11** and isopropylamine. Each acylation/substitution step was monitored by the chloranil test (GP019). The resin was split and from one half the Boc and TIPS protecting groups were removed (GP011) and the peptoid was cleaved from the resin (GP012). The peptoid was washed off the resin with DCM and dried. $-R_1$=Boc, $-R_2$=TIPS – *MALDI-TOF* (matrix: CHCA), m/z (%): 914.72 (100) $[M+H]^+$, 530.38 (65), 758.56 (55). – *MALDI-TOF/TOF* (matrix: CHCA), m/z (%) [fragment]: 858.49 (30) $[M-tBu]^+$, 814.53 (50) $[M-Boc]^+$, 559.35 (25) $[Y_5+2\,H]^+$, 468.34 (18) $[B_3]^+$, 355.25 (100) $[B_2]^+$, 284.18 (20), 256.19 (12) $[Y_5+2\,H]^+$, 229.13

(10) $[Z_4]^+$. -R_1=H, -R_2=H – *MALDI-TOF* (matrix: CHCA), m/z (%): 811.65 (100), 797.63 (43), 754.51 (58), 658.54 (20) $[M+H]^+$. – *MALDI-TOF/TOF* (matrix: CHCA), m/z (%) [fragment]: 559.38 (35) $[Y_6+2 H]^+$, 403.26 (100) $[Y_5+2 H]^+$, 369.31 (40) $[B_3]^+$, 290.18 (2) $[Y_4+2 H]^+$, 256.22 (38) $[B_2]^+$, 228.22 (18), 142.10 (18).
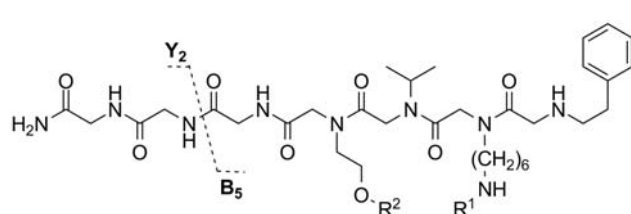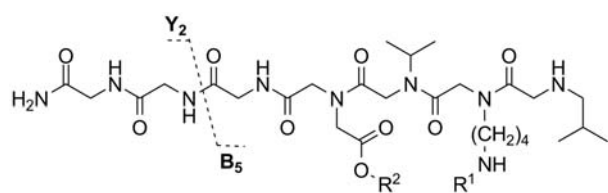

H_2N-GGG-Nser^{+1}Nval^{+0}Nlys^{+2}Nphe^{+1}-H **40**: The resin **36** was acylated with bromoacetic acid (GP005) and washed (GP002). Bromine was substituted with **10** (GP006) and the resin was washed (GP002). The cycle of acylation (GP005), washing (GP002), substitution (GP006), washing (GP002) was repeated with the remaining amines: Isopropylamine, **11** and 2-phenylethanamine. Each acylation/substitution step was monitored by the chloranil test (GP019). The resin was split and from one half the Boc and TIPS protecting groups were removed (GP011) and the peptoid was cleaved from the resin (GP012). The peptoid was washed off the resin with DCM and dried. -R_1=Boc, -R_2=TIPS – *MALDI-TOF* (matrix: CHCA), m/z (%): 962.71 (100) $[M+H]^+$, 808.57 (63), 904.67 (45). – *MALDI-TOF/TOF* (matrix: CHCA), m/z (%) [fragment]: 906.51 (100) $[M-tBu]^+$, 863.52 (15) $[M-Boc]^+$, 801.50 (15) $[Y_6+2 H]^+$, 689.40 (15), 602.36 (15), 585.35 (20), 545.35 (60) $[Y_5+2 H]^+$, 517.34 (15) $[B_3]^+$, 418.27 (20) $[B_2]^+$, 362.21 (15), 229.12 $[Z_4]^+$. -R_1=H, -R_2=H – *MALDI-TOF* (matrix: CHCA), m/z (%): 867.67 (100), 631.47 (90), 706.56 (18) $[M+H]^+$. – *MALDI-TOF/TOF* (matrix: CHCA), m/z (%) [fragment]: 545.38 (13) $[Y_6+2 H]^+$, 417.32 (45) $[B_3]^+$, 389.25 (100) $[Y_5+2 H]^+$, 363.31 (10), 318.24 (23) $[B_2]^+$, 290.25 (15) $[Y_4+2 H]^+$, 148.10 (13).
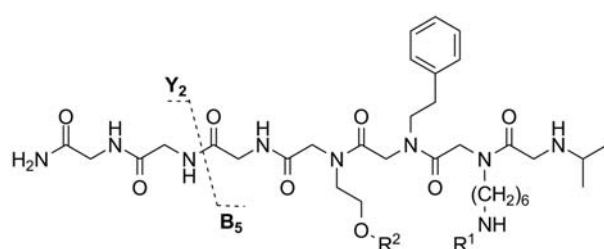
H_2N-GGG-Nser^{+1}Nphe^{+1}Nlys^{+2}Nval^{+0}-H **41**: The resin **36** was acylated with bromoacetic acid (GP005) and washed (GP002). Bromine was substituted with **10** (GP006) and the resin was washed (GP002). The cycle of acylation (GP005), washing (GP002), substitution (GP006), washing (GP002) was repeated with the remaining amines: Isopropylamine, **11** and 2-phenylethanamine. Each acylation/substitution step was monitored by the chloranil test (GP019). The resin was split and from one half the Boc and TIPS protecting groups were removed (GP011) and the peptoid was cleaved from the resin (GP012). The peptoid was washed off the resin with DCM and dried. -R_1=Boc, -R_2=TIPS – *MALDI-TOF* (matrix: CHCA), m/z (%): 962.73 (100) $[M+H]^+$, 806.57 (60), 904.68 (30). – *MALDI-TOF/TOF* (matrix: CHCA), m/z (%) [fragment]: 906.52 (40) $[M-tBu]^+$, 802.56 (50) $[M-Boc]^+$ and $[Y_6+2 H]^+$, 773.54 (3) $[B_4]^+$, 607.37 (30) $[Y_5+2 H]^+$, 516.36 (15) $[B_3]^+$, 355.27 (100) $[B_2]^+$, 284.20 (18), 229.12 (13) $[Z_4]^+$. -R_1=H, -R_2=H – *MALDI-TOF* (matrix: CHCA), m/z (%): 907.67 (100), 748.57 (50), 706.56 (25) $[M+H]^+$. – *MALDI-TOF/TOF* (matrix: CHCA), m/z (%) [fragment]: 607.39 (25) $[Y_6+2 H]^+$, 451.27 (100) $[Y_5+2 H]^+$, 417.32 (40) $[B_3]^+$, 290.18 (2) $[Y_4+2 H]^+$, 256.23 (28) $[B_2]^+$, 228.23 (15), 190.11 (25).
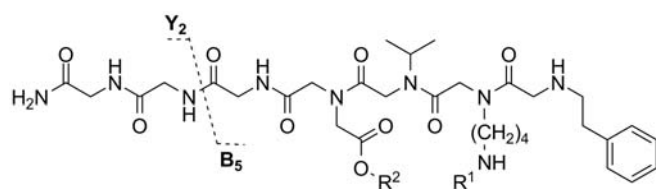
H_2N-GGG-Nasp^{+0}Nval^{+0}Nlys^{+0}Nleu^{+0}-H **42**: The resin **36** was acylated with bromoacetic acid (GP005) and washed (GP002). Bromine was substituted with L-glycine-*tert*-butyl ester acetate (GP006) and the resin was washed (GP002). T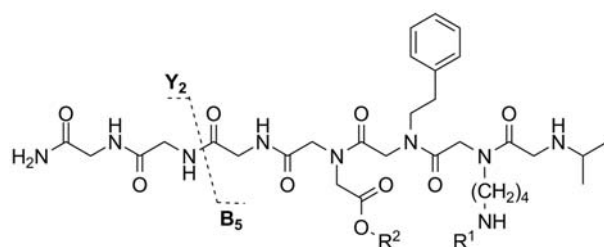he cycle of acylation (GP005), washing (GP002), substitution (GP006), washing (GP002) was repeated with the remaining amines: Isopropylamine, **12** and isobutylamine. Each acylation/substitution step was monitored by the chloranil test (GP019). The resin was split and from one half the Boc and *t*Bu protecting groups were removed (GP011) and the peptoid was cleaved from the resin (GP012). The peptoid was washed off the resin with DCM and dried. -R$_1$=Boc, -R$_2$=tBu – *MALDI-TOF* (matrix: CHCA), m/z (%): 800.58 (100) [M+H]$^+$, 686.52 (26), 857.60 (12). – *MALDI-TOF/TOF* (matrix: CHCA), m/z (%) [fragment]: 744.39 (100) [M-tBu]$^+$, 701.40 (10) [M-Boc]$^+$, 687.38 (5) [Y$_6$+2 H]$^+$, 682.45 (18), 459.25 (18) [Y$_5$+2 H]$^+$, 441.29 (7) [B$_3$]$^+$, 342.23 (13) [B$_2$]$^+$. -R$_1$=H, -R$_2$=H – *MALDI-TOF* (matrix: CHCA), m/z (%): 644.49 (100) [M+H]$^+$, 740.49 (75), 626.42 (35) . – *MALDI-TOF/TOF* (matrix: CHCA), m/z (%) [fragment]: 531.31 (30) [Y$_6$+2 H]$^+$, 456.30 (3) [B$_4$]$^+$, 403.21 (45) [Y$_5$+2 H]$^+$, 341.27 (25) [B$_3$]$^+$, 242.20 (100) [B$_2$]$^+$.
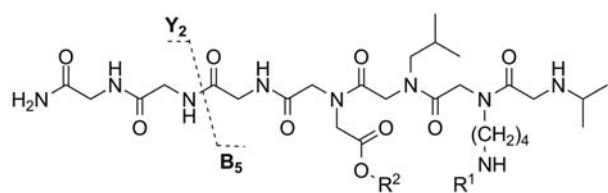
H_2N-GGG-Nasp^{+0}Nleu^{+0}Nlys^{+0}Nval^{+0}-H **43**: The resin **36** was acylated with bromoacetic acid (GP005) and washed (GP002). Bromine was substituted with glycine *tert*-butyl ester acetate (GP006) and the resin was washed (GP002). The cycle of acylation (GP005), washing (GP002), substitution (GP006), washing (GP002) was repeated with the remaining amines: Isobutylamine, **12** and isopropylamine. Each acylation/substitution step was monitored by the chloranil test (GP019). The resin was split and from one half the Boc and *t*Bu protecting groups were removed (GP011) and the peptoid was cleaved from the resin (GP012). The peptoid was washed off the resin with DCM and dried. -R$_1$=Boc, -R$_2$=tBu – *MALDI-TOF* (matrix: CHCA), m/z (%): 800.58 (100) [M+H]$^+$, 686.52 (45), 857.61 (15). – *MALDI-TOF/TOF* (matrix: CHCA), m/z (%) [fragment]: 744.40 (100) [M-tBu]$^+$, 701.40 (15) [M-Boc]$^+$ and [Y$_6$+2 H]$^+$, 473.26 (10) [Y$_5$+2 H]$^+$, 441.30 (3) [B$_3$]$^+$, 328.22 (8) [B$_2$]$^+$. -R$_1$=H, -R$_2$=H – *MALDI-TOF* (matrix: CHCA), m/z (%): 740.49 (100), 644.48 (86) [M+H]$^+$, 774.52 (58). – *MALDI-TOF/TOF* (matrix: CHCA), m/z (%) [fragment]: 545.32 (40) [Y$_6$+2 H]$^+$, 417.24 (50) [Y$_5$+2 H]$^+$, 341.27 (30) [B$_3$]$^+$, 338.20 (15), 228.19 (100) [B$_2$]$^+$.

H_2N-GGG-Nasp^{+0}Nval^{+0}Nlys^{+0}Nphe^{+1}-H **44**: The resin **36** was acylated with bromoacetic acid (GP005) and washed (GP002). Bromine was substituted with glycine *tert*-butyl ester acetate (GP006) and the resi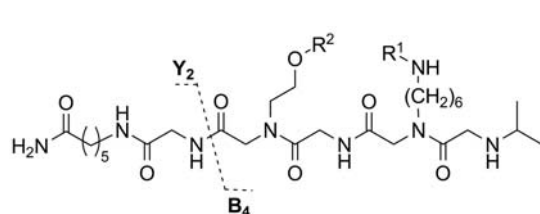n was washed (GP002). The cycle of acylation (GP005), washing (GP002), substitution (GP006), washing (GP002) was repeated with the remaining amines: Isopropylamine, **12** and 2-phenylethanamine. Each acylation/substitution step was monitored by the chloranil test (GP019). The resin was split and from one half the Boc and *t*Bu protecting groups were removed (GP011) and the peptoid was cleaved from the resin (GP012). The peptoid was washed off the resin with

DCM and dried. $-R_1=$Boc, $-R_2=t$Bu – *MALDI-TOF* (matrix: CHCA), m/z (%): 848.57 (100) $[M+H]^+$, 677.49 (45), 734.52 (23). – *MALDI-TOF/TOF* (matrix: CHCA), m/z (%) [fragment]: 792.38 (100) $[M-tBu]^+$, 749.38 (10) $[M-Boc]^+$, 730.46 (15), 687.32 (5) $[Y_6+2\ H]^+$, 489.29 (9) $[B_3]^+$, 459.24 (20) $[Y_5+2\ H]^+$, 390.16 (18) $[B_2]^+$. $-R_1=$H, $-R_2=$H – *MALDI-TOF* (matrix: CHCA), m/z (%): 788.49 (100), 296.43 (73) $[M+H]^+$, 674.43 (73). – *MALDI-TOF/TOF* (matrix: CHCA), m/z (%) [fragment]: 531.32 (25) $[Y_6+2\ H]^+$, 504.31 (2) $[B_4]^+$, 403.22 (45) $[Y_5+2\ H]^+$, 389.28 (25) $[B_3]^+$, 290.21 (100) $[B_2]^+$.

H_2N-*GGG-Nasp^{+0}Nphe^{+1}Nlys^{+0}Nval^{+0}*-H **45**: The resin **36** was acylated with bromoacetic acid (GP005) and washed (GP002). Bromine was substituted with glycine *tert*-butyl ester acetate (GP006) and the resin was washed (GP002). The cycle of acylation (GP005), washing (GP002), substitution (GP006), washing (GP002) was repeated with the remaining amines: 2-phenylethanamine, **12** and isopropylamine. Each acylation/substitution step was monitored by the chloranil test (GP019). The resin was split and from one half the Boc and *t*Bu protecting groups were removed (GP011) and the peptoid was cleaved from the resin (GP012). The peptoid was washed off the resin with DCM and dried. $-R_1=$Boc, $-R_2=t$Bu – *MALDI-TOF* (matrix: CHCA), m/z (%): 848.56 (100) $[M+H]^+$, 910.58 (30), 734.51 (28). – *MALDI-TOF/TOF* (matrix: CHCA), m/z (%) [fragment]: 792.39 (100) $[M-tBu]^+$, 749.40 (15) $[M-Boc]^+$ and $[Y_6+2\ H]^+$, 521.26 (12) $[Y_5+2\ H]^+$, 489.29 (3) $[B_3]^+$, 328.21 (8) $[B_2]^+$. $-R_1=$H, $-R_2=$H – *MALDI-TOF* (matrix: CHCA), m/z (%): 850.51 (100), 788.48 (75), 692.48 (40) $[M+H]^+$. – *MALDI-TOF/TOF* (matrix: CHCA), m/z (%) [fragment]: 593.33 (40) $[Y_6+2\ H]^+$, 504.23 (2) $[B_4]^+$, 465.25 (98) $[Y_5+2\ H]^+$, 389.28 (30), 386.21 (55) $[B_3]^+$, 228.19 (100) $[B_2]^+$, 190.11 (30).

H_2N-*Ahx-G-Nser^{+1}GlyNlys^{+2}Nval^{+0}*-H **46**: The resin **37** was acylated with bromoacetic acid (GP005) and washed (GP002). Bromine was substituted with **10** (GP006) and the resin was washed (GP002). Fmoc-N-glycine was attached (GP007, A) and the resin was washed (GP002). The cycle of acylation (GP005), washing (GP002), substitution (GP006), washing (GP002) was repeated with the remaining amines: **11** and isopropylamine. Each acylation/substitution step was monitored by the chloranil test (GP019). The peptoid was cleaved from the resin (GP012). The peptoid was washed off the resin with DCM and dried. $-R_1=$Boc, $-R_2=$TIPS – *MALDI-TOF* (matrix: CHCA), m/z (%): 744.53 (100), 857.62 (65) $[M+H]^+$, 686.48 (23). – *MALDI-TOF/TOF* (matrix: CHCA), m/z (%) [fragment]: 801.45 (40) $[M-tBu]^+$, 758.47 (100) $[M-Boc]^+$, 669.43 (12) $[B_4]^+$, 665.99 (35), 445.30 (8) $[Y_3+2\ H]^+$, 412.26 (15) $[B_3]^+$, 355.24 (85) $[B_2]^+$, 284.17 (15), 256.18 (13).
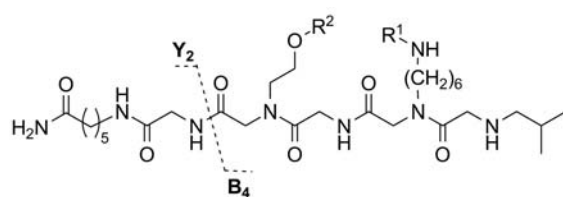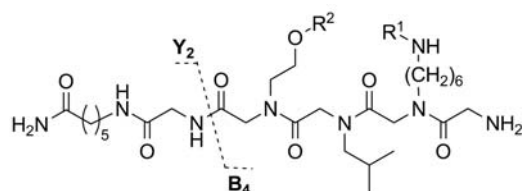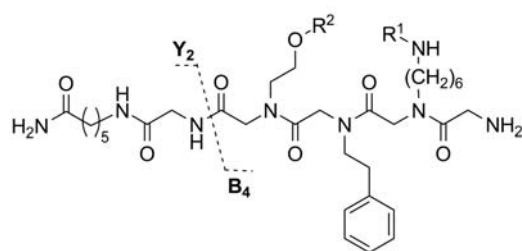

H_2N-*Ahx-G-Nser^{+1}GlyNlys^{+2}Nleu^{+0}*-H **47**: The resin **37** was acylated with bromoacetic acid (GP005) and washed (GP002). Bromine was substituted with **10** (GP006) and the resin was washed (GP002). Fmoc-N-glycine was attached (GP007, A) and the resin was washed (GP002). The cycle

of acylation (GP005), washing (GP002), substitution (GP006), washing (GP002) was repeated with the remaining amines: **11** and isobutylamine. Each acylation/substitution step was monitored by the chloranil test (GP019). The peptoid was cleaved from the resin (GP012). The peptoid was washed off the resin with DCM and dried. -R_1=Boc, -R_2=TIPS – *MALDI-TOF* (matrix: CHCA), m/z (%): 771.59 (100), 871.65 (63) [M+H]$^+$, 700.52 (40). – *MALDI-TOF/TOF* (matrix: CHCA), m/z (%) [fragment]: 815.48 (100) [M-tBu]$^+$, 772.48 (68) [M-Boc]$^+$, 681.94 (8) [B_4]$^+$, 445.29 (3) [Y_2+2 H]$^+$, 370.23 (5) [B_2]$^+$, 239.23 (11).
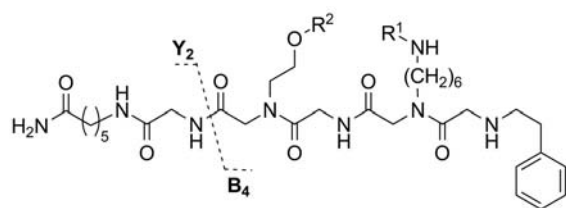
H_2N-Ahx-G-Nser^{+1}GlyNlys^{+2}Nphe^{+1}-H **48**: The resin **37** was acylated with bromoacetic acid (GP005) and washed (GP002). Bromine was substituted with **10** (GP006) and the resin was washed (GP002). Fmoc-N-glycine was attached (GP007, A) and the resin was washed (GP002). The cycle of acylation (GP005), washing (GP002), substitution (GP006), washing (GP002) was repeated with the remaining amines: **11** and isobutylamine. Each acylation/substitution step was monitored by the chloranil test (GP019). Protecting groups were removed (GP011) and the peptoid was cleaved from the resin (GP012). The peptoid was washed off the resin with DCM and dried. -R_1=H, -R_2=H – *MALDI-TOF* (matrix: CHCA), m/z (%): 571.52 (100), 864.61 (35), 663.50 (6) [M+H]$^+$. – *MALDI-TOF/TOF* (matrix: CHCA), m/z (%) [fragment]: 533.31 (5) [B_5]$^+$, 502.33 (100) [Y_5+2 H]$^+$, 476.28 (18) [B_4]$^+$, 375.24 (35) [B_3]$^+$, 346.20 (25) [Y_4+2 H]$^+$, 318.21 (70) [B_2]$^+$, 290.22 (100) [Y_3+2 H]$^+$, 188.14 (10) [Y_2+2 H]$^+$.
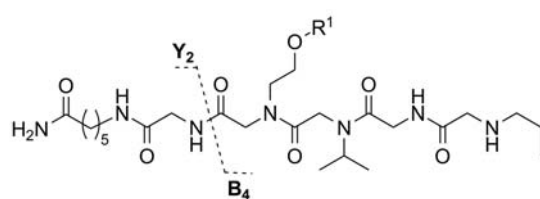

H_2N-Ahx-G-Nser^{+1}Nval^{+0}Nlys^{+2}Gly-H **49**: The resin **37** was acylated with bromoacetic acid (GP005) and washed (GP002). Bromine was substituted with **10** (GP006) and the resin was washed (GP002). The cycle of acylation (GP005), washing (GP002), substitution (GP006), washing (GP002) was repeated with the remaining amines: isobutylamine and **11**. Each acylation/substitution step was monitored by the chloranil test (GP019). Fmoc-N-glycine was attached (GP007, A) and the resin was washed (GP002). The peptoid was cleaved from the resin (GP012). The peptoid was washed off the resin with DCM and dried. -R_1=Boc, -R_2=TIPS – *MALDI-TOF* (matrix: CHCA), m/z (%): 871.67 (100) [M+H]$^+$, 893.65 (70), 758.57 (60). – *MALDI-TOF/TOF* (matrix: CHCA), m/z (%) [fragment]: 851.65 (35), 809.64 (30), 684.63 (18) [B_4]$^+$, 681.97 (100), 558.32 (15) [Y_4+2 H]$^+$.

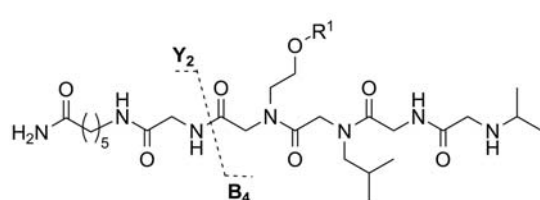*H_2N-Ahx-G-Nser^{+1}Nphe^{+1}Nlys^{+2}Gly-H* **50**: The resin **37** was acylated with bromoacetic acid (GP005) and washed (GP002). Bromine was substituted with **10** (GP006) and the resin was washed (GP002). The cycle of acylation (GP005), washing (GP002), substitution (GP006), washing (GP002) was repeated with the remaining amines: 2-phenylethanamine and **11**. Each acylation/substitution step was monitored by the chloranil test (GP019). Fmoc-N-glycine was attached (GP007, A) and the resin was washed (GP002). The resin was split and from one half the Boc and TIPS

protecting groups were removed (GP011) and the peptoid was cleaved from the resin (GP012). The peptoid was washed off the resin with DCM and dried. -R_1=Boc, -R_2=TIPS – *MALDI-TOF* (matrix: CHCA), m/z (%): 919.66 (100) $[M+H]^+$, 861.62 (85), 806.57 (58). – *MALDI-TOF/TOF* (matrix: CHCA), m/z (%) [fragment]: 857.63 (35) $[M-tBu]^+$, 819.51 (30) $[M-Boc]^+$, 644.40 (30), 606.40 (100) $[Y_4+2\ H]^+$, 472.27 (25) $[B_3]^+$, 311.17 (20) $[B_2]^+$. -R_1=H, -R_2=H – *MALDI-TOF* (matrix: CHCA), m/z (%): 1096.80 (100), 788.48 (75), 663.51 (70) $[M+H]^+$, 926.67 (60). – *MALDI-TOF/TOF* (matrix: CHCA), m/z (%) [fragment]: 533.33 (7) $[B_5]^+$, 490.29 (30), 476.26 (5) $[B_4]^+$, 462.30 (40), 450.27 (100) $[Y_4+2\ H]^+$, 375.24 (30) $[B_3]^+$, 214.20 (9) $[B_2]^+$.

H_2N-Ahx-G-Nser^{+1}Nval^{+0}GlyNleu^{+0}-H **51**: The resin **37** was acylated with bromoacetic acid (GP005) and washed (GP002). Bromine was substituted with **10** (GP006) and the resin was washed (GP002). The cycle of acylation (GP005), washing (GP002), substitution (GP006), washing (GP002) was repeated with isopropylamine. Fmoc-N-glycine was attached (GP007, A) and the resin was washed (GP002). Another cycle of acylation (GP005), washing (GP002), substitution (GP006), washing (GP002) was performed with isobutylamine. Each acylation/substitution step was monitored by the chloranil test (GP019). The resin was split and from one half the TIPS protecting group was removed (GP011) and the peptoid was cleaved from the resin (GP012). The peptoid was washed off the resin with DCM and dried. -R_1=TIPS – *MALDI-TOF* (matrix: CHCA), m/z (%): 613.43 (100), 756.52 (53), 714.52 (15) $[M+H]^+$. – *MALDI-TOF/TOF* (matrix: CHCA), m/z (%) [fragment]: 708.00 (45), 544.36 (58) $[Y_4+2\ H]^+$, 527.32 (45) $[B_4]^+$, 445.30 (50) $[Y_3+2\ H]^+$, 270.17 (100) $[B_3]^+$. -R_1=H – *MALDI-TOF* (matrix: CHCA), m/z (%): no target signal. – *MALDI-TOF/TOF* (matrix: CHCA), m/z (%) [fragment]: 388.25 (40) $[Y_4+2\ H]^+$, 371.23 (20) $[B_4]^+$, 289.19 (10) $[Y_3+2\ H]^+$, 270.18 (100) $[B_3]^+$.

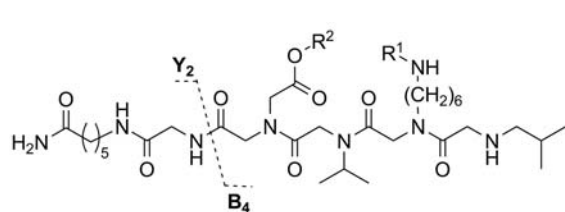H_2N-Ahx-G-Nser^{+1}Nleu^{+0}GlyNval^{+0}-H **52**: The resin **37** was acylated with bromoacetic acid (GP005) and washed (GP002). Bromine was substituted with **10** (GP006) and the resin was washed (GP002). The cycle of acylation (GP005), washing (GP002), substitution (GP006), washing (GP002) was repeated with isobutylamine. Fmoc-N-glycine was attached (GP007, A) and the resin was washed (GP002). Another cycle of acylation (GP005), washing (GP002), substitution (GP006), washing (GP002) was performed with isopropylamine. Each acylation/substitution step was monitored by the chloranil test (GP019). The resin was split and from one half the TIPS protecting group was removed (GP011) and the peptoid was cleaved from the resin (GP012). The peptoid was washed off the resin with DCM and dried. -R_1=TIPS – *MALDI-TOF* (matrix: CHCA), m/z (%): 627.46 (100), 601.44 (75), 714.54 (55) $[M+H]^+$. – *MALDI-TOF/TOF* (matrix: CHCA), m/z (%) [fragment]: 558.38 (80) $[Y_4+2\ H]^+$, 527.33 (90) $[B_4]^+$, 445.29 (80) $[Y_3+2\ H]^+$, 270.17 (100) $[B_3]^+$. -R_1=H – *MALDI-TOF* (matrix: CHCA), m/z (%): 584.44 (100), 558.42 (25) $[M+H]^+$. – *MALDI-TOF/TOF* (matrix: CHCA), m/z (%) [fragment]: 459.29 (8) $[Y_5+2\ H]^+$, 428.25 (4) $[B_5]^+$, 402.27 (50) $[Y_4+2\ H]^+$, 371.23 (23) $[B_4]^+$, 289.19 (12) $[Y_3+2\ H]^+$, 270.19 (100) $[B_3]^+$, 157.10 (2) $[B_2]^+$.

7 Materials and Methods
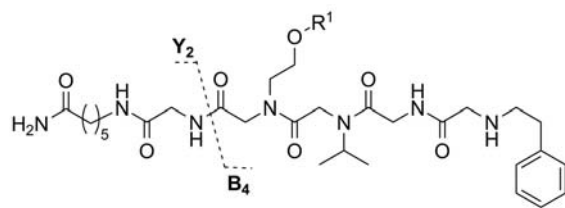
H₂N-Ahx-G-Nser⁺¹Nval⁺⁰GlyNphe⁺¹-H **53**: The resin **37** was acylated with bromoacetic acid (GP005) and washed (GP002). Bromine was substituted with **10** (GP006) and the resin was washed (GP002). The cycle of acylation (GP005), washing (GP002), substitution (GP006), washing (GP002) was repeated with isopropylamine. Fmoc-N-glycine was attached (GP007, A) and the resin was washed (GP002). Another cycle of acylation (GP005), washing (GP002), substitution (GP006), washing (GP002) was performed with 2-phenylethanamine. Each acylation/substitution step was monitored by the chloranil test (GP019). The resin was split and from one half the TIPS protecting group was removed (GP011) and the peptoid was cleaved from the resin (GP012). The peptoid was washed off the resin with DCM and dried. -R₁=TIPS – *MALDI-TOF* (matrix: CHCA), m/z (%): 627.45 (100), 649.45 (65), 762.54 (40) [M+H]⁺. – *MALDI-TOF/TOF* (matrix: CHCA), m/z (%) [fragment]: 575.48 (40) [B₄]⁺, 544.37 (50) [Y₄+2 H]⁺, 445.47 (35) [Y₃+2 H]⁺, 318.17 (100) [B₃]⁺. -R₁=H – *MALDI-TOF* (matrix: CHCA), m/z (%): 606.42 (100) [M+H]⁺, 570.41 (98). – *MALDI-TOF/TOF* (matrix: CHCA), m/z (%) [fragment]: 476.26 (2) [B₅]⁺, 445.28 (4) [Y₅+2 H]⁺, 419.24 (15) [B₄]⁺, 388.26 (40) [Y₄+2 H]⁺, 318.19 (100) [B₃]⁺, 289.20 (8) [Y₃+2 H]⁺.
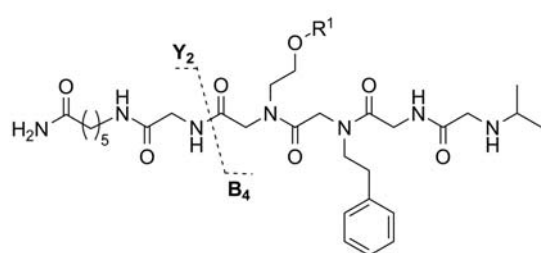
H₂N-Ahx-G-Nser⁺¹Nphe⁺¹GlyNval⁺⁰-H **54**: The resin **37** was acylated with bromoacetic acid (GP005) and washed (GP002). Bromine was substituted with **10** (GP006) and the resin was washed (GP002). The cycle of acylation (GP005), washing (GP002), substitution (GP006), washing (GP002) was repeated with 2-phenyletha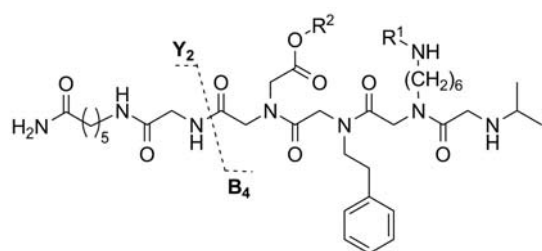namine. Fmoc-N-glycine was attached (GP007, A) and the resin was washed (GP002). Another cycle of acylation (GP005), washing (GP002), substitution (GP006), washing (GP002) was performed with isopropylamine. Each acylation/substitution step was monitored by the chloranil test (GP019). The resin was split and from one half the TIPS protecting group was removed (GP011) and the peptoid was cleaved from the resin (GP012). The peptoid was washed off the resin with DCM and dried. -R₁=TIPS – *MALDI-TOF* (matrix: CHCA), m/z (%): 649.43 (100), 731.54 (85), 762.53 (40) [M+H]⁺. – *MALDI-TOF/TOF* (matrix: CHCA), m/z (%) [fragment]: 754.44 (100), 606.39 (90) [Y₄+2 H]⁺, 575.38 (45) [B₄]⁺, 445.29 (40) [Y₃+2 H]⁺, 318.18 (85) [B₃]⁺. -R₁=H – *MALDI-TOF* (matrix: CHCA), m/z (%): 632.44 (100), 575.41 (75) [M+H]⁺, 606.43 (30). – *MALDI-TOF/TOF* (matrix: CHCA), m/z (%) [fragment]: 507.29 (5) [Y₅+2 H]⁺, 450.27 (50) [Y+2 H]⁺, 419.23 (23) [B₅]⁺, 318.19 (100) [B₃]⁺, 289.19 (9) [Y₃+2 H]⁺, 157,10 [B₂]⁺.

H₂N-Ahx-G-Nasp⁺⁰Nval⁺⁰Nlys⁺²Nleu⁺⁰-H **55**: The resin **37** was acylated with bromoacetic acid (GP005) and washed (GP002). Bromine was substituted with glycine *tert*-butyl ester acetate (GP006) and the resin was washed (GP002). The 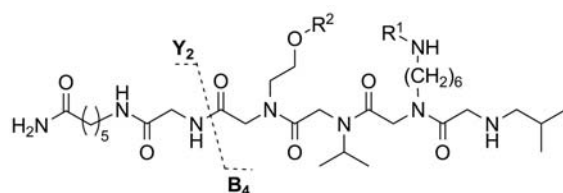cycle of acylation (GP005), washing (GP002), substitution (GP006), washing (GP002) was repeated with the remaining amines: isopropylamine, **11** and isobutylamine. Each acylation/substitution step was monitored by the chloranil test (GP019). The resin was
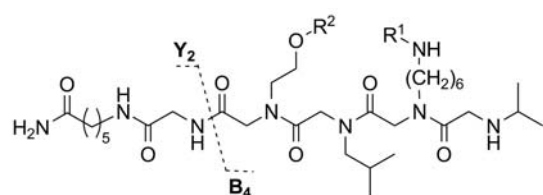
split and from one half the Boc and tBu protecting groups were removed (GP011) and the peptoid was cleaved from the resin (GP012). The peptoid was washed off the resin with DCM and dried. $-R_1$=Boc, $-R_2$=tBu – *MALDI-TOF* (matrix: CHCA), m/z (%): 714.52 (100), 828.59 (75) [M+H]$^+$, 666.47 (23) . – *MALDI-TOF/TOF* (matrix: CHCA), m/z (%) [fragment]: 772.41 (100) [M-tBu]$^+$, 728.44 (15) [M-Boc]$^+$, 520.33 (20), 458.29 (23) [Y$_4$+2 H]$^+$, 370.25 (13) [B$_2$]$^+$. $-R_1$=H, $-R_2$=H – *MALDI-TOF* (matrix: CHCA), m/z (%): 671.52 (100) [M+H]$^+$, 713.54 (95), 784.62 (90). – *MALDI-TOF/TOF* (matrix: CHCA), m/z (%) [fragment]: 558.35 (35) [Y$_5$+2 H]$^+$, 484.30 (4) [B$_4$]$^+$, 402.23 (100) [Y+2 H]$^+$, 369.28 (45) [B$_3$]$^+$, 270.21 (60) [B$_2$]$^+$.

H_2N-*Ahx*-*G*-*Nasp*$^{+0}$*Nleu*$^{+0}$*Nlys*$^{+2}$*Nval*$^{+0}$-*H* **56**: The resin **37** was acylated with bromoacetic acid (GP005) and washed (GP002). Bromine was substituted with glycine *tert*-butyl ester acetate (GP006) and the resin was washed (GP002). The cycle of acylation (GP005), washing (GP002), substitution (GP006), washing (GP002) was repeated with the remaining amines: isobutylamine, **11** and isopropylamine. Each acylation/substitution step was monitored by the chloranil test (GP019). The resin was split and from one half the Boc and tBu protecting groups were removed (GP011) and the peptoid was cleaved from the resin (GP012). The peptoid was washed off the resin with DCM and dried. $-R_1$=Boc, $-R_2$=tBu – *MALDI-TOF* (matrix: CHCA), m/z (%): 714.51 (100), 827.60 (50) [M+H]$^+$, 656.43 (20) . – *MALDI-TOF/TOF* (matrix: CHCA), m/z (%) [fragment]: 771.44 (100) [M-tBu]$^+$, 728.46 (15) [M-Boc]$^+$, 671.42 (10), 472.29 (15) [Y$_5$+2 H]$^+$, 355.25 (18) [B$_2$]$^+$. $-R_1$=H, $-R_2$=H – *MALDI-TOF* (matrix: CHCA), m/z (%): 500.37 (100), 770.60 (68), 671.52 (63) [M+H]$^+$. – *MALDI-TOF/TOF* (matrix: CHCA), m/z (%) [fragment]: 614.38 (10), 572.37 (50) [Y$_5$+2 H]$^+$, 416.25 (100) [Y$_4$+2 H]$^+$, 369.29 (60) [B$_3$]$^+$, 256.20 (80) [B$_2$]$^+$.

H_2N-*Ahx*-*G*-*Nasp*$^{+0}$*Nval*$^{+0}$*Nlys*$^{+2}$*Nphe*$^{+1}$-*H* **57**: The resin **37** was acylated with bromoacetic acid (GP005) and washed (GP002). Bromine was substituted with glycine *tert*-butyl ester acetate (GP006) and the resin was washed (GP002). The cycle of acylation (GP005), washing (GP002), substitution (GP006), washing (GP002) was repeated with the remaining amines: isobutylamine, **11** and 2-phenylethanamine. Each acylation/substitution step was monitored by the chloranil test (GP019). The peptoid was cleaved from the resin (GP012), washed off the resin with DCM and dried. $-R_1$=Boc, $-R_2$=tBu – *MALDI-TOF* (matrix: CHCA), m/z (%): 762.49 (100), 875.58 (50) [M+H]$^+$, 704.45 (20). – *MALDI-TOF/TOF* (matrix: CHCA), m/z (%) [fragment]: 819.44 (100) [M-tBu]$^+$, 775.45 (15) [M-Boc]$^+$, 681.99 (35), 517.32 (15) [B$_3$]$^+$, 458.28 (25) [Y$_4$+2 H]$^+$, 418.25 (15) [B$_2$]$^+$.

H_2N-Ahx-G-$Nasp^{+0}Nphe^{+1}Nlys^{+2}Nval^{+0}$-H **58**: The resin **37** was acylated with bromoacetic acid (GP005) and washed (GP002). Bromine was substituted with glycine *tert*-butyl ester acetate (GP006) and the resin was washed (GP002). The cycle of acylation (GP005), washing (GP002), substitution (GP006), washing (GP002) was repeated with the remaining amines: 2-phenylethanamine, **11** and isobutylamine. Each acylation/substitution step was monitored by the chloranil test (GP019). The peptoid was cleaved from the resin (GP012), washed off the resin with DCM and dried. -R_1=Boc, -R_2=tBu – *MALDI-TOF* (matrix: CHCA), m/z (%): 858.58 (100), 800.54 (20), 875.66 (8) [M+H]$^+$. – *MALDI-TOF/TOF* (matrix: CHCA), m/z (%) [fragment]: 802.44 (100) [M-tBu]$^+$, 758.47 (90) [M-Boc]$^+$, 412.28 (12), 355.26 (55) [B$_2$]$^+$, 284.19 (12).
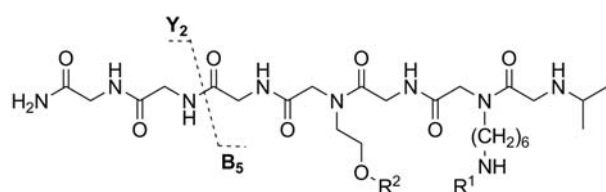

H_2N-Ahx-G-$Nser^{+1}Nval^{+0}Nlys^{+2}Nleu^{+0}$-H **59**: The resin **37** was acylated with bromoacetic acid (GP005) and washed (GP002). Bromine was substituted with 2-[(triisopropylsilyl)oxy]ethylamine (GP006) and the resin was washed (GP002). The cycle of acylation (GP005), washing (GP002), substitution (GP006), washing (GP002) was repeated with the remaining amines: isopropylamine, **11** and isobutylamine. Each acylation/substitution step was monitored by the chloranil test (GP019). The resin was split and from one half the Boc and TIPS protecting groups were removed (GP011) and the peptoid was cleaved from the resin (GP012). The peptoid was washed off the resin with DCM and dried. -R_1=Boc, -R_2=TIPS – *MALDI-TOF* (matrix: CHCA), m/z (%): 800.60 (100), 913.69 (55) [M+H]$^+$, 742.56 (43). – *MALDI-TOF/TOF* (matrix: CHCA), m/z (%) [fragment]: 857.53 (90) [M-tBu]$^+$, 813.56 (40) [M-Boc]$^+$, 544.37 (100) [Y$_4$+2 H]$^+$, 469.32 (30) [B$_3$]$^+$, 370.25 (28) [B$_3$]$^+$, 314.19 (13), 229.11 (58). -R_1=H, -R_2=H – *MALDI-TOF* (matrix: CHCA), m/z (%): 1198.92 (100), 699.55 (90), 657.53 (66) [M+H]$^+$. – *MALDI-TOF/TOF* (matrix: CHCA), m/z (%) [fragment]: 544.36 (25) [Y$_5$+2 H]$^+$, 470.32 (2) [B$_4$]$^+$, 388.25 (100) [Y$_4$+2 H]$^+$, 369.28 (35) [B$_3$]$^+$, 270.21 (40) [B$_2$]$^+$.

H_2N-Ahx-G-$Nser^{+1}Nleu^{+0}Nlys^{+2}Nval^{+0}$-H **60**: The resin **37** was acylated with bromoacetic acid (GP005) and washed (GP002). Bromine was substituted with 2-[(triisopropylsilyl)oxy]ethylamine (GP006) and the resin was washed (GP002). The cycle of acylation (GP005), washing (GP002),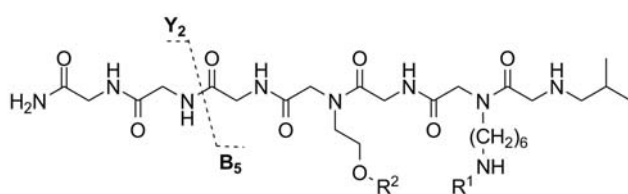 substitution (GP006), washing (GP002) was repeated with the remaining amines: isobutylamine, **11** and isopropylamine. Each acylation/substitution step was monitored by the chloranil test (GP019). The resin was split and from one half the Boc and TIPS protecting groups were removed (GP011) and the peptoid was cleaved from the resin (GP012). The peptoid was washed off the resin with DCM and dried. -R_1=Boc, -R_2=TIPS – *MALDI-TOF* (matrix: CHCA), m/z (%): 800.60 (100), 913.70 (55) [M+H]$^+$, 742.56 (35). – *MALDI-TOF/TOF* (matrix: CHCA), m/z (%) [fragment]: 857.53 (45) [M-tBu]$^+$, 814.56 (50) [M-Boc]$^+$, 558.39 (45) [Y$_4$+2 H]$^+$, 468.34 (20) [B$_3$]$^+$, 355.26 (100) [B$_2$]$^+$, 284.18 (18). -R_1=H, -R_2=H – *MALDI-TOF* (matrix: CHCA), m/z (%): 699.54 (100), 657.53 (95), [M+H]$^+$, 756.61

(73). – *MALDI-TOF/TOF* (matrix: CHCA), m/z (%) [fragment]: 558.38 (45) $[Y_5+2\ H]^+$, 470.32 (3) $[B_4]^+$, 402.27 (100) $[Y_4+2\ H]^+$, 369.28 (45) $[B_3]^+$, 256.20 (55) $[B_2]^+$.
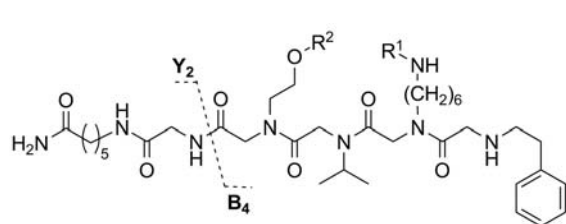
H_2N-Ahx-G-Nser^{+1}Nval^{+0}Nlys^{+2}Nphe^{+1}-H **61**: The resin **37** was acylated with bromoacetic acid (GP005) and washed (GP002). Bromine was substituted with 2-[(triisopropylsilyl)oxy]ethylamine (GP006) and the resin was washed (GP002). The cycle of acylation (GP005), washing (GP002), substitution (GP006), washing (GP002) was repeated with the remaining amines: isopropylamine, **11** and 2-phenylethanamine. Each acylation/substitution step was monitored by the chloranil test (GP019). The resin was split and from one half the Boc and TIPS protecting groups were removed (GP011) and the peptoid was cleaved from the resin (GP012). The peptoid was washed off the resin with DCM and dried. -R_1=Boc, -R_2=TIPS – *MALDI-TOF* (matrix: CHCA), m/z (%): 848.61 (100), 961.70 (43) $[M+H]^+$, 909.64 (38). – *MALDI-TOF/TOF* (matrix: CHCA), m/z (%) [fragment]: 905.52 (35) [M-tBu]$^+$, 862.55 (20) [M-Boc]$^+$, 544.36 (35) $[Y_4+2\ H]^+$, 517.29 (20) $[B_3]^+$, 418.25 (15) $[B_2]^+$, 229.10 (25). -R_1=H, -R_2=H – *MALDI-TOF* (matrix: CHCA), m/z (%): 705.52 (100) $[M+H]^+$, 866.62 (97), 747.54 (75). – *MALDI-TOF/TOF* (matrix: CHCA), m/z (%) [fragment]: 544.37 (20) $[Y_5+2\ H]^+$, 518.32 (4) $[B_4]^+$, 417.28 (40) $[B_3]^+$, 388.25 (100) $[Y_4+2\ H]^+$, 318.21 (50) $[B_2]^+$, 290.22 (18) $[Y_3+2\ H]^+$.
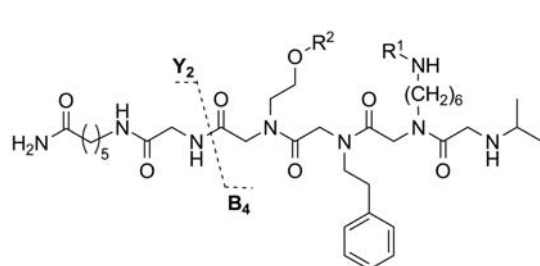
H_2N-Ahx-G-Nser^{+1}Nphe^{+1}Nlys^{+2}Nval^{+1}-H **62**: The resin **37** was acylated with bromoacetic acid (GP005) and washed (GP002). Bromine was substituted with 2-[(triisopropylsilyl)oxy]ethylamine (GP006) and the resin was washed (GP002). The cycle of acylation (GP005), washing (GP002), substitution (GP006), washing (GP002) was repeated with the remaining amines: 2-phenylethanamine, **11** and isopropylamine. Each acylation/substitution step was monitored by the chloranil test (GP019). The resin was split and from one half the Boc and TIPS protecting groups were removed (GP011) and the peptoid was cleaved from the resin (GP012). The peptoid was washed off the resin with DCM and dried. -R_1=Boc, -R_2=TIPS – *MALDI-TOF* (matrix: CHCA), m/z (%): 848.61 (100), 961.70 (43) $[M+H]^+$, 790.56 (32). – *MALDI-TOF/TOF* (matrix: CHCA), m/z (%) [fragment]: 905.51 (50) [M-tBu]$^+$, 861.59 (65) [M-Boc]$^+$, 606.38 (55) $[Y_4+2\ H]^+$, 517.29 (20) $[B_3]^+$, 355.25 (100) $[B_2]^+$. -R_1=H, -R_2=H – *MALDI-TOF* (matrix: CHCA), m/z (%): 1294.92 (100), 705.54 (77) $[M+H]^+$, 747.55 (75). – *MALDI-TOF/TOF* (matrix: CHCA), m/z (%) [fragment]: 606.38 (40) $[Y_5+2\ H]^+$, 518.32 (3) $[B_4]^+$, 450.27 (100) $[Y_4+2\ H]^+$, 417.28 (40) $[B_3]^+$, 256.20 (50) $[B_2]^+$, 228.20 (17).

H_2N-GGG-Nser^{+1}GlyNlys^{+2}Nval^{+0}-H **63**: The resin **36** was acylated with bromoacetic acid (GP005) and washed (GP002). Bromine was substituted with **10** (GP006) and the resin was washed (GP002). Fmoc-N-glycine was attached (G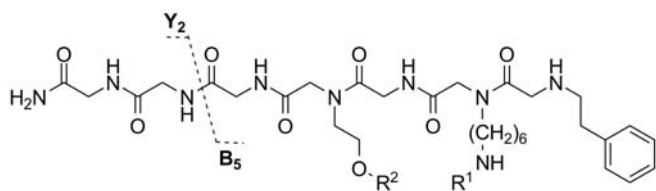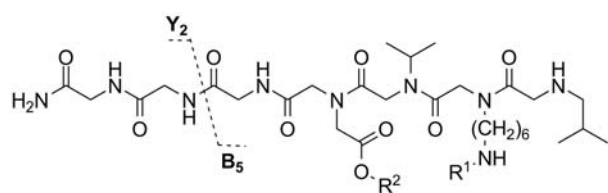P007, A) and the resin was washed (GP002). The cycle of acylation (GP005), washing (GP002), substitution (GP006), washing (GP002) was repeated

with the remaining amines: **11** and isopropylamine. Each acylation/substitution step was monitored by the chloranil test (GP019). The resin was split and from one half the Boc and TIPS protecting groups were removed (GP011) and the peptoid was cleaved from the resin (GP012). The peptoid was washed off the resin with DCM and dried. -R_1=Boc, -R_2=TIPS – *MALDI-TOF* (matrix: CHCA), m/z (%): 858.59 (100), 800.54 (20) [M+H]$^+$, 897.59 (20). – *MALDI-TOF/TOF* (matrix: CHCA), m/z (%) [fragment]: 802.44 (55) [M-tBu]$^+$, 758.48 (100) [M-Boc]$^+$ and [Y_6+2 H]$^+$, 669.46 (7) [B_4]$^+$, 503.30 (2) [Y_5+2 H]$^+$, 446.27 (3) [Y_4+2 H]$^+$, 412.28 (10) [B_3]$^+$, 355.26 (45) [B_2]$^+$, 284.19 (10). -R_1=H, -R_2=H – *MALDI-TOF* (matrix: CHCA), m/z (%): 702.48 (100), 732.43 (50), 602.41 (28) [M+H]$^+$. – *MALDI-TOF/TOF* (matrix: CHCA), m/z (%) [fragment]: 503.29 (100) [Y_6+2 H]$^+$, 414.25 (5) [B_4]$^+$, 347.17 (15) [Y_5+2 H]$^+$, 313.23 (12) [B_3]$^+$, 290.15 (12) [Y_4+2 H]$^+$, 256.20 (60) [B_2]$^+$, 228.21 (35).

H_2N-GGG-Nser^{+1}GlyNlys^{+2}Nleu^{+0}-H **64**: The resin **36** was acylated with bromoacetic acid (GP005) and washed (GP002). Bromine was substituted with **10** (GP006) and the resin was washed (GP002). Fmoc-N-g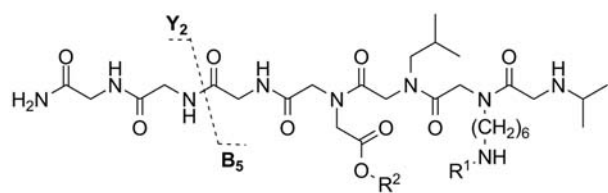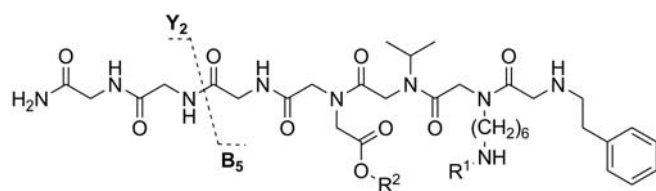lycine was attached (GP007, A) and the resin was washed (GP002). The cycle of acylation (GP005), washing (GP002), substitution (GP006), washing (GP002) was repeated with the remaining amines: **11** and isobutylamine. Each acylation/substitution step was monitored by the chloranil test (GP019). The resin was split and from one half the Boc and TIPS protecting groups were removed (GP011) and the peptoid was cleaved from the resin (GP012). The peptoid was washed off the resin with DCM and dried. -R_1=Boc, -R_2=TIPS – *MALDI-TOF* (matrix: CHCA), m/z (%): 872.59 (100) [M+H]$^+$, 885.63 (80) , 814.58 (48). – *MALDI-TOF/TOF* (matrix: CHCA), m/z (%) [fragment]: 816.43 (100) [M-tBu]$^+$, 773.44 (20) [M-Boc]$^+$, 758.42 (7) [Y_6+2 H]$^+$, 503.28 (2) [Y_5+2 H]$^+$. -R_1=H, -R_2=H – *MALDI-TOF* (matrix: CHCA), m/z (%): 769.52 (100), 746.45 (52), 616.44 (20) [M+H]$^+$. – *MALDI-TOF/TOF* (matrix: CHCA), m/z (%) [fragment]: 503.28 (100) [Y_6+2 H]$^+$, 485.30 (5) [B_5]$^+$, 428.28 (8) [B_4]$^+$, 383.30 (13), 327.16 (17) [B_3]$^+$, 290.14 (10) [Y_4+2 H]$^+$, 270.21 (55) [B_2]$^+$, 242.22 (45).

H_2N-GGG-Nser^{+1}GlyNlys^{+2}Nphe^{+1}-H **65**: The resin **36** was acylated with bromoacetic acid (GP005) and washed (GP002). Bromine was substituted with **10** (GP006) and the resin was washed (GP002). Fmoc-N-glycine was attached (GP007, A) and the resin was washed (GP002). The cycle of acylation (GP005), washing (GP002), substitution (GP006), washing (GP002) was repeated with the remaining amines: **11** and 2-phenylethanamine. Each acylation/substitution step was monitored by the chloranil test (GP019). The peptoid was cleaved from the resin (GP012) and washed off the resin with DCM and dried. -R_1=Boc, -R_2=TIPS – *MALDI-TOF* (matrix: CHCA), m/z (%): 920.60 (100) [M+H]$^+$, 981.64 (80) , 862.56 (55). – *MALDI-TOF/TOF* (matrix: CHCA), m/z (%) [fragment]: 864.43 (100) [M-tBu]$^+$, 821.45 (18) [M-Boc]$^+$, 758.42 (8) [Y_6+2 H]$^+$.

H₂N-GGG-Nser⁺¹Nval⁺⁰Nlys⁺²Gly-H **66**: The resin **36** was acylated with bromoacetic acid (GP005) and washed (GP002). Bromine was substituted with **10** (GP006) and the resin was washed (GP002). The cycle of acylation (GP005), washing (GP002), substitution (GP006), washing (GP002) was repeated with the remaining amines: isopropylamine and **11**. Each acylation/substitution step was monitored by the chloranil test (GP019). Fmoc-N-glycine was attached (GP007, A) and the resin was washed (GP002). The peptoid was cleaved from the resin (GP012) and washed off the resin with DCM and dried. -R_1=Boc, -R_2=TIPS – *MALDI-TOF* (matrix: CHCA), m/z (%): 670.46 (100), 727.49 (15), 858.59 (13) [M+H]⁺. – *MALDI-TOF/TOF* (matrix: CHCA), m/z (%) [fragment]: 802.44 (55) [M-tBu]⁺ and [Y_6+2 H]⁺, 758.46 (30) [M-Boc]⁺, 642.40 (27), 557.34 (20), 545.34 (100) [Y_5+2 H]⁺, 413.23 (10) [B_3]⁺, 410.24 (15), 314.20 [B_2]⁺, 308.20 (20).

H₂N-GGG-Nser⁺¹Nleu⁺⁰Nlys⁺²Gly-H **67**: The resin **36** was acylated with bromoacetic acid (GP005) and washed (GP002). Bromine was substituted with **10** (GP006) and the resin was washed (GP002). The cycle of acylation (GP005), washing (GP002), substitution (GP006), washing (GP002) was repeated with the remaining amines: isobutylamine and **11**. Each acylation/substitution step was monitored by the chloranil test (GP019). Fmoc-N-glycine was attached (GP007, A) and the resin was washed (GP002). The peptoid was cleaved from the resin (GP012) and washed off the resin with DCM and dried. -R_1=Boc, -R_2=TIPS – *MALDI-TOF* (matrix: CHCA), m/z (%): 684.48 (100), 872.60 (70), 814.56 (50) [M+H]⁺. – *MALDI-TOF/TOF* (matrix: CHCA), m/z (%) [fragment]: 816.44 (65) [M-tBu]⁺, 772.46 (33) [M-Boc]⁺, 616.36 (15), 559.35 (100) [Y_5+2 H]⁺, 427.22 (4) [B_3]⁺, 424.24 (20), 314.18 (8) [B_2]⁺, 311.16 (20).

H₂N-GGG-Nser⁺¹Nphe⁺⁰Nlys⁺²Gly-H **68**: The resin **36** was acylated with bromoacetic acid (GP005) and washed (GP002). Bromine was substituted with **10** (GP006) and the resin was washed (GP002). The cycle of acylation (GP005), washing (GP002), substitution (GP006), washing (GP002) was repeated with the remaining amines: 2-phenylethanamine and **11**. Each acylation/substitution step was monitored by the chloranil test (GP019). Fmoc-N-glycine was attached (GP007, A) and the resin was washed (GP002). The peptoid was cleaved from the resin (GP012) and washed off the resin with DCM and dried. -R_1=Boc, -R_2=TIPS – *MALDI-TOF* (matrix: CHCA), m/z (%): 732.48 (100), 920.60 (60) [M+H]⁺, 862.56 (30). – *MALDI-TOF/TOF* (matrix: CHCA), m/z (%) [fragment]: 864.43 (55) [M-tBu]⁺, 820.46 (35) [M-Boc]⁺, 664.36 (18), 647.39 (22), 607.35 (100) [Y_5+2 H]⁺, 472.25 (20) [B_3]⁺, 314.19 (10) [B_2]⁺, 311.17 (19).

H_2N-GGG-Nasp^{+0}Nval^{+0}Nlys^{+2}Nleu^{+0}-H **69**: The resin **36** was acylated with bromoacetic acid (GP005) and washed (GP002). Bromine was substituted with glycine *tert*-butyl ester acetate (GP006) and the resin was washed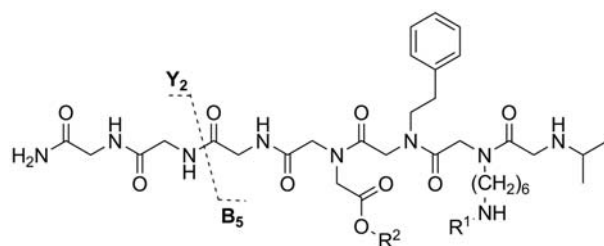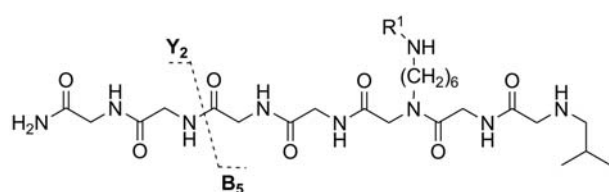 (GP002). The cycle of acylation (GP005), washing (GP002), substitution (GP006), washing (GP002) was repeated with the remaining amines: isopropylamine, **11**, isobutylamine. Each acylation/substitution step was monitored by the chloranil test (GP019). The resin was split and from one half the Boc and TIPS protecting groups were removed (GP011) and the peptoid was cleaved from the resin (GP012). The peptoid was washed off the resin with DCM and dried. -R$_1$=Boc, -R$_2$=tBu – *MALDI-TOF* (matrix: CHCA), m/z (%): 828.55 (100) [M+H]$^+$, 881.58 (30), 772.49 (15). – *MALDI-TOF/TOF* (matrix: CHCA), m/z (%) [fragment]: 772.39 (100) [M-tBu]$^+$, 729.40 (8) [M-Boc]$^+$, 469.30 (5) [B$_3$]$^+$, 459.23 (15) [Y$_5$+2 H]$^+$, 370.25 (8) [B$_2$]$^+$, 229.10 (13). -R$_1$=H, -R$_2$=H – *MALDI-TOF* (matrix: CHCA), m/z (%): 825.55 (100), 802.45 (30), 672.46 (23) [M+H]$^+$. – *MALDI-TOF/TOF* (matrix: CHCA), m/z (%) [fragment]: 559.31 (35) [Y$_6$+2 H]$^+$, 484.36 (3) [B$_4$]$^+$, 403.19 (100) [Y$_5$+2 H]$^+$, 383.31 (25), 369.28 (35) [B$_3$]$^+$, 270.22 (55) [B$_2$]$^+$, 242.22 (20).

H_2N-GGG-Nasp^{+0}Nleu^{+0}Nlys^{+2}Nval^{+0}-H **70**: The resin **36** was acylated with bromoacetic acid (GP005) and washed (GP002). Bromine was substituted with glycine *tert*-butyl ester acetate (GP006) and the resin was washed (GP002). The cycle of acylation (GP005), washing (GP002), substitution (GP006), washing (GP002) was repeated with the remaining amines: isobutylamine, **11**, isopropylamine. Each acylation/substitution step was monitored by the chloranil test (GP019). The resin was split and from one half the Boc and TIPS protecting groups were removed (GP011) and the peptoid was cleaved from the resin (GP012). The peptoid was washed off the resin with DCM and dried. -R$_1$=Boc, -R$_2$=tBu – *MALDI-TOF* (matrix: CHCA), m/z (%): 828.55 (100) [M+H]$^+$, 714.50 (23), 772.49 (17). – *MALDI-TOF/TOF* (matrix: CHCA), m/z (%) [fragment]: 772.40 (100) [M-tBu]$^+$, 729.39 (10) [M-Boc]$^+$, 473.24 (7) [Y$_5$+2 H]$^+$, 355.25 (6) [B$_2$]$^+$. -R$_1$=H, -R$_2$=H – *MALDI-TOF* (matrix: CHCA), m/z (%): 811.55 (100), 825.56 (97), 672.46 (48) [M+H]$^+$. – *MALDI-TOF/TOF* (matrix: CHCA), m/z (%) [fragment]: 573.31 (80) [Y$_6$+2 H]$^+$, 457.20 (20), 417.21 (100) [Y$_5$+2 H]$^+$, 369.29 (55) [B$_3$]$^+$, 256.20 (85) [B$_2$]$^+$, 228.20 (33).

H_2N-GGG-Nasp^{+0}Nval^{+0}Nlys^{+2}Nphe^{+1}-H **71**: The resin **36** was acylated with bromoacetic acid (GP005) and washed (GP002). Bromine was substituted with glycine *tert*-butyl ester acetate (GP006) and the resin was washed (GP002). The cycle of acylation (GP005), washing (GP002), substitution (GP006), washing (GP002) was repeated with the remaining amines: isobutylamine, **11**, 2-phenylethanamine. Each acylation/substitution step was monitored by the chloranil test (GP019). The resin was split and from one half the Boc and TIPS protecting groups were removed (GP011) and the peptoid was cleaved from the resin (GP012). The peptoid was washed off the

resin with DCM and dried. -R_1=Boc, -R_2=tBu – *MALDI-TOF* (matrix: CHCA), m/z (%): 876.54 (100) [M+H]$^+$, 977.57 (40) , 937.57 (30). – *MALDI-TOF/TOF* (matrix: CHCA), m/z (%) [fragment]: 820.40 (100) [M-tBu]$^+$, 777.40 (7) [M-Boc]$^+$, 720.39 (9), 479.27 (9), 459.23 (12) [Y_5+2 H]$^+$, 418.25 (7) [B_2]$^+$. -R_1=H, -R_2=H – *MALDI-TOF* (matrix: CHCA), m/z (%): 881.56 (100), 720.46 (80) [M+H]$^+$, 762.48 (50). – *MALDI-TOF/TOF* (matrix: CHCA), m/z (%) [fragment]: 559.31 (35) [Y_6+2 H]$^+$, 532.32 (3) [B_4]$^+$, 417.29 (40) [B_3]$^+$, 403.20 (100) [Y_5+2 H]$^+$, 318.22 (70) [B_2]$^+$.

H_2N-GGG-Nasp^{+0}Nval^{+0}Nlys^{+2}Nphe^{+1}-H **72**: The resin **36** was acylated with bromoacetic acid (GP005) and washed (GP002). Bromine was substituted with glycine *tert*-butyl ester acetate (GP006) and the resin was washed (GP002). The cycle of acylation (GP005), washing (GP002), substitution (GP006), washing (GP002) was repeated with the remaining amines: isobutylamine, **11**, 2-phenylethanamine. Each acylation/substitution step was monitored by the chloranil test (GP019). The resin was split and from one half the Boc and TIPS protecting groups were removed (GP011) and the peptoid was cleaved from the resin (GP012). The peptoid was washed off the resin with DCM and dried. -R_1=Boc, -R_2=tBu – *MALDI-TOF* (matrix: CHCA), m/z (%): 876.54 (100) [M+H]$^+$, 858.48 (40) , 902.56 (38). – *MALDI-TOF/TOF* (matrix: CHCA), m/z (%) [fragment]: 820.40 (100) [M-tBu]$^+$, 777.41 (10) [M-Boc]$^+$, 521.25 (8) [Y_5+2 H]$^+$, 356.23 (6) [B_2]$^+$. -R_1=H, -R_2=H – *MALDI-TOF* (matrix: CHCA), m/z (%): 859.52 (100), 921.54 (95), 720.44 (50) [M+H]$^+$. – *MALDI-TOF/TOF* (matrix: CHCA), m/z (%) [fragment]: 621.34 (55) [Y_6+2 H]$^+$, 465.22 (100) [Y_5+2 H]$^+$, 417.29 (40) [B_3]$^+$, 256.20 (55) [B_2]$^+$, 228.21 (20).
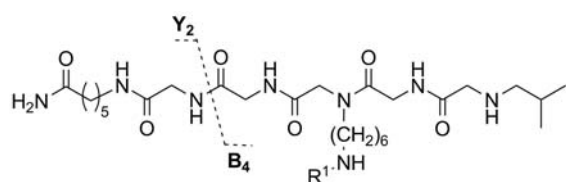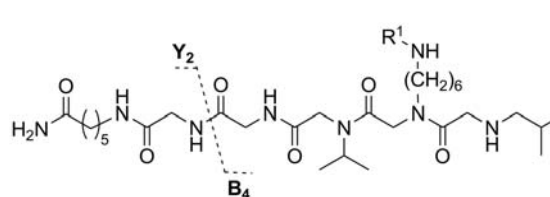

H_2N-Ahx-G-GlyNlys^{+2}GlyNleu^{+0}-H **73**: Fmoc-N-glycine was attached to resin **37** (GP007, A) and the resin was washed (GP002). The resin was then acylated with bromoacetic acid (GP005) and washed (GP002). Bromine was substituted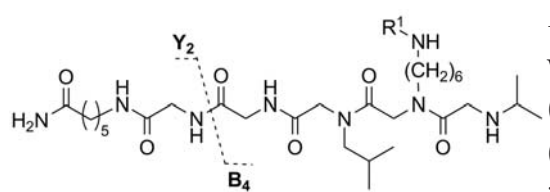 with **11** (GP006) and the resin was washed (GP002). Fmoc-N-glycine was attached (GP007, A) and the resin was washed (GP002). The cycle of acylation (GP005), washing (GP002), substitution (GP006), washing (GP002) was repeated with isobutylamine. Each acylation/substitution step was monitored by the chloranil test (GP019). The resin was split and from one half the Boc protecting group was removed (GP011) and the peptoid was cleaved from the resin (GP012). The peptoid was washed off the resin with DCM and dried. -R_1=Boc – *MALDI-TOF* (matrix: CHCA), m/z (%): 671.45 (100) [M+H]$^+$, 571.86 (93), 1103.71 (60). – *MALDI-TOF/TOF* (matrix: CHCA), m/z (%) [fragment]: 615.36 (30) [M-tBu]$^+$, 571.38 (50) [M-Boc]$^+$, 555.32 (45) [Y_5+2 H]$^+$, 498.31 (100) [Y_4+2 H]$^+$, 481.27 (30) [B_4]$^+$, 424.25 (98), [B_3]$^+$. -R_1=H – *MALDI-TOF* (matrix: CHCA), m/z (%): 668.44 (100), 741.53 (70), 571.41 (50) [M+H]$^+$. – *MALDI-TOF/TOF* (matrix: CHCA), m/z (%) [fragment]: 458.32 (45) [Y_5+2 H]$^+$, 441.29 (10) [B_5]$^+$, 401.30 (100) [Y_4+2 H]$^+$, 384.27 (15) [B_4]$^+$, 327.25 (40) [B_3]$^+$, 299.28 (12), 242.16 (3) [Y_3+2 H]$^+$, 214.17 (12).
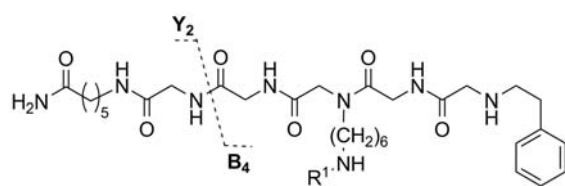
$H_2N\text{-}Ahx\text{-}G\text{-}GlyNlys^{+2}GlyNphe^{+1}\text{-}H$ **74**: Fmoc-N-glycine was attached to resin **37** (GP007, A) and the resin was washed (GP002). The resin was then acylated with bromoacetic acid (GP005) and washed (GP002). Bromine was substituted with **11** (GP006) and the resin was washed (GP002). Fmoc-N-glycine was attached (GP007, A) and the resin was washed (GP002). The cycle of acylation (GP005), washing (GP002), substitution (GP006), washing (GP002) was repeated with 2-phenylethanamine. Each acylation/substitution step was monitored by the chloranil test (GP019). The resin was split and from one half the Boc protecting group was removed (GP011) and the peptoid was cleaved from the resin (GP012). The peptoid was washed off the resin with DCM and dried. -R_1=Boc – *MALDI-TOF* (matrix: CHCA), m/z (%): 719.48 (100) [M+H]$^+$, 619.42 (68), 837.53 (62). – *MALDI-TOF/TOF* (matrix: CHCA), m/z (%) [fragment]: 663.36 (50) [M-tBu]$^+$, 619.38 (85) [M-Boc]$^+$, 555.33 (30) [Y$_5$+2 H]$^+$, 498.31 (100) [Y$_4$+2 H]$^+$, 472.26 (75) [B$_3$]$^+$. -R_1=H – *MALDI-TOF* (matrix: CHCA), m/z (%): 619.44 (100) [M+H]$^+$, 837.56 (85), 1122.73 (60). – *MALDI-TOF/TOF* (matrix: CHCA), m/z (%) [fragment]: 489.28 (10), 458.31 (40) [Y$_5$+2 H]$^+$, 432.26 (15) [B$_4$]$^+$, 401.29 (100) [Y$_4$+2 H]$^+$, 375.24 (60) [B$_3$]$^+$, 347.25 (10), 219.11 (3) [B$_2$]$^+$.
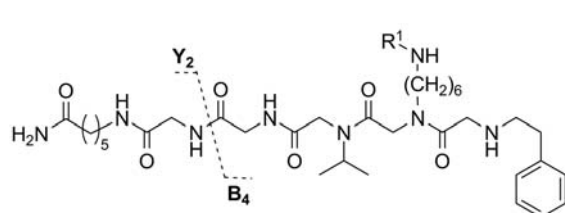

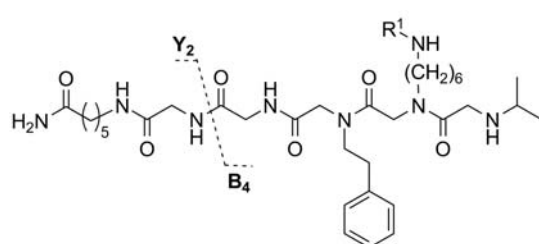$H_2N\text{-}GGG\text{-}GlyNlys^{+2}GlyNleu^{+0}\text{-}H$ **75**: Fmoc-N-glycine was attached to resin **36** (GP007, A) and the resin was washed (GP002). The resin was then acylated with bromoacetic acid (GP005) and washed (GP002). Bromine was substituted with **11** (GP006) and the resin was washed (GP002). Fmoc-N-glycine was attached (GP007, A) and the resin was washed (GP002). The cycle of acylation (GP005), washing (GP002), substitution (GP006), washing (GP002) was repeated with isobutylamine. Each acylation/substitution step was monitored by the chloranil test (GP019). The resin was split and from one half the Boc protecting group was removed (GP011) and the peptoid was cleaved from the resin (GP012). The peptoid was washed off the resin with DCM and dried. -R_1=Boc – *MALDI-TOF* (matrix: CHCA), m/z (%): 715.48 (100), 658.46 (98), 672.44 (53) [M+H]$^+$. – *MALDI-TOF/TOF* (matrix: CHCA), m/z (%) [fragment]: 616.31 (40) [M-tBu]$^+$, 595.33 (15), 556.30 (45), 499.26 (100) [Y$_5$+2 H]$^+$, 424.25 (65) [B$_3$]$^+$, 197.16 (80). -R_1=H – *MALDI-TOF* (matrix: CHCA), m/z (%): no target signal. – *MALDI-TOF/TOF* (matrix: CHCA), m/z (%) [fragment]: 459.26 (45) [Y$_6$+2 H]$^+$, 441.27 (10), 407.22 (15), 402.24 (100) [Y$_5$+2 H]$^+$, 384.25 (10) [B$_4$]$^+$, 327.23 (45) [B$_3$]$^+$, 214.14 (10), 190.06 (65) [Y$_3$+2 H]$^+$, 172.10 (15) [B$_2$]$^+$.
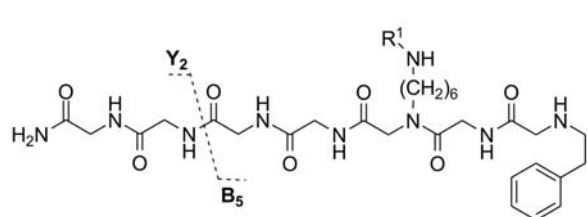

$H_2N\text{-}GGG\text{-}GlyNlys^{+2}GlyNphe^{+1}\text{-}H$ **76**: Fmoc-N-glycine was attached to resin **36** (GP007, A) and the resin was washed (GP002). The resin was then acylated with bromoacetic acid (GP005) and washed (GP002). Bromine was substituted with **11** (GP006) and the resin was washed (GP002). Fmoc-N-glycine was attached (GP007, A) and the resin was washed (GP002). The cycle of acylation (GP005), washing (GP002), substitution (GP006), washing (GP002) was repeated with 2-phenylethanamine. Each acylation/substitution step was monitored by the chloranil test (GP019). The

resin was split and from one half the Boc protecting group was removed (GP011) and the peptoid was cleaved from the resin (GP012). The peptoid was washed off the resin with DCM and dried. $-R_1=$Boc – *MALDI-TOF* (matrix: CHCA), m/z (%): 720.44 (100) $[M+H]^+$, 838.49 (80), 620.38 (40) . – *MALDI-TOF/TOF* (matrix: CHCA), m/z (%) [fragment]: 664.32 (45) $[M-tBu]^+$, 556.31 (35) $[Y_6+2\,H]^+$, 499.26 (100) $[Y_5+2\,H]^+$, 472.27 (80) $[B_3]^+$. $-R_1=$H – *MALDI-TOF* (matrix: CHCA), m/z (%): 717.42 (100), 838.52 (70), 620.40 (10). – *MALDI-TOF/TOF* (matrix: CHCA), m/z (%) [fragment]: 489.29 (10) $[B_5]^+$, 459.27 (50) $[Y_6+2\,H]^+$, 432.26 (10) $[B_4]^+$, 402.25 (100) $[Y_5+2\,H]^+$, 375.24 (45) $[B_3]^+$, 347.25 (20), 219.12 (2) $[B_2]^+$.

H_2N-Ahx-G-GlyNval^{+0}Nlys^{+2}Nleu^{+0}-H **77**: Fmoc-N-glycine was attached to resin **37** (GP007, A) and the resin was washed (GP002). The resin was then acylated with bromoacetic acid (GP005) and washed (GP002). Bromine was substituted with isopropylamine (GP006) and the resin was washed (GP002). The cycle of acylation (GP005), washing (GP002), substitution (GP006), washing (GP002) was repeated with **11** and isobutylamine. Each acylation/substitution step was monitored by the chloranil test (GP019). The resin was split and from one half the Boc protecting group was removed (GP011) and the peptoid was cleaved from the resin (GP012). The peptoid was washed off the resin with DCM and dried. $-R_1=$Boc – *MALDI-TOF* (matrix: CHCA), m/z (%): 714.50 (100) $[M+H]^+$, 727.53 (60), 655.46 (25). – *MALDI-TOF/TOF* (matrix: CHCA), m/z (%) [fragment]: 657.40 (100) $[M-tBu]^+$, 614.40 (60) $[M-Boc]^+$, 370.26 (8) $[B_2]^+$. $-R_1=$H – *MALDI-TOF* (matrix: CHCA), m/z (%): 726.55 (100), 613.46 (73) $[M+H]^+$, 655.47 (52). – *MALDI-TOF/TOF* (matrix: CHCA), m/z (%) [fragment]: 500,36 (85) $[Y_5+2\,H]^+$, 483.33 (5) $[B_5]^+$, 457.32 (12), 427.24 (5) $[B_4]^+$, 399.23 (12), 369.29 (45) $[B_3]^+$, 344.24 (90) $[Y_4+2\,H]^+$, 330.21 (10), 270.22 (100) $[B_2]^+$, 242.23 (50).

H_2N-Ahx-G-GlyNleu^{+0}Nlys^{+2}Nval^{+0}-H **78**: Fmoc-N-glycine was attached to resin **37** (GP007, A) and the resin was washed (GP002). The resin was then acylated with bromoacetic acid (GP005) and washed (GP002). Bromine was substituted with isobutylamine (GP006) and the resin was washed (GP002). The cycle of acylation (GP005), washing (GP002), substitution (GP006), washing (GP002) was repeated with **11** and isopropylamine. Each acylation/substitution step was monitored by the chloranil test (GP019). The resin was split and from one half the Boc protecting group was removed (GP011) and the peptoid was cleaved from the resin (GP012). The peptoid was washed off the resin with DCM and dried. $-R_1=$Boc – *MALDI-TOF* (matrix: CHCA), m/z (%): 713.52 (100) $[M+H]^+$. – *MALDI-TOF/TOF* (matrix: CHCA), m/z (%) [fragment]: 657.39 (95) $[M-tBu]^+$, 613.42 (100) $[M-Boc]^+$, 468.33 (8) $[B_3]^+$, 355.26 (48) $[Y_4+2\,H]^+$ and $[B_2]^+$. $-R_1=$H – *MALDI-TOF* (matrix: CHCA), m/z (%): 712.55 (100), 1110.80 (90), 613.47 (75) $[M+H]^+$. – *MALDI-TOF/TOF* (matrix: CHCA), m/z (%) [fragment]: 514.37 (100) $[Y_5+2\,H]^+$, 483.32 (5) $[B_5]^+$, 426.31 (6) $[B_4]^+$, 369.29 (35) $[B_3]^+$, 358.25 (60) $[Y_4+2\,H]^+$, 256.20 (85) $[B_2]^+$.

H_2N-Ahx-G-Gly$Nval^{+0}Nlys^{+2}Nphe^{+1}$-H **79**: Fmoc-N-glycine was attached to resin **37** (GP007, A) and the resin was washed (GP002). The resin was then acylated with bromoacetic acid (GP005) and washed (GP002). Bromine was substituted with isopropylamine (GP006) and the resin was washed (GP002). The cycle of acylation (GP005), washing (GP002), substitution (GP006), washing (GP002) was repeated with **11** and 2-phenylethanamine. Each acylation/substitution step was monitored by the chloranil test (GP019). The resin was split and from one half the Boc protecting group was removed (GP011) and the peptoid was cleaved from the resin (GP012). The peptoid was washed off the resin with DCM and dried. -R_1=Boc – *MALDI-TOF* (matrix: CHCA), m/z (%): 762.52 (100) [M+H]$^+$, 823.55 (70), 704.47 (25). – *MALDI-TOF/TOF* (matrix: CHCA), m/z (%) [fragment]: 705.40 (100) [M-tBu]$^+$, 662.40 (65) [M-Boc]$^+$, 600.39 (5) [Y_5+2 H]$^+$, 517.32 (5) [B_3]$^+$, 418.26 (12) [B_2]$^+$. -R_1=H – *MALDI-TOF* (matrix: CHCA), m/z (%): 822.58 (100), 1304.93 (65), 661.48 (40) [M+H]$^+$. – *MALDI-TOF/TOF* (matrix: CHCA), m/z (%) [fragment]: 531.33 (3) [B_5]$^+$, 500.36 (43) [Y_5+2 H]$^+$, 474.31 (6) [B_4]$^+$, 417.29 (45) [B_3]$^+$, 389.29 (15), 344.23 (100) [Y_4+2 H]$^+$, 318.22 (55) [B_2]$^+$, 290.22 (58).

H_2N-Ahx-G-Gly$Nphe^{+1}Nlys^{+2}Nval^{+0}$-H **80**: Fmoc-N-glycine was attached to resin **37** (GP007, A) and the resin was washed (GP002). The resin was then acylated with bromoacetic acid (GP005) and washed (GP002). Bromine was substituted with 2-phenylethanamine (GP006) and the resin was washed (GP002). The cycle of acylation (GP005), washing (GP002), substitution (GP006), washing (GP002) was repeated with **11** and isopropylamine. Each acylation/substitution step was monitored by the chloranil test (GP019). The resin was split and from one half the Boc protecting group was removed (GP011) and the peptoid was cleaved from the resin (GP012). The peptoid was washed off the resin with DCM and dried. -R_1=Boc – *MALDI-TOF* (matrix: CHCA), m/z (%): 761.53 (100) [M+H]$^+$, 703.48 (15). – *MALDI-TOF/TOF* (matrix: CHCA), m/z (%) [fragment]: 705.41 (100) [M-tBu]$^+$, 661.44 (65) [M-Boc]$^+$, 516.35 (5) [B_3]$^+$, 406.25 (5) [Y_4+2 H]$^+$, 355.27 (10) [B_2]$^+$. -R_1=H – *MALDI-TOF* (matrix: CHCA), m/z (%): 1206.83 (100), 760.57 (85), 661.49 (70) [M+H]$^+$. – *MALDI-TOF/TOF* (matrix: CHCA), m/z (%) [fragment]: 562.37 (100) [Y_5+2 H]$^+$, 531.33 (4) [B_5]$^+$, 474.31 (6) [B_4]$^+$, 417.29 (40) [B_3]$^+$, 406.25 (80) [Y_4+2 H]$^+$, 256.20 (85) [B_2]$^+$, 228.21 (55).
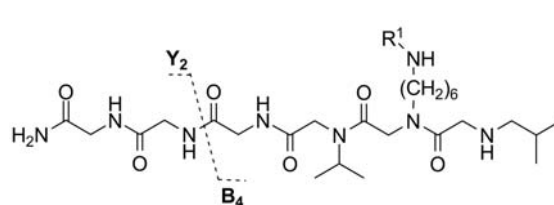
H_2N-GGG-$Nval^{+0}Nlys^{+2}Nleu^{+0}$-H **81**: The resin **36** was acylated with bromoacetic acid (GP005) and washed (GP002). Bromine was substituted with isopropylamine (GP006) and the resin was washed (GP002). The cycle of acylation (GP005), washing (GP002), substitution (GP006), washing (GP002) was repeated with **11** and isobutylamine. Each acylation/substitution step was monitored by the chloranil test (GP019). The resin was split and from one half the Boc protecting group was removed (GP011) and the peptoid was cleaved from the resin (GP012). The peptoid was washed off the resin with DCM and dried. -R_1=Boc – *MALDI-TOF* (matrix: CHCA), m/z (%): 657.48 (100) [M+H]$^+$, 670.49 (45),

710.49 (20). – *MALDI-TOF/TOF* (matrix: CHCA), m/z (%) [fragment]: 601.36 (100) [M-tBu]$^+$, 557.38 (8) [M-Boc]$^+$, 544.33 (5) [Y$_5$+2 H]$^+$, 469.33 (2) [B$_3$]$^+$, 302.23 (3) [Y$_4$+2 H]$^+$. -R$_1$=H – *MALDI-TOF* (matrix: CHCA), m/z (%): 670.51 (100), 557.42 (49) [M+H]$^+$, 599.43 (45). – *MALDI-TOF/TOF* (matrix: CHCA), m/z (%) [fragment]: 444.29 (70) [Y$_6$+2 H]$^+$, 426.31 (2) [B$_4$]$^+$, 383.31 (20), 369.29 (25) [B$_3$]$^+$, 288.17 (35) [Y$_5$+2 H]$^+$, 270.22 (100) [B$_2$]$^+$, 242.23 (43).
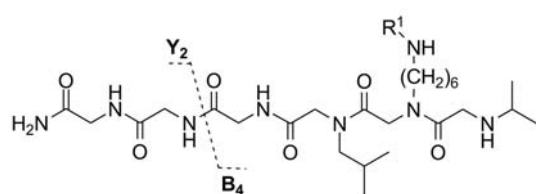
*H$_2$N-GGG-Nleu^{+0}Nlys^{+2}Nval^{+0}-H* **82**: The resin **36** was acylated with bromoacetic acid (GP005) and washed (GP002). Bromine was substituted with isobutylamine (GP006) and the resin was washed (GP002). The cycle of acylation (GP005), washing (GP002), substitution (GP006), washing (GP002) was repeated with **11** and isopropylamine. Each acylation/substitution step was monitored by the chloranil test (GP019). The resin was split and from one half the Boc protecting group was removed (GP011) and the peptoid was cleaved from the resin (GP012). The peptoid was washed off the resin with DCM and dried. -R$_1$=Boc – *MALDI-TOF* (matrix: CHCA), m/z (%): 657.45 (100) [M+H]$^+$, 696.46 (15). – *MALDI-TOF/TOF* (matrix: CHCA), m/z (%) [fragment]: 601.38 (100) [M-tBu]$^+$, 557.39 (35) [M-Boc]$^+$, 469.33 (3) [B$_3$]$^+$, 355.27 (15) [B$_2$]$^+$, 302.23 (3) [Y$_4$+2 H]$^+$. -R$_1$=H – *MALDI-TOF* (matrix: CHCA), m/z (%): 656.49 (100), 696.50 (80), 557.42 (58) [M+H]$^+$. – *MALDI-TOF/TOF* (matrix: CHCA), m/z (%) [fragment]: 458.31 (100) [Y$_6$+2 H]$^+$, 369.29 (25) [B$_3$]$^+$, 302.19 (25) [Y$_5$+2 H]$^+$, 256.20 [B$_2$]$^+$, 228.21 (43).
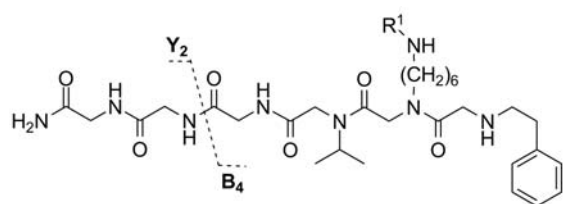
H$_2$N-GGG-Nval^{+0}Nlys^{+2}Nphe^{+1}-H **83**: The resin **36** was acylated with bromoacetic acid (GP005) and washed (GP002). Bromine was substituted with isopropylamine (GP006) and the resin was washed (GP002). The cycle of acylation (GP005), washing (GP002), substitution (GP006), washing (GP002) was repeated with **11** and 2-phenylethanamine. Each acylation/substitution step was monitored by the chloranil test (GP019). The resin was split and from one half the Boc protecting group was removed (GP011) and the peptoid was cleaved from the resin (GP012). The peptoid was washed off the resin with DCM and dried. -R$_1$=Boc – *MALDI-TOF* (matrix: CHCA), m/z (%): 705.44 (100) [M+H]$^+$, 766.48 (85), 806.48 (23). – *MALDI-TOF/TOF* (matrix: CHCA), m/z (%) [fragment]: 649.36 (100) [M-tBu]$^+$, 605.38 (10) [M-Boc]$^+$, 544.34 (5) [Y$_5$+2 H]$^+$, 517.33 (2) [B$_3$]$^+$, 418.26 (6) [B$_2$]$^+$. -R$_1$=H – *MALDI-TOF* (matrix: CHCA), m/z (%): 766.51 (100), 647.43 (30), 605.42 (25) [M+H]$^+$. – *MALDI-TOF/TOF* (matrix: CHCA), m/z (%) [fragment]: 531.32 (5) [B$_5$]$^+$, 474.30 (5) [B$_4$]$^+$, 444.29 (70) [Y$_6$+2 H]$^+$, 417.28 (50) [B$_3$]$^+$, 389.29 (15), 318.21 (100) [B$_2$]$^+$, 290.22 (95), 288.16 (65) [Y$_5$+2 H]$^+$.
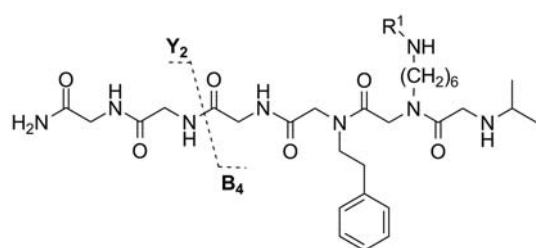
H$_2$N-GGG-Nphe^{+1}Nlys^{+2}Nval^{+0}-H **84**: The resin **36** was acylated with bromoacetic acid (GP005) and washed (GP002). Bromine was substituted with 2-phenylethanamine (GP006) and the resin was washed (GP002). The cycle of acylation (GP005), washing (GP002), substitution (GP006), washing (GP002) was repeated with **11** and isopropylamine. Each acy-

lation/substitution step was monitored by the chloranil test (GP019). The resin was split and from one half the Boc protecting group was removed (GP011) and the peptoid was cleaved from the resin (GP012). The peptoid was washed off the resin with DCM and dried. -R$_1$=Boc – *MALDI-TOF* (matrix: CHCA), m/z (%): 705.44 (100) [M+H]$^+$, 806.47 (15). – *MALDI-TOF/TOF* (matrix: CHCA), m/z (%) [fragment]: 649.38 (100) [M-tBu]$^+$, 605.39 (45) [Y$_5$+2 H]$^+$, 516.36 (3) [B$_3$]$^+$, 355.27 (25) [B$_2$]$^+$, 350.18 (3) [Y$_4$+2 H]$^+$, 229.11 (10). -R$_1$=H – *MALDI-TOF* (matrix: CHCA), m/z (%): 806.51 (100), 704.48 (78), 605.41 (53) [M+H]$^+$. – *MALDI-TOF/TOF* (matrix: CHCA), m/z (%) [fragment]: 531.32 (4) [B$_5$]$^+$, 506.30 (100) [Y$_6$+2 H]$^+$, 474.30 (5) [B$_4$]$^+$, 417.28 (35) [B$_3$]$^+$, 350.18 (45) [Y$_5$+2 H]$^+$, 256.20 (90) [B$_2$]$^+$, 228.20 (55).

H$_2$N-AKWRMVLRI--Ahx--ADTLMRTQ on TentaGel MB HMBA, TG-IL8RPLoops **85**: Synthesis by K. Brahm and W. Blum (Liberty synthesizer, Thiele group, TU Darmstadt). Amino acids with side-chain protecting groups used: Fmoc-Lys(Boc)-OH, Fmoc-Trp(Boc)-OH, Fmoc-Arg(Pbf)-OH, Fmoc-His(Trt)-OH, Fmoc-Asp(O*t*Bu)-OH Fmoc-Thr(*t*Bu)-OH. 100 mg TG-HMBA macrobeads (ø 300 μm, 0.24 mmol/g) were swollen according to GP001. The first amino acid was attached manually (by K. Brahm): 44.0 mg (0.07 mmol, 3.00 eq) Nα-Fmoc-Nδ-trityl-L-glutamine and 0.293 mg (0.002 mmol, 0.10 eq) DMAP were added (dissolved in DMF) and incubated over night. 14.9 μL (0.096 mmol, 5.00 eq) DIC were added and the mixture was shaken at 600 rpm overnight. The Fmoc-group was removed (GP008) and the resin was washed (GP002). The remaining residues were attached according to GP018 using a peptide synthesizer (W. Blum at the Thiele group, TUD). The protecting groups were removed (GP011), the resin was washed (GP002) and dried. A small amount of resin beads was treated with ammonia gas (GP012) and analyzed. – *MALDI-TOF* (matrix: CHCA), m/z (%): 2244.37 (100) [M+H]$^+$, 2226.38 (40), 2114.28 (22). – *MALDI-TOF/TOF* (matrix: CHCA), m/z (%) [fragment]: 1495.97 (100) [B$_2$]$^+$, 1478.94 (22), 1397.97 (68) [C$_{11}$]$^+$, 1381.90 (15), 1316.83 (7), 1083.71 (9) [B$_8$]$^+$, 1047.60 (3) [Y$_9$+2 H]$^+$, 748.43 (9) [Y$_6$+2 H]$^+$.

Fluo-AKWRMVLRI-Ahx-ADTLMRTQ, Fluo-IL8RPLoops **86**: Synthesis on 50 mg 2-chlorotrityl chloride resin by K. Brahm and H. Fittler (Liberty synthesizer, Kolmar group, TU Darmstadt). Amino acids with side-chain protections used: Fmoc-Lys(Boc)-OH, Fmoc-Trp(Boc)-OH, Fmoc-Arg(Pbf)-OH, Fmoc-His(Trt)-OH, Fmoc-Asp(O*t*Bu)-OH Fmoc-Thr(*t*Bu)-OH. Coupling of amino acids: 4.00 equivalents of amino acid, 4.00 equivalents of HBTU and 8.00 equivalents of DIPEA. See Avrutina *et al.*[336] for further details on synthesizer program and LC/MS settings. The peptide was purified by HPLC (K. Brahm, 1 CV linear gradient 0-5 % eluent B, over 5 CV linear gradient 5-80 % eluent B), the product eluted after 56 min. – *ESI LC/MS* (C4 LC column), m/z (%): 641.2 (100) [M+4H]$^{4+}$, 854.7 (45) [M+3H]$^{3+}$, 513.2 (15) [M+5H]$^{5+}$, 1281.5 (5) [M+2H]$^{2+}$.

H$_2$N-AKWRMVLRI-Ahx-ADTLMRTQ, IL8RPLoops **87**: Synthesis on 50 mg 2-chlorotrityl chloride resin by K. Brahm and H. Fittler (Liberty synthesizer, Kolmar group, TUD). Amino acids with side-chain protections used: Fmoc-Lys(Boc)-OH, Fmoc-Trp(Boc)-OH, Fmoc-Arg(Pbf)-OH, Fmoc-His(Trt)-OH, Fmoc-Asp(O*t*Bu)-OH Fmoc-Thr(*t*Bu)-OH. Coupling of amino acids: 4.00 equivalents of amino acid, 4.00 equivalents of HBTU and 8.00 equivalents of DIPEA. See Avrutina *et al.*[336] for further details on synthesizer program and LC/MS settings. The peptide was purified by HPLC (K. Brahm) (5 CV linear gradient 0-55 % eluent B), the product eluted after 32.5 min. – *ESI LC/MS* (C4 LC column), m/z (%): 551.7 (100) [M+4H]$^{4+}$, 735.3 (50) [M+3H]$^{3+}$, 1102.4 (8) [M+2H]$^{2+}$.
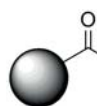
H₂N-FWLDFW-CONH₂[150] *on TentaGel MB HMBA, TG-WFDLWF* **88**: Synthesis by K. Brahm and W. Blum (Liberty synthesizer, Thiele group, TUD). 100 mg TG-HMBA macrobeads (Ø 300 µm, 0.24 $^{mmol}/_g$) were swollen according to GP001. The first amino acid was attached manually (by K. Brahm): 44.0 mg (0.07 mmol, 3.00 eq) N_α-Fmoc-N_δ-trityl-L-glutamine and 0.293 mg (0.002 mmol, 0.10 eq) DMAP were added (dissolved in DMF). 14.9 µL (0.096 mmol, 5.00 eq) DIC were added and the mixture was shaken at 600 rpm overnight. The Fmoc-group was removed (GP008) and the resin was washed (GP002). The remaining residues were attached according to GP018 using a peptide synthesizer (W. Blum at the Thiele group, TUD). The protecting group was removed (GP011), the resin was washed (GP002) and dried. A small amount of resin beads was treated with ammonia gas (GP012) and analyzed. – *MALDI-TOF* (matrix: CHCA), m/z (%): 895.58 (100), 912.56 (85) [M+H]⁺, 863.58 (47). – *MALDI-TOF/TOF* (matrix: CHCA), m/z (%) [fragment]: 895.34 (40), 867.42 (20), 782.36 (8), 709.34 (100) [B_2]⁺, 681.65 (13) [C_2]⁺, 580.29 (13) [Y_4+2 H]⁺, 562.27 (35) [B_4]⁺, 466.22 (5) [Y_3+2 H]⁺, 44724 (12) [B_3]⁺, 353.19 (2) [Y_2+2 H]⁺, 334.46 (5) [B_2]⁺.

Fluo-MWDFDD-Ahx-MPPADEDYSP, Fluo-CXCR1-p1 **89**: Synthesis by K. Schmitz and P. Wadhwani (Syro II multiple peptide synthesizer, Institute of Biological Interfaces 2, KIT), see also Girrbach *et al.*.[337] The peptide was purified over a C18 RP column on an ÄKTA purifier HPLC system (0.10 min 10 % eluent B, linear gradient 10-75 min to 80 % eluent B) and eluted after 45 min.

RhoB-SAKELRCQCI CXCL8(1-10) (N-terminus) labelled with Rhodamine B **90**: 150 mg 2-chlorotrityl chloride resin (225 µmol, 1.00 eq) were swollen according to GP001. The first amino acid was attached according to GP004: 238 mg Fmoc-Ile-OH (673 µmol, 3.00 eq) were dissolved in DMF, 115 µL DIPEA (975 µmol, 3.00 eq) were added and the mixture was added to the resin. The suspension was shaken at 600 rpm overnight. The resin was washed (GP002). Resin loading was determined according to GP016 and gave 1.35 $^{mmol}/_g$ (90 %). The Fmoc-group was removed (GP008) and the resin was washed (GP002). The cycle washing (GP002), amino acid attachment (GP007, B), washing (GP002) and removal of the Fmoc-Group (GP008) was repeated for remaining amino acids. Rhodamine B was attached according to GP015. The product was cleaved from the resin according to GP013. The peptide was purified by C18 RP HPLC (20 % eluent B from 0.5 min followed by a linear gradient to 90 % eluent B from 5-25 min. The product eluted after 15.5 min). – *MALDI-TOF* (matrix: CHCA), m/z (%): 1574.89 (100) [M+H]⁺.

7.6.2 Mix-and Split Synthesis

GP020: Calculation of resin mass

In order to increase the statistical probability of synthesizing any possible sequence in a mix-and-split procedure, the number of resin-beads employed for the synthesis should amount to three times the number of possible sequences.[173] The number of possible sequences was calculated as follows:

$$N_{tot} = n_{step1} \cdot n_{step2} \cdot n_{step3} \cdot \cdots n_{stepn} \tag{7.2}$$

7 Materials and Methods

where N_{tot} represents the total number of possible sequences, and n_{stepx} represents the number of different amines in synthesis step x. The resin mass for the synthesis was calculated as follows:

$$m = N_{tot} \cdot 3 \cdot m_{bead} \tag{7.3}$$

where m_{bead} is the mass of one resin bead.

GP021: Mix-and-Split Synthesis

Attachment of bromoacetic acid was executed according to general procedure GP005. The reaction was performed in polypropylene filter frits for resin amounts under 1.00 g or in a glass filter frit (3 cm diameter, 29 ground glass joint, frit pore size 3) with a teflon stopcock for resin amounts higher than 1.00 g. If necessary more solvent was added to create an easily shakable suspension. After a washing step (GP002) attachment of primary amines was conducted in individual polypropylene filter frits according to GP006. Each acylation/substitution step was monitored by the chloranil test (GP019). The simplest way to split the reaction mixture after attachment of bromoacetic acid proved to be vigurous shaking of the frit while using a pipet (with a large tip outlet, preferably 5.00 mL tips) to take out the desired fraction of the suspension. To ensure the right amount of suspension in the frit, the frit was marked on the outside at the appropriate total volume prior to synthesis steps (i.e. if seven different amines are to be coupled and 3 mL of suspension per splitting step is desired, the frit is marked at $7 \cdot 3$ mL on the outside). The frit was closed with a septum equipped with a needle for the maintenance of a gas equilibrium. The frit was shaken at room temperature.

Peptoid Library **91**
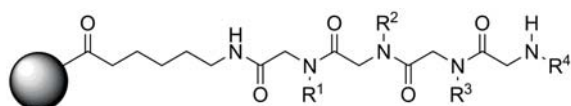
R^1	R^2	R^3	R^4
$Nser^{+1}$	$Nval^{+0}$	$Nlys^{+2}$	$Nval^{+0}$
$Nasp^{+0}$	$Nphe^{+1}$	$Nlys^{+0}$	$Nphe^{+1}$

Figure 7.1: Mix-and-split library **91** with $2^4 = 16$ possible sequences.

The mix-and-split synthesis of **91** was carried out on 100 mg TG-HMBA macrobeads (Ø 300 µm) with a capacity of 0.24 ᵍ/mmol according to GP021. The synthesis and analysis was executed by M. Hau*. 50 randomly chosen beads were analyzed by MALDI-TOF and MALDI TOF/TOF mass spectrometry. 12 of the 16 possible sequences were identified and are listed below.

---

* See Bachelor Thesis M. Hau, Hochschule Reutlingen 2012, "Screening und Dekonvolution potentieller Interleukin-8 Liganden"
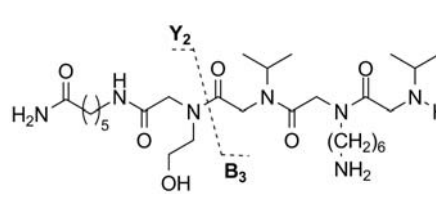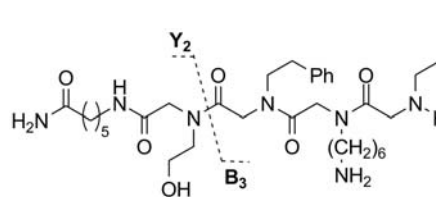
$H_2N\text{-}Ahx\text{-}\text{-}Nser^{+1}Nval^{+0}Nlys^{+2}Nval^{+0}\text{-}H$ **92**: Positively identified in single-bead MALDI-TOF/TOF MS analysis with 50 randomly chosen beads from library **91**. – *MALDI-TOF* (matrix: CHCA), m/z: 586.23 $[M+H]^+$. – *MALDI-TOF/TOF* (matrix: CHCA), m/z (%) [fragment]: 485.35 (25) $[Y_4+2\ H]^+$, 355.25 (100) $[B_3]^+$, 331.21 (8) $[Y_3+2\ H]^+$, 256.19 (5) $[B_2]^+$, 228.21 (3) $[Y_2+2\ H]^+$.
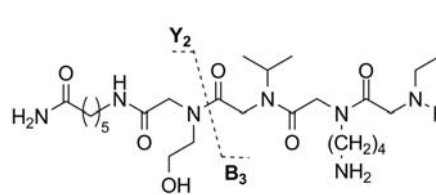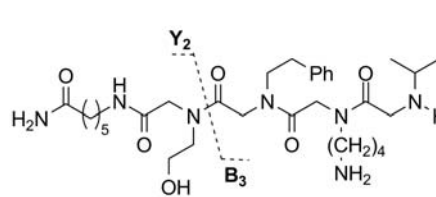
$H_2N\text{-}Ahx\text{-}Nser^{+1}Nval^{+0}Nlys^{+2}Nphe^{+1}\text{-}H$ **93**: Positively identified in single-bead MALDI-TOF/TOF MS analysis with 50 randomly chosen beads from library **91**. – *MALDI-TOF* (matrix: CHCA), m/z: 620.10 $[M+H]^+$. – *MALDI-TOF/TOF* (matrix: CHCA), m/z (%) [fragment]: 459.33 (8) $[Y_4+2\ H]^+$, 433.01 (25) $[Y_2+2\ H]^+$, 389.26 (25) $[B_3]^+$, 331.24 (45) $[Y_3+2\ H]^+$, 290.19 (100) $[B_2]^+$.
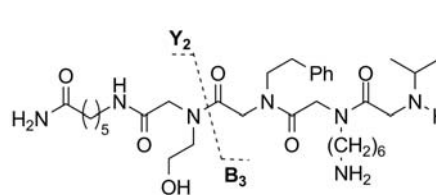
$H_2N\text{-}Ahx\text{-}Nser^{+1}Nphe^{+1}Nlys^{+2}Nval^{+0}\text{-}H$ **94**: Positively identified in single-bead MALDI-TOF/TOF MS analysis with 50 randomly chosen beads from library **91**. – *MALDI-TOF* (matrix: CHCA), m/z: 648.30 $[M+H]^+$. – *MALDI-TOF/TOF* (matrix: CHCA), m/z (%) [fragment]: 547.42 (28) $[Y_4+2\ H]^+$, 355.28 (100) $[B_3]^+$, 256.21 (8) $[B_2]^+$.

$H_2N\text{-}Ahx\text{-}Nser^{+1}Nphe^{+1}Nlys^{+2}Nphe^{+1}\text{-}H$ **95**: Positively identified in single-bead MALDI-TOF/TOF MS analysis with 50 randomly chosen beads from library **91**. – *MALDI-TOF* (matrix: CHCA), m/z: 710.92 $[M+H]^+$. – *MALDI-TOF/TOF* (matrix: CHCA), m/z (%) [fragment]: 547.38 (15) $[Y_4+2\ H]^+$, 479.28 (100) $[B_3]^+$, 318.21 (8) $[B_2]^+$, 230.18 (3) $[Y_2+2\ H]^+$.
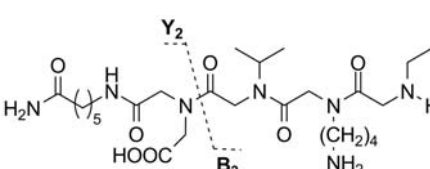
$H_2N\text{-}Ahx\text{-}Nser^{+1}Nphe^{+1}Nlys^{+0}Nval^{+0}\text{-}H$ **96**: Positively identified in single-bead MALDI-TOF/TOF MS analysis with 50 randomly chosen beads from library **91**. – *MALDI-TOF* (matrix: CHCA), m/z: 620.25 $[M+H]^+$. – *MALDI-TOF/TOF* (matrix: CHCA), m/z (%) [fragment]: 521.38 (13) $[Y_4+2\ H]^+$, 393.26 (33) $[Y_3+2\ H]^+$, 389.26 (20) $[B_3]^+$, 228.17 (100) $[B_2]^+$.
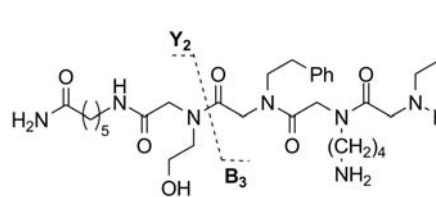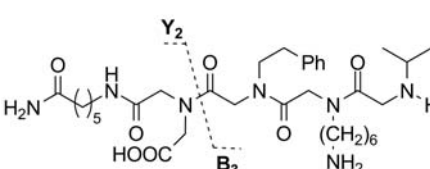
$H_2N\text{-}Ahx\text{-}Nser^{+1}Nphe^{+1}Nlys^{+0}Nphe^{+1}\text{-}H$ **97**: Positively identified in single-bead MALDI-TOF/TOF MS analysis with 50 randomly chosen beads from library **91**. – *MALDI-TOF* (matrix: CHCA), m/z: 681.40 $[M+H]^+$. – *MALDI-TOF/TOF* (matrix: CHCA), m/z (%) [fragment]: 521.35 (15) $[Y_4+2\ H]^+$, 451.28 (25) $[B_3]^+$, 393.26 (40) $[Y_3+2\ H]^+$, 290.19 (100) $[B_2]^+$.
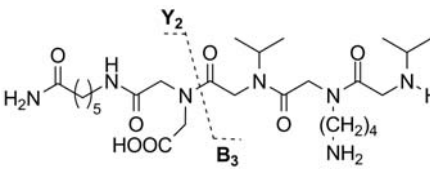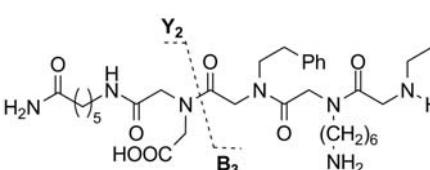
H_2N-*Ahx-Nasp*$^{+0}$*Nval*$^{+0}$*Nlys*$^{+0}$*Nval*$^{+0}$-*H* **98**: Positively identified in single-bead MALDI-TOF/TOF MS analysis with 50 randomly chosen beads from library **91**. – *MALDI-TOF* (matrix: CHCA), m/z: 572.41 $[M+H]^+$. – *MALDI-TOF/TOF* (matrix: CHCA), m/z (%) [fragment]: 473.32 (10) $[Y_4+2\ H]^+$, 345.23 (20) $[Y_3+2\ H]^+$, 327.25 (33) $[B_3]^+$, 228.18 (100) $[B_2]^+$.
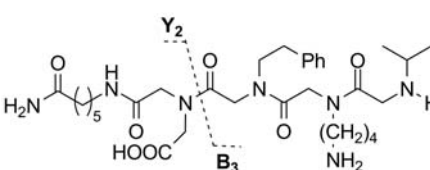

H_2N-*Ahx-Nasp*$^{+0}$*Nval*$^{+0}$*Nlys*$^{+0}$*Nphe*$^{+1}$-*H* **99**: Positively identified in single-bead MALDI-TOF/TOF MS analysis with 50 randomly chosen beads from library **91**. – *MALDI-TOF* (matrix: CHCA), m/z: 633.40 $[M+H]^+$. – *MALDI-TOF/TOF* (matrix: CHCA), m/z (%) [fragment]: 473.31 (13) $[Y_4+2\ H]^+$, 389.25 (28) $[B_3]^+$, 345.22 (25) $[Y_3+2\ H]^+$, 290.19 (100) $[B_2]^+$, 245.22 (13) $[Y_2+2\ H]^+$.

H_2N-*Ahx-Nasp*$^{+0}$*Nphe*$^{+1}$*Nlys*$^{+2}$*Nval*$^{+0}$-*H* **100**: Positively identified in single-bead MALDI-TOF/TOF MS analysis with 50 randomly chosen beads from library **91**. – *MALDI-TOF* (matrix: CHCA), m/z: 761.29 $[M+H]^+$. – *MALDI-TOF/TOF* (matrix: CHCA), m/z (%) [fragment]: 662.37 (25) $[Y_4+2\ H]^+$, 516.33 (25) $[B_3]^+$, 407.19 (5) $[Y_3+2\ H]^+$, 335.24 (100) $[B_2]^+$.

H_2N-*Ahx-Nasp*$^{+0}$*Nphe*$^{+1}$*Nlys*$^{+2}$*Nphe*$^{+1}$-*H* **101**: Positively identified in single-bead MALDI-TOF/TOF MS analysis with 50 randomly chosen beads from library **91**. – *MALDI-TOF* (matrix: CHCA), m/z: 724.29 $[M+H]^+$. – *MALDI-TOF/TOF* (matrix: CHCA), m/z (%) [fragment]: 561.44 (12) $[Y_4+2\ H]^+$, 479.32 (75) $[B_3]^+$, 407.24 (50) $[Y_3+2\ H]^+$, 318.23 (15) $[B_2]^+$, 245.22 (10) $[Y_2+2\ H]^+$.

H_2N-*Ahx-Nasp*$^{+0}$*Nphe*$^{+1}$*Nlys*$^{+0}$*Nval*$^{+0}$-*H* **102**: Positively identified in single-bead MALDI-TOF/TOF MS analysis with 50 randomly chosen beads from library **91**. – *MALDI-TOF* (matrix: CHCA), m/z: 634.05 $[M+H]^+$. – *MALDI-TOF/TOF* (matrix: CHCA), m/z (%) [fragment]: 535.31 (15) $[Y_4+2\ H]^+$, 407.22 (20) $[Y_3+2\ H]^+$, 389.25 (25) $[B_3]^+$, 246.17 (2) $[Y_2+2\ H]^+$, 228.17 (100) $[B_2]^+$.
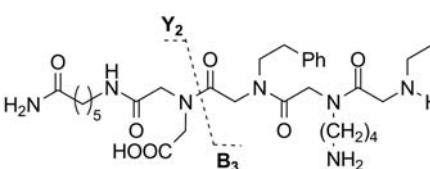
H_2N-*Ahx-Nasp*$^{+0}$*Nphe*$^{+1}$*Nlys*$^{+0}$*Nphe*$^{+1}$-*H* **103**: Positively identified in single-bead MALDI-TOF/TOF MS analysis with 50 randomly chosen beads from library **91**. – *MALDI-TOF* (matrix: CHCA), m/z: 696.73 $[M+H]^+$. – *MALDI-TOF/TOF* (matrix: CHCA), m/z (%) [fragment]: 535.34 (10) $[Y_4+2\ H]^+$, 451.28 (22) $[B_3]^+$, 407.24 (20) $[Y_3+2\ H]^+$, 290.19 (100) $[B_2]^+$, 245.21 (6) $[Y_2+2\ H]^+$.
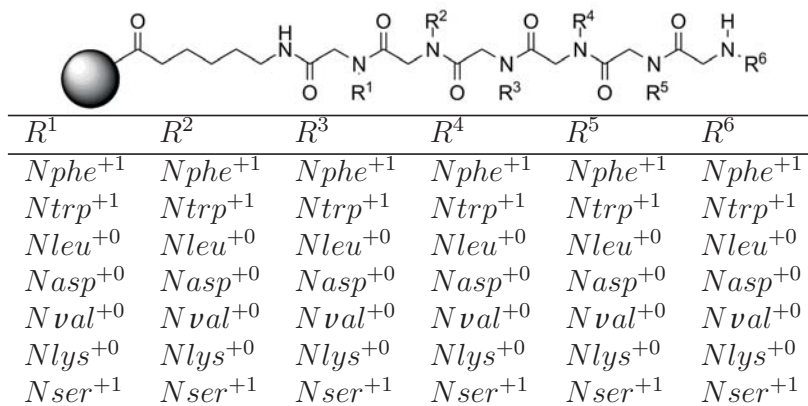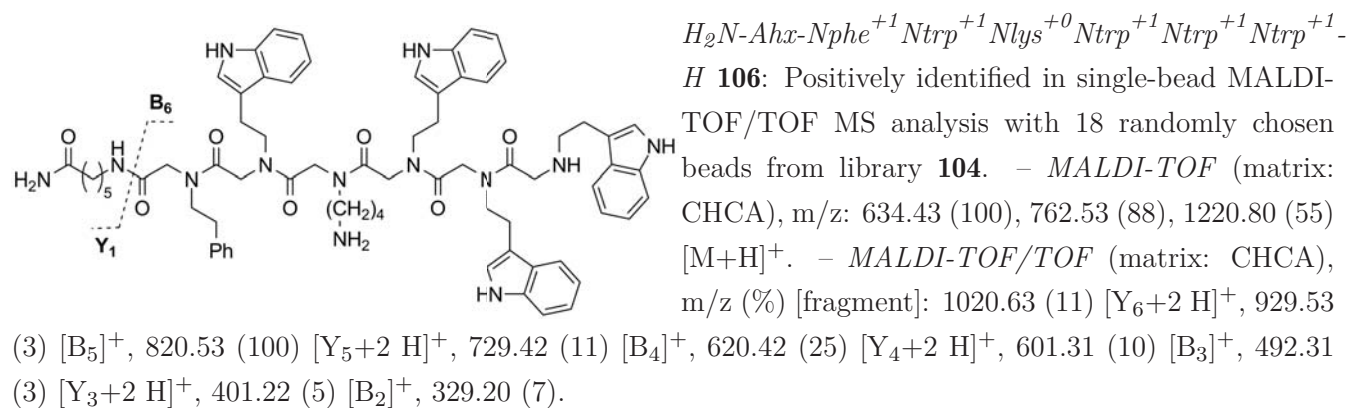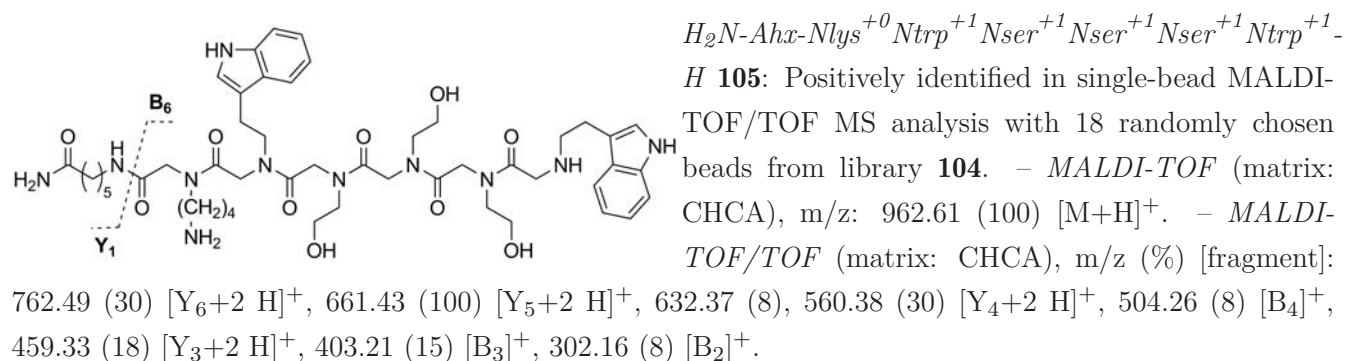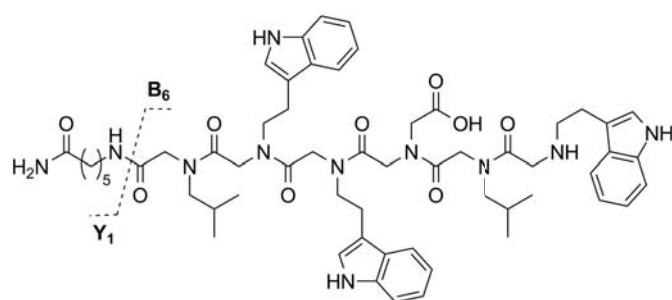
R^1	R^2	R^3	R^4	R^5	R^6
$Nphe^{+1}$	$Nphe^{+1}$	$Nphe^{+1}$	$Nphe^{+1}$	$Nphe^{+1}$	$Nphe^{+1}$
$Ntrp^{+1}$	$Ntrp^{+1}$	$Ntrp^{+1}$	$Ntrp^{+1}$	$Ntrp^{+1}$	$Ntrp^{+1}$
$Nleu^{+0}$	$Nleu^{+0}$	$Nleu^{+0}$	$Nleu^{+0}$	$Nleu^{+0}$	$Nleu^{+0}$
$Nasp^{+0}$	$Nasp^{+0}$	$Nasp^{+0}$	$Nasp^{+0}$	$Nasp^{+0}$	$Nasp^{+0}$
$Nval^{+0}$	$Nval^{+0}$	$Nval^{+0}$	$Nval^{+0}$	$Nval^{+0}$	$Nval^{+0}$
$Nlys^{+0}$	$Nlys^{+0}$	$Nlys^{+0}$	$Nlys^{+0}$	$Nlys^{+0}$	$Nlys^{+0}$
$Nser^{+1}$	$Nser^{+1}$	$Nser^{+1}$	$Nser^{+1}$	$Nser^{+1}$	$Nser^{+1}$

Figure 7.2: Mix-and-split library **104** with 7^6=117649 possible sequences.

The mix-and-split synthesis of library **104** was carried out on 2.40 g TG-HMBA macrobeads (Ø 300 μm) with a capacity of 0.24 ^{g}/$_{mmol}$ according to GP021. 18 randomly chosen beads were analyzed by MALDI-TOF and MALDI TOF/TOF mass spectrometry. All 18 sequences were identified and are listed below. Two of the sequences (**111** and **112**) showed unsuccessful coupling in the last coupling step of glycine *tert*-butyl ester acetate.
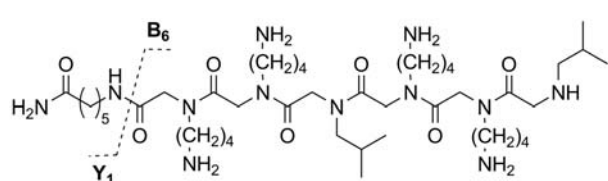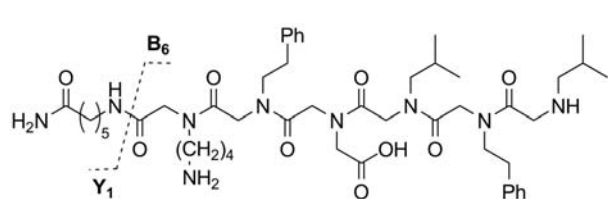

H_2N-Ahx-Nlys^{+0}Ntrp^{+1}Nser^{+1}Nser^{+1}Nser^{+1}Ntrp^{+1}-H **105**: Positively identified in single-bead MALDI-TOF/TOF MS analysis with 18 randomly chosen beads from library **104**. – *MALDI-TOF* (matrix: CHCA), m/z: 962.61 (100) [M+H]$^+$. – *MALDI-TOF/TOF* (matrix: CHCA), m/z (%) [fragment]: 762.49 (30) [Y$_6$+2 H]$^+$, 661.43 (100) [Y$_5$+2 H]$^+$, 632.37 (8), 560.38 (30) [Y$_4$+2 H]$^+$, 504.26 (8) [B$_4$]$^+$, 459.33 (18) [Y$_3$+2 H]$^+$, 403.21 (15) [B$_3$]$^+$, 302.16 (8) [B$_2$]$^+$.

H_2N-Ahx-Nphe^{+1}Ntrp^{+1}Nlys^{+0}Ntrp^{+1}Ntrp^{+1}Ntrp^{+1}-H **106**: Positively identified in single-bead MALDI-TOF/TOF MS analysis with 18 randomly chosen beads from library **104**. – *MALDI-TOF* (matrix: CHCA), m/z: 634.43 (100), 762.53 (88), 1220.80 (55) [M+H]$^+$. – *MALDI-TOF/TOF* (matrix: CHCA), m/z (%) [fragment]: 1020.63 (11) [Y$_6$+2 H]$^+$, 929.53 (3) [B$_5$]$^+$, 820.53 (100) [Y$_5$+2 H]$^+$, 729.42 (11) [B$_4$]$^+$, 620.42 (25) [Y$_4$+2 H]$^+$, 601.31 (10) [B$_3$]$^+$, 492.31 (3) [Y$_3$+2 H]$^+$, 401.22 (5) [B$_2$]$^+$, 329.20 (7).

H₂N-Ahx-Nleu⁺⁰Ntrp⁺¹Ntrp⁺¹Nasp⁺⁰Nleu⁺⁰Ntrp⁺¹-H **107**: Positively identified in single-bead MALDI-TOF/TOF MS analysis with 18 randomly chosen beads from library **104**. – *MALDI-TOF* (matrix: CHCA), m/z: 1072.70 (1000) [M+H]⁺, 644.45 (33). – *MALDI-TOF/TOF* (matrix: CHCA), m/z (%) [fragment]: 872.53 (11) [Y₆+2 H]⁺, 829.42 (5) [B₅]⁺, 759.51 (100) [Y₅+2 H]⁺, 629.38 (10) [B₄]⁺, 644.45 (20) [Y₄+2 H]⁺, 429.33 (40) [B₃]⁺, 444.21 (3) [Y₃+2 H]⁺, 314.31 (6) [B₂]⁺.
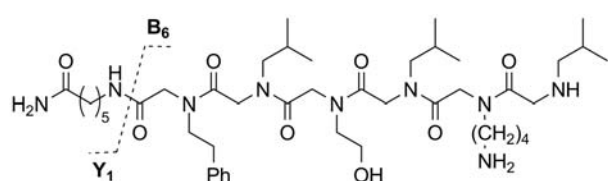
H₂N-Ahx-Nphe⁺¹Nleu⁺⁰Nser⁺¹Nleu⁺⁰Nlys⁺⁰Nleu⁺⁰-H **108**: Positively identified in single-bead MALDI-TOF/TOF MS analysis with 18 randomly chosen beads from library **104**. – *MALDI-TOF* (matrix: CHCA), m/z: 860.68 (100) [M+H]⁺. – *MALDI-TOF/TOF* (matrix: CHCA), m/z (%) [fragment]: 747.53 (23) [Y₆+2 H]⁺, 619.44 (100) [Y₅+2 H]⁺, 569.43 (6) [B₅]⁺, 506.36 (33) [Y₄+2 H]⁺, 456.33 (13) [B₄]⁺, 405.30 (3) [Y₃+2 H]⁺, 355.28 (40) [B₃]⁺, 242.20 (93) [B₂]⁺.

H₂N-Ahx-Nlys⁺⁰Nlys⁺⁰Nleu⁺⁰Nlys⁺⁰Nlys⁺⁰Nleu⁺⁰-H **109**: Positively identified in single-bead MALDI-TOF/TOF MS analysis with 18 randomly chosen beads from library **104**. – *MALDI-TOF* (matrix: CHCA), m/z: 869.75 (100) [M+H]⁺, 891.73 (53), 1003.79 (15). – *MALDI-TOF/TOF* (matrix: CHCA), m/z (%) [fragment]: 756.62 (13) [Y₆+2 H]⁺, 628.51 (100) [Y₅+2 H]⁺, 611.47 (5) [B₅]⁺, 500.41 (20) [Y₄+2 H]⁺, 483.38 (13) [B₄]⁺, 387.31 (4) [Y₃+2 H]⁺, 370.29 (24) [B₃]⁺, 242.19 (33) [B₂]⁺.

H₂N-Ahx-Nlys⁺⁰Nphe⁺¹Nasp⁺⁰Nleu⁺⁰Nphe⁺¹Nleu⁺⁰-H **110**: Positively identified in single-bead MALDI-TOF/TOF MS analysis with 18 randomly chosen beads from library **104**. – *MALDI-TOF* (matrix: CHCA), m/z: 922.67 (100) [M+H]⁺. – *MALDI-TOF/TOF* (matrix: CHCA), m/z (%) [fragment]: 809.52 (27) [Y₆+2 H]⁺, 664.40 (3) [B₅]⁺, 648.43 (100) [Y₅+2 H]⁺, 535.35 (22) [Y₄+2 H]⁺, 503.31 (7) [B₄]⁺, 420.31 (8) [Y₃+2 H]⁺, 388.27 (48) [B₃]⁺, 275.18 (10) [B₂]⁺, 259.22 (2) [Y₂+2 H]⁺.
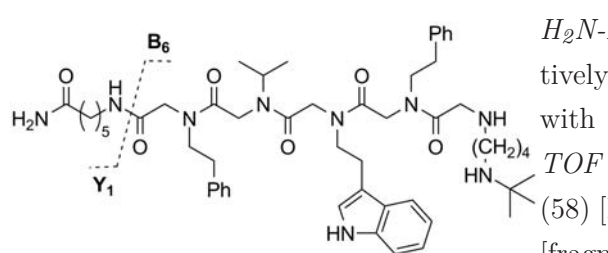
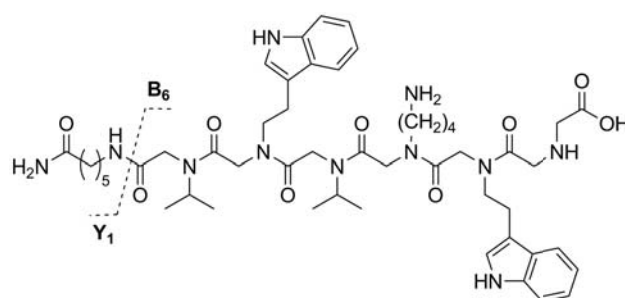*H₂N-Ahx-Nphe⁺¹Nval⁺⁰Ntrp⁺¹Nphe⁺¹Nlys⁺⁰-H* **111**: Positively identified in single-bead MALDI-TOF/TOF MS analysis with 18 randomly chosen beads from library **104**. – *MALDI-TOF* (matrix: CHCA), m/z: 752.52 (100), 661.50 (73), 938.64 (58) [M+H]⁺. – *MALDI-TOF/TOF* (matrix: CHCA), m/z (%) [fragment]: 865.53 (30), 752.49 (100) [Y₅+2 H]⁺, 591.40 (40) [Y₄+2 H]⁺, 548.32 (25) [B₃]⁺, 391.30 (5) [Y₃+2 H]⁺, 348.21 (13) [B₂]⁺, 187.11 (2) [B₁]⁺.
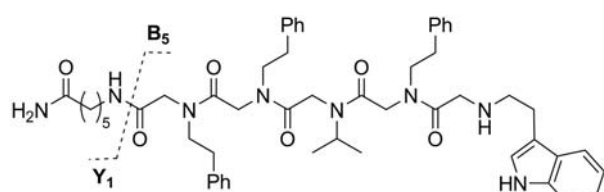
$H_2N\text{-}Ahx\text{-}Nphe^{+1}Nphe^{+1}Nval^{+0}Nphe^{+1}Ntrp^{+1}\text{-}H$ **112**: Positively identified in single-bead MALDI-TOF/TOF MS analysis with 18 randomly chosen beads from library **104**. – *MALDI-TOF* (matrix: CHCA), m/z: 913.62 (100) [M+H]$^+$, 639.42 (53), 752.00 (45). – *MALDI-TOF/TOF* (matrix: CHCA), m/z (%) [fragment]: 840.48 (30), 713.47 (50) [Y$_5$+2 H]$^+$, 622.35 (12) [B$_4$]$^+$, 552.38 (100) [Y$_4$+2 H]$^+$, 461.26 (67) [B$_3$]$^+$, 453.31 (15) [Y$_3$+2 H]$^+$, 362.18 (7) [B$_2$]$^+$.

$H_2N\text{-}Ahx\text{-}Nval^{+0}Ntrp^{+1}Nval^{+0}Nlys^{+0}Ntrp^{+1}Nasp^{+0}\text{-}H$ **113**: Positively identified in single-bead MALDI-TOF/TOF MS analysis with 18 randomly chosen beads from library **104**. – *MALDI-TOF* (matrix: CHCA), m/z: 972.67 (100) [M+H]$^+$, 657.50 (50), 614.46 (33). – *MALDI-TOF/TOF* (matrix: CHCA), m/z (%) [fragment]: 857.56 (16) [Y$_6$+2 H]$^+$, 743.42 (3) [B$_5$]$^+$, 657.47 (100) [Y$_5$+2 H]$^+$, 543.31 (7) [B$_4$]$^+$, 529.37 (43) [Y$_4$+2 H]$^+$, 444.24 (15) [B$_3$]$^+$, 430.29 (10) [Y$_3$+2 H]$^+$, 316.14 (7) [B$_2$]$^+$.
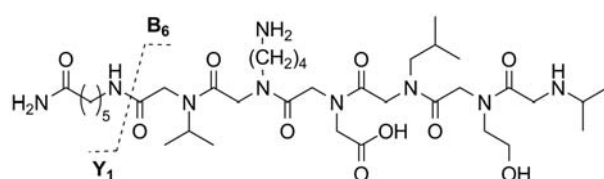
$H_2N\text{-}Ahx\text{-}Nval^{+0}Nlys^{+0}Nasp^{+0}Nleu^{+0}Nser^{+1}Nval^{+0}\text{-}H$ **114**: Positively identified in single-bead MALDI-TOF/TOF MS analysis with 18 randomly chosen beads from library **104**. – *MALDI-TOF* (matrix: CHCA), m/z: 786.57 (100) [M+H]$^+$, 808.55 (33), 920.61 (25). – *MALDI-TOF/TOF* (matrix: CHCA), m/z (%) [fragment]: 697.49 (5), 687.45 (27) [Y$_6$+2 H]$^+$, 586.41 (100) [Y$_5$+2 H]$^+$, 557.36 (7) [B$_5$]$^+$, 473.33 (32) [Y$_4$+2 H]$^+$, 429.25 (4) [B$_4$]$^+$, 358.29 (17) [Y$_3$+2 H]$^+$, 314.22 (50) [B$_3$]$^+$, 230.19 (2) [Y$_2$+2 H]$^+$, 201.13 (10) [B$_2$]$^+$.
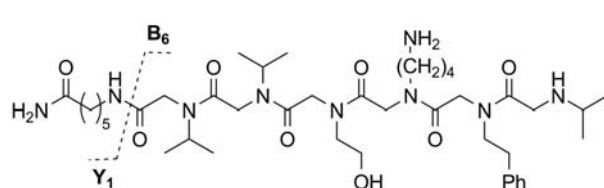
$H_2N\text{-}Ahx\text{-}Nval^{+0}Nval^{+0}Nser^{+1}Nlys^{+0}Nphe^{+1}Nval^{+0}\text{-}H$ **115**: Positively identified in single-bead MALDI-TOF/TOF MS analysis with 18 randomly chosen beads from library **104**. – *MALDI-TOF* (matrix: CHCA), m/z: 818.61 (100) [M+H]$^+$, 717.55 (32), 840.59 (20). – *MALDI-TOF/TOF* (matrix: CHCA), m/z (%) [fragment]: 719.50 (12) [Y$_6$+2 H]$^+$, 589.39 (4) [B$_5$]$^+$, 558.42 (100) [Y$_5$+2 H]$^+$, 490.32 (10) [B$_4$]$^+$, 430.32 (23) [Y$_4$+2 H]$^+$, 389.27 (25) [B$_3$]$^+$, 329.26 (3) [Y$_3$+2 H]$^+$, 261.17 (4) [B$_2$]$^+$.
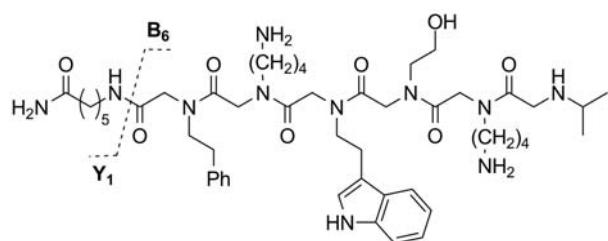
H_2N-Ahx-Nphe^{+1}Nlys^{+0}Ntrp^{+1}Nser^{+1}Nlys^{+0}Nval^{+0}-H **116**: Positively identified in single-bead MALDI-TOF/TOF MS analysis with 18 randomly chosen beads from library **104**. – *MALDI-TOF* (matrix: CHCA), m/z: 948.67 (100) [M+H]$^+$. – *MALDI-TOF/TOF* (matrix: CHCA), m/z (%) [fragment]: 849.56 (23) [Y$_6$+2 H]$^+$, 721,47 (90) [Y$_5$+2 H]$^+$, 657,43 (8) [Y$_4$+2 H]$^+$ and [B$_5$]$^+$, 620.42 (43), 529.34 (21) [B$_4$]$^+$, 420.31 (12) [Y$_3$+2 H]$^+$, 329.22 (5) [B$_3$]$^+$, 228.18 (100) [B$_2$]$^+$.

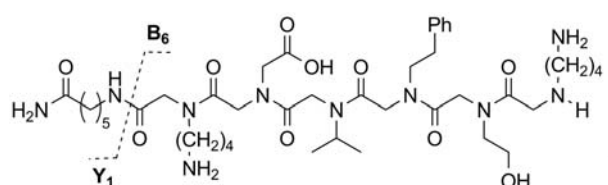H_2N-Ahx-Nlys^{+0}Nasp^{+0}Nval^{+0}Nphe^{+1}Nser^{+1}Nlys^{+0}-H **117**: Positively identified in single-bead MALDI-TOF/TOF MS analysis with 18 randomly ch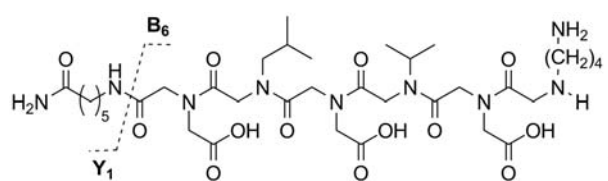osen beads from library **104**. – *MALDI-TOF* (matrix: CHCA), m/z: 863.60 (100) [M+H]$^+$, 885.58 (20), 620.46 (15). – *MALDI-TOF/TOF* (matrix: CHCA), m/z (%) [fragment]: 792.46 (12), 735.45 (20) [Y$_6$+2 H]$^+$, 634.41 (100) [Y$_5$+2 H]$^+$, 605.34 (15) [B$_5$]$^+$, 490.31 (37) [B$_4$]$^+$, 473.31 (22) [Y$_4$+2 H]$^+$, 391.23 (11) [B$_3$]$^+$, 374.23 (6) [Y$_3$+2 H]$^+$, 230.15 (6) [B$_2$]$^+$.

H_2N-Ahx-Nasp^{+0}Nleu^{+0}Nasp^{+0}Nval^{+0}Nasp^{+0}Nlys^{+0}-H **118**: Positively identified in single-bead MALDI-TOF/TOF MS analysis with 18 randoml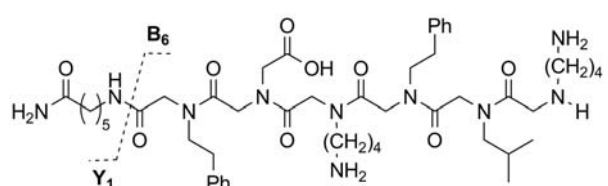y chosen beads from library **104**. – *MALDI-TOF* (matrix: CHCA), m/z: 816.51 (100) [M+H]$^+$, 798.50 (50), 701.47 (47). – *MALDI-TOF/TOF* (matrix: CHCA), m/z (%) [fragment]: 746.40 (12), 688.39 (23) [Y$_6$+2 H]$^+$, 589.34 (8), 573.36 (100) [Y$_5$+2 H]$^+$, 474.29 (48) [Y$_4$+2 H]$^+$, 458.26 (10) [B$_4$]$^+$, 359.25 (13) [Y$_3$+2 H]$^+$, 343.22 (83) [B$_3$]$^+$, 325.19 (15), 272.13 (18), 246.17 (5) [B$_2$]$^+$ and [Y$_2$+2 H]$^+$.

H_2N-Ahx-Nphe^{+1}Nasp^{+0}Nlys^{+0}Nphe^{+0}Nleu^{+0}Nlys^{+0}-H **119**: Positively identified in single-bead MALDI-TOF/TOF MS analysis with 18 randomly chosen beads from library **104**. – *MALDI-TOF* (matrix: CHCA), m/z: 937.67 (100) [M+H]$^+$. – *MALDI-TOF/TOF* (matrix: CHCA), m/z (%) [fragment]: 866.51 (10), 809.49 (20) [Y$_6$+2 H]$^+$, 696.42 (100) [Y$_5$+2 H]$^+$, 646.40 (10) [B$_5$]$^+$, 535.33 (23) [Y$_4$+2 H]$^+$, 531.37 (33) [B$_4$]$^+$, 403.27 (10) [B$_3$]$^+$, 290.18 (10) [Y$_2$+2 H]$^+$, 242.19 (10) [B$_2$]$^+$.

H_2N-Ahx-Nser^{+1}Nser^{+1}Nlys^{+0}Nasp^{+0}Nphe^{+1}Nser^{+1}-H **120**: Positively identified in single-bead MALDI-TOF/TOF MS analysis with 18 randomly chosen beads from library **104**. – *MALDI-TOF* (matrix: CHCA), m/z: 838.53 (100) [M+H]$^+$. – *MALDI-TOF/TOF* (matrix: CHCA), m/z

(%) [fragment]: 737.43 (15) $[Y_6+2\,H]^+$, 607.32 (7) $[B_5]^+$, 576.35 (100) $[Y_5+2\,H]^+$, 506.27 (27) $[B_4]^+$, 461.32 (22) $[Y_4+2\,H]^+$, 333.22 (17) $[Y_3+2\,H]^+$, 263.14 (37) $[B_2]^+$.

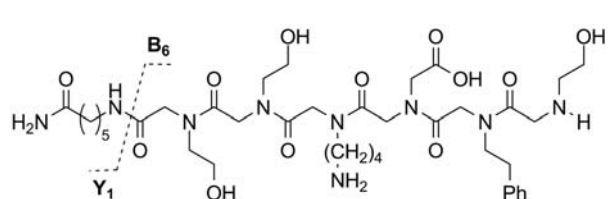*H_2N-Ahx-Nser^{+1}Nphe^{+1}Nval^{+0}Nleu^{+0}Nphe^{+1}Nser^{+1}-H* **121**: Positively identified in single-bead MALDI-TOF/TOF MS analysis with 18 randomly chosen beads from library **104**. – *MALDI-TOF* (matrix: CHCA), m/z: 867.62 (100) $[M+H]^+$, 754.52 (30), 653.46 (20). – *MALDI-TOF/TOF* (matrix: CHCA), m/z (%) [fragment]: 766.50 (12) $[Y_6+2\,H]^+$, 636.38 (4) $[B_5]^+$, 605.42 (100) $[Y_5+2\,H]^+$, 492.33 (33) $[Y_4+2\,H]^+$, 475.30 (23) $[B_4]^+$, 393.25 (3) $[Y_3+2\,H]^+$, 376.23 (14) $[B_3]^+$, 263.14 (5) $[B_2]^+$.

H_2N-Ahx-Nleu^{+0}Nasp^{+0}Nphe^{+1}Nlys^{+0}Nser^{+1}Nser^{+1}-H **122**: Positively identified in single-bead MALDI-TOF/TOF MS analysis with 18 randomly chosen beads from library **104**. – *MALDI-TOF* (matrix: CHCA), m/z: 850.58 (100) $[M+H]^+$, 605.42 (35). – *MALDI-TOF/TOF* (matrix: CHCA), m/z (%) [fragment]: 749.47 (15) $[Y_6+2\,H]^+$, 648.43 (100) $[Y_5+2\,H]^+$, 607.33 (3) $[B_5]^+$, 520.34 (17) $[Y_4+2\,H]^+$, 492.30 (23) $[B_4]^+$, 331.21 (19) $[B_3]^+$.

7.7 Screening of Peptoid Libraries

In order to simplify identification of the peptoid-sequences by MALDI TOF/TOF mass spectrometry the individual suspensions in the frits of the last amine coupling step were not pooled and screened individually.
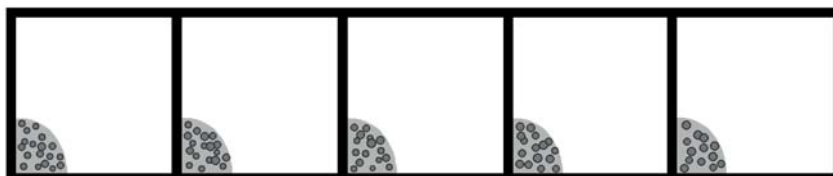

Figure 7.3: Placing little suspension droplets on the upper edge of 384 well MTP with consecutive centrifugation ensures quick bead distribution without formation of multiple bead layers.

After the cleavage of side chain protecting groups, the seven synthesis frits of library **104** (approximately 340 mg resin per frit) were washed with low-salt PBS until the supernatants reached a neutral pH value. The supernatant was removed and individual frits were incubated with 1.00 mL of 10.0 µM labelled CXCL8 **23** for 3-5 h in the dark at room temperature. The resin was washed three times with 2.00 mL low-salt PBS. The 348 wells of black-wall, transparent-bottom microtiter plates (MTP) were filled with 20.0 µL low-salt PBS. The resin was suspended in 2.00 mL low-salt PBS and the beads were distributed into the 384 wells of the MTP by using a cut-off 20.0 µL pipet-tip (to increase the outlet space of the tip). In order to distribute the resin beads quickly and evenly without formation of double layers in the MTP wells, the placement of little suspension droplets in the top edges of the wells is advised (see Figure 7.3). The plates were centrifuged at 2000 rpm (Hettich Rotina 420R) for 30 sec. Fluorescence images of the beads

(FITC- and RHO-channel) were taken in an automated fashion using the 6D 'mark-and-find' function in combination with the automated x/y-table. Immediately after taking the images, they were visually scanned for red beads in the RHO-channel. The beads of a well that contained one or more red beads where pipetted out and dispensed as individual beads in individual wells of another 384 well black-wall, transparent-bottom MTP filled with 20.0 μL low-salt PBS. Another set of images was taken to identify the single red bead. The bead was placed in a microcentrifuge tube, washed with DCM and lyophilized. The peptoids were cleaved from the resin bead (GP012) and analyzed by MALDI TOF and TOF/TOF mass spectrometry. 63 % of the analyzed peptoid sequences were identified. Omitting the highly hydrophobic sequences **123**-**136** 29 sequences (one sequence was found twice) were chosen as potentially interesting hits and are listed below. The peptoids were re-snythesized with fluorescein labels by parallel synthesis and are listed below.
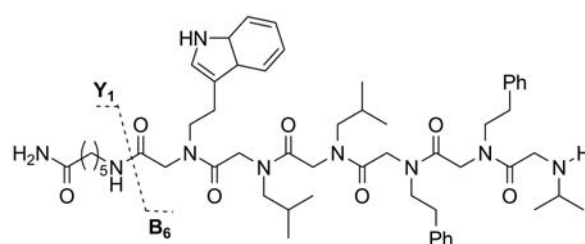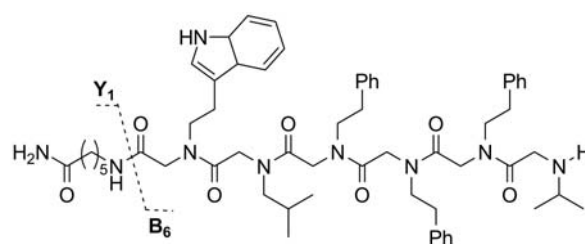

H_2N-Ahx-Ntrp^{+1}Nleu^{+0}Nval^{+0}Nphe^{+1}Nphe^{+1}Nval^{+0}-H **123**: Positively identified as binding to IL8S72C-DL550 **23** in a screen of library **104**. Later omitted due to highly hydrophobic side chains. – *MALDI-TOF* (matrix: CHCA), m/z: 978.78 (100) [M+H]$^+$, 835.68 (65), 1010.77 (21). – *MALDI-TOF/TOF* (matrix: CHCA), m/z (%) [fragment]:

880.53 (20) [Y$_6$+2 H]$^+$, 718.48 (100) [Y$_5$+2 H]$^+$, 648.42 (8) [B$_5$]$^+$, 557.40 (24) [Y$_4$+2 H]$^+$, 535.34 (21) [B$_4$]$^+$, 444.31 (5) [Y$_3$+2 H]$^+$, 422.25 (25) [B$_3$]$^+$, 261.18 (5) [B$_2$]$^+$.
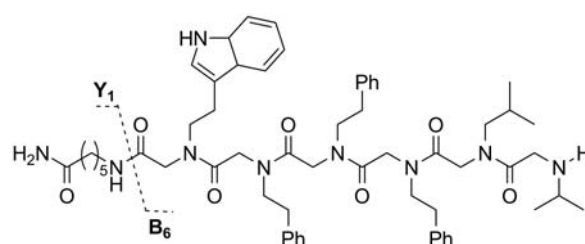

H_2N-Ahx-Ntrp^{+1}Nleu^{+0}Nphe^{+1}Nphe^{+1}Nphe^{+1}Nval^{+0}-H **124**: Positively identified as binding to IL8S72C-DL550 **23** in a screen of library **104**. Later omitted due to highly hydrophobic side chains. – *MALDI-TOF* (matrix: CHCA), m/z: 883.68 (100), 1027.00 (83) [M+H]$^+$, 714.54 (54). – *MALDI-TOF/TOF* (matrix: CHCA), m/z (%) [fragment]:

928.53 (20) [Y$_6$+2 H]$^+$, 767.48 (100) [Y$_5$+2 H]$^+$, 696.42 (8) [B$_5$]$^+$, 606.39 (23) [Y$_4$+2 H]$^+$, 583.35 (21) [B$_4$]$^+$, 444.30 (4) [Y$_3$+2 H]$^+$, 422.25 (28) [B$_3$]$^+$, 261.16 (6) [B$_2$]$^+$.

H_2N-Ahx-Ntrp^{+1}Nphe^{+1}Nphe^{+1}Nphe^{+1}Nleu^{+0}Nval^{+0}-H **125**: Positively identified as binding to IL8S72C-DL550 **23** in a screen of library **104**. Later omitted due to highly hydrophobic side chains. – *MALDI-TOF* (matrix: CHCA), m/z: 1027.01 (100) [M+H]$^+$, 883.00 (98), 925.69 (44). – *MALDI-TOF/TOF* (matrix: CHCA), m/z (%) [fragment]:

928.56 (19) [Y$_6$+2 H]$^+$, 815.48 (100) [Y$_5$+2 H]$^+$, 696.42 (6) [B$_5$]$^+$, 653.41 (20) [Y$_4$+2 H]$^+$, 535.34 (23) [B$_4$]$^+$, 492.31 (5) [Y$_3$+2 H]$^+$, 374.25 (27) [B$_3$]$^+$, 213.17 (7) [B$_2$]$^+$.
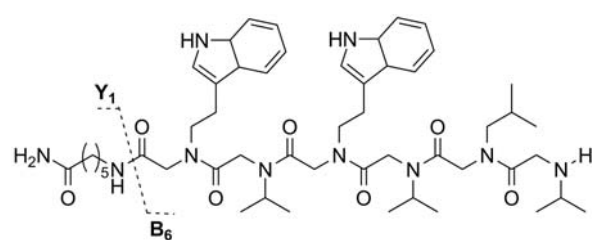
H_2N-Ahx-Ntrp^{+1}Nval^{+0}Ntrp^{+1}Nval^{+0}Nleu^{+0}Nval^{+0}-H **126**: Positively identified as binding to IL8S72C-DL550 **23** in a screen of library **104**. Later omitted due to highly hydrophobic side chains. – *MALDI-TOF* (matrix: CHCA), m/z: 941.34 (100) [M+H]$^+$, 741.61 (72), 798.64 (44). – *MALDI-TOF/TOF* (matrix: CHCA), m/z (%) [fragment]: 842.56 (10) [Y$_6$+2 H]$^+$, 729.48 (100) [Y$_5$+2 H]$^+$, 630.41 (37) [Y$_4$+2 H]$^+$, 611.43 (5) [B$_5$]$^+$, 512.36 (18) [B$_4$]$^+$, 430.33 (5) [Y$_3$+2 H]$^+$, 312.26 (18) [B$_3$]$^+$, 213.18 (3) [B$_2$]$^+$.

H_2N-Ahx-Ntrp^{+1}Nleu^{+0}Ntrp^{+1}Nphe^{+1}Nleu^{+0}Nval^{+0}-H **127**: Positively identified as binding to IL8S72C-DL550 **23** in a screen of library **104**. Later omitted due to highly hydrophobic side chains. – *MALDI-TOF* (matrix: CHCA), m/z: 1018.79 (100) [M+H]$^+$, 874.69 (93), 815.6 (22). – *MALDI-TOF/TOF* (matrix: CHCA), m/z (%) [fragment]: 919.58 (17) [Y$_6$+2 H]$^+$, 806.51 (100) [Y$_5$+2 H]$^+$, 687.46 (7) [B$_5$]$^+$, 644.43 (32) [Y$_4$+2 H]$^+$, 574.37 (14) [B$_4$]$^+$, 444.32 (5) [Y$_3$+2 H]$^+$, 374.26 (20) [B$_3$]$^+$, 213.17 (5) [B$_2$]$^+$.
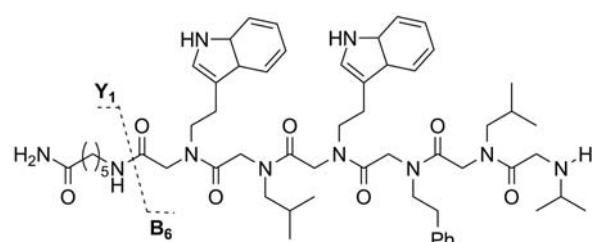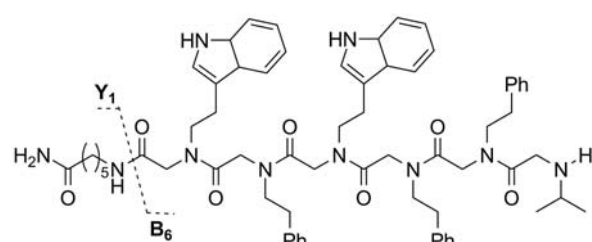

H_2N-Ahx-Ntrp^{+1}Nphe^{+1}Ntrp^{+1}Nphe^{+1}Nphe^{+1}Nval^{+0}-H **128**: Positively identified as binding to IL8S72C-DL550 **23** in a screen of library **104**. Later omitted due to highly hydrophobic side chains. – *MALDI-TOF* (matrix: CHCA), m/z: 970.71 (100), 1114.80 (86) [M+H]$^+$, 827.60 (19). – *MALDI-TOF/TOF* (matrix: CHCA), m/z (%) [fragment]: 1015.56 (18) [Y$_6$+2 H]$^+$, 854.50 (100) [Y$_5$+2 H]$^+$, 783.45 (5) [B$_5$]$^+$, 693.41 (33) [Y$_4$+2 H]$^+$, 622.37 (16) [B$_4$]$^+$, 492.33 (5) [Y$_3$+2 H]$^+$, 422.26 (18) [B$_3$]$^+$, 261.18 (4) [B$_2$]$^+$.
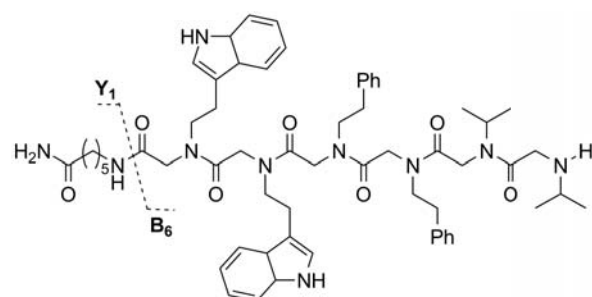
H_2N-Ahx-Ntrp^{+1}Ntrp^{+1}Nphe^{+1}Nphe^{+1}Nval^{+0}Nval^{+0}-H **129**: Positively identified as binding to IL8S72C-DL550 **23** in a screen of library **104**. Later omitted due to highly hydrophobic side chains. – *MALDI-TOF* (matrix: CHCA), m/z: 1052.79 (100) [M+H]$^+$, 908.70 (70), 1081.79 (16). – *MALDI-TOF/TOF* (matrix: CHCA), m/z (%) [fragment]: 953.58 (32) [Y$_6$+2 H]$^+$, 854.51 (100) [Y$_5$+2 H]$^+$, 721.44 (4) [B$_5$]$^+$, 692.43 (17) [Y$_4$+2 H]$^+$, 531.35 (7) [Y$_3$+2 H]$^+$, 521.35 (14) [B$_4$]$^+$, 360.26 (17) [B$_3$]$^+$, 199.16 (6) [B$_2$]$^+$.
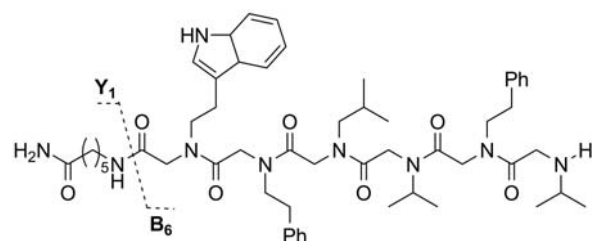
H_2N-Ahx-Ntrp^{+1}Nphe^{+1}Nleu^{+0}Nval^{+0}Nphe^{+1}Nval^{+0}-H **130**: Positively identified as binding to IL8S72C-DL550 **23** in a screen of library **104**. Later omitted due to highly hydrophobic side chains. – *MALDI-TOF* (matrix: CHCA), m/z: 821.66 (100), 964.77 (84) [M+H]$^+$, 996.77 (55). – *MALDI-TOF/TOF* (matrix: CHCA), m/z (%) [fragment]: 865.55

(11) $[Y_6+2\,H]^+$, 704.47 (100) $[Y_5+2\,H]^+$, 634.41 (4) $[B_5]^+$, 605.41 (21) $[Y_4+2\,H]^+$, 492.29 (3) $[Y_3+2\,H]^+$, 473.33 (15) $[B_4]^+$, 360.25 (33) $[B_3]^+$, 261.16 (5) $[B_2]^+$.

H_2N-Ahx-Nval^{+0}Nleu^{+0}Ntrp^{+1}Nphe^{+1}Ntrp^{+1}Nval^{+0}-H **131**: Positively identified as binding to IL8S72C-DL550 **23** in a screen of library **104**. Later omitted due to highly hydrophobic side chains. – *MALDI-TOF* (matrix: CHCA), m/z: 803.63 (100), 926.74 (100), 1003.77 (63) $[M+H]^+$. – *MALDI-TOF/TOF* (matrix: CHCA), m/z (%) [fragment]: 904.56 (16) $[Y_6+2\,H]^+$, 704.46 (100) $[Y_5+2\,H]^+$, 661.38 (14) $[B_4]^+$, 543.39 (30) $[Y_4+2\,H]^+$, 461.26 (18) $[B_3]^+$, 343.26 (4) $[Y_3+2\,H]^+$, 300.19 (8) $[B_2]^+$, 229.11 (3) $[Y_2+2\,H]^+$.
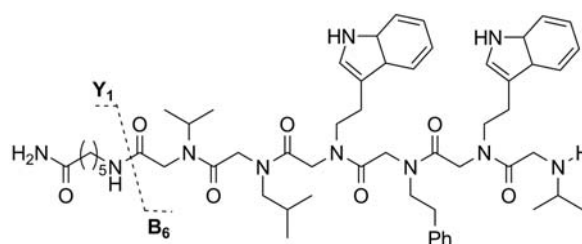
H_2N-Ahx-Ntrp^{+1}Nval^{+0}Nleu^{+0}Nval^{+0}Nphe^{+1}Nval^{+0}-H **132**: Positively identified as binding to IL8S72C-DL550 **23** in a screen of library **104**. Later omitted due to highly hydrophobic side chains. – *MALDI-TOF* (matrix: CHCA), m/z: 902.72 (100) $[M+H]^+$, 759.62 (38), 981.72 (29). – *MALDI-TOF/TOF* (matrix: CHCA), m/z (%) [fragment]: 803.52 (10) $[Y_6+2\,H]^+$, 642.45 (100) $[Y_5+2\,H]^+$, 572.39 (5) $[B_5]^+$, 543.38 (26) $[Y_4+2\,H]^+$, 473.32 (17) $[B_4]^+$, 430.29 (4) $[Y_3+2\,H]^+$, 360.23 (25) $[B_3]^+$, 261.17 (3) $[B_2]^+$.

H_2N-Ahx-Ntrp^{+1}Nphe^{+1}Nphe^{+1}Nval^{+0}Nleu^{+0}Nval^{+0}-H **133**: Positively identified as binding to IL8S72C-DL550 **23** in a screen of library **104**. Later omitted due to highly hydrophobic side chains. – *MALDI-TOF* (matrix: CHCA), m/z: 821.66 (100), 964.75 (87) $[M+H]^+$, 996.74 (47). – *MALDI-TOF/TOF* (matrix: CHCA), m/z (%) [fragment]: 866.52 (12) $[Y_6+2\,H]^+$, 752.46 (100) $[Y_5+2\,H]^+$, 653.40 (22) $[Y_4+2\,H]^+$, 634.39 (4) $[B_5]^+$, 492.29 (3) $[Y_3+2\,H]^+$, 473.33 (13) $[B_4]^+$, 312.24 (31) $[B_3]^+$, 213.16 (5) $[B_2]^+$.
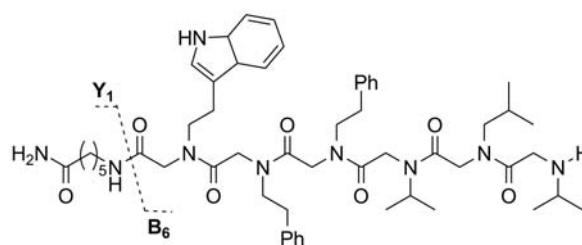
H_2N-Ahx-Ntrp^{+1}Ntrp^{+1}Nleu^{+0}Nleu^{+0}Nser^{+1}Nval^{+0}-H **134**: Positively identified as binding to IL8S72C-DL550 **23** in a screen of library **104**. Later omitte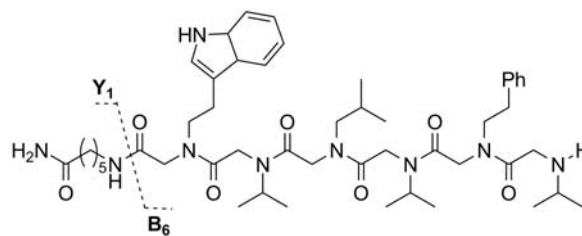d due to highly hydrophobic side chains. – *MALDI-TOF* (matrix: CHCA), m/z: 957.72 (100) $[M+H]^+$, 814.63 (47), 987.71 (17). – *MALDI-TOF/TOF* (matrix: CHCA), m/z (%) [fragment]: 859.52 (21) $[Y_6+2\,H]^+$, 758.50 (100) $[Y_5+2\,H]^+$, 644.43 (34) $[Y_4+2\,H]^+$, 627.41 (8) $[B_5]^+$, 531.35 (10) $[Y_3+2\,H]^+$, 427.31 (26) $[B_4]^+$, 314.22 (17) $[B_3]^+$, 201.13 (3) $[B_2]^+$.
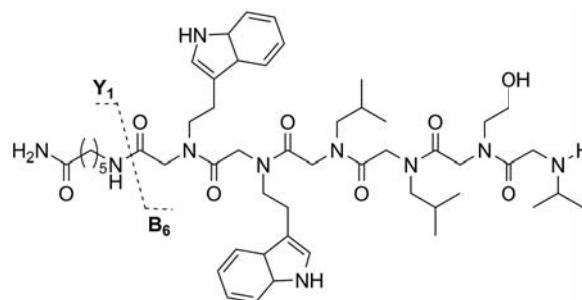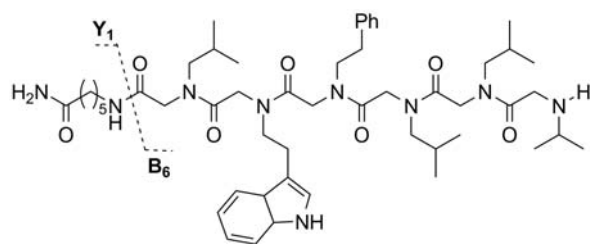
$H_2N\text{-}Ahx\text{-}Nleu^{+0}Ntrp^{+1}Nphe^{+1}Nleu^{+0}Nleu^{+0}Nval^{+0}\text{-}H$ **135**: Positively identified as binding to IL8S72C-DL550 **23** in a screen of library **104**. Later omitted due to highly hydrophobic side chains. – *MALDI-TOF* (matrix: CHCA), m/z: 930.74 (100) [M+H]$^+$, 787.64 (53), 959.73 (42). – *MALDI-TOF/TOF* (matrix: CHCA), m/z (%) [fragment]: 835.60 (20) [Y$_6$+2 H]$^+$, 798.48 (100) [Y$_5$+2 H]$^+$, 685.39 (22) [B$_5$]$^+$, 487.36 (22) [B$_4$]$^+$, 326.26 (30) [B$_3$]$^+$, 213.18 (8) [B$_2$]$^+$.
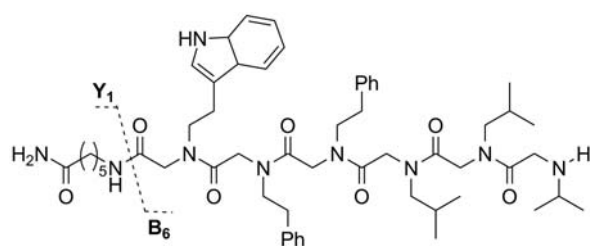
$H_2N\text{-}Ahx\text{-}Ntrp^{+1}Nphe^{+1}Nphe^{+1}Nleu^{+0}Nleu^{+0}Nval^{+0}\text{-}H$ **136**: Positively identified as binding to IL8S72C-DL550 **23** in a screen of library **104**. Later omitted due to highly hydrophobic side chains. – *MALDI-TOF* (matrix: CHCA), m/z: 978.77 (100) [M+H]$^+$, 835.67 (93), 1010.76 (46). – *MALDI-TOF/TOF* (matrix: CHCA), m/z (%) [fragment]: 880.53 (20) [Y$_6$+2 H]$^+$, 767.47 (100) [Y$_5$+2 H]$^+$, 653.41 (21) [Y$_4$+2 H]$^+$, 648.42 (6) [B$_5$]$^+$, 487.34 (22) [B$_4$]$^+$, 326.25 (29) [B$_3$]$^+$, 213.17 (8) [B$_2$]$^+$.
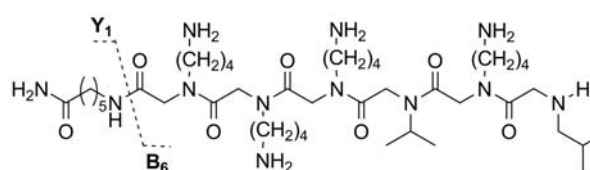
$H_2N\text{-}Ahx\text{-}Nlys^{+0}Nlys^{+0}Nlys^{+0}Nval^{+0}Nlys^{+0}Nleu^{+0}\text{-}H$ **137**: Positively identified as binding to IL8S72C-DL550 **23** in a screen of library **104**. – *MALDI-TOF* (matrix: CHCA), m/z: 855.82 (100) [M+H]$^+$, 877.81 (92). – *MALDI-TOF/TOF* (matrix: CHCA), m/z (%) [fragment]: 742.55 (16) [Y$_6$+2 H]$^+$, 614.48 (100) [Y$_5$+2 H]$^+$, 597.45 (6) [B$_5$]$^+$, 515.42 (40) [Y$_4$+2 H]$^+$, 469.36 (13) [B$_4$]$^+$, 387.29 (7) [Y$_3$+2 H]$^+$, 341.27 (17) [B$_3$]$^+$, 242.19 (47) [B$_2$]$^+$.
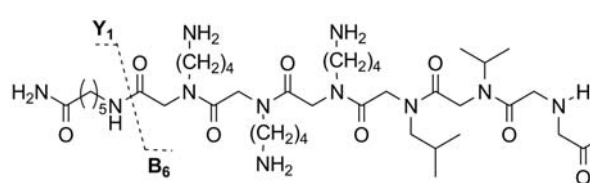
$H_2N\text{-}Ahx\text{-}Nlys^{+0}Nlys^{+0}Nlys^{+0}Nleu^{+0}Nval^{+0}Nasp^{+0}\text{-}H$ **138**: Positively identified as binding to IL8S72C-DL550 **23** in a screen of library **104**. – *MALDI-TOF* (matrix: CHCA), m/z: 842.71 (100) [M+H]$^+$, 1396.25 (45). – *MALDI-TOF/TOF* (matrix: CHCA), m/z (%) [fragment]: 727.51 (36) [Y$_6$+2 H]$^+$, 628.47 (100) [Y$_5$+2 H]$^+$, 584.38 (8) [B$_5$]$^+$, 515.38 (28) [Y$_4$+2 H]$^+$, 456.28 (10) [B$_4$]$^+$, 387.30 (14) [Y$_3$+2 H]$^+$, 328.18 (8) [B$_3$]$^+$, 215.10 (4) [B$_2$]$^+$.

$H_2N\text{-}Ahx\text{-}Nlys^{+0}Nlys^{+0}Nser^{+1}Nlys^{+0}Nlys^{+0}Nleu^{+0}\text{-}H$ **139**: Positively identified as binding to IL8S72C-DL550 **23** in a screen of library **104**. – *MALDI-TOF* (matrix: CHCA), m/z: 879.80 (100), 857.82 (87) [M+H]$^+$, 656.21 (38). – *MALDI-TOF/TOF* (matrix: CHCA), m/z (%) [fragment]: 744.53 (18) [Y$_6$+2 H]$^+$, 616.46 (100) [Y$_5$+2 H]$^+$, 599.44 (6) [B$_5$]$^+$, 488.38 (21) [Y$_4$+2 H]$^+$, 471.33 (9) [B$_4$]$^+$, 387.31 (6) [Y$_3$+2 H]$^+$, 370.28 (27) [B$_3$]$^+$, 257.21 (2) [Y$_2$+2 H]$^+$, 242.20 (34) [B$_2$]$^+$.

H_2N-Ahx-Nlys^{+0}Nlys^{+0}Nleu^{+0}Nlys^{+0}Nval^{+0}Nleu^{+0}-H **140**: Positively identified as binding to IL8S72C-DL550 **23** in a screen of library **104**. – *MALDI-TOF* (matrix: CHCA), m/z: 862.82 (100), 840.82 (86) [M+H]$^+$. – *MALDI-TOF/TOF* (matrix: CHCA), m/z (%) [fragment]: 727.58 (28) [Y$_6$+2 H]$^+$, 628.51 (100) [Y$_5$+2 H]$^+$, 582.47 (2) [B$_5$]$^+$, 500.41 (12) [Y$_4$+2 H]$^+$, 454.35 (6) [B$_4$]$^+$, 387.31 (4) [Y$_3$+2 H]$^+$, 341.26 (9) [B$_3$]$^+$, 213.18 (5) [B$_2$]$^+$.

H_2N-Ahx-Nlys^{+0}Nlys^{+0}Nval^{+0}Nlys^{+0}Nphe^{+1}Nleu^{+0}-H **141**: Positively identified as binding to IL8S72C-DL550 **23** in a screen of library **104**. – *MALDI-TOF* (matrix: CHCA), m/z: 888.85 (100) [M+H]$^+$, 760.72 (50), 1302.24 (20). – *MALDI-TOF/TOF* (matrix: CHCA), m/z (%) [fragment]: 775.57 (14) [Y$_6$+2 H]$^+$, 630.47 (4) [B$_5$]$^+$, 614.50 (100) [Y$_5$+2 H]$^+$, 502.35 (18) [B$_4$]$^+$, 486.40 (33) [Y$_4$+2 H]$^+$, 403.29 (19) [B$_3$]$^+$, 387.32 (7) [Y$_3$+2 H]$^+$, 275.18 (4) [B$_2$]$^+$.
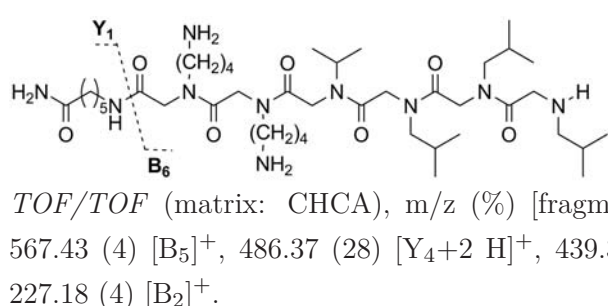
H_2N-Ahx-Nlys^{+0}Nlys^{+0}Nval^{+0}Nleu^{+0}Nleu^{+0}Nleu^{+0}-H **142**: Positively identified as binding to IL8S72C-DL550 **23** in a screen of library **104**. – *MALDI-TOF* (matrix: CHCA), m/z: 825.83 (100) [M+H]$^+$, 847.79 (35). – *MALDI-TOF/TOF* (matrix: CHCA), m/z (%) [fragment]: 712.52 (20) [Y$_6$+2 H]$^+$, 599.45 (100) [Y$_5$+2 H]$^+$, 567.43 (4) [B$_5$]$^+$, 486.37 (28) [Y$_4$+2 H]$^+$, 439.31 (22) [B$_4$]$^+$, 387.30 (7) [Y$_3$+2 H]$^+$, 340.26 (20) [B$_3$]$^+$, 227.18 (4) [B$_2$]$^+$.
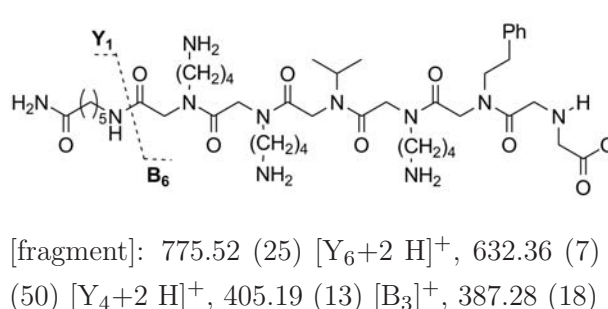
H_2N-Ahx-Nlys^{+0}Nlys^{+0}Nval^{+0}Nlys^{+0}Nphe^{+1}Nasp^{+0}-H **143**: Positively identified as binding to IL8S72C-DL550 **23** in a screen of library **104**. – *MALDI-TOF* (matrix: CHCA), m/z: 890.72 (100) [M+H]$^+$, 762.59 (23), 962.75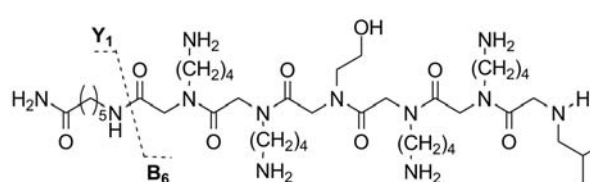 (21). – *MALDI-TOF/TOF* (matrix: CHCA), m/z (%) [fragment]: 775.52 (25) [Y$_6$+2 H]$^+$, 632.36 (7) [B$_5$]$^+$, 614.44 (100) [Y$_5$+2 H]$^+$, 504.28 (7) [B$_4$]$^+$, 486.36 (50) [Y$_4$+2 H]$^+$, 405.19 (13) [B$_3$]$^+$, 387.28 (18) [Y$_3$+2 H]$^+$, 277.11 (13) [B$_2$]$^+$.
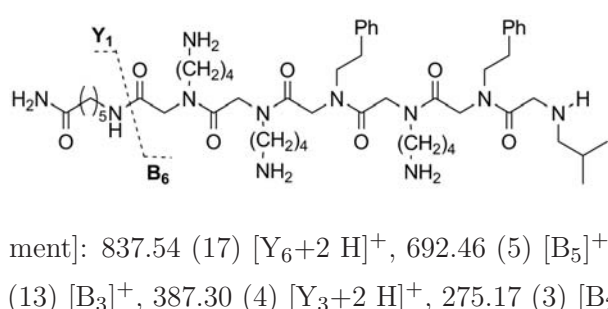
H_2N-Ahx-Nlys^{+0}Nlys^{+0}Nphe^{+1}Nlys^{+0}Nphe^{+1}Nleu^{+0}-H **144**: Positively identified as binding to IL8S72C-DL550 **23** in a screen of library **104**. – *MALDI-TOF* (matrix: CHCA), m/z: 950.85 (100) [M+H]$^+$, 972.79 (31), 1554.38 (21). – *MALDI-TOF/TOF* (matrix: CHCA), m/z (%) [fragment]: 837.54 (17) [Y$_6$+2 H]$^+$, 692.46 (5) [B$_5$]$^+$, 676.49 (100) [Y$_5$+2 H]$^+$, 564.40 (23) [Y$_4$+2 H]$^+$, 403.27 (13) [B$_3$]$^+$, 387.30 (4) [Y$_3$+2 H]$^+$, 275.17 (3) [B$_2$]$^+$.
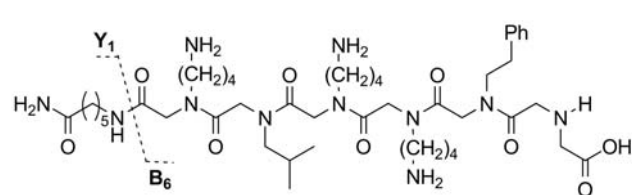
H_2N-Ahx-Nlys^{+0}Nleu^{+0}Nlys^{+0}Nlys^{+0}Nphe^{+1}Nasp^{+0}-H **145**: Positively identified as binding to IL8S72C-DL550 **23** in a screen of library **104**. – *MALDI-TOF* (matrix: CHCA), m/z: 904.70 (100) [M+H]$^+$, 976.74 (36), 1734.38 (15). – *MALDI-TOF/TOF* (matrix: CHCA), m/z (%) [fragment]: 789.52 (23) [Y$_6$+2 H]$^+$, 646.37 (4) [B$_5$]$^+$, 628.47 (100) [Y$_5$+2 H]$^+$, 533.29 (20) [B$_4$]$^+$, 500.37 (50) [Y$_4$+2 H]$^+$, 405.19 (8) [B$_3$]$^+$, 372.29 (4) [Y$_3$+2 H]$^+$, 277.10 (6) [B$_2$]$^+$.
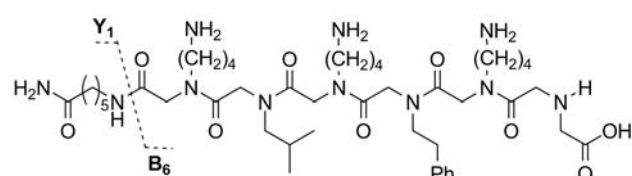
H_2N-Ahx-Nlys^{+0}Nleu^{+0}Nlys^{+0}Nphe^{+1}Nlys^{+0}Nasp^{+0}-H **146**: Positively identified as binding to IL8S72C-DL550 **23** in a screen of library **104**. – *MALDI-TOF* (matrix: CHCA), m/z: 904.71 (100) [M+H]$^+$, 671.56 (60), 1201.99 (15). – *MALDI-TOF/TOF* (matrix: CHCA), m/z (%) [fragment]: 789.56 (23) [Y$_6$+2 H]$^+$, 661.48 (100) [Y$_5$+2 H]$^+$, 646.37 (8) [B$_5$]$^+$, 533.29 (16) [B$_4$]$^+$, 500.39 (45) [Y$_4$+2 H]$^+$, 405.21 (2) [B$_3$]$^+$, 372.29 (6) [Y$_3$+2 H]$^+$, 244.14 (11) [B$_2$]$^+$.
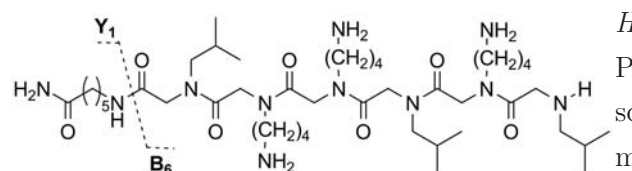
H_2N-Ahx-Nleu^{+0}Nlys^{+0}Nlys^{+0}Nleu^{+0}Nlys^{+0}Nleu^{+0}-H **147**: Positively identified as binding to IL8S72C-DL550 **23** in a screen of library **104**. – *MALDI-TOF* (matrix: CHCA), m/z: 854.85 (100) [M+H]$^+$, 656.62 (62), 876.81 (56). – *MALDI-TOF/TOF* (matrix: CHCA), m/z (%) [fragment]: 741.58 (26) [Y$_6$+2 H]$^+$, 613.50 (100) [Y$_5$+2 H]$^+$, 500.41 (50) [Y$_4$+2 H]$^+$, 372.32 (8) [Y$_3$+2 H]$^+$, 355.29 (17) [B$_3$]$^+$, 242.19 (55) [B$_2$]$^+$.
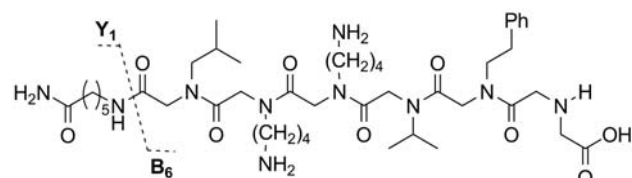
H_2N-Ahx-Nleu^{+0}Nlys^{+0}Nlys^{+0}Nval^{+0}Nphe^{+1}Nasp^{+0}-H **148** : Positively identified as binding to IL8S72C-DL550 **23** in a screen of library **104**. – *MALDI-TOF* (matrix: CHCA), m/z: 875.68 (100) [M+H]$^+$, 1400.18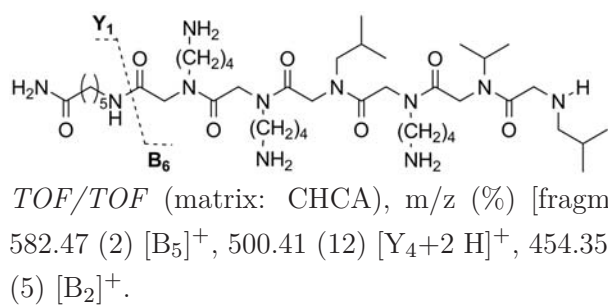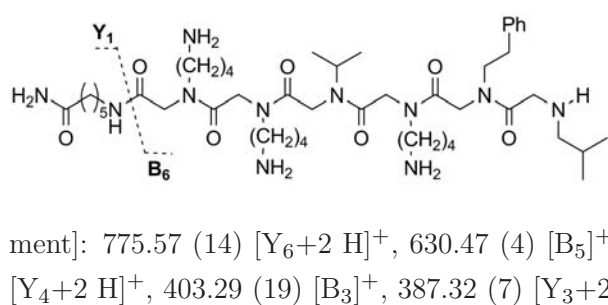 (33). – *MALDI-TOF/TOF* (matrix: CHCA), m/z (%) [fragment]: 760.49 (18) [Y$_6$+2 H]$^+$, 632.34 (6) [B$_5$]$^+$, 599.43 (100) [Y$_5$+2 H]$^+$, 504.25 (11) [B$_4$]$^+$, 500.37 (55) [Y$_4$+2 H]$^+$, 376.18 (16) [B$_3$]$^+$, 372.28 (14) [Y$_3$+2 H]$^+$, 277.10 (4) [B$_2$]$^+$.
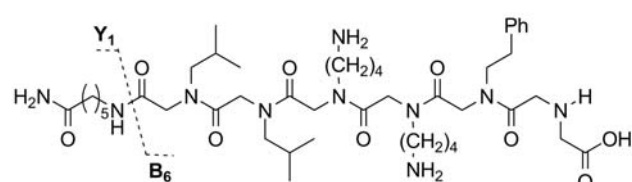
H_2N-Ahx-Nleu^{+0}Nleu^{+0}Nlys^{+0}Nlys^{+0}Nphe^{+1}Nasp^{+0}-H **149**: Positively identified as binding to IL8S72C-DL550 **23** in a screen of library **104**. – *MALDI-TOF* (matrix: CHCA), m/z: 889.72 (100) [M+H]$^+$, 1428.23 (90), 1095.94 (75). – *MALDI-TOF/TOF* (matrix: CHCA), m/z (%) [fragment]: 774.53 (21) [Y$_6$+2 H]$^+$, 646.38 (4) [B$_5$]$^+$, 613.46 (100) [Y$_5$+2 H]$^+$, 533.30 (23) [B$_4$]$^+$, 485.37 (50) [Y$_4$+2 H]$^+$, 405.21 (9) [B$_3$]$^+$, 357.27 (4) [Y$_3$+2 H]$^+$, 277.10 (4) [B$_2$]$^+$.
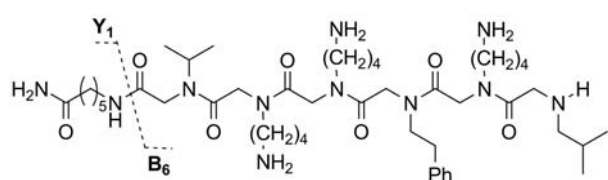
H_2N-Ahx-Nval^{+0}Nlys^{+0}Nlys^{+0}Nphe^{+1}Nlys^{+0}Nleu^{+0}-H **150**: Positively identified as binding to IL8S72C-DL550 **23** in a screen of library **104**. – *MALDI-TOF* (matrix: CHCA), m/z: 888.82 (100) [M+H]$^+$, 1174.04 (55), 1130.99 (36). – *MALDI-TOF/TOF* (matrix: CHCA), m/z (%) [fragment]: 775.54 (24) [Y$_6$+2 H]$^+$, 659.45 (6) [B$_5$]$^+$, 647.46 (100) [Y$_5$+2 H]$^+$, 531.36 (22) [B$_4$]$^+$, 486.37 (42) [Y$_4$+2 H]$^+$, 403.27 (17) [B$_3$]$^+$, 358.28 (12) [Y$_3$+2 H]$^+$, 242.20 (54) [B$_2$]$^+$.
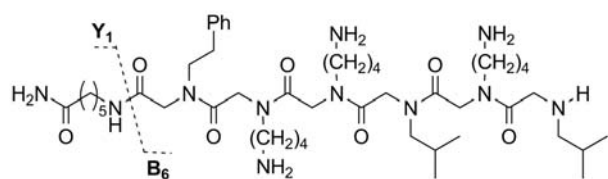
H_2N-Ahx-Nphe^{+1}Nlys^{+0}Nlys^{+0}Nleu^{+0}Nlys^{+0}Nleu^{+0}-H **151**: Positively identified as binding to IL8S72C-DL550 **23** in a screen of library **104**. – *MALDI-TOF* (matrix: CHCA), m/z: 902.85 (100) [M+H]$^+$, 752.64 (85). – *MALDI-TOF/TOF* (matrix: CHCA), m/z (%) [fragment]: 789.56 (26) [Y$_6$+2 H]$^+$, 661.48 (100) [Y$_5$+2 H]$^+$, 611.48 (4) [B$_5$]$^+$, 548.40 (40) [Y$_4$+2 H]$^+$, 483.37 (19) [B$_4$]$^+$, 420.30 (8) [Y$_3$+2 H]$^+$, 355.27 (17) [B$_3$]$^+$, 242.19 (67) [B$_2$]$^+$.
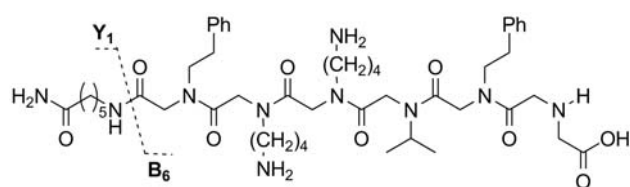
H_2N-Ahx-Nphe^{+1}Nlys^{+0}Nlys^{+0}Nval^{+0}Nphe^{+1}Nasp^{+0}-H **152**: Positively identified as binding to IL8S72C-DL550 **23** in a screen of library **104**. – *MALDI-TOF* (matrix: CHCA), m/z: 923.70 (100) [M+H]$^+$, 1093.86 (14), 1236.00 (12). – *MALDI-TOF/TOF* (matrix: CHCA), m/z (%) [fragment]: 808.52 (18) [Y$_6$+2 H]$^+$, 647.46 (100) [Y$_5$+2 H]$^+$, 632.36 (7) [B$_5$]$^+$, 548.39 (50) [Y$_4$+2 H]$^+$, 504.28 (10) [B$_4$]$^+$, 420.30 (12) [Y$_3$+2 H]$^+$, 376.19 (15) [B$_3$]$^+$, 277.11 (3) [B$_2$]$^+$.
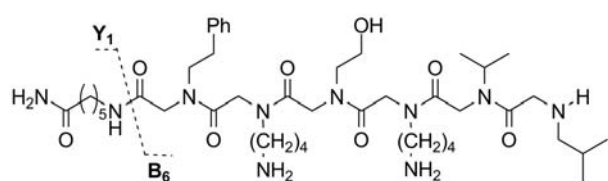
H_2N-Ahx-Nphe^{+1}Nlys^{+0}Nser^{+1}Nlys^{+0}Nval^{+0}Nleu^{+0}-H **153**: Positively identified as binding to IL8S72C-DL550 **23** in a screen of library **104**. – *MALDI-TOF* (matrix: CHCA), m/z: 752.63 (100), 837.71 (72), 861.78 (56) [M+H]$^+$. – *MALDI-TOF/TOF* (matrix: CHCA), m/z (%) [fragment]: 748.52 (24) [Y$_6$+2 H]$^+$, 649.46 (100) [Y$_5$+2 H]$^+$, 570.39 (2) [B$_5$]$^+$, 521.35 (13) [Y$_4$+2 H]$^+$, 442.31 (5) [B$_4$]$^+$, 420.31 (4) [Y$_3$+2 H]$^+$, 341.27 (10) [B$_3$]$^+$, 213.16 (4) [B$_2$]$^+$.
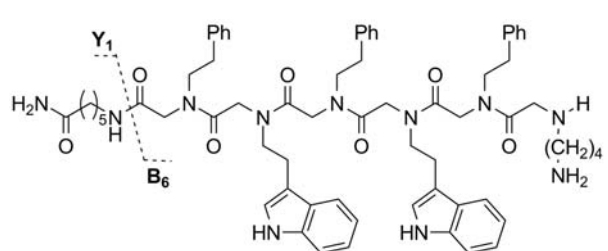
H_2N-Ahx-Nphe^{+1}Ntrp^{+1}Nphe^{+1}Ntrp^{+1}Nphe^{+1}Nlys^{+0}-H **154**: Positively identified as binding to IL8S72C-DL550 **23** in a screen of library **104**. – *MALDI-TOF* (matrix: CHCA), m/z: 1000.70 (100), 857.59 (47), 1143.79 (43) [M+H]$^+$. – *MALDI-TOF/TOF* (matrix: CHCA), m/z (%) [fragment]: 1014.58 (14) [Y$_6$+2 H]$^+$, 854.48 (100) [Y$_5$+2 H]$^+$, 654.38 (15) [Y$_4$+2 H]$^+$, 651.37 (13) [B$_4$]$^+$, 490.31 (10) [B$_3$]$^+$, 290.20 (17) [B$_2$]$^+$.

H_2N-Ahx-Ntrp^{+1}Ntrp^{+1}Nphe^{+1}Nlys^{+0}Nlys^{+0}Nleu^{+0}-H **155**: Positively identified as binding to IL8S72C-DL550 **23** in a screen of library **104**. – *MALDI-TOF* (matrix: CHCA), m/z: 1061.94 (100) [M+H]$^+$, 918.82 (80). – *MALDI-TOF/TOF* (matrix: CHCA), m/z (%) [fragment]: 948.56 (15) [Y$_6$+2 H]$^+$, 820.50 (100) [Y$_5$+2 H]$^+$, 731.47 (5) [B$_5$]$^+$, 692.41 (25) [Y$_4$+2 H]$^+$, 531.36 (18) [Y$_3$+2 H]$^+$ and [B$_4$]$^+$, 370.28 (20) [B$_3$]$^+$, 242.18 (36) [B$_2$]$^+$.

H_2N-Ahx-Ntrp^{+1}Ntrp^{+1}Nlys^{+0}Nlys^{+0}Ntrp^{+1}Nlys^{+0}-H **156**: Positively identified as binding to IL8S72C-DL550 **23** in a screen of library **104**. – *MALDI-TOF* (matrix: CHCA), m/z: 646.40 (100), 786.53 (58), 1115.82 (54) [M+H]$^+$. – *MALDI-TOF/TOF* (matrix: CHCA), m/z (%) [fragment]: 987.61 (20) [Y$_6$+2 H]$^+$, 787.52 (100) [Y$_5$+2 H]$^+$, 659.44 (27) [Y$_4$+2 H]$^+$, 585.41 (16) [B$_4$]$^+$, 531.32 (6) [Y$_3$+2 H]$^+$, 547.24 (9) [B$_3$]$^+$, 329.24 (8) [B$_2$]$^+$.

H_2N-Ahx-Ntrp^{+1}Ntrp^{+1}Nser^{+1}Nphe^{+1}Ntrp^{+1}Nlys^{+0}-H **157**: Positively identified as binding to IL8S72C-DL550 **23** in a screen of library **104**. – *MALDI-TOF* (matrix: CHCA), m/z: 1122.76 (100) [M+H]$^+$, 1134.78 (60), 979.66 (52). – *MALDI-TOF/TOF* (matrix: CHCA), m/z (%) [fragment]: 994.50 (24) [Y$_6$+2 H]$^+$, 858.47 (17), 794.43 (100) [Y$_5$+2 H]$^+$, 633.35 (12) [Y$_4$+2 H]$^+$, 591.34 (10) [B$_4$]$^+$, 532.28 (9) [Y$_3$+2 H]$^+$, 490.28 (17) [B$_3$]$^+$, 329.20 (22) [B$_2$]$^+$.

H_2N-Ahx-Ntrp^{+1}Nphe^{+1}Nval^{+0}Ntrp^{+1}Nser^{+1}Nlys^{+0}-H **158**: Positively identified as binding to IL8S72C-DL550 **23** in a screen of library **104**. – *MALDI-TOF* (matrix: CHCA), m/z: 820.60 (100), 1021.74 (76) [M+H]$^+$, 878.63 (55). – *MALDI-TOF/TOF* (matrix: CHCA), m/z (%) [fragment]: 892.52 (12) [Y$_6$+2 H]$^+$, 792.45 (100) [Y$_5$+2 H]$^+$, 592.38 (28) [Y$_4$+2 H]$^+$, 529.34 (18) [B$_4$]$^+$, 493.31 (10) [Y$_3$+2 H]$^+$, 430.26 (17) [B$_3$]$^+$, 230.15 (5) [B$_2$]$^+$.

H_2N-Ahx-Ntrp^{+1}Nphe^{+1}Ntrp^{+1}Nphe^{+1}Nser^{+1}Nser^{+1}-H **159**: Positively identified as binding to IL8S72C-DL550 **23** in a screen of library **104**. – *MALDI-TOF* (matrix: CHCA), m/z: 1056.67 (100) [M+H]$^+$, 913.56 (95), 1088.66 (25). – *MALDI-TOF/TOF* (matrix: CHCA), m/z (%) [fragment]: 955.47 (14) [Y$_6$+2 H]$^+$, 854.45

(100) $[Y_5+2\,H]^+$, 725.35 (7) $[B_5]^+$, 693.37 (36) $[Y_4+2\,H]^+$, 564.28 (22) $[B_4]^+$, 493.27 (4) $[Y_3+2\,H]^+$, 364.18 (8) $[B_3]^+$, 203.10 (3) $[B_2]^+$.
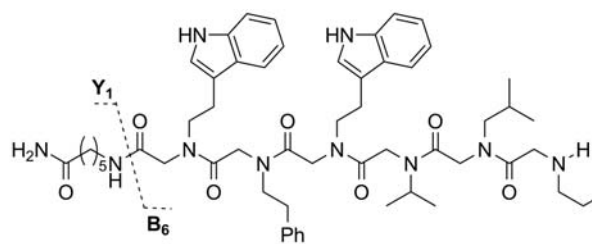
H₂N-Ahx-Ntrp⁺¹Nphe⁺¹Ntrp⁺¹Nval⁺⁰Nleu⁺⁰Nser⁺¹-H **160**: Positively identified as binding to IL8S72C-DL550 **23** in a screen of library **104**. – *MALDI-TOF* (matrix: CHCA), m/z: 1006.68 (100) [M+H]⁺, 863.59 (53), 893.59 (19). – *MALDI-TOF/TOF* (matrix: CHCA), m/z (%) [fragment]: 905.51 (8) $[Y_6+2\,H]^+$, 792.44 (100) $[Y_5+2\,H]^+$, 693.37 (29) $[Y_4+2\,H]^+$, 675.38 (3) $[B_5]^+$, 514.31 (14) $[B_4]^+$, 493.28 (2) $[Y_3+2\,H]^+$, 314.51 (9) $[B_3]^+$, 215.14 (3) $[B_2]^+$.
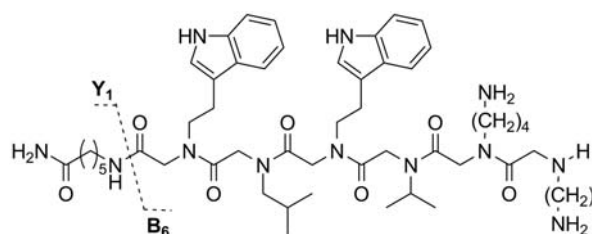
H₂N-Ahx-Ntrp⁺¹Nleu⁺⁰Ntrp⁺¹Nval⁺⁰Nlys⁺⁰Nlys⁺⁰-H **161**: Positively identified as binding to IL8S72C-DL550 **23** in a screen of library **104**. – *MALDI-TOF* (matrix: CHCA), m/z: 856.65 (100), 999.75 (65) [M+H]⁺, 1029.73 (36). – *MALDI-TOF/TOF* (matrix: CHCA), m/z (%) [fragment]: 871.56 (19) $[Y_6+2\,H]^+$, 743.48 (100) $[Y_5+2\,H]^+$, 669.48 (7) $[B_5]^+$, 644.43 (37) $[Y_4+2\,H]^+$, 556.35 (14) $[B_4]^+$, 444.33 (12) $[Y_3+2\,H]^+$, 356.27 (35) $[B_3]^+$, 257.20 (83) $[B_2]^+$.
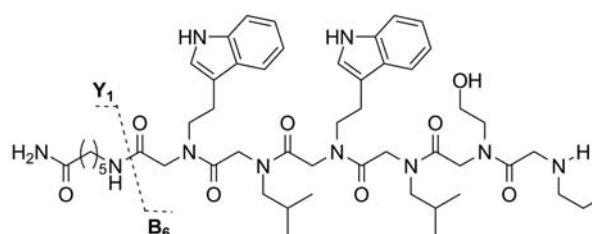
H₂N-Ahx-Ntrp⁺¹Nleu⁺⁰Ntrp⁺¹Nleu⁺⁰Nser⁺¹Nser⁺¹-H **162**: Positively identified as binding to IL8S72C-DL550 **23** in a screen of library **104**. – *MALDI-TOF* (matrix: CHCA), m/z: 960.65 (100) [M+H]⁺, 816.55 (62), 859.58 (25). – *MALDI-TOF/TOF* (matrix: CHCA), m/z (%) [fragment]: 859.51 (14) $[Y_6+2\,H]^+$, 758.49 (100) $[Y_5+2\,H]^+$, 645.40 (38) $[Y_4+2\,H]^+$, 629.38 (8) $[B_5]^+$, 516.29 (23) $[B_4]^+$, 444.29 (4) $[Y_3+2\,H]^+$, 316.20 (8) $[B_3]^+$, 203.11 (3) $[B_2]^+$.
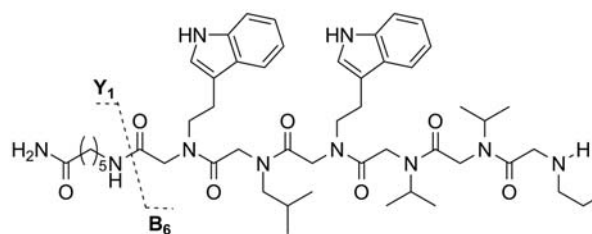
H₂N-Ahx-Ntrp⁺¹Nleu⁺⁰Ntrp⁺¹Nval⁺⁰Nval⁺⁰Nser⁺¹-H **163**: Positively identified as binding to IL8S72C-DL550 **23** in a screen of library **104**. – *MALDI-TOF* (matrix: CHCA), m/z: 944.66 (100) [M+H]⁺, 800.57 (72), 815.54 (32). – *MALDI-TOF/TOF* (matrix: CHCA), m/z (%) [fragment]: 843.48 (14) $[Y_6+2\,H]^+$, 744.45 (100) $[Y_5+2\,H]^+$, 645.38 (20) $[Y_4+2\,H]^+$, 613.36 (3) $[B_5]^+$, 500.29 (8) $[B_4]^+$, 444.28 (2) $[Y_3+2\,H]^+$, 300.19 (8) $[B_3]^+$, 201.13 (6) $[B_2]^+$.
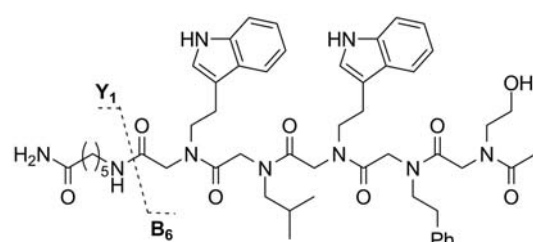
H_2N-Ahx-$Ntrp^{+1}Nleu^{+0}Ntrp^{+1}Nphe^{+1}Nser^{+1}Nser^{+1}$-$H$ **164**: Positively identified as binding to IL8S72C-DL550 **23** in a screen of library **104**. – *MALDI-TOF* (matrix: CHCA), m/z: 1008.65 (100) [M+H]$^+$, 865.57 (77), 815.55 (23). – *MALDI-TOF/TOF* (matrix: CHCA), m/z (%) [fragment]: 907.48 (14) [Y$_6$+2 H]$^+$, 806.45 (100) [Y$_5$+2 H]$^+$, 677.36 (9) [B$_5$]$^+$, 645.37 (37) [Y$_4$+2 H]$^+$, 564.28 (22) [B$_4$]$^+$, 444.28 (5) [Y$_3$+2 H]$^+$, 364.18 (8) [B$_3$]$^+$, 203.09 (2) [B$_2$]$^+$.
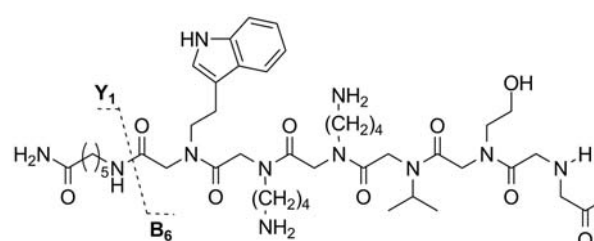
H_2N-Ahx-$Ntrp^{+1}Nlys^{+0}Nlys^{+0}Nval^{+0}Nser^{+1}Nasp^{+0}$-$H$ **165**: Positively identified as binding to IL8S72C-DL550 **23** in a screen of library **104**. – *MALDI-TOF* (matrix: CHCA), m/z: 931.69 (100), 916.69 (76), 902.71 (49) [M+H]$^+$. – *MALDI-TOF/TOF* (matrix: CHCA), m/z (%) [fragment]: 787.52 (19) [Y$_6$+2 H]$^+$, 730.46 (20), 718.42 (23), 715.46 (27), 690.41 (77), 686.46 (100) [Y$_5$+2 H]$^+$, 619.38 (17), 591.6 (51), 587.41 (67) [Y$_4$+2 H]$^+$, 572.32 (26) [B$_5$]$^+$, 459.31 (25) [Y$_3$+2 H]$^+$, 444.21 (27) [B$_4$]$^+$, 316.17 (30) [B$_3$]$^+$.

The 18 peptoid hits from library **104** (peptoids **137-153** and **165**) were synthesized with fluorescein labels for further testing. HPLC purification of peptoids **167-184** was executed by K. Brahm.
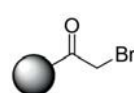
Bromoacetic acid on chlorotritylchloride resin **166**: 310 mg (0.465 mmol, 1.00 eq) chlorotritylchloride resin was swollen according to GP001. 1136 mg (4.65 mmol, 3.00 eq) bromoacetic acid (1.2 M in NMP) were mixed with 635 µL (4.65 mmol, 3.00 eq) DIPEA and the mixture was added to the resin. The mixture was shaken at 600 rpm overnight (GP004). The resin was washed (GP002).
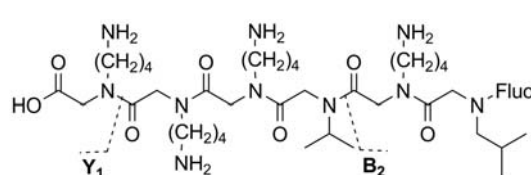
HO-$Nlys^{+0}Nlys^{+0}Nlys^{+0}Nval^{+0}Nlys^{+0}Nleu^{+0}$-*Fluo* **167**: 10.0 mg (0.015 mmol, 1.00 eq) resin **166** was substituted with **12** (GP006) and the resin was washed (GP002). The cycle of acylation (GP005), washing (GP002), substitution (GP006), washing (GP002) was repeated with the remaining amines: **12** twice, isopropylamine, **12** and isobutylamine. Each acylation/substitution step was monitored by the chloranil test (GP019). 5(6)-Carboxyfluorescein was attached according to GP015. Protecting groups were removed and the peptoid was cleaved off the resin (GP013). TFA was removed *in vacuo* and the peptoid was isolated by HPLC (C18 RP, linear gradient over 5 CV: 0 %-60 % eluent B) and eluted after 29 min. Yield: 1.4 mg.
– *MALDI-TOF* (matrix: CHCA), m/z: 1101.96 (100) [M+H]$^+$, 743.79 (9). – *MALDI-TOF/TOF* (matrix: CHCA), m/z (%) [fragment]: 955.56 (17) [B$_5$]$^+$, 827.46 (21) [B$_4$]$^+$, 699.34 (19) [B$_3$]$^+$, 630.51 (100) [Y$_5$+2 H]$^+$, 600.25 (10) [B$_2$]$^+$, 502.41 (70) [Y$_4$+2 H]$^+$, 473.19 (8) [B$_1$]$^+$, 403.32 (41) [Y$_3$+2 H]$^+$.

HO-Nlys^{+0}Nlys^{+0}Nlys^{+0}Nleu^{+0}Nval^{+0}Nasp^{+0}-Fluo **168**: 10.0 mg (0.015 mmol, 1.00 eq) resin **166** was substituted with **12** (GP006) and the resin was washed (GP002). The cycle of acylation (GP005), washing (GP002), substitution (GP006), washing (GP002) was repeated with the remaining amines: **12**, isobutylamine, isopropylamine, glycine *tert*-butyl ester acetate. Each acylation/substitution step was monitored by the chloranil test (GP019). 5(6)-carboxyfluorescein was attached according to GP015. Protecting groups were removed and the peptoid was cleaved off the resin (GP013). TFA was removed *in vacuo* and the peptoid was isolated by HPLC (C18 RP, linear gradient over 5 CV: 0 %-60 % eluent B) and eluted after 30.5 min. Yield: 0.7 mg. – *MALDI-TOF* (matrix: CHCA), m/z: 1088.91 (100) [M+H]$^+$. – *MALDI-TOF/TOF* (matrix: CHCA), m/z (%) [fragment]: 942.53 (31) [B$_5$]$^+$, 814.40 (39) [B$_4$]$^+$, 686.31 (25) [B$_3$]$^+$, 615.51 (98) [Y$_5$+2 H]$^+$, 574.18 (4) [B$_2$]$^+$, 516.43 (100) [Y$_4$+2 H]$^+$, 403.35 (64) [Y$_3$+2 H]$^+$, 275.22 (7) [Y$_2$+2 H]$^+$.

HO-Nlys^{+0}Nlys^{+0}Nser^{+1}Nlys^{+0}Nlys^{+0}Nleu^{+0}-Fluo **169**: 10.0 mg (0.015 mmol, 1.00 eq) resin **166** was substituted with **12** (GP006) and the resin was washed (GP002). The cycle of acylation (GP005), washing (GP002), substitution (GP006), washing (GP002) was repeated with the remaining amines: **12**, **10** and isobutylamine. Each acylation/substitution step was monitored by the chloranil test (GP019). 5(6)-carboxyfluorescein was attached according to GP015. Protecting groups were removed and the peptoid was cleaved off the resin (GP013). TFA was removed *in vacuo* and the peptoid was isolated by HPLC (C18 RP, linear gradient over 5 CV: 0 %-60 % eluent B) and eluted after 28 min. Yield: 0.7 mg. – *MALDI-TOF* (matrix: CHCA), m/z: 1103.98 (100) [M+H]$^+$. – *MALDI-TOF/TOF* (matrix: CHCA), m/z (%) [fragment]: 958.54 (15) [B$_5$]$^+$, 829.44 (7) [B$_4$]$^+$, 728.38 (31) [B$_3$]$^+$, 632.50 (100) [Y$_5$+2 H]$^+$, 600.28 (7) [B$_2$]$^+$, 504.38 (49) [Y$_4$+2 H]$^+$, 473.20 (5) [B$_1$]$^+$, 376.25 (5) [Y$_3$+2 H]$^+$.

HO-Nlys^{+0}Nlys^{+0}Nleu^{+0}Nlys^{+0}Nval^{+0}Nleu^{+0}-Fluo **170**: 10.0 mg (0.015 mmol, 1.00 eq) resin **166** was substituted with **12** (GP006) and the resin was washed (GP002). The cycle of acylation (GP005), washing (GP002), substitution (GP006), washing (GP002) was repeated with the remaining amines: **12**, isobutylamine and isopropylamine. Each acylation/substitution step was monitored by the chloranil test (GP019). 5(6)-carboxyfluorescein was attached according to GP015. Protecting groups were removed and the peptoid was cleaved off the resin (GP013). TFA was removed *in vacuo* and the peptoid was isolated by HPLC (C18 RP, linear gradient over 5 CV: 0 %-60 % eluent B) and eluted after 50.5 min. Yield: 0.1 mg. – *MALDI-TOF* (matrix: CHCA), m/z: 1086.97 (100) [M+H]$^+$. – *MALDI-TOF/TOF* (matrix: CHCA), m/z (%) [fragment]: 940.59 (10) [B$_5$]$^+$, 812.50 (5) [B$_4$]$^+$, 699.39 (20) [B$_3$]$^+$, 615.52 (100) [Y$_5$+2 H]$^+$, 571.26 (13) [B$_2$]$^+$, 516.44 (57) [Y$_4$+2 H]$^+$, 472.18 (9) [B$_1$]$^+$, 388.32 (8) [Y$_3$+2 H]$^+$.

HO-Nlys^{+0}Nlys^{+0}Nval^{+0}Nlys^{+0}Nphe^{+1}Nleu^{+0}-Fluo **171**: 10.0 mg (0.015 mmol, 1.00 eq) resin **166** was substituted with **12** (GP006) and the resin was washed (GP002). The cycle of acylation (GP005), washing (GP002), substitution (GP006), washing (GP002) was repeated with the remaining amines: **12**, isopropylamine, 2-phenylethanamine, isobutylamine. Each acylation/substitution step was monitored by the chloranil test (GP019). 5(6)-Carboxyfluorescein was attached according to GP015. Protecting groups were removed and the peptoid was cleaved off the resin (GP013). TFA was removed *in vacuo* and the peptoid was isolated by HPLC (C18 RP, linear gradient over 5 CV: 0 %-60 % eluent B) and eluted after 26 min. Yield: 0.1 mg. – *MALDI-TOF* (matrix: CHCA), m/z: 1134.98 (100) [M+H]$^+$, 1156.98 (6). – *MALDI-TOF/TOF* (matrix: CHCA), m/z (%) [fragment]: 988.56 (23) [B$_5$]$^+$, 860.45 (11) [B$_4$]$^+$, 761.41 (43) [B$_3$]$^+$, 663.53 (100) [Y$_5$+2 H]$^+$, 633.28 (8) [B$_2$]$^+$, 502.42 (73) [Y$_4$+2 H]$^+$, 472.20 (13) [B$_1$]$^+$, 374.32 (16) [Y$_3$+2 H]$^+$.
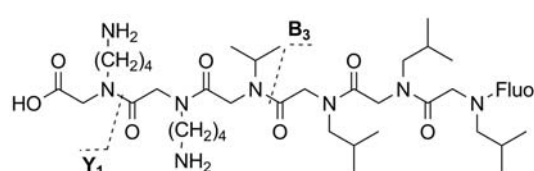
HO-Nlys^{+0}Nlys^{+0}Nval^{+0}Nleu^{+0}Nleu^{+0}Nleu^{+0}-Fluo **172**: 10.0 mg (0.015 mmol, 1.00 eq) resin **166** was substituted with **12** (GP006) and the resin was washed (GP002). The cycle of acylation (GP005), washing (GP002), substitution (GP006), washing (GP002) was repeated with the remaining amines: **12**, isopropylamine, and isobutylamine. Each acylation/substitution step was monitored by the chloranil test (GP019). 5(6)-Carboxyfluorescein was attached according to GP015. Protecting groups were removed and the peptoid was cleaved off the resin (GP013). TFA was removed *in vacuo* and the peptoid was isolated by HPLC (C18 RP, linear gradient over 5 CV: 0 %-60 % eluent B) and eluted after 42.5 min. Yield: 0.9 mg. – *MALDI-TOF* (matrix: CHCA), m/z: 1071.95 (100) [M+H]$^+$, 1093.94 (18). – *MALDI-TOF/TOF* (matrix: CHCA), m/z (%) [fragment]: 925.53 (12) [B$_5$]$^+$, 797.44 (33) [B$_4$]$^+$, 698.36 (54) [B$_3$]$^+$, 600.48 (100) [Y$_5$+2 H]$^+$, 585.26 (10) [B$_2$]$^+$, 487.37 (54) [Y$_4$+2 H]$^+$, 572.17 (5) [B$_1$]$^+$, 374.30 (21) [Y$_3$+2 H]$^+$, 275.21 (4) [Y$_2$+2 H]$^+$.
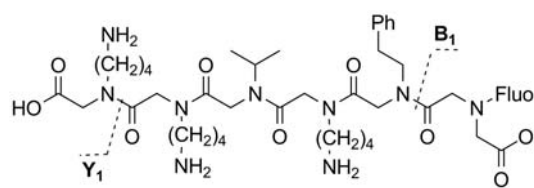
HO-Nlys^{+0}Nlys^{+0}Nval^{+0}Nlys^{+0}Nphe^{+1}Nasp^{+0}-Fluo **173**: 10.0 mg (0.015 mmol, 1.00 eq) resin **166** was substituted with **12** (GP006) and the resin was washed (GP002). The cycle of acylation (GP005), washing (GP002), substitution (GP006), washing (GP002) was repeated with the remaining amines: **12**, isopropylamine, 2-phenylethanamine and glycine *tert*-butyl ester acetate. Each acylation/substitution step was monitored by the chloranil test (GP019). 5(6)-Carboxyfluorescein was attached according to GP015. Protecting groups were removed and the peptoid was cleaved off the resin (GP013). TFA was removed *in vacuo* and the peptoid was isolated by HPLC (C18 RP, linear gradient over 5 CV: 0 %-60 % eluent B) and eluted after 32 min. Yield: 1.0 mg. – *MALDI-TOF* (matrix: CHCA), m/z: 1136.92 (100) [M+H]$^+$. – *MALDI-TOF/TOF* (matrix: CHCA), m/z (%) [fragment]: 990.54 (34) [B$_5$]$^+$, 862.43 (36) [B$_4$]$^+$, 844.41 (11), 763.34 (80) [B$_3$]$^+$, 663.52 (73) [Y$_5$+2 H]$^+$, 636.23 (3) [B$_2$]$^+$, 502.42 (100) [Y$_4$+2 H]$^+$, 374.30 (41) [Y$_3$+2 H]$^+$, 275.25 (6) [Y$_2$+2 H]$^+$.
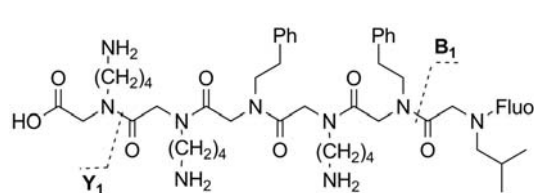
HO-Nlys^{+0}*Nlys*$^{+0}$*Nphe*$^{+1}$*Nlys*$^{+0}$*Nphe*$^{+1}$*Nleu*$^{+0}$*-Fluo* **174**: 10.0 mg (0.015 mmol, 1.00 eq) resin **166** was substituted with **12** (GP006) and the resin was washed (GP002). The cycle of acylation (GP005), washing (GP002), substitution (GP006), washing (GP002) was repeated with the remaining amines: **12**, 2-phenylethanamine and isobutylamine. Each acylation/substitution step was monitored by the chloranil test (GP019). 5(6)-Carboxyfluorescein was attached according to GP015. Protecting groups were removed and the peptoid was cleaved off the resin (GP013). TFA was removed *in vacuo* and the peptoid was isolated by HPLC (C18 RP, linear gradient over 5 CV: 0 %-60 % eluent B) and eluted after 40.5 min. Yield: 1.0 mg. – *MALDI-TOF* (matrix: CHCA), m/z: 1197.01 (100) [M+H]$^+$, 1219.00 (33). – *MALDI-TOF/TOF* (matrix: CHCA), m/z (%) [fragment]: 1050.57 (23) [B$_5$]$^+$, 922.49 (7) [B$_4$]$^+$, 761.40 (34) [B$_3$]$^+$, 725.52 (100) [Y$_5$+2 H]$^+$, 633.30 (8) [B$_2$]$^+$, 564.43 (66) [Y$_4$+2 H]$^+$, 472.18 (13) [B$_1$]$^+$, 436.35 (15) [Y$_3$+2 H]$^+$.
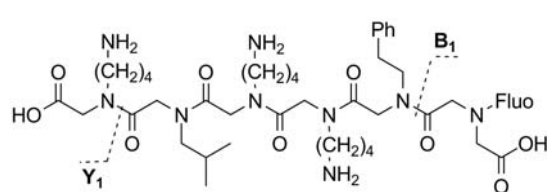
HO-Nlys^{+0}*Nleu*$^{+0}$*Nlys*$^{+0}$*Nlys*$^{+0}$*Nphe*$^{+1}$*Nasp*$^{+0}$*-Fluo* **175**: 10.0 mg (0.015 mmol, 1.00 eq) resin **166** was substituted with **12** (GP006) and the resin was washed (GP002). The cycle of acylation (GP005), washing (GP002), substitution (GP006), washing (GP002) was repeated with the remaining amines: isobutylamine, **12**, 2-phenylethanamine and glycine *tert*-butyl ester acetate. Each acylation/substitution step was monitored by the chloranil test (GP019). 5(6)-Carboxyfluorescein was attached according to GP015. Protecting groups were removed and the peptoid was cleaved off the resin (GP013). TFA was removed *in vacuo* and the peptoid was isolated by HPLC (C18 RP, linear gradient over 5 CV: 0 %-60 % eluent B) and eluted after 33.5 min. Yield: 0.7 mg. – *MALDI-TOF* (matrix: CHCA), m/z: 1150.94 (100) [M+H]$^+$, 1035.87 (18), 1172.92 (6). – *MALDI-TOF/TOF* (matrix: CHCA), m/z (%) [fragment]: 1004.50 (28) [B$_5$]$^+$, 891.44 (40) [B$_4$]$^+$, 763.34 (43) [B$_3$]$^+$, 677.53 (72) [Y$_5$+2 H]$^+$, 516.42 (100) [Y$_4$+2 H]$^+$, 388.32 (92) [Y$_3$+2 H]$^+$.
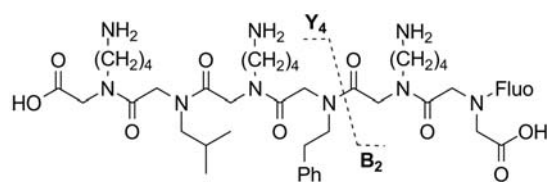
HO-Nlys^{+0}*Nleu*$^{+0}$*Nlys*$^{+0}$*Nphe*$^{+1}$*Nlys*$^{+0}$*Nasp*$^{+0}$*-Fluo* **176**: 10.0 mg (0.015 mmol, 1.00 eq) resin **166** was substituted with **12** (GP006) and the resin was washed (GP002). The cycle of acylation (GP005), washing (GP002), substitution (GP006), washing (GP002) was repeated with the remaining amines: isobutylamine, **12**, 2-phenylethanamine and glycine *tert*-butyl ester acetate. Each acylation/substitution step was monitored by the chloranil test (GP019). 5(6)-Carboxyfluorescein was attached according to GP015. Protecting groups were removed and the peptoid was cleaved off the resin (GP013). TFA was removed *in vacuo* and the peptoid was isolated by HPLC (C18 RP, linear gradient over 5 CV: 0 %-60 % eluent B) and eluted after 32.5 min. Yield: 0.7 mg. – *MALDI-TOF* (matrix: CHCA), m/z: 1150.93 (100) [M+H]$^+$, 1035.86 (13). – *MALDI-TOF/TOF* (matrix: CHCA), m/z (%) [fragment]: 1004.50 (32) [B$_5$]$^+$, 891.41 (43) [B$_4$]$^+$, 763.32 (36) [B$_3$]$^+$, 677.53 (92) [Y$_5$+2 H]$^+$, 602.24 (8) [B$_2$]$^+$, 549.42 (100) [Y$_4$+2 H]$^+$, 388.32 (82) [Y$_3$+2 H]$^+$.
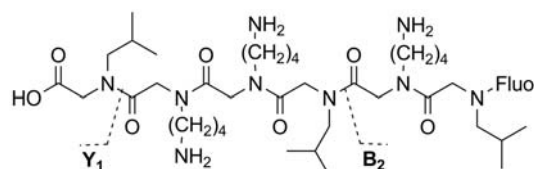
HO-Nleu^{+0}Nlys^{+0}Nlys^{+0}Nleu^{+0}Nlys^{+0}Nleu^{+0}-Fluo **177**: 10.0 mg (0.015 mmol, 1.00 eq) resin **166** was substituted with isobutylamine (GP006) and the resin was washed (GP002). The cycle of acylation (GP005), washing (GP002), substitution (GP006), washing (GP002) was repeated with the remaining amines: **12** and isobutylamine. Each acylation/substitution step was monitored by the chloranil test (GP019). 5(6)-carboxyfluorescein was attached according to GP015. Protecting groups were removed and the peptoid was cleaved off the resin (GP013). TFA was removed *in vacuo* and the peptoid was isolated by HPLC (C18 RP, linear gradient over 5 CV: 0 %-60 % eluent B) and eluted after 36 min. Yield: 1.1 mg. – *MALDI-TOF* (matrix: CHCA), m/z: 1100.96 (100) [M+H]$^+$. – *MALDI-TOF/TOF* (matrix: CHCA), m/z (%) [fragment]: 969.61 (10) [B$_5$]$^+$, 841.49 (20) [B$_4$]$^+$, 713.39 (17) [B$_3$]$^+$, 629.52 (100) [Y$_5$+2 H]$^+$, 600.32 (10) [B$_2$]$^+$, 501.42 (40) [Y$_4$+2 H]$^+$, 473.16 (8) [B$_1$]$^+$, 388.34 (31) [Y$_3$+2 H]$^+$, 260.22 (3) [Y$_2$+2 H]$^+$.
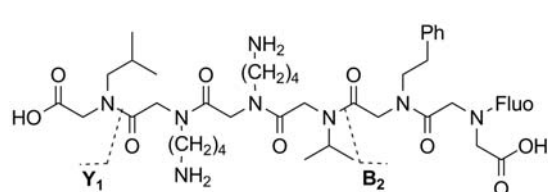
HO-Nleu^{+0}Nlys^{+0}Nlys^{+0}Nval^{+0}Nphe^{+1}Nasp^{+0}-Fluo **178**: 10.0 mg (0.015 mmol, 1.00 eq) resin **166** was substituted with isobutylamine (GP006) and the resin was washed (GP002). The cycle of acylation (GP005), washing (GP002), substitution (GP006), washing (GP002) was repeated with the remaining amines: **12**, isopropylamine, 2-phenylethylamine and glycine *tert*-butyl ester acetate. Each acylation/substitution step was monitored by the chloranil test (GP019). 5(6)-Carboxyfluorescein was attached according to GP015. Protecting groups were removed and the peptoid was cleaved off the resin (GP013). TFA was removed *in vacuo* and the peptoid was isolated by HPLC (C18 RP, linear gradient over 5 CV: 0 %-60 % eluent B) and eluted after 38 min. Yield: 0.5 mg. – *MALDI-TOF* (matrix: CHCA), m/z: 1121.87 (100) [M+H]$^+$, 1006.80 (23), 1451.36 (9). – *MALDI-TOF/TOF* (matrix: CHCA), m/z (%) [fragment]: 990.51 (17) [B$_5$]$^+$, 862.41 (49) [B$_4$]$^+$, 734.31 (54) [B$_3$]$^+$, 648.53 (57) [Y$_5$+2 H]$^+$, 635.20 (4) [B$_2$]$^+$, 487.41 (83) [Y$_4$+2 H]$^+$, 388.34 (100) [Y$_3$+2 H]$^+$, 260.23 (7) [Y$_2$+2 H]$^+$.

HO-Nleu^{+0}Nleu^{+0}Nlys^{+0}Nlys^{+0}Nphe^{+1}Nasp^{+0}-Fluo **179**: 10.0 mg (0.015 mmol, 1.00 eq) resin **166** was substituted with isobutylamine (GP006) and the resin was washed (GP002). The cycle of acylation (GP005), washing (GP002), substitution (GP006), washing (GP002) was repeated with the remaining amines: **12**, 2-phenylethylamine and glycine *tert*-butyl ester acetate. Each acylation/substitution step was monitored by the chloranil test (GP019). 5(6)-carboxyfluorescein was attached according to GP015. Protecting groups were removed and the peptoid was cleaved off the resin (GP013). TFA was removed *in vacuo* and the peptoid was isolated by HPLC (C18 RP, linear gradient over 5 CV: 0 %-60 % eluent B) and eluted after 41 min. Yield: 0.6 mg. – *MALDI-TOF* (matrix: CHCA), m/z: 1135.87 (100) [M+H]$^+$, 657.64 (19), 1479.36 (9). – *MALDI-TOF/TOF* (matrix: CHCA), m/z (%) [fragment]: 1004.55 (23) [B$_5$]$^+$, 891.46 (33) [B$_4$]$^+$, 763.35 (48) [B$_3$]$^+$, 662.52 (58) [Y$_5$+2 H]$^+$, 501.43 (100) [Y$_4$+2 H]$^+$, 373.31 (75) [Y$_3$+2 H]$^+$.

HO-Nval^{+0}Nlys^{+0}Nlys^{+0}Nphe^{+1}Nlys^{+0}Nleu^{+0}-Fluo **180**: 10.0 mg (0.015 mmol, 1.00 eq) resin **166** was substituted with isopropylamine (GP006) and the resin was washed (GP002). The cycle of acylation (GP005), washing (GP002), substitution (GP006), washing (GP002) was repeated with the remaining amines: **12**, 2-phenylethylamine and isobutylamine. Each acylation/substitution step was monitored by the chloranil test (GP019). 5(6)-carboxyfluorescein was attached according to GP015. Protecting groups were removed and the peptoid was cleaved off the resin (GP013). TFA was removed *in vacuo* and the peptoid was isolated by HPLC (C18 RP, linear gradient over 5 CV: 0 %-60 % eluent B) and eluted after 47 min. Yield: 0.2 mg. – *MALDI-TOF* (matrix: CHCA), m/z: 1134.93 (100) $[M+H]^+$. – *MALDI-TOF/TOF* (matrix: CHCA), m/z (%) [fragment]: 1017.61 (27) $[B_5]^+$, 889.51 (23) $[B_4]^+$, 761.41 (15) $[B_3]^+$, 663.53 (100) $[Y_5+2\,H]^+$, 600.30 (10) $[B_2]^+$, 535.41 (42) $[Y_4+2\,H]^+$, 473.18 (7) $[B_1]^+$, 374.32 (30) $[Y_3+2\,H]^+$.

HO-Nphe^{+1}Nlys^{+0}Nlys^{+0}Nleu^{+0}Nlys^{+0}Nleu^{+0}-Fluo **181**: 10.0 mg (0.015 mmol, 1.00 eq) resin **166** was substituted with 2-phenylethanamine (GP006) and the resin was washed (GP002). The cycle of acylation (GP005), washing (GP002), substitution (GP006), washing (GP00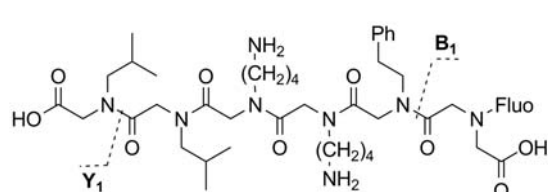2) was repeated with the remaining amines: **12** and isobutylamine. Each acylation/substitution step was monitored by the chloranil test (GP019). 5(6)-carboxyfluorescein was attached according to GP015. Protecting groups were removed and the peptoid was cleaved off the resin (GP013). TFA was removed *in vacuo* and the peptoid was isolated by HPLC (C18 RP, linear gradient over 5 CV: 0 %-60 % eluent B) and eluted after 49 min. Yield: 0.2 mg. – *MALDI-TOF* (matrix: CHCA), m/z: 1148.98 (100) $[M+H]^+$. – *MALDI-TOF/TOF* (matrix: CHCA), m/z (%) [fragment]: 841.51 (9) $[B_4]^+$, 713.38 (15) $[B_3]^+$, 677.54 (100) $[Y_5+2\,H]^+$, 600.28 (12) $[B_2]^+$, 549.43 (44) $[Y_4+2\,H]^+$, 473.16 (7) $[B_1]^+$, 436.32 (30) $[Y_3+2\,H]^+$, 308.20 (3) $[Y_2+2\,H]^+$.

HO-Nphe^{+1}Nlys^{+0}Nlys^{+0}Nval^{+0}Nphe^{+1}Nasp^{+0}-Fluo **182**: 10.0 mg (0.015 mmol, 1.00 eq) resin **166** was substituted with 2-phenylethanamine (GP006) and the resin was washed (GP002). The cycle of acylation (GP005), washing (GP002), substitution (GP006), washing (GP002) was repeated with the remaining amines: **12**, isopropylamine, 2-phenylethanamine and glycine *tert*-butyl ester acetate. Each acylation/substitution step was monitored by the chloranil test (GP019). 5(6)-carboxyfluorescein was attached according to GP015. Protecting groups were removed and the peptoid was cleaved off the resin (GP013). TFA was removed *in vacuo* and the peptoid was isolated by HPLC (C18 RP, linear gradient over 5 CV: 0 %-60 % eluent B) and eluted after 40 min. Yield: 0.9 mg. – *MALDI-TOF* (matrix: CHCA), m/z: 1169.89 (100) $[M+H]^+$, 1547.42 (65), 919.88 (11). – *MALDI-TOF/TOF* (matrix: CHCA), m/z (%) [fragment]: 990.54 (18) $[B_5]^+$, 862.46 (55) $[B_4]^+$, 734.35 (80) $[B_3]^+$, 696.57 (60) $[Y_5+2\,H]^+$, 636.24 (7) $[B_2]^+$, 535.45 (100) $[Y_4+2\,H]^+$, 436.37 (98) $[Y_3+2\,H]^+$, 308.25 (8) $[Y_2+2\,H]^+$.

HO-Nphe^{+1}Nlys^{+0}Nser^{+1}Nlys^{+0}Nval^{+0}Nleu^{+0}-Fluo **183**: 10.0 mg (0.015 mmol, 1.00 eq) resin **166** was substituted with 2-phenylethanamine (GP006) and the resin was washed (GP002). The cycle of acylation (GP005), washing (GP002), substitution (GP006), washing (GP002) was repeated with the remaining amines: **12**, **10**, isopropylamine and isobutylamine. Each acylation/substitution step was monitored by the chloranil test (GP019). 5(6)-carboxyfluorescein was attached according to GP015. Protecting groups were removed and the peptoid was cleaved off the resin (GP013). TFA was removed *in vacuo* and the peptoid was isolated by HPLC (C18 RP, linear gradient over 5 CV: 0 %-60 % eluent B) and eluted after 40 min. Yield: 0.8 mg. – *MALDI-TOF* (matrix: CHCA), m/z: 1107.89 (100) [M+H]$^+$, 1129.90 (6). – *MALDI-TOF/TOF* (matrix: CHCA), m/z (%) [fragment]: 928.55 (8) [B$_5$]$^+$, 800.44 (8) [B$_4$]$^+$, 699.38 (27) [B$_3$]$^+$, 636.47 (100) [Y$_5$+2 H]$^+$, 571.26 (11) [B$_2$]$^+$, 537.40 (63) [Y$_4$+2 H]$^+$, 472.20 (8) [B$_1$]$^+$, 409.26 (3) [Y$_3$+2 H]$^+$.
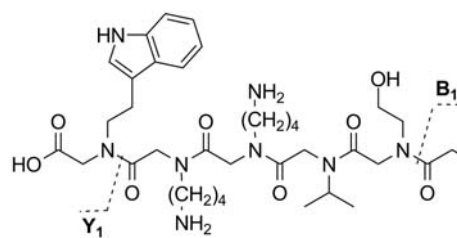
HO-Ntrp^{+1}Nlys^{+0}Nlys^{+0}Nval^{+0}Nser^{+1}Nasp^{+0}-Fluo **184**: 10.0 mg (0.015 mmol, 1.00 eq) resin **166** was substituted with **13** (GP006) and the resin was washed (GP002). The cycle of acylation (GP005), washing (GP002), substitution (GP006), washing (GP002) was repeated with the remaining amines: **12**, isopropylamine, **10** and glycine *tert*-butyl ester acetate. Each acylation/substitution step was monitored by the chloranil test (GP019). 5(6)-carboxyfluorescein was attached according to GP015. Protecting groups were removed and the peptoid was cleaved off the resin (GP013). TFA was removed *in vacuo* and the peptoid was isolated by HPLC (C18 RP, linear gradient over 5 CV: 15 %-75 % eluent B) and eluted after 19 min. Yield: Yield: 0.1 mg. – *MALDI-TOF* (matrix: CHCA), m/z: 1148.87 (100) [M+H]$^+$, 948.71 (17), 1047.79 (13). – *MALDI-TOF/TOF* (matrix: CHCA), m/z (%) [fragment]: 930.48 (22) [B$_5$]$^+$, 802.38 (46) [B$_4$]$^+$, 675.51 (47) [Y$_5$+2 H]$^+$ and [B$_3$]$^+$, 574.43 (58) [Y$_4$+2 H]$^+$ and [B$_2$]$^+$, 475.35 (100) [Y$_3$+2 H]$^+$ and [B$_1$]$^+$, 347.25 (8) [Y$_2$+2 H]$^+$.

7.7.1 Verification of Library Hits

GP022: Fluorescence Anisotropy Binding Assay
Fluorescence anisotropy was measured with a Tecan Infinite M1000 microplate reader. Measurements were conducted according to Moerke in low-volume black, transparent flat-bottom 384-well microtiter plates.[338] 16 consecutive 1:2-dilutions of protein in *ls*-PBS were prepared to give a final volume of 31.5 µL each. To each of these dilutions 3.50 µL of fluorescent ligand was added. Additionally, a sample of 31.5 µL of low-salt PBS with 3.50 µL of fluorescent ligand (free ligand control) was prepared. The components were gently mixed and three times 10 µL of each solution were transferred into three adjacent cavities of the 384-well microtiter plate. As a blank three times 10 µL of *ls*-PBS were transferred into three additional cavities. For ligands labelled with 5(6)-carboxyfluorescein fluorescence anisotropy was measured at an LED excitation wavelength of 470 nm and an emission wavelength of 520 nm. For ligands labelled with DyLight550, LED was set to 530 nm excitation and emission wavelength was set to 576 nm. Data was processed with Systat Software 'SigmaPlot 12.0'.

GP023: Isolation of Human Neutrophil Granulocytes from Buffy Coats

Isolations were executed by I. Rink. 3 mL histopaque®-1119 were carefully overlaid with 3 mL lympho-prep™in a 15 mL microcentrifuge tube. The 2-phase system was left to reach rt before continuing the protocol. The two phases were carefully overlaid with 6.00 mL buffy coat (DRK Blutspendedienst Frankfurt/Main) and consecutively centrifuged at $700 \times g$ for 30 min at room temperature with the breaks turned off. Plasma and monocyte layers on top were removed and the neutrophil fraction was collected and transferred into a 15 mL microcentrifuge tube. Neutrophils were mixed with PBS to give 15 mL of cell suspension. The suspension was centrifuged at $200 \times g$ for 10 min at room temperature. PBS supernatant was removed and the washing step was repeated. Another washing step with $RPMI_{(-)}$ instead of PBS was performed before suspending the cells in the same medium and adjusting the number of cells to $10 \cdot 10^6$ cells/mL.

GP024: Isolation of Human Neutrophil Granulocytes from Full Blood

Isolations were executed by I. Rink. Equal volumes of human blood (roughly 10 mL per experiment, from the university medical office, TU Darmstadt), dextran 500 (6 % solution in water) and PBS were mixed and incubated at 37 °C for 30 min. Sedimented erythrocytes were discarded. The supernatant was transferred into a new tube and centrifuged for 10 min at 15 °C at $240 \times g$. The supernatant was discarded and the pellet was washed with PBS buffer and centrifuged for 10 min at 15 °C at $240 \times g$. The pellet was re-suspended in 10 mL PBS buffer and added to 30 mL Lymphoprep™. The mixture was centrifuged for 20 min at 4 °C at $600 \times g$. The white layer formed in the middle of the tube was carefully removed, suspended in PBS buffer and centrifuged for 10 min at 4 °C with $240 \times g$. The pellet was washed in PBS, and then re-suspended in 5.00 mL PBS buffer. Erythrocytes were lysed by addition of 25.0 mL deionized water. After 30 s 17.2 mL 3.6 % NaCl solution in water was added. The suspension was centrifuged for 10 min at 4 °C at $240 \times g$. The pellet was consecutively washed with PBS buffer and $RPMI_{(BSA-)}$. The cells were suspended in $RPMI_{(BSA-)}$ and should be used immediately.

Actin Polymerization Assay

Human neutrophil granulocytes were isolated as described in GP024. Per sample 10 wells of a black flat-bottom 96-well plate were filled with 50.0 μL 6 % formaldehyde (v/v) in PBS for lysis of cells at different activation times. 400 μL of $RPMI_{(-)}$, chemoattractant CXCL8 (100 $^{ng}/_{mL}$, 11.93 nM), CXCL8 with anti-CXCL8 (11.93 nM CXCL8 and) and desired mixtures of CXCL8 and inhibitors were prepared in $RPMI_{(-)}$. The samples were mixed with 100 μL of human neutrophil granulocytes each and at 0, 10, 20, 30, 40, 50, 60, 120, 240, 300 seconds 50.0 μL of each sample was transferred into one well with the prepared formaldehyde solutions. Cells were incubated in formaldehyde for 30-60 min at room temperature. The plate was centrifuged at 4000 rpm (Hettich Rotina 420R) for 5 min. The supernatant was removed and 100 μL of 0.2 % Triton X-100 (v/v) in PBS was added to each well and incubated for 5 min at room temperature. The plate was centrifuged at 4000 rpm (Hettich Rotina 420R) for 5 min. The supernatant was removed. For 80 wells of a microtiter-plate (8 samples) 1.00 μg Phalloidin-iFluor$_{555}$ (1 mg/mL solution in DMSO) was mixed with 4.10 mL of PBS and 50.0 μL of the solution was transferred onto the fixed cells. Cells

were incubated for 1 h in the dark at room temperature. The plate was centrifuged at 4000 rpm (Hettich Rotina 420R) for 5 min. The supernatant was removed and the wells were washed with 100 μL PBS each. The plate was centrifuged at 4000 rpm (Hettich Rotina 420R) for 5 min and fluorescence intensity was measured using the Tecan M1000 plate reader (excitation: 556 nm, emission: 574 nm).

Neutrophil Migration Assay

Human neutrophil granulocytes were isolated as described in GP024. 24-well Corning Transwell plates (3 μm) were used without coating. Final concentration of chemoattractants like CXCL8 and fMLP of 10.0 nM in RPMI$_{(BSA-)}$ proved to be effective. Inhibitors were mixed with the chemoattractants at appropriate concentrations. The cavities of the 24-well bottom plate were filled with 595 μL of the chemokine/inhibitor solutions. Each solution was prepared in triplicate. To determine the maximum cell number, a plain cell suspension was added to three cavities. As a negative control, plain buffer was added to three more cavities. Anti-CXCL8 antibody (10.8 μL of mouse anti-human IL8, monoclonal, 500 μg/mL) in 900 μL chemotaxis buffer served as a positive inhibitor control. The inserts of the top plate were filled with 150 μL of neutrophil suspension ($5{\times}10^6$ cells/mL) in RPMI$_{(-)}$. After incubation for 1.5 h at 37 °C in a carbon dioxide incubator the inserts were removed and 50 μL of cell suspension were mixed with 50 μL trypan blue solution (0.5 % (w/v) in PBS). Cells were incubated with trypan blue for 5 min at rt. Living cells of each well were counted using a Neubauer chamber. Resulting absolute cell numbers were divided by the maximum cell number to obtain relative cell numbers for evaluation.

Toxicity Assay by Resazurin Staining

Human neutrophil granulocytes were isolated as described in GP024. Cells were counted using an improved Neubauer chamber and diluted in RPMI$_{(BSA-)}$ to give a final titer of $5{\times}10^6$ cells/mL. Target substances were diluted consecutively in 1:2 steps in RPMI$_{(BSA-)}$ to give 20 μL dilution per well of a 384-well black microtiter plate. 20 μL of cell suspension were added to each of the dilutions. One row of the MTP served as positive control: 20 μL RPMI$_{(BSA-)}$ mixed with 20 μL of cell suspension. The negative control consisted of one row of 40 μL RPMI$_{(BSA-)}$. Plates were incubated for 4 h in the incubator at 37 °C. Resazurin was dissolved in MilliQ water to give a final concentration of 0.1 $\mathrm{mg/mL}$ and 4 μL of the resazurin solution were added to each of the wells and the MTP was incubated overnight. Fluorescence intensity was analyzed using the Tecan M-1000 plate reader at 535 nm excitation and 585 nm emission. The intensity value of the positive control was interpreted as 100 % living neutrophils and all measured values were calculated in relation to that value. The intensity value of the buffer without cells was interpreted as 0 % living neutrophils.

Bibliography

[1] S. D. Kobayashi, F. R. DeLeo, *Wiley Interdiscip. Rev. Syst. Biol. Med.* **2009**, *1*, 309-333.

[2] M. P. Pruchniak, M. Arazna, U. Demkow, *Respir. Physiol. Neurobiol.* **2013**, *187*, 68-73.

[3] P. Friedl, B. Weigelin, *Nat. Immunol.* **2008**, *9*, 960-969.

[4] N. Dixit, S. I. Simon, *Front. Immunol.* **2012**, *3*, 1-9.

[5] B. Petri, M. G. Bixel, *FEBS J.* **2006**, *273*, 4399-4407.

[6] W. A. Muller, *Circ. Res.* **2009**, *105*, 223-230.

[7] M. Majka, A. Janowska, Wieczorek *et al.*, *Blood* **2001**, *97*, 3075-3085.

[8] I. Oynebraten, O. Bakke *et al.*, *Blood* **2004**, *104*, 314-320.

[9] N. Janabi, I. Hau, M. Tardieu, *J. Immunol.* **1999**, *162*, 1701-1706.

[10] J. Henningsen, B. K. Pedersen, I. Kratchmarova, *Mol. BioSyst.* **2011**, *7*, 311-321.

[11] S. J. Allen, S. E. Crown, T. M. Handel, *Annu. Rev. Immunol.* **2007**, *25*, 787-820.

[12] Z. Johnson, A. E. Proudfoot, T. M. Handel, *Cytokine Growth Factor Rev.* **2005**, *16*, 625-636.

[13] R. M. Strieter, P. J. Polverini *et al.*, *J. Biol. Chem.* **1995**, *270*, 27348-27357.

[14] E. J. Fernandez, E. Lolis, *Annu. Rev. Pharmacol. Toxicol.* **2002**, *42*, 469-499.

[15] T. Yoshimura, K. Matsushima *et al.*, *Proc. Natl. Acad. Sci. U. S. A.* **1987**, *84*, 9233-9237.

[16] T. Yoshimura, E. A. Robinson *et al.*, *Mol. Immunol.* **1989**, *26*, 87-93.

[17] M. Baggiolini, I. Clarklewis, *FEBS Lett.* **1992**, *307*, 97-101.

[18] E. Gasteiger, A. Gattiker *et al.*, *Nucleic Acids Res.* **2003**, *31*, 3784-3788.

[19] A. Mortier, N. Berghmans *et al.*, *PLoS One* **2011**, *6*, e23913 1-9.

[20] C. A. Hebert, J. B. Baker, *Cancer Investigation* **1993**, *11*, 743-750.

[21] J. van Damme, J. Vanbeeumen *et al.*, *Eur. J. Biochem.* **1989**, *181*, 337-344.

[22] D. P. Witt, A. D. Lander, *Curr. Biol.* **1994**, *4*, 394-400.

[23] G. S. V. Kuschert, A. J. Hoogewerf *et al.*, *Biochemistry* **1998**, *37*, 11193-11201.

[24] J. Middleton, S. Neil *et al.*, *Cell* **1997**, *91*, 385-395.

[25] G. M. Clore, E. Appella *et al.*, *Biochemistry* **1990**, *29*, 1689-1696.

[26] R. T. Clubb, J. G. Omichinski *et al.*, *FEBS Lett.* **1994**, *338*, 93-97.

[27] S. H. Park, F. Casagrande *et al.*, *J. Mol. Biol.* **2011**, *414*, 194-203.

[28] E. T. Baldwin, I. T. Weber *et al.*, *Proc. Natl. Acad. Sci. U. S. A.* **1991**, *88*, 502-506.

[29] I. Clark-Lewis, C. Schumacher *et al.*, *J. Biol. Chem.* **1991**, *266*, 23128-23134.

[30] C. A. Hebert, R. V. Vitangcol, J. B. Baker, *J. Biol. Chem.* **1991**, *266*, 18989-18994.

[31] S. R. Leong, R. C. Kabakoff, C. A. Hebert, *J. Biol. Chem.* **1994**, *269*, 19343-19348.

[32] W. E. Holmes, J. Lee *et al.*, *Science* **1991**, *253*, 1278-1280.

[33] P. M. Murphy, H. L. Tiffany, *Science* **1991**, *253*, 1280-1283.

[34] J. Lee, R. Horuk *et al.*, *J. Biol. Chem.* **1992**, *267*, 16283-16287.

[35] M. Wolf, M. B. Delgado *et al.*, *Eur. J. Immunol.* **1998**, *28*, 164-170.

[36] M. Baggiolini, B. Dewald, B. Moser, *Annu. Rev. Immunol.* **1997**, *15*, 675-705.

[37] A. Chuntarapai, J. Lee *et al.*, *J. Immunol.* **1994**, *153*, 5682-5688.

[38] G. J. LaRosa, K. M. Thomas *et al.*, *J. Biol. Chem.* **1992**, *267*, 25402-25406.

[39] I. Clark-Lewis, B. Dewald *et al.*, *J. Biol. Chem.* **1994**, *269*, 16075-16081.

[40] C. A. Hebert, A. Chuntharapai *et al.*, *J. Biol. Chem.* **1993**, *268*, 18549-53.

[41] I. Clark-Lewis, K. S. Kim *et al.*, *J. Leukocyte Biol.* **1995**, *57*, 703-711.

[42] N. J. Skelton, C. Quan *et al.*, *Struct. Fold. Des.* **1999**, *7*, 157-168.

[43] L. Rajagopalan, K. Rajarathnam, *Biosci. Rep.* **2006**, *26*, 325-339.

[44] E. F. Barter, M. J. Stone, *Biochemistry* **2012**, *51*, 1322-1331.

[45] G. M. Clore, A. M. Gronenborn, *FASEB J.* **1995**, *9*, 57-62.

[46] H. B. Lowman, W. J. Fairbrother *et al.*, *Protein Sci.* **1997**, *6*, 598-608.

[47] S. D. Burrows, M. L. Doyle *et al.*, *Biochemistry* **1994**, *33*, 12741-12745.

[48] H. Fernando, C. Chin *et al.*, *J. Biol. Chem.* **2004**, *279*, 36175-36178.

[49] K. Rajarathnam, B. D. Sykes *et al.*, *Science* **1994**, *264*, 90-92.

[50] S. T. Das, L. Rajagopalan *et al.*, *PLoS One* **2010**, *5*, e11754 1-12.

[51] P. Gangavarapu, L. Rajagopalan *et al.*, *J. Leukocyte Biol.* **2012**, *91*, 259-265.

[52] M. W. Nasser, S. K. Raghuwanshi *et al.*, *J. Immunol.* **2009**, *183*, 3425-3432.

[53] A. Ravindran, P. R. B. Joseph, K. Rajarathnam, *Biochemistry* **2009**, *48*, 8795-8805.

[54] K. Rajarathnam, I. Clarklewis, B. D. Sykes, *Biochemistry* **1995**, *34*, 12983-12990.

[55] K. Rajarathnam, G. N. Prado *et al.*, *Biochemistry* **2006**, *45*, 7882-7888.

[56] T. J. Daly, G. J. Larosa *et al.*, *J. Biol. Chem.* **1995**, *270*, 23282-23292.

[57] M. A. Williams, C. M. Cave *et al.*, *Shock* **2005**, *23*, 371-376.

[58] M. Horcher, A. Rot *et al.*, *Cytokine* **1998**, *10*, 1-12.

[59] K. Rajarathnam, C. M. Kay *et al.*, *Chemokines* **1997**, *287*, 89-105.

[60] H. Fernando, G. T. Nagle, K. Rajarathnam, *FEBS J.* **2007**, *274*, 241-251.

[61] A. Rot, *Eur. J. Immunol.* **1993**, *23*, 303-306.

[62] A. J. Hoogewerf, G. S. V. Kuschert *et al.*, *Biochemistry* **1997**, *36*, 13570-13578.

[63] J. Middleton, A. M. Patterson *et al.*, *Blood* **2002**, *100*, 3853-3860.

[64] D. J. Hamel, I. Sielaff *et al.*, *Methods in Enzymology, Vol 461: Chemokines, Part B* **2009**, *461*, 71-102.

[65] A. D. Lander, S. B. Selleck, *J. Cell Biol.* **2000**, *148*, 227-232.

[66] A. D. Cardin, H. J. R. Weintraub, *Arteriosclerosis* **1989**, *9*, 21-32.

[67] R. E. Hileman, J. R. Fromm *et al.*, *BioEssays* **1998**, *20*, 156-167.

[68] S. Akira, K. Takeda, T. Kaisho, *Nat. Immunol.* **2001**, *2*, 675-680.

[69] N. Fitzner, S. Clauberg *et al.*, *Clin. Vaccine Immunol.* **2008**, *15*, 138-146.

[70] E. Levy, G. Xanthou *et al.*, *Pediatr. Res.* **2009**, *66*, 179-184.

[71] K. Takeda, T. Kaisho, S. Akira, *Annu. Rev. Immunol.* **2003**, *21*, 335-376.

[72] K. Ley, C. Laudanna *et al.*, *Nat. Rev. Immunol.* **2007**, *7*, 678-689.

[73] S. A. Mousa, *Mol. Biotechnol.* **2008**, *38*, 33-40.

[74] K. Ley, *Trends Mol. Med.* **2003**, *9*, 263-268.

[75] P. Mehta, R. D. Cummings, R. P. McEver, *J. Biol. Chem.* **1998**, *273*, 32506-32513.

[76] K. Croce, S. J. Freedman *et al.*, *Biochemistry* **1998**, *37*, 16472-16480.

[77] K. L. Moore, K. D. Patel *et al.*, *J. Cell Biol.* **1995**, *128*, 661-671.

[78] T. Yago, J. H. Wu *et al.*, *J. Cell Biol.* **2004**, *166*, 913-923.

[79] P. Sundd, M. K. Pospieszalska, K. Ley, *Mol. Immunol.* **2013**, *55*, 59-69.

[80] B. H. Luo, C. V. Carman, T. A. Springer, *Annu. Rev. Immunol.* **2007**, *25*, 619-647.

[81] G. Constantin, *J. Neuroimmunol.* **2008**, *198*, 20-26.

[82] C. V. Carman, T. A. Springer, *Curr. Opin. Cell Biol.* **2003**, *15*, 547-556.

[83] T. Kinashi, *Nat. Rev. Immunol.* **2005**, *5*, 546-559.

[84] R. O. Hynes, *Cell* **1992**, *69*, 11-25.

[85] R. J. Faull, M. H. Ginsberg, *Journal of the American Society of Nephrology* **1996**, *7*, 1091-1097.

[86] H. Watanabe, S. Hattori *et al.*, *Journal of Biochemistry* **1990**, *108*, 753-759.

[87] T. D. Pollard, G. G. Borisy, *Cell* **2003**, *112*, 453-465.

[88] T. Oda, M. Iwasa *et al.*, *Nature* **2009**, *457*, 441-445.

[89] R. Dominguez, K. C. Holmes, *Annual Review of Biophysics, Vol 40* **2011**, *40*, 169-186.

[90] M. A. Conti, R. S. Adelstein, *J. Cell Sci.* **2008**, *121*, 11-18.

[91] F. Lynen, U. Wieland, *Ann. Chem.* **1937**, *533*, 93-117.

[92] J. A. Cooper, *J. Cell Biol.* **1987**, *105*, 1473-1478.

[93] W. F. Westlin, J. M. Kiely, M. A. Gimbrone, *J. Leukocyte Biol.* **1992**, *52*, 43-51.

[94] A. E. Proudfoot, T. N. C. Wells, C. A. Power, *Humana Press* **2000**, ISBN 0-89603-722-3.

[95] J. M. Vasiliev, *J. Cell Sci.* **1991**, *98*, 1-4.

[96] D. A. Lauffenburger, A. F. Horwitz, *Cell* **1996**, *84*, 359-369.

[97] R. J. Eddy, L. M. Pierini, F. R. Maxfield, *Mol. Biol. Cell* **2002**, *13*, 4470-4483.

[98] J. V. Small, B. Geiger *et al.*, *Nat. Rev. Mol. Cell Biol.* **2002**, *3*, 957-964.

[99] C. le Clainche, M. F. Carlier, *Physiol. Rev.* **2008**, *88*, 489-513.

[100] L. G. Tilney, E. M. Bonder, D. J. Derosier, *J. Cell Biol.* **1981**, *90*, 485-494.

[101] A. Mogilner, G. Oster, *Biophys. J.* **1996**, *71*, 3030-3045.

[102] M. Vicente, Manzanares, C. K. Choi, A. R. Horwitz, *J. Cell Sci.* **2009**, *122*, 199-206.

[103] A. Y. Alexandrova, K. Arnold *et al.*, *PLoS One* **2008**, *3*, e3234 1-9.

[104] D. Wirtz, S. B. Khatau, *Nat. Mater.* **2010**, *9*, 788-790.

[105] G. Cicchetti, P. G. Allen, M. Glogauer, *Crit. Rev. Oral Biol. M.* **2002**, *13*, 220-228.

[106] C. Knall, S. Young *et al.*, *J. Biol. Chem.* **1996**, *271*, 2832-2838.

[107] D. Chodniewicz, D. V. Zhelev, *Blood* **2003**, *101*, 1181-1184.

[108] H. C. Lane, A. R. Anand, R. K. Ganju, *Int. Immunol.* **2006**, *18*, 1315-1325.

[109] D. J. J. Waugh, C. Wilson, *Clin. Cancer Res.* **2008**, *14*, 6735-6741.

[110] M. Thelen, P. Peveri *et al.*, *FASEB J.* **1988**, *2*, 2702-2706.

[111] E. L. Becker, J. C. Kermode *et al.*, *J. Cell Biol.* **1985**, *100*, 1641-1646.

[112] F. A. P. Ribeiro-Neto, M. Rodbell, *Proc. Natl. Acad. Sci. U. S. A.* **1989**, *86*, 2577-2581.

[113] A. Katz, D. Q. Wu, M. I. Simon, *Nature* **1992**, *360*, 686-689.

[114] D. Q. Wu, A. Katz, M. I. Simon, *Proc. Natl. Acad. Sci. U. S. A.* **1993**, *90*, 5297-5301.

[115] D. G. Park, D. Y. Jhon *et al.*, *J. Biol. Chem.* **1993**, *268*, 4573-4576.

[116] G. P. Downey, C. K. Chan *et al.*, *J. Cell Biol.* **1990**, *110*, 1975-1982.

[117] H. Arai, I. F. Charo, *J. Biol. Chem.* **1996**, *271*, 21814-21819.

[118] N. Tapon, A. Hall, *Curr. Opin. Cell Biol.* **1997**, *9*, 86-92.

[119] D. Franciotta, G. Martino *et al.*, *J. Neuroimmunol.* **2001**, *115*, 192-198.

[120] L. A. Boven, L. Montagne *et al.*, *Clin. Exp. Immunol.* **2000**, *122*, 257-263.

[121] J. E. Simpson, J. Newcombe *et al.*, *J. Neuroimmunol.* **1998**, *84*, 238-249.

[122] A. Szczucinski, J. Losy, *Acta Neurol. Scand.* **2007**, *115*, 137-146.

[123] B. Engelhardt, *J. Neural Transm.* **2006**, *113*, 477-485.

[124] Z. Szekanecz, M. M. Halloran *et al.*, *Arthritis Research & Therapy* **2001**, *3*, 1266-1277.

[125] S. A. Luther, J. G. Cyster, *Nat. Immunol.* **2001**, *2*, 102-107.

[126] M. M. Wong, E. N. Fish, *Semin. Immunol.* **2003**, *15*, 5-14.

[127] S. M. Pope, P. C. Fulkerson *et al.*, *J. Biol. Chem.* **2005**, *280*, 13952-13961.

[128] A. Zlotnik, *Int. J. Cancer* **2006**, *119*, 2026-2029.

[129] I. Takanami, *Int. J. Cancer* **2003**, *105*, 186-189.

[130] M. B. Sporn, A. B. Roberts, *Nature* **1985**, *313*, 745-747.

[131] D. Schadendorf, A. Moller *et al.*, *J. Immunol.* **1993**, *151*, 2667-2675.

[132] R. Brew, J. S. Erikson *et al.*, *Cytokine* **2000**, *12*, 78-85.

[133] M. Miyamoto, Y. Shimizu *et al.*, *Cancer Immunol. Immun.* **1998**, *47*, 47-57.

[134] V. M. Dong, D. H. McDermott, R. Abdi, *Eur. J. Dermatol.* **2003**, *13*, 224-230.

[135] T. Dragic, V. Litwin *et al.*, *Nature* **1996**, *381*, 667-673.

[136] L. Weiss, A. SiMohamed *et al.*, *J. Infect. Dis.* **1997**, *176*, 1621-1624.

[137] E. A. Eugenin, K. Osiecki *et al.*, *J. Neurosci.* **2006**, *26*, 1098-1106.

[138] E. J. Miller, A. Kurdowska *et al.*, *Agents Actions* **1993**, *40*, 200-208.

[139] R. A. Houghten, C. Pinilla *et al.*, *Nature* **1991**, *354*, 84-86.

[140] S. Hayashi, A. Kurdowska *et al.*, *J. Immunol.* **1995**, *154*, 814-824.

[141] S. M. Miller, R. J. Simon *et al.*, *Drug Dev. Res.* **1995**, *35*, 20-32.

[142] S. Hayashi, A. Kurdowska *et al.*, *J. Clin. Invest.* **1997**, *99*, 2581-2587.

[143] S. Hayashi, J. Yatsunami *et al.*, *Lung* **2002**, *180*, 339-348.

[144] M. R. Attwood, N. Borkakoti *et al.*, *Bioorg. Med. Chem. Lett.* **1996**, *6*, 1869-1874.

[145] M. R. Attwood, E. A. Conway *et al.*, *Bioorg. Med. Chem. Lett.* **1997**, *7*, 429-432.

[146] J. R. White, J. M. Lee *et al.*, *J. Biol. Chem.* **1998**, *273*, 10095-10098.

[147] L. Rajagopalan, K. Rajarathnam, *J. Biol. Chem.* **2004**, *279*, 30000-30008.

[148] C. Ezerzer, M. Dolgin *et al.*, *Peptides* **2009**, *30*, 1296-1305.

[149] M. Houimel, P. Loetscher *et al.*, *Eur. J. Immunol.* **2001**, *31*, 3535-3545.

[150] M. Houimel, L. Mazzucchelli, *J. Leukocyte Biol.* **2009**, *85*, 728-738.

[151] A. Datta-Mannan, M. J. Stone, *Biochemistry* **2004**, *43*, 14602-14611.

[152] C. Bizzarri, S. Pagliei *et al.*, *Biochem. Pharmacol.* **2001**, *61*, 1429-1437.

[153] S. Paskauskas, A. Parseliunas *et al.*, *BMC Immunology* **2011**, *12*, 64-73.

[154] M. Hachet-Haas, K. Balabanian *et al.*, *J. Biol. Chem.* **2008**, *283*, 23189-23199.

[155] F. Daubeuf, M. Hachet, Haas *et al.*, *J. Biol. Chem.* **2013**, *288*, 11865-11876.

[156] O. Kulkarni, R. D. Pawar *et al.*, *Journal of the American Society of Nephrology* **2007**, *18*, 2350-2358.

[157] J. Hoellenriegel, D. Zboralski *et al.*, *Blood* **2014**, *123*, 1032-1039.

[158] D. Grainger, J. Reckless *et al.*, *Allergy* **2009**, *64*, 539-539.

[159] A. Frauenschuh, C. A. Power *et al.*, *J. Biol. Chem.* **2007**, *282*, 27250-27258.

[160] B. T. Seet, G. McFadden, *J. Leukocyte Biol.* **2002**, *72*, 24-34.

[161] A. Alcami, S. A. Lira, *Curr. Opin. Immunol.* **2010**, *22*, 482-487.

[162] A. S. Lalani, K. Graham *et al.*, *J. Virol.* **1997**, *71*, 4356-4363.

[163] W. Bannwarth, B. Hinzen, *Wiley-VCH* **2006**, ISBN 3-527-30693-5.

[164] R. B. Merrifield, *J. Am. Chem. Soc.* **1963**, *85*, 2149-2154.

[165] E. M. Southern, *Methods in Molecular Biology* **2001**, *170*, 1-15.

[166] F. C. Kafatos, C. W. Jones, A. Efstratiadis, *Nucleic Acids Res.* **1979**, *7*, 1541-1552.

[167] M. Schena, D. Shalon *et al.*, *Science* **1995**, *270*, 467-470.

[168] J. D. Hoheisel, M. T. Ross *et al.*, *J. Biotechnol.* **1994**, *35*, 121-134.

[169] J. R. Falsey, M. Renil *et al.*, *Bioconjugate Chem.* **2001**, *12*, 346-353.

[170] G. MacBeath, A. N. Koehler, S. L. Schreiber, *J. Am. Chem. Soc.* **1999**, *121*, 7967-7968.

[171] A. Furka, F. Sebestyen *et al.*, *Int. J. Pept. Prot. Res.* **1991**, *37*, 487-493.

[172] K. S. Lam, S. E. Salmon *et al.*, *Nature* **1991**, *354*, 82-84.

[173] K. S. Lam, M. Lebl, V. Krchnak, *Chem. Rev.* **1997**, *97*, 411-448.

[174] B. T. Chait, R. Wang *et al.*, *Science* **1993**, *262*, 89-92.

[175] A. Thakkar, A. S. Cohen *et al.*, *J. Comb. Chem.* **2009**, *11*, 294-302.

[176] R. W. Liu, J. Mark, K. S. Lam, *J. Am. Chem. Soc.* **2002**, *124*, 7678-7680.

[177] S. H. Hwang, A. Lehman *et al.*, *Org. Lett.* **2004**, *6*, 3829-3832.

[178] M. G. Paulick, K. M. Hart *et al.*, *J. Comb. Chem.* **2006**, *8*, 417-426.

[179] T. Carell, E. A. Wintner *et al.*, *Angew. Chem., Int. Ed. Engl.* **1994**, *33*, 2059-2061.

[180] T. Carell, E. A. Wintner, J. Rebek, *Angew. Chem., Int. Ed. Engl.* **1994**, *33*, 2061-2064.

[181] R. A. Houghten, *Proc. Natl. Acad. Sci. U. S. A.* **1985**, *82*, 5131-5135.

[182] K. C. Nicolaou, X. Y. Xiao *et al.*, *Angew. Chem., Int. Ed. Engl.* **1995**, *34*, 2289-2291.

[183] R. S. Roberts, *J. Comb. Chem.* **2005**, *7*, 21-32.

[184] D. K. Kolmel, D. Furniss *et al.*, *Pharmaceuticals* **2012**, *5*, 1265-1281.

[185] H. M. Geysen, R. H. Meloen, S. J. Barteling, *Proc. Natl. Acad. Sci. U. S. A.* **1984**, *81*, 3998-4002.

[186] S. P. A. Fodor, J. L. Read *et al.*, *Science* **1991**, *251*, 767-773.

[187] S. P. A. Fodor, R. P. Rava *et al.*, *Nature* **1993**, *364*, 555-556.

[188] A. P. Blanchard, R. J. Kaiser, L. E. Hood, *Biosens. Bioelectron.* **1996**, *11*, 687-690.

[189] E. M. Southern, U. Maskos, J. K. Elder, *Genomics* **1992**, *13*, 1008-1017.

[190] R. Frank, *Tetrahedron* **1992**, *48*, 9217-9232.

[191] M. C. Needels, D. G. Jones *et al.*, *Proc. Natl. Acad. Sci. U. S. A.* **1993**, *90*, 10700-10704.

[192] M. Oh, J. H. Lee *et al.*, *Proc. Natl. Acad. Sci. U. S. A.* **2014**, *111*, 11007-11012.

[193] G. P. Smith, *Science* **1985**, *228*, 1315-1317.

[194] K. Fukunaga, M. Taki, *J. Nucl. Acids* **2012**, *2012*, 1-9.

[195] C. Neylon, *Nucleic Acids Res.* **2004**, *32*, 1448-1459.

[196] T. Lindner, H. Kolmar *et al.*, *Molecules* **2011**, *16*, 1625-1641.

[197] D. R. Burton, C. F. Barbas *et al.*, *Proc. Natl. Acad. Sci. U. S. A.* **1991**, *88*, 10134-10137.

[198] R. Freudl, S. Macintyre *et al.*, *J. Mol. Biol.* **1986**, *188*, 491-494.

[199] E. T. Boder, K. D. Wittrup, *Nat. Biotechnol.* **1997**, *15*, 553-557.

[200] L. C. Mattheakis, R. R. Bhatt, W. J. Dower, *Proc. Natl. Acad. Sci. U. S. A.* **1994**, *91*, 9022-9026.

[201] C. Zahnd, P. Amstutz, A. Pluckthun, *Nat. Methods* **2007**, *4*, 269-279.

[202] L. C. Huang, X. Y. Pan *et al.*, *Sci. Rep.* **2013**, *3*, 1-9.

[203] L. A. A. de Jong, D. R. A. Uges *et al.*, *J. Chromatogr. B* **2005**, *829*, 1-25.

[204] P. Cariuk, M. J. Gardener, T. J. Vaughan, *Pharmaceuticals* **2013**, *6*, 681-688.

[205] B. Valeur, *Wiley-VCH* **2001**, ISBN 3-527-60024-8.

[206] J. R. Lakowicz, *Springer* **2006**, ISBN 0-387-31278-1.

[207] H. Fu, *Methods in Molecular Biology 261*, 161-165.

[208] F. Perrin, *J. Phys. Radium V* **1926**, *7*, 390-401.

[209] D. M. Jameson, J. A. Ross, *Chem. Rev.* **2010**, *110*, 2685-2708.

[210] G. Weber, *Adv. Protein Chem.* **1953**, *8*, 415-459.

[211] A. M. Rossi, C. W. Taylor, *Nat. Protoc.* **2011**, *6*, .

[212] W. B. Dandliker, M. L. Hsu *et al.*, *Methods Enzymol.* **1981**, *74*, 3-28.

[213] Invitrogen, *Fluorescence Polarization Technical Resource Guide* **2006**, *4*, part 1-8.

[214] P. S. Farmer, E. J. Ariens, *Trends Pharmacol. Sci.* **1982**, *3*, 362-365.

[215] J. Vagner, H. C. Qu, V. J. Hruby, *Curr. Opin. Chem. Biol.* **2008**, *12*, 292-296.

[216] A. Grauer, B. Konig, *Eur. J. Org. Chem.* **2009**, 5099-5111.

[217] R. J. Simon, R. S. Kania *et al.*, *Proc. Natl. Acad. Sci. U. S. A.* **1992**, *89*, 9367-9371.

[218] R. N. Zuckermann, J. M. Kerr *et al.*, *J. Am. Chem. Soc.* **1992**, *114*, 10646-10647.

[219] R. N. Zuckermann, *Abstr. Pap. Am. Chem. Soc.* **1994**, *208*, 376-377.

[220] D. Buckley, S. Dunstan, H. B. Henbest, *J. Chem. Soc.* **1957**, 4901-4905.

[221] K. Fickentscher, *Arch. Pharm. Ber. Dtsch. Pharm. Ges.* **1969**, *302*, 119-125.

[222] I. Masip, N. Cortes *et al.*, *Bioorg. Med. Chem.* **2005**, *13*, 1923-1929.

[223] R. J. Simon, E. J. Martin *et al.*, *Techniques in Protein Chemistry V* **1994**, 533-539 569.

[224] E. W. Taylor, J. A. Gibbons, R. A. Braeckman, *Pharm. Res.* **1997**, *14*, 572-577.

[225] K. Moehle, H. J. Hofmann, *Biopolymers* **1996**, *38*, 781-790.

[226] Q. Sui, D. Borchardt, D. L. Rabenstein, *J. Am. Chem. Soc.* **2007**, *129*, 12042-12048.

[227] G. L. Butterfoss, P. D. Renfrew *et al.*, *J. Am. Chem. Soc.* **2009**, *131*, 16798-16807.

[228] D. E. Stewart, A. Sarkar, J. E. Wampler, *J. Mol. Biol.* **1990**, *214*, 253-260.

[229] H. Tran, S. L. Gael *et al.*, *J. Vis. Exp.* **2012**, *57*, e3373 1-6.

[230] H. J. Olivos, P. G. Alluri *et al.*, *Org. Lett.* **2002**, *4*, 4057-4059.

[231] Y. B. Feng, G. Melacini *et al.*, *Biopolymers* **1996**, *39*, 859-872.

[232] P. Armand, K. Kirshenbaum *et al.*, *Fold. Des.* **1997**, *2*, 369-375.

[233] P. Armand, K. Kirshenbaum *et al.*, *Proc. Natl. Acad. Sci. U. S. A.* **1998**, *95*, 4309-4314.

[234] K. Kirshenbaum, A. E. Barron *et al.*, *Proc. Natl. Acad. Sci. U. S. A.* **1998**, *95*, 4303-4308.

[235] M. Rainaldi, V. Moretto *et al.*, *J. Pept. Sci.* **2002**, *8*, 241-252.

[236] T. J. Sanborn, C. W. Wu *et al.*, *Biopolymers* **2002**, *63*, 12-20.

[237] J. A. Crapster, I. A. Guzei, H. E. Blackwell, *Angew. Chem., Int. Ed. Engl.* **2013**, *52*, 5079-5084.

[238] B. C. Lee, R. N. Zuckermann, K. A. Dill, *J. Am. Chem. Soc.* **2005**, *127*, 10999-11009.

[239] B. C. Lee, T. K. Chu *et al.*, *J. Am. Chem. Soc.* **2008**, *130*, 8847-8855.

[240] B. Sanii, R. Kudirka *et al.*, *J. Am. Chem. Soc.* **2011**, *133*, 20808-20815.

[241] S. Ostergaard, A. Holm, *Mol. Diversity* **1997**, *3*, 17-27.

[242] T. A. Tran, R. H. Mattern *et al.*, *J. Med. Chem.* **1998**, *41*, 2679-2685.

[243] S. Ng, B. Goodson *et al.*, *Bioorg. Med. Chem.* **1999**, *7*, 1781-1785.

[244] N. P. Chongsiriwatana, J. A. Patch *et al.*, *Proc. Natl. Acad. Sci. U. S. A.* **2008**, *105*, 2794-2799.

[245] A. R. Statz, A. E. Barron, P. B. Messersmith, *Soft Matter* **2008**, *4*, 131-139.

[246] P. A. Wender, D. J. Mitchell *et al.*, *Proc. Natl. Acad. Sci. U. S. A.* **2000**, *97*, 13003-13008.

[247] I. Peretto, R. M. Sanchez, Martin *et al.*, *Chem. Comm.* **2003**, 2312-2313.

[248] T. Schroder, N. Niemeier *et al.*, *J. Med. Chem.* **2008**, *51*, 376-379.

[249] C. Anne, M. C. Fournie, Zaluski *et al.*, *Tetrahedron Lett.* **1998**, *39*, 8973-8974.

[250] G. M. Figliozzi, R. Goldsmith *et al.*, *Methods Enzymol.* **1996**, *267*, 437-447.

[251] R. Volkmer, Engert, B. Hoffmann, J. Schneider, Mergener, *Tetrahedron Lett.* **1997**, *38*, 1029-1032.

[252] N. Heine, T. Ast *et al.*, *Tetrahedron* **2003**, *59*, 9919-9930.

[253] M. Humet, T. Carbonell *et al.*, *J. Comb. Chem.* **2003**, *5*, 597-605.

[254] H. S. Lim, M. M. Reddy *et al.*, *Bioorg. Med. Chem. Lett.* **2009**, *19*, 3866-3869.

[255] T. Kodadek, K. Bachhawat, Sikder, *Mol. BioSyst.* **2006**, *2*, 25-35.

[256] J. J. Devlin, L. C. Panganiban, P. E. Devlin, *Science* **1990**, *249*, 404-406.

[257] P. C. Weber, M. W. Pantoliano, L. D. Thompson, *Biochemistry* **1992**, *31*, 9350-9354.

[258] E. K. Bradley, *J. Magn. Reson. Ser. B* **1996**, *110*, 195-197.

[259] E. K. Bradley, J. M. Kerr *et al.*, *Mol. Diversity* **1997**, *3*, 1-15.

[260] C. W. Wu, K. Kirshenbaum *et al.*, *J. Am. Chem. Soc.* **2003**, *125*, 13525-13530.

[261] W. Heerma, C. Versluis *et al.*, *Rapid Commun. Mass Spectrom.* **1996**, *10*, 459-464.

[262] W. Heerma, J. P. J. L. Boon *et al.*, *J. Mass Spectrom.* **1997**, *32*, 697-704.

[263] D. Wiese, K. Schmitz, *J. Immunol. Methods* **2011**, *364*, 77-82.

[264] J. Inglese, P. Samama *et al.*, *Biochemistry* **1998**, *37*, 2372-2377.

[265] E. Kownatzki, A. Kapp, S. Uhrich, *Clin. Exp. Immunol.* **1986**, *64*, 214-222.

[266] A. L. van Dervort, C. Lam *et al.*, *J. Leukocyte Biol.* **1998**, *64*, 511-518.

[267] D. H. A. Correa, C. H. I. Ramos, *Afr. J. Biochem. Res.* **2009**, *3*, 164-173.

[268] W. Kabsch, C. Sander, *Biopolymers* **1983**, *22*, 2577-2637.

[269] L. Pohjala, P. Tammela, *Molecules* **2012**, *17*, 10774-10790.

[270] X. C. Zhang, J. K. Jackson, H. M. Burt, *J. Biochem. Biophys. Meth.* **1996**, *31*, 145-150.

[271] A. Helenius, K. Simons, *J. Biol. Chem.* **1972**, *247*, 3656-3661.

[272] E. Fries, *Biochim. Biophys. Acta* **1976**, *455*, 928-936.

[273] K. M. Misura, D. Chivian *et al.*, *Proc. Natl. Acad. Sci. U. S. A.* **2006**, *103*, 5361-6.

[274] S. H. Park, B. B. Das *et al.*, *Nature* **2012**, *491*, 779-783.

[275] E. F. Pettersen, T. D. Goddard *et al.*, *J. Comput. Chem.* **2004**, *25*, 1605-12.

[276] E. N. Baker, R. E. Hubbard, *Prog. Biophys. Mol. Biol.* **1984**, *44*, 97-179.

[277] I. Y. Torshin, I. T. Weber, R. W. Harrison, *Protein Eng.* **2002**, *15*, 359-363.

[278] C. Bissantz, B. Kuhn, M. Stahl, *J. Med. Chem.* **2010**, *53*, 6241-6241.

[279] I. Clark-Lewis, B. Dewald *et al.*, *Proc. Natl. Acad. Sci. U. S. A.* **1993**, *90*, 3574-3577.

[280] I. U. Schraufstatter, M. Ma *et al.*, *J. Biol. Chem.* **1995**, *270*, 10428-10431.

[281] M. E. W. Hammond, V. Shyamala *et al.*, *J. Biol. Chem.* **1996**, *271*, 8228-8235.

[282] G. Williams, N. Borkakoti *et al.*, *J. Biol. Chem.* **1996**, *271*, 9579-9586.

[283] G. N. Prado, K. Suetomi *et al.*, *Biochemistry* **2007**, *46*, 11660-11660.

[284] F. Xu, H. Wu *et al.*, *Science* **2011**, *332*, 322-7.

[285] P. R. B. Joseph, J. M. Sarmiento *et al.*, *J. Biol. Chem.* **2010**, *285*, 29262-29269.

[286] J. Sarmiento, C. Shumate *et al.*, *PLoS One* **2011**, *6*, e27967 1-7.

[287] G. S. V. Kuschert, F. Coulin *et al.*, *Biochemistry* **1999**, *38*, 12959-12968.

[288] D. Spillmann, D. Witt, U. Lindahl, *J. Biol. Chem.* **1998**, *273*, 15487-15493.

[289] J. W. Liou, F. T. Chang *et al.*, *PLoS One* **2014**, *9*, e94178 1-13.

[290] C. . G. . I. Chemical *Molecular Operating Environment (MOE)* **2013**, H3A 2R7.

[291] G. B. Fields, R. L. Noble, *Int. J. Pept. Protein Res.* **1990**, *35*, 161-214.

[292] Y. Cheng, W. H. Prusoff, *Biochem. Pharmacol.* **1973**, *22*, 3099-3108.

[293] M. A. Holden, P. S. Cremer, *J. Am. Chem. Soc.* **2003**, *125*, 8074-8075.

[294] M. A. Holden, S. Y. Jung, P. S. Cremer, *Anal. Chem.* **2004**, *76*, 1838-1843.

[295] J. M. Belisle, J. P. Correia *et al.*, *Lab Chip* **2008**, *8*, 2164-2167.

[296] A. Waldbaur, B. Waterkotte *et al.*, *Small* **2012**, *8*, 1570-1578.

[297] L. Da Vinci, *Mona Lisa retouched, wikicommons public domain* **1503**, accessed 2012.

[298] W. S. Rasband, *ImageJ, U. S. National Institutes of Health* **1997-2014**, http://imagej.nih.gov/ij/.

[299] A. S. Culf, R. J. Ouellette, *Molecules* **2010**, *15*, 5282-5335.

[300] T. Schroder, *Logos* **2007**, *Dissertation*, ISBN 978-3-8325-1768-7.

[301] J. D. White, Y. Li, D. C. Ihle, *J. Org. Chem.* **2010**, *75*, 3569-3577.

[302] R. Fischer, O. Mader *et al.*, *Bioconjugate Chem.* **2003**, *14*, 653-660.

[303] X. Zhu, I. A. Papayannopoulos, *J. Biomol. Tech.* **2003**, *14*, 298-307.

[304] M. Pursch, G. Schlotterbeck *et al.*, *Angew. Chem., Int. Ed. Engl.* **1996**, *35*, 2867-2869.

[305] H. I. Olivos, K. Bachhawat, Sikder, T. Kodadek, *ChemBioChem* **2003**, *4*, 1242-1245.

[306] J. Canny, *IEEE T. Pattern. Anal.* **1986**, *8*, 679-698.

[307] P. V. C. Hough, *US Patent* **1962**, US3069654 A.

[308] J. K. Bowmaker, H. J. A. Dartnall, *Journal of Physiology-London* **1980**, *298*, 501-511.

[309] N. D. Spencer, *World Scientific Publishing Co. Pte. Ltd.* **2011**, ISBN 981-4289-42-6.

[310] N. Y. Yount, A. J. Waring *et al.*, *Biochim. Biophys. Acta, Biomembr.* **2007**, *1768*, 598-608.

[311] J. O'Brien, I. Wilson *et al.*, *Eur. J. Biochem.* **2000**, *267*, 5421-5426.

[312] Y. L. Yan, G. Marriott, *Curr. Opin. Chem. Biol.* **2003**, *7*, 635-640.

[313] J. W. Choi, D. K. Kang *et al.*, *Anal. Chem.* **2012**, *84*, 3849-3854.

[314] S. Dedier, S. Reinelt *et al.*, *J. Immunol. Methods* **2001**, *255*, 57-66.

[315] J. Kyte, R. F. Doolittle, *J. Mol. Biol.* **1982**, *157*, 105-132.

[316] X. L. Xie, L. Sun *et al.*, *PLoS One* **2013**, *8*, e78042.

[317] K. Palczewski, T. Kumasaka *et al.*, *Science* **2000**, *289*, 739-745.

[318] T. Okada, M. Sugihara *et al.*, *J. Mol. Biol.* **2004**, *342*, 571-583.

[319] B. G. Tehan, A. Bortolato *et al.*, *Pharmacol. Ther.* **2014**, *143*, 51-60.

[320] H. M. Berman, J. Westbrook *et al.*, *Nucleic Acids Res.* **2000**, *28*, 235-242.

[321] I. Ispolatov, A. Yuryev *et al.*, *Nucleic Acids Res.* **2005**, *33*, 3629-3635.

[322] A. Boeijen, R. M. J. Liskamp, *Tetrahedron Lett.* **1998**, *39*, 3589-3592.

[323] E. Bayer, M. Dengler, B. Hemmasi, *Int. J. Pept. Protein Res.* **1985**, *25*, 178-186.

[324] E. Bayer, *Angew. Chem., Int. Ed. Engl.* **1991**, *30*, 113-129.

[325] B. J. Egner, S. Rana *et al.*, *Chem. Comm.* **1997**, 735-736.

[326] P. G. Alluri, M. M. Reddy *et al.*, *J. Am. Chem. Soc.* **2003**, *125*, 13995-14004.

[327] B. Hintersteiner, M. Auer, *Methods Appl. Fluoresc.* **2013**, *1*, 1-7.

[328] K. S. Lam, A. L. Lehman *et al.*, *Methods Enzymol.* **2003**, *369*, 298-322.

[329] M. M. Reddy, K. Bachhawat, Sikder, T. Kodadek, *Chem. Biol.* **2004**, *11*, 1127-1137.

[330] M. Hintersteiner, C. Buehler *et al.*, *J. Comb. Chem.* **2009**, *11*, 886-894.

[331] Y. U. Kwon, T. Kodadek, *Chem. Comm.* **2008**, 5704-5706.

[332] B. H. Hu, M. R. Jones, P. B. Messersmith, *Anal. Chem.* **2007**, *79*, 7275-7285.

[333] M. Sturm, A. Bertsch *et al.*, *BMC Bioinformatics* **2008**, *9*, 1-11.

[334] N. Ebner, *Dissertation* **2006**, University of Karlsruhe.

[335] M. Gude, J. Ryf, P. D. White, *Lett. Pept. Sci.* **2002**, *9*, 203-206.

[336] O. Avrutina, H. Fittler *et al.*, *Org. Biomol. Chem.* **2012**, *10*, 7753-7762.

[337] M. Girrbach, I. Meliciani *et al.*, *Phys. Chem. Chem. Phys.* **2014**, *16*, 8036-8043.

[338] N. Moerke, *Curr. Protoc. Chem. Biol.* **2009**, *1*, 1-15.

8 Abbreviations

aa	Amino acid
AIDS	Acquired immumodefficiency syndrome
AU	Anisotropy units
BSA	Bovine serum albumin
CAM	Cell adhesion molecule
CD	Circular dichroism
CD4, CD14	Cluster of differentiation 4, 14
cmc	Critical micelle concentration
CV	Column volume
DAPI	4',6-diamidino-2-phenylindole (microscopy channel)
DIPEA	N,N-Diisopropylethylamine
ECD	Extracellular domain
EGF	Epidermal growth factor
em	Emission
ESGL	E-selectin glycoprotein ligand
ex	Excitation
FACS	Fluorescence-activated cell sorting
FITC	Fluorescein isothiocyanate
Fluo	Fluorescein-label of peptides, 5(6)-carboxyfluorescein
GAG	Glycosaminoglycan
GPCR	G-protein coupled receptor
HBTU	N,N,N',N'-Tetramethyl-O-(1H-benzotriazol-1-yl)uronium hexafluorophosphate
HIV	Human immunodeficiency virus
HOBt	Hydroxybenzotriazole
ICAM	Intercellular adhesion molecule
IDA	Iminodiacetic acid
IP3	Inositol trisphosphate
ITC	Isothermal titration calorimetry
IVTT	*In vitro* transcription/translation
K_d	Dissociation constant
LBP	Lipopolysaccharide binding protein
LPS	Lipopolysaccharide
M-PVA	Superparamegnetic particles in polyvinylalcohol matrix
MALDI TOF MS	Matrix assisted laser desorption/ionisation time-of-flight mass spectrometry
MALDI TOF MS/MS	Matrix assisted laser desorption/ionisation time-of-flight mass spectrometry with ion selection and fragmentation
man	manual (setting of the PMTG)
MB HMBA	Macrobeads with 4-(hydroxymethyl)benzoic acid linker
MCP-1	Monocyte chemoattractant protein-1, chemokine CCL2
MS	Mass spectrometry
MTP	Microtiter plate
NMR	Nuclear magnetic resonance (spectroscopy)

OBOC	One-bead-one-compound
opt	optimal (setting of the PMTG)
PEG	Polyethylene glycol
PIP2	Phosphatidylinositol-4,5-bisphosphate
PIP3	Phosphatidylinositol-3,4,5-trisphosphate
PKB	Protein kinase B
PMN	Polymorphonuclear leukocyte
PMTG	Photomultiplier tube gain
PSGL	P-selectin glycoprotein ligand
PVA	Polyvinylalcohol
RANTES	Regulated on Activation, Normal T-Cell Expressed, chemokine CCL5
REC	Radio frequency encoded combinatorial chemistry
RHO	Rhodamine (microscopy channel)
RhoB	Rhodamine B
ROS	Reactive oxygen species
RPMI	Roswell Park Memorial Institute medium
RU	Relative fluorescence units
SDF1-α	Stromal cell-derived factor 1, chemokine CXCL12
SEA	Staphylococcal enterotoxin A
SMART	Single or Multiple Addressable Radiofrequency Tag
SPR	Surface Plasmon Resonance
TG	TentaGel
TLR	Toll-like receptor
TMH	Transmembrane helix
XRC	X-ray crystallography

9 Appendix

Peptoid Binding Affinity for CXCL8, see Section 5.5.3

Peptoids **167-184** were tested for their affinity for CXCL8wt in fluorescence anisotropy measurements.
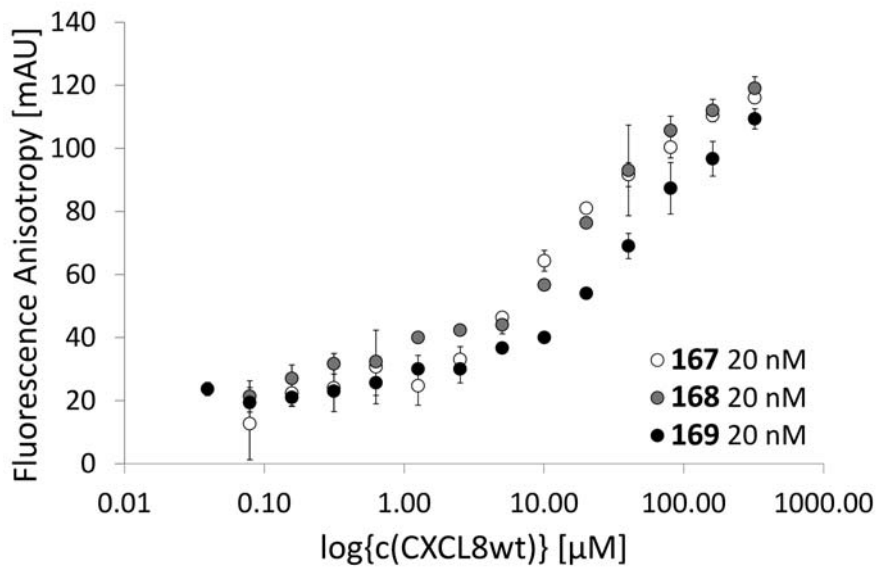
Figure 9.1: Fluorescence anisotropy measurement of the binding of peptoids **167**, **168**, **169** to CXCL8 in *ls*-PBS.
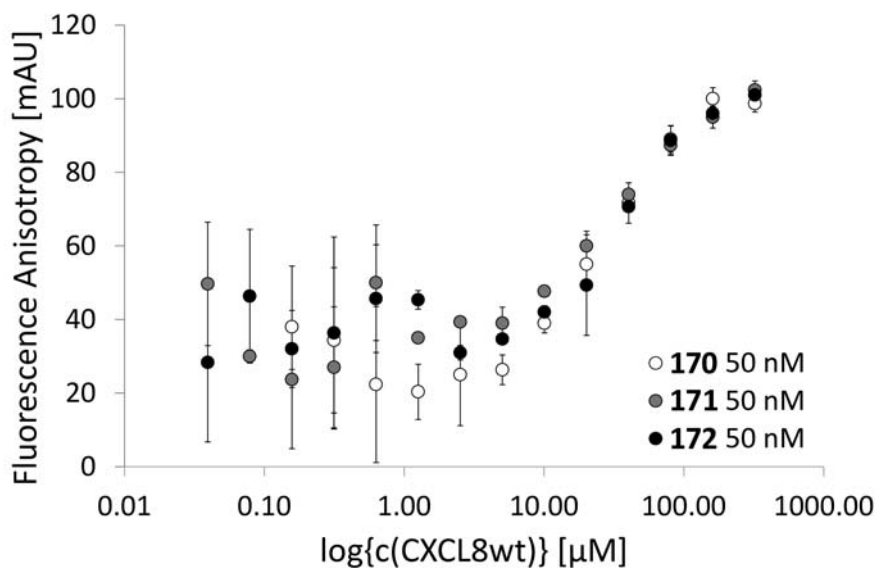
Figure 9.2: Fluorescence Anisotropy measurement of the binding of peptoids **170**, **171**, **172** to CXCL8 in *ls*-PBS.
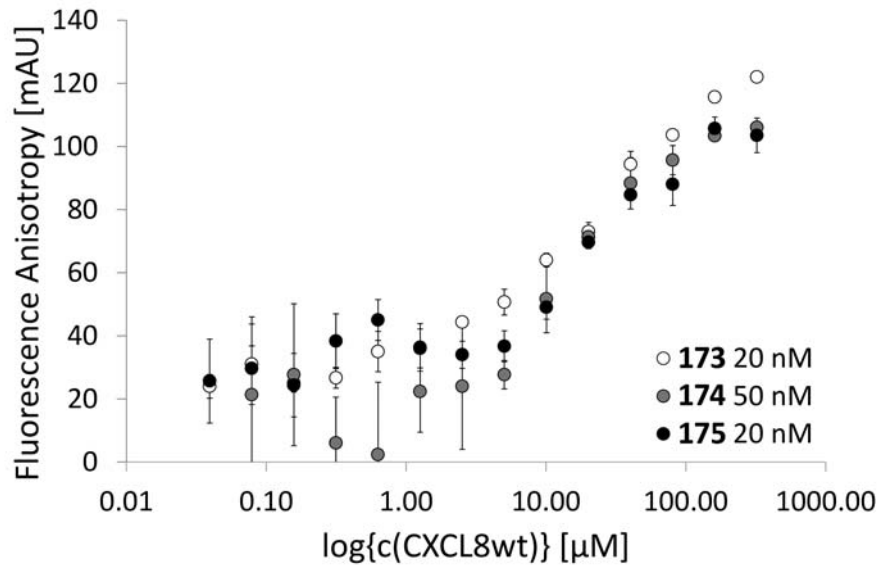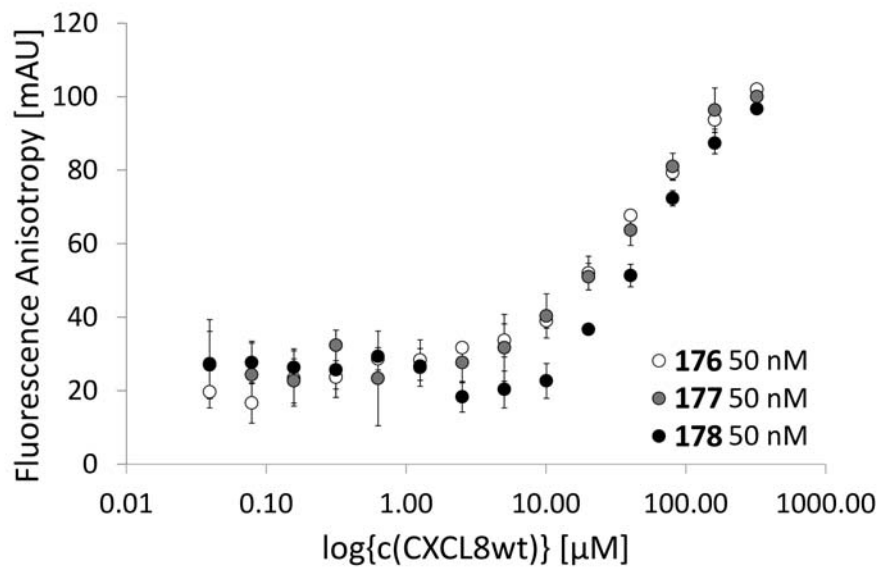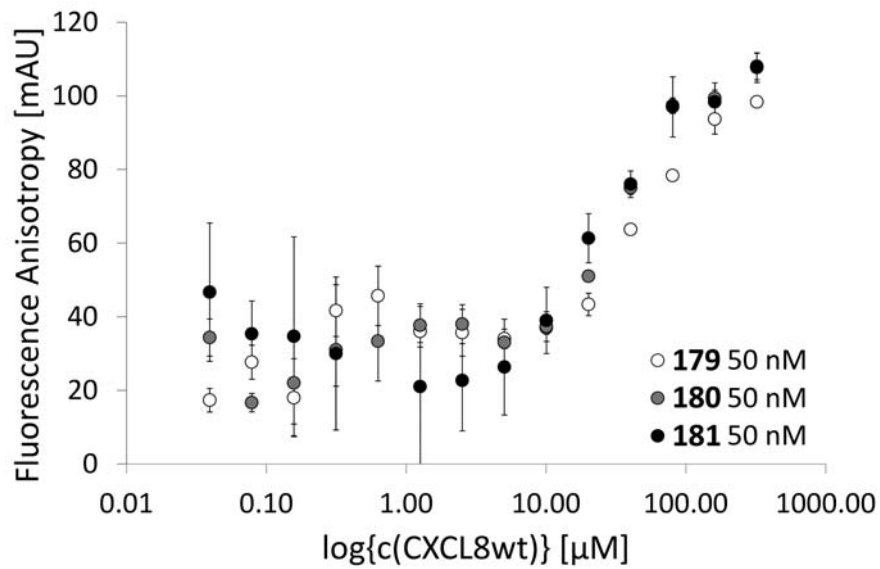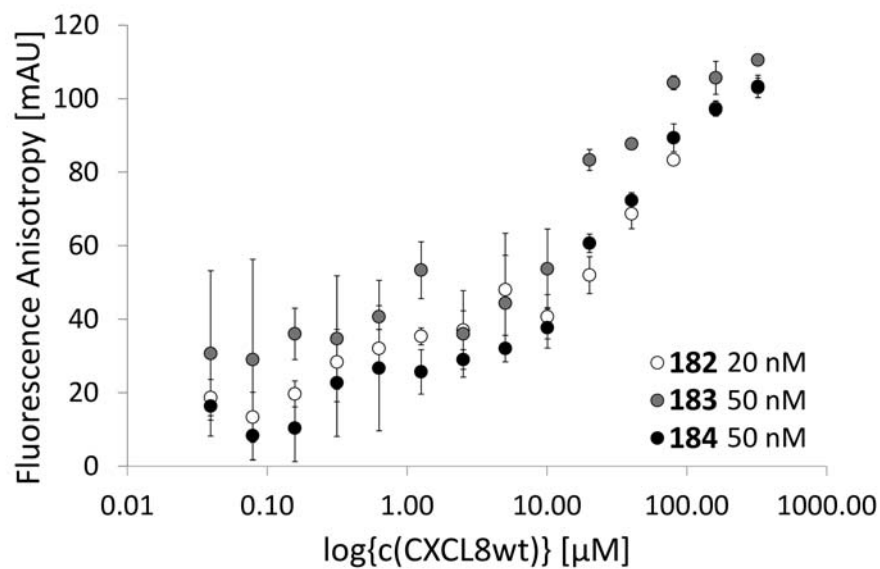
Figure 9.3: Fluorescence Anisotropy measurement of the binding of peptoids **173**, **174**, **175** to CXCL8 in *ls*-PBS.

Figure 9.4: Fluorescence Anisotropy measurement of the binding of peptoids **176**, **177**, **178** to CXCL8 in *ls*-PBS.

Figure 9.5: Fluorescence Anisotropy measurement of the binding of peptoids **179**, **180**, **181** to CXCL8 in *ls*-PBS.

Figure 9.6: Fluorescence Anisotropy measurement of the binding of peptoids **182**, **183**, **184** to CXCL8 in *ls*-PBS.

Peptoids **167**-**179** and **182**-**183** were tested for their toxic effect on human neutrophils by a resazurin viability assay. Peptoids show no toxic effect on human neutrophils.
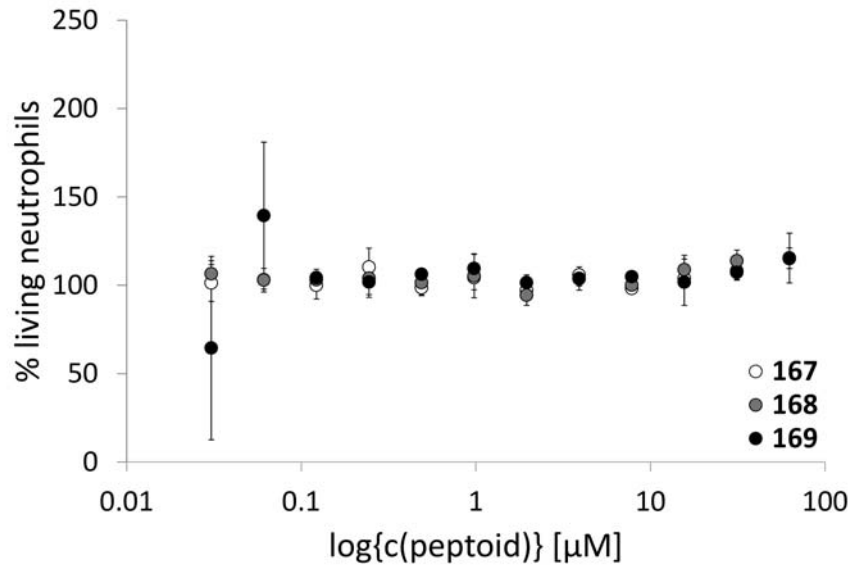
Figure 9.7: **167**, **168**, **169** show no toxic effect on human neutrophil granulocytes stained with resazurin.
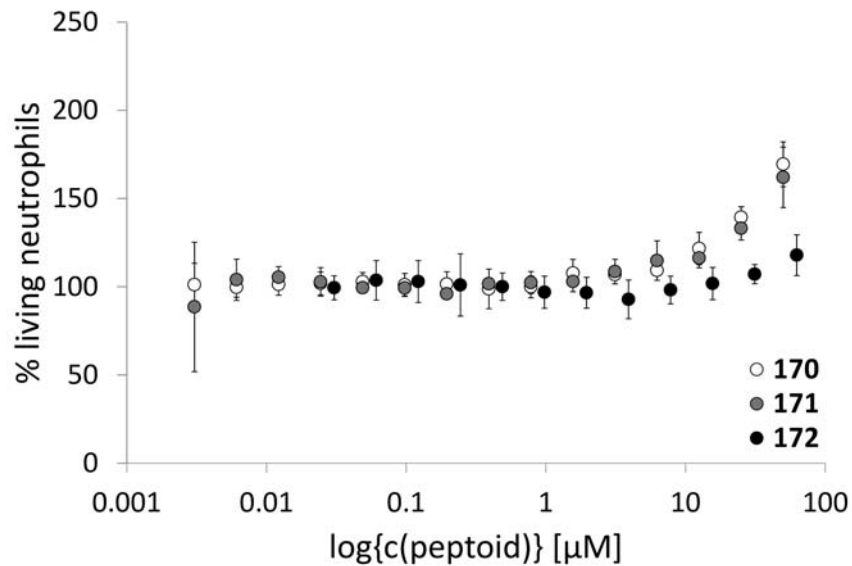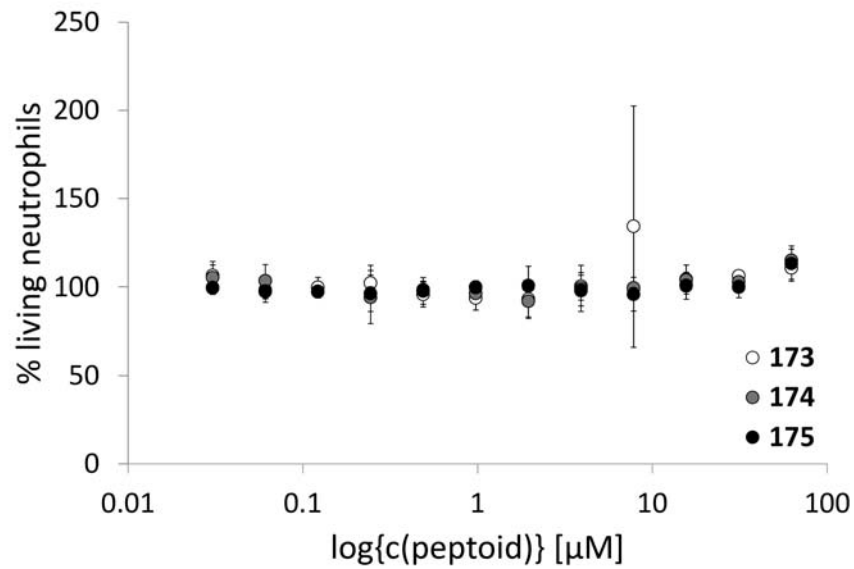

Figure 9.8: **170**, **171**, **172** show no toxic effect on human neutrophil granulocytes stained with resazurin.

Figure 9.9: **173**, **174**, **175** show no toxic effect on human neutrophil granulocytes stained with resazurin.
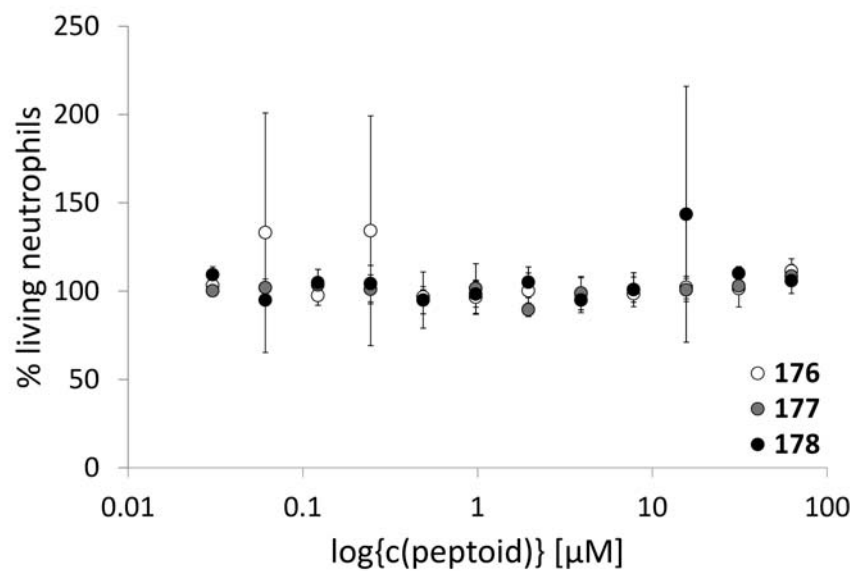

Figure 9.10: **176**, **177**, **178** show no toxic effect on human neutrophil granulocytes stained with resazurin.
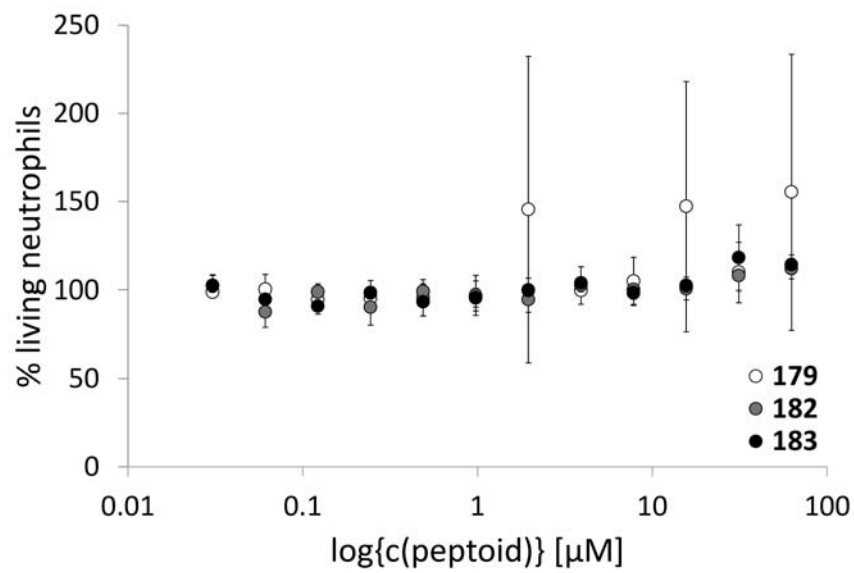
Figure 9.11: **179**, **182** and **183** show no toxic effect on human neutrophil granulocytes stained with resazurin.

Peptoids **174**, **180**, **181** and **182** influenced CXCL8-induced actin polymerization in human neutrophils by decreasing amounts of filamentous F-actin. Amount of F-actin was determined by fluorescence intensity measurements after phalloidin-iFluor555 staining.
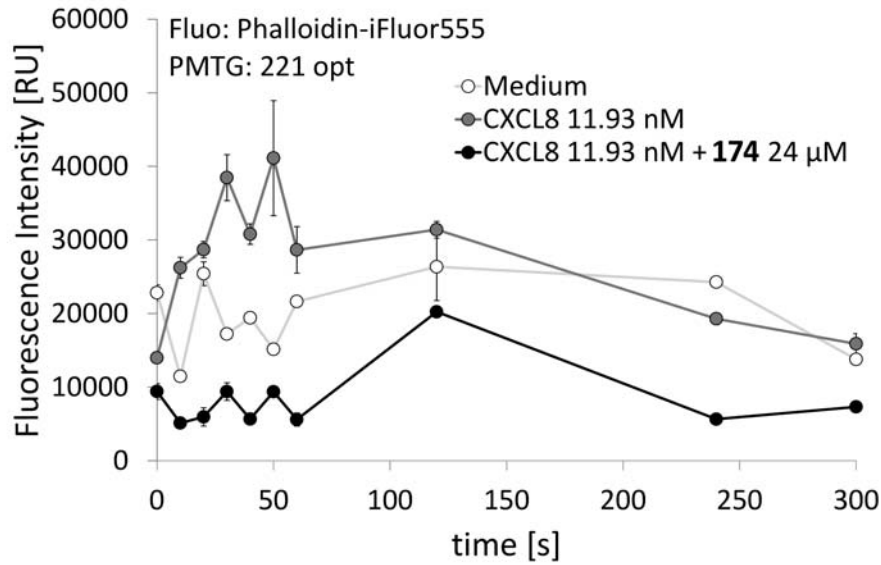

Figure 9.12: Actin polymerisation assay with human neutrophil granulocytes stimulated with CXCL8wt and a mixture of CXCL8 and peptoid **174** in RPMI$_{(-)}$. Peptoid **174** significantly reduces the amount of F-actin visualized by staining with phalloidin-iFluor555.

Figure 9.13: Actin polymerisation assay with human neutrophil granulocytes stimulated with CXCL8wt and a mixture of CXCL8 and peptoid **180** in RPMI$_{(-)}$. Peptoid **180** significantly reduces the amount of F-actin visualized by staining with phalloidin-iFluor555.
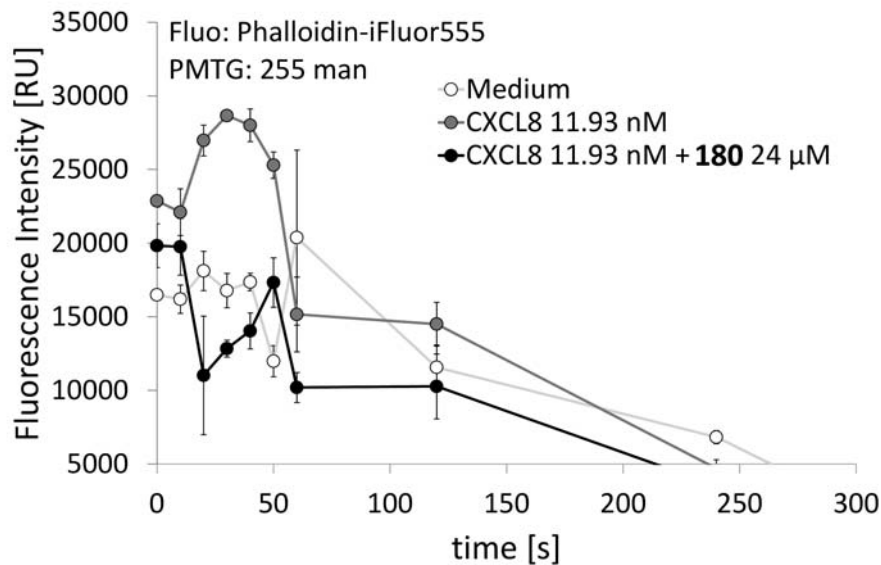
Figure 9.14: Actin polymerisation assay with human neutrophil granulocytes stimulated with CXCL8wt and a mixture of CXCL8 and peptoid **181** in RPMI$_{(-)}$. Peptoid **181** significantly reduces the amount of F-actin visualized by staining with phalloidin-iFluor555.
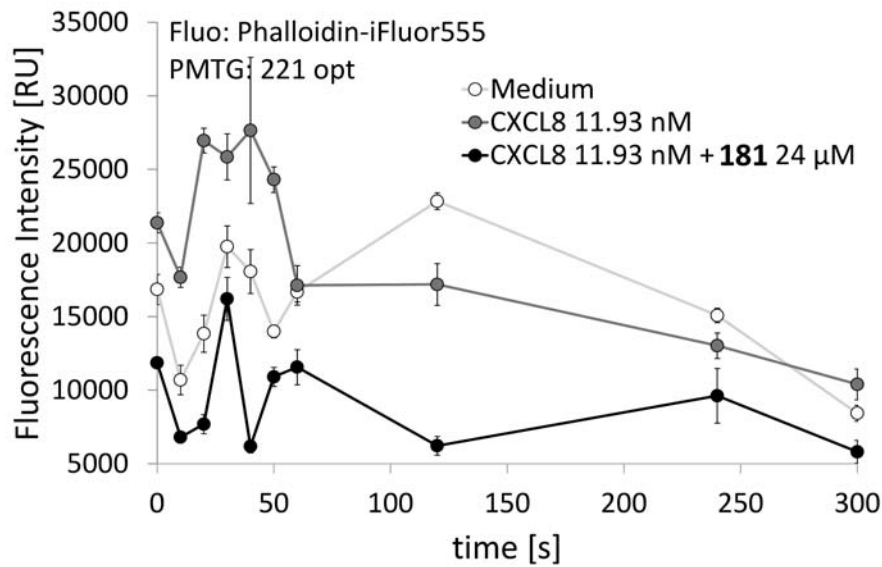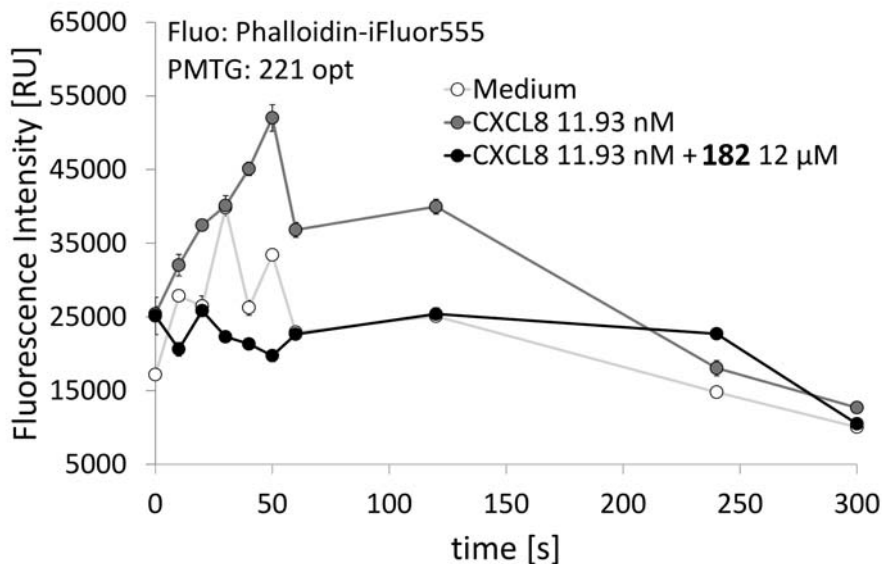

Figure 9.15: Actin polymerisation assay with human neutrophil granulocytes stimulated with CXCL8wt and a mixture of CXCL8 and peptoid **182** in RPMI$_{(-)}$. Peptoid **182** significantly reduces the amount of F-actin visualized by staining with phalloidin-iFluor555.

Publications

Manuscripts

- D. Helmer, I. Rink, J. A. R. Dalton, K. Brahm, M. Jöst, T. M. Nargang, W. Blum, P. Wadhwani, G. Brenner-Weiss, B. E. Rapp, J. Giraldo, K. Schmitz, "Rational design of a peptide capture agent for CXCL8 based on a model of the CXCL8:CXCR1 complex", *RSC Advances* **2015**, *5*, 25657-25668.

Speeches

- "Synthesis and semi-automated screening of one-bead-one-compound libraries of potential chemokine inhibitor peptoids", 8th Peptoid Summit, LBNL, Berkeley, California, 2012.

- "Synthesis and semi-automated screening of one-bead-one-compound libraries of potential chemokine inhibitor peptoids", Doktorandentag, TU Darmstadt, 2012.

- "Synthesis and Test of Peptoids for the Inhibition of Cytokines", BioInterfaces International Graduate School Retreat, Bad Herrenalb, 2011.

Posters

- "Synthesis and semi-automated screening of one-bead-one-compound libraries of potential chemokine inhibitors", Status Seminar Chemical Biology, DECHEMA Frankfurt, 2013.

- "Peptoids for the Inhibition of Cytokines", Helmer, D., Schmitz, K., 7th Peptoid Summit, LBNL, Berkeley, California, 2010.

- "Effects of Inhibitors and Immobilization on Chemokine Activity" Braun, M., Helmer, D., Waterkotte, B. and Schmitz, K., European Lab Automation, Hamburg, 2011.

- "Peptoids for the Inhibition of Cytokines", Helmer, D., Reischl, M., Schmitz, K., European Lab Automation, Hamburg, 2011.

- "Peptoids for the Inhibition of Cytokines", Helmer, D., Schmitz, K., EMBL Chemical Biology, Heidelberg 2011.

10 Danksagung

Danksagungen werden dem Beitrag der Erwähnten nie gerecht. Ich möchte dennoch versuchen, meine aufrichtige Dankbarkeit zum Ausdruck zu bringen.

Frau Prof. Katja Schmitz danke ich für Ideen, Betreuung, Interesse, Beistand, Verständnis, kritische Diskussionen, Fachgespräche, Spontanität, und für die Freude an der Arbeit, die wir in Karlsruhe und in Darmstadt nie verloren haben. Ich habe so viel von dir gelernt, es war eine tolle, lehrreiche Zeit.

Herrn Prof. Harald Kolmar danke ich für die freundliche Übernahme des Korreferats.

Herrn Dr. Bastian E. Rapp möchte ich für seine Unterstützung danken. Ohne dich gäbe es diese Arbeit nicht, ich werde das nicht vergessen. Ich danke Tobias Nargang für seine Hilfe bei der maskenlosen Lithographie und dem Rest der Rappschen Truppe für sonstige moralische und experimentelle Unterstützung bei meinen vielen Besuchen.

Der Analytik-Crew des IFG (KIT) aus Gerald Brenner-Weiss, Frank Kirschhöfer, Michael 'Numi' Nusser und Boris Kühl danke ich sehr für die Möglichkeit MALDI TOF MS messen zu können, für die stets unterhaltsamen Messzeiten und die prompte Hilfe bei allen fachlichen Fragen.

Dank auch an James Dalton aus der Gruppe von Jesús Giraldo (UA Barcelona) für MD Simulationen und Docking, sowie Philipp Czechowski für die Messung der CD Spektren, Witali Blum für Peptidsynthesen am Synthesizer und Sebastian Hörner sowie Heiko Fittler für LC/MS Messungen. Parvesh Wadhwani und seiner Gruppe vom IBG-2 (KIT) danke ich für die Synthese von Fluo-CXCR1-p1.

Aus meiner Zeit in Darmstadt möchte ich insbesondere Ina Rink danken. Ohne deine Hilfe und Untestützung wäre ich nicht ans Ziel gekommen. Ich danke dir für alle Experimente bei denen du mir neben deiner eigenen Arbeit immer sofort bereitwillig geholfen hast. Du bist einmalig und nicht zu ersetzen. Ganz besonders möchte ich auch Anke Imrich danken für viele schöne aufmunternde Gespräche und Nachschub an Interleukin-8. Für großartige Abende und beste Unterhaltung danke ich außerdem Kerstin Bathon. Des Weiteren gilt mein Dank meinen Kollegen Kevin *'HPLC-König'* Brahm und Marina Jöst für die praktische Unterstützung, die alten Zeiten und den Kuchen.

Für eine unbeschreibliche Zeit in Karlsruhe und für das beste Abschiedsgeschenk der Welt danke ich insbesondere Ebru Diler - du hast mir in Darmstadt oft gefehlt. Außerdem Ingo Fischer, Tobias Müller, Miklos Szantai-Kis, Christian Morhardt, Matthias Franzreb, Martín Silvestre, Christine Müller, Markus Gärtner und Mirjam Hau. Unvergesslich bleibt für mich außerdem die Zeit in Karlsruhe mit Katharina Güse, Sabrina Hanke, Irene Meliciani, Anna-Marie Zorn, Carlos Azucena, Marina Albrizio, Barbara Vezzoni, Tatiana Losovskaya und Dana Wiese.

Isabella Hebeiß danke ich für ihre Freundschaft, ihren Rat und für zwei Jahre wunderbare Wohngemeinschaft. Ich werde dich immer bewundern.

Am meisten danke ich meiner Familie. Mama, Papa, Chris, ihr seid die Besten! And James, thank you!

Erklärung zur Dissertation

Ich erkläre hiermit, dass ich meine Dissertation selbstständig und nur mit den angegebenen Hilfsmitteln angefertigt habe und dass ich noch keinen Promotionsversuch unternommen habe.

Gernsbach, den

Dorothea Helmer